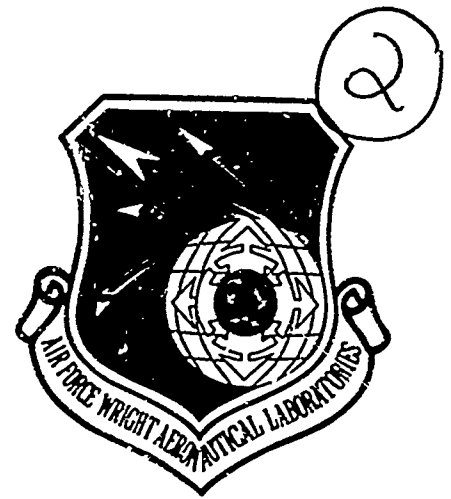


DTIC FILE COPY

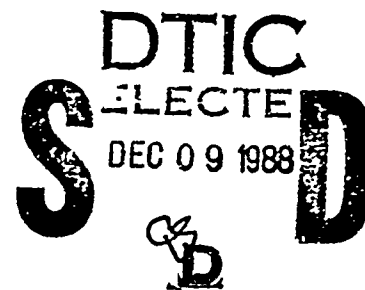
AFWAL-TR-87-3008
VOLUME II



**SUPERPLASTIC FORMED ALUMINUM AIRFRAME STRUCTURES
VOLUME II - TECHNICAL DETAILS**

H. R. ZAMANI
S. P. AGRAWAL
R. VASTAVA

NORTHROP CORPORATION - AIRCRAFT DIVISION
HAWTHORNE, CALIFORNIA 90250-3277



JULY 1987
FINAL REPORT FOR PERIOD NOVEMBER 1981 - JULY 1986

Approved for public release; distribution unlimited

88 12 9 009

FLIGHT DYNAMICS LABORATORY
AIR FORCE WRIGHT AERONAUTICAL LABORATORIES
AIR FORCE SYSTEMS COMMAND
WRIGHT-PATTERSON AIR FORCE BASE, OHIO 45433-6553

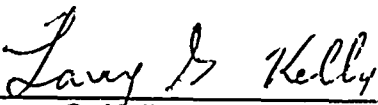
AD-A201 941


NOTICE

When Government drawings, specifications, or other data are used for any purpose other than in connection with a definitely related Government procurement operation, the United States Government thereby incurs no responsibility nor any obligation whatsoever; and the fact that the government may have formulated, furnished, or in any way supplied the said drawings, specifications, or other data, is not to be regarded by implication or otherwise as in any manner licensing the holder or any other person or corporation, or conveying any rights or permission to manufacture use, or sell any patented invention that may in any way be related thereto.

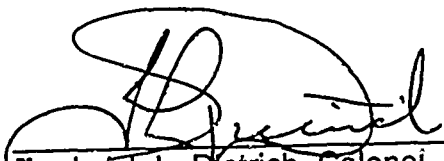
This report has been reviewed by the Office of Public Affairs (ASD/PA) and is releasable to the National Technical Information Service (NTIS). At NTIS, it will be available to the general public, including foreign nations.

This technical report has been reviewed and is approved for publication.


Larry G. Kelly, Chief
Structural Concepts Branch
Structures Division


Richard L. Rolles, Project Engineer
Structural Concepts Branch
Structures Division

FOR THE COMMANDER


Frederick L. Dietrich, Colonel, USAF
Chief, Structures Division

"If your address has changed, if you wish to be removed from our mailing list, or if the addressee is no longer employed by your organization please notify AFWAL/FIBCB W-PAFB, OH 45433 to help us maintain a current mailing list".

Copies of this report should not be returned unless return is required by security considerations, contractual obligations, or notice on a specific document.

UNCLASSIFIED

SECURITY CLASSIFICATION OF THIS PAGE

REPORT DOCUMENTATION PAGE

1a. REPORT SECURITY CLASSIFICATION UNCLASSIFIED		1b. RESTRICTIVE MARKINGS													
2a. SECURITY CLASSIFICATION AUTHORITY		3. DISTRIBUTION/AVAILABILITY OF REPORT Approved for public release; distribution unlimited.													
2b. DECLASSIFICATION/DOWNGRADING SCHEDULE															
4. PERFORMING ORGANIZATION REPORT NUMBER(S) NOR 86-204		5. MONITORING ORGANIZATION REPORT NUMBER(S) AFWAL-TR-87-3008, Volume II													
6a. NAME OF PERFORMING ORGANIZATION NORTHROP CORPORATION Aircraft Division	6b. OFFICE SYMBOL (if applicable) AFWAL/FIBCB	7a. NAME OF MONITORING ORGANIZATION AIR FORCE WRIGHT AERONAUTICAL LABORATORIES Flight Dynamics Laboratory, AFWAL/FIBCB													
6c. ADDRESS (City, State and ZIP Code) One Northrop Avenue Hawthorne, California 90250		7b. ADDRESS (City, State and ZIP Code) Wright-Patterson AFB, Ohio 45433-6553													
8a. NAME OF FUNDING/SPONSORING ORGANIZATION Air Force Wright-Aeronautical Laboratories	8b. OFFICE SYMBOL (if applicable) AFWAL/FIBCB	9. PROCUREMENT INSTRUMENT IDENTIFICATION NUMBER F33615-81-C-3227													
8c. ADDRESS (City, State and ZIP Code) Wright-Patterson Air Force Base Ohio 45433-6553		10. SOURCE OF FUNDING NOS. <table border="1"><thead><tr><th>PROGRAM ELEMENT NO.</th><th>PROJECT NO.</th><th>TASK NO.</th><th>WORK UNIT NO.</th></tr></thead><tbody><tr><td>62201F</td><td>2401</td><td>03</td><td>56</td></tr></tbody></table>		PROGRAM ELEMENT NO.	PROJECT NO.	TASK NO.	WORK UNIT NO.	62201F	2401	03	56				
PROGRAM ELEMENT NO.	PROJECT NO.	TASK NO.	WORK UNIT NO.												
62201F	2401	03	56												
11. TITLE (Include Security Classification) SEE REVERSE SIDE															
12. PERSONAL AUTHOR(S) H. Zamani, S. P. Agrawal, and R. Vastava															
13a. TYPE OF REPORT FINAL	13b. TIME COVERED FROM 11/81 TO 07/86	14. DATE OF REPORT (Yr., Mo., Day) 1987 JULY	15. PAGE COUNT 254												
16. SUPPLEMENTARY NOTATION															
17. COSATI CODES <table border="1"><thead><tr><th>FIELD</th><th>GROUP</th><th>SUB. GR.</th></tr></thead><tbody><tr><td></td><td></td><td></td></tr><tr><td></td><td></td><td></td></tr><tr><td></td><td></td><td></td></tr></tbody></table>		FIELD	GROUP	SUB. GR.										18. SUBJECT TERMS (Continue on reverse if necessary and identify by block number)	
FIELD	GROUP	SUB. GR.													
19. ABSTRACT (Continue on reverse if necessary and identify by block number) This report contains the technical details of the work done on Contract F33615-81-C-3227, "Superplastic Formed Aluminum Airframe Structures." The scope of this program was to select, design, fabricate, evaluate and test superplastically formed (SPF) aluminum airframe parts. The program was conducted in the following five tasks: In Task I, several candidate structural components were evaluated for SPF production design and two parts, namely, Leading Edge Extension (LEX) and avionics deck compartment, showing the most benefits from SPF, were selected. Task II dealt with selection of a suitable alloy for fabrication of structural components. After a detailed evaluation, Reynold's aluminum alloy MD254 was selected for part fabrication. <i>(Signature)</i>															
20. DISTRIBUTION/AVAILABILITY OF ABSTRACT UNCLASSIFIED/UNLIMITED <input type="checkbox"/> SAME AS RPT. <input checked="" type="checkbox"/> DTIC USERS <input type="checkbox"/>		21. ABSTRACT SECURITY CLASSIFICATION UNCLASSIFIED													
22a. NAME OF RESPONSIBLE INDIVIDUAL R. ROLFES	22b. TELEPHONE NUMBER (Include Area Code) (513) 255-2521	22c. OFFICE SYMBOL AFWAL/FIBCB													

11. Superplastic Formed Aluminum Airframe Structures (Technical Details), Volume II

19. ABSTRACT (Continued)

In Task II, subcomponents, which represented the most severe forming areas of each component were fabricated and tested. The selected subcomponents represented the critical forming areas of the full-scale components.

Task IV involved fabricating and assembling the avionics deck. In addition, corrugations for the LEX were superplastically formed.

Part evaluation and structural verification were carried out in Task V. Structural verification involved static and fatigue tests of the avionics deck compartment.

The studies carried out in this program have shown that complex aluminum structural parts can be superplastically formed, resulting in substantial cost and weight savings.



Accession For	
NTIS CRA&I	<input checked="" type="checkbox"/>
DTIC TAB	<input checked="" type="checkbox"/>
Unannounced	<input type="checkbox"/>
Justification	
By	
Distribution /	
Availability Codes	
Dist	Avail and/or Special
A-1	

PREFACE

This report was prepared by the Northrop Corporation, Aircraft Division, Hawthorne, California, covering work done under the United States Air Force Contract F33615-81-C-3227 between November 1981 and July 1986. The contract was administered by the Wright Aeronautical Laboratories, Flight Dynamics Laboratory, Wright-Patterson Air Force Base, Ohio. Mr. J. Tuss was the AFWAL/FBCB Project Engineer from November 1981 to November 1985 and Mr. R. Rolfes from November 1985 to July 1986.

The work was performed in the Northrop Advanced Structural Concepts Department under the program management of Mr. L. Bernhardt from November 1981 to July 1984 and Dr. M. M. Ratwani from August 1984 to July 1986. Mr. H. Zamani was the Principal Investigator on this program. The following Northrop personnel were the major contributors to the program:

DESIGN:	L. Bernhardt & E. Youm
ANALYSIS:	H. Zamani & J. Spradley
MATERIALS EVALUATIONS:	S. P. Agrawal
FABRICATION OF SPF PARTS:	R. Vastava, J. Akana and J. Fabre
MANUFACTURING COORDINATION:	S. Cormany & J. Wilkes
DOCUMENTATION:	K. Gonzalez & K. Clayton

TABLE OF CONTENTS

<u>SECTION</u>	<u>PAGE</u>
1	INTRODUCTION.
	1
1.1	Background
	1
1.2	Objective.
	2
1.3	Approach
	3
2	PART SELECTION.
	5
2.1	Selection Criteria
	5
2.1.1	Cost and Weight Considerations.
	6
2.1.2	Manufacturing Considerations.
	8
2.2	Selected Components.
	9
2.2.1	Description of Components
	9
2.2.2	Manufacturing Plans
	18
2.2.2.1	Forward Avionics Deck.
	18
2.2.2.2	Nose Gear Wheel Door
	23
2.2.2.3	Trailing Edge Flap
	29
2.2.2.3.1	Spar Assembly
	31
2.2.2.3.2	Leading Edge Skin Assembly.
	31
2.2.2.3.3	Leading Edge Assembly
	33
2.2.2.3.4	Trailing Edge Skin Assembly
	33
2.2.2.3.5	Final Assembly.
	34
2.2.2.4	Wing Leading Edge Extension.
	36
2.3	Component Ranking.
	43
2.4	Final Selection.
	54
3	DESIGN AND ANALYSIS
	55
3.1	Preliminary Part Design.
	55
3.1.1	Forward Lower Avionics Deck
	55
3.1.2	Leading Edge Extension.
	56

TABLE OF CONTENTS (Continued)

<u>SECTION</u>	<u>PAGE</u>
3.2 Preliminary Analysis	58
3.3 Final Design	65
3.3.1 Forward Avionics Deck	65
3.4 Design Considerations.	80
3.5 Final Analysis	81
3.6 Tool Design.	91
4 MATERIAL EVALUATION AND SELECTION	93
4.1 Material Screening	93
4.1.1 Selection of Candidate Materials.	93
4.1.1.1 Characteristics of 7475 Alloy.	94
4.1.1.2 Characteristics of 7050 Alloy.	94
4.1.1.3 Characteristics of X7091 Alloy	95
4.1.2 Material Procurement.	95
4.1.3 Preliminary Material Evaluation	96
4.1.4 Post-SPF Microstructural Evaluation	112
4.2 Final Material Selection and Evaluation.	123
4.2.1 Material Evaluation	126
4.2.2 Microstructural evaluation.	132
4.2.3 Property Evaluation	135
4.2.3.1 Superplastic Forming of Pans	135
4.2.3.2 Post-SPF Evaluations	138
4.2.3.3 Post-SPF Material Properties	138
4.2.3.3.1 Tensile Tests	138
4.2.3.3.2 Notched Tensile Tests	141
4.2.3.3.3 Compression Tests	141
4.2.3.3.4 Bearing Tests	142
4.2.3.3.5 Shear Punch Tests	143
4.2.3.3.6 Fatigue Tests	145
4.2.3.3.7 Fatigue Crack Growth Tests.	147
4.2.3.3.8 Stress Corrosion Tests.	148
4.2.3.3.9 Exfoliation Corrosion Tests	149

TABLE OF CONTENTS (Continued)

<u>SECTION</u>		<u>PAGE</u>
	4.2.3.4 Secondary Processability Evaluations .	150
	4.2.3.4.1 Anodizing Test.	150
	4.2.3.4.2 Painting Test	150
	4.2.3.4.3 Chem Milling.	150
	4.2.3.4.4 Adhesive Bonding.	151
	4.2.3.4.5 Climbing Drum Peel Test . .	151
	4.2.3.4.6 Resistance Seam Welding . .	152
	4.2.3.4.7 Weldbonding	152
	4.2.4 Development of Forming Parameters	155
	4.3 Material Substitution to MD254	156
5	PRODUCIBILITY FORMING TESTS	165
	5.1 Producibility Subcomponent Selection	165
	5.1.1 Leading Edge Extension.	166
	5.1.2 Avionics Deck Lower Compartment	167
	5.2 Producibility Forming.	168
	5.2.1 LEX Producibility Subcomponent Forming.	168
	5.2.2 Avionics Deck Producibility Subcomponent Forming	170
	5.3 Subcomponent Modifications	170
	5.3.1 LEX Subcomponent Redesign	172
	5.3.2 Avionics Deck Subcomponent Redesign	172
6	PART AND TOOL FABRICATION	179
	6.1 Tool Fabrication	179
	6.1.1 Conventional Machining of LEX Corrugation Die .	179
	6.1.2 Numeric Control Data Generation	180
	6.1.3 Numeric Control Machining	182
	6.1.4 Numeric Tool Inspection	183

TABLE OF CONTENTS

<u>SECTION</u>	<u>PAGE</u>
6.2 Part Fabrication	188
6.2.1 IEX Corrugation Fabrication	189
6.2.2 Avionics Deck Upper Skin Fabrication.	189
6.2.3 Avionics Deck Lower Skin Fabrication.	198
6.2.4 Avionics Deck Waffle Pan Fabrication.	198
6.3 Avionics Deck Substructure Detail Fabrication.	206
7 ASSEMBLY AND TEST	213
7.1 Lower Avionics Deck Assembly	213
7.1.1 Preliminary Assembly.	213
7.1.2 Final Assembly.	215
7.2 Component Testing.	220
7.2.1 Test Load Generation.	221
7.2.2 Test Setup.	229
7.2.3 Instrumentation	229
7.2.4 Preliminary Static Testing.	231
7.2.5 Fatigue Testing	237
7.2.6 Residual Strength Testing	245
8 SUMMARY AND CONCLUSIONS	249
8.1 Summary.	249
8.2 Conclusions.	250
REFERENCES.	253

LIST OF ILLUSTRATIONS

<u>FIGURE</u>		<u>PAGE</u>
2-1	Baseline and Original SPF Avionics Deck	10
2-2	Baseline and SPF Nose Gear Wheel Door	12
2-3	Baseline and SPF Trailing Edge Flap	15
2-4	Baseline and Original SPF LEX	17
2-5	Cumulative Average Hours Comparison for Three Shipsets. . .	48
2-6	Cumulative Average Hours Comparison for 300 Shipsets. . . .	48
2-7	Direct Labor Hours Comparison (Avionics Deck)	49
2-8	Direct Labor Hours Comparison (Nose Gear Door).	49
2-9	Direct Labor Hours Comparison (Trailing Edge Flap).	50
2-10	Direct Labor Hours Comparison (Leading Edge Extension . . .	50
3-1	Modified Avionics Deck SPF Design	57
3-2	One-Piece Skin SPF LEX Design	59
3-3	Two-Piece Skin SPF LEX Design	60
3-4	SPF Avionics Deck NASTRAN Model	62
3-5	SPF Leading Edge Extension NASTRAN Model.	63
3-6	Leading Edge Extension Corrugation Thicknesses Variations .	64
3-7	Leading Edge Extension Cross Sectional Pressure Loading . .	66
3-8	Final Avionics Deck SPF Design.	67
3-9	Avionics Deck Waffle Pan Redesign	68
3-10	Avionics Deck Waffle Pan Flange Modifications	70
3-11	Avionics Deck Upper Skin Design	71
3-12	Avionics Deck Lower Skin Design.	73

LIST OF ILLUSTRATIONS (Continued)

<u>FIGURE</u>		<u>PAGE</u>
3-13	Avionics Deck Waffle Pan Design	75
3-14	Avionics Deck Assembly.	77
3-15	Modified Leading Edge Extension SPF Design.	79
3-16	Superimposed Plot of the Deformed and Undeformed Avionics Deck.	83
3-17	Comparison of Avionics Deck Waffle Pan Sections With Different Draft Angles	85
3-18	High Stress Element Locations (LEX)	87
3-19	LEX Major Principal Stresses (Ksi).	88
3-20	LEX Upper Skin Chordwise Stresses (Ksi)	89
3-21	LEX Upper Skin Spanwise Stresses (Ksi).	90
4-1	As Received Microstructure of SPF Aluminum Alloy Sheet 7475-I (0.125-Inch Thickness)	99
4-2	As Received Microstructure of SPF Aluminum Alloy Sheet 7050-I (0.125-Inch Thickness)	100
4-3	As Received microstructure of SPF Aluminum Alloy Sheet X7091-I (0.125-Inch Thickness).	101
4-4	Plots of Log Flow Stress Versus Log True Strain Rate for 7475-II Material at Various Temperatures.	105
4-5	Plots of Log Flow Stress Versus Log True Strain Rate for 7050-II Material at Various Temperatures.	106
4-6	Plots of Log Flow Stress Versus Log True Strain Rate for P/M X7091-III and X7091-IV Materials at 970°F Temperature	107
4-7	Plots of Strain-Rate Sensitivity (m) Versus Log True Strain Rate for 7475-II Material at Various Temperatures	108
4-8	Plots of Strain-Rate Sensitivity (m) Versus Log True Strain Rate for 7050-II Material at Various Temperatures	109
4-9	Plots of Strain-Rate Sensitivity (m) Versus Log True Strain Rate for P/M X7091-III and X7091-IV Materials at 970°F Temperature	110

LIST OF ILLUSTRATIONS (Continued)

<u>FIGURE</u>		<u>PAGE</u>
4-10	Microstructure of a 7475 Alloy Cone Specimen (ID 7475-II-P7, Cone 4) at Various Strain Locations, Initial Sheet Thickness 0.090 Inch, Test Temperature 970°F	117
4-11	Effect of Strain on cavitation During Superplastic Deformation of 7475 Alloy Sheet, 7475-II (0.090-Inch Thickness), at Various Temperatures and Strain Rates.	122
4-12	Effect of SPF Strain on Grain Size (A) in a 7475 Alloy Sheet, 7475-II (0.090-Inch Thickness), at Various Temperatures	124
4-13	Effect of SPF Strain on Grain Size (b) in a 7475 Alloy Sheet, 7475-II (0.090-Inch Thickness), at Various Temperatures	125
4-14	Log Flow Stress Versus Log True Strain Rate Plot for the Laboratory and Mill Produced 7475 Aluminum Alloy Sheets (Gauge Thickness 0.125 Inch).	130
4-15	Log Flow Stress Versus Log True Strain Rate Plot for the Laboratory and Mill Produced 7475 Aluminum Alloy Sheets (Gauge Thickness 0.090 Inch).	131
4-16	Microstructure of the Mill Produced SPF Aluminum Alloy Sheet M7475-I (0.125-Inch Thickness).	133
4-17	Microstructure of the Mill Produced SPF Aluminum Alloy Sheet M7475-II (0.090-Inch Thickness)	134
4-18	Pressure-Time Profiles (Forming Cycles) Used for Fabricating SPF Pans of Three Geometries.	137
4-19	SPF Pans of Aluminum Alloy 7475 With Varying Severity of Forming	137
4-20	Effect of SPF Strain on 7475-T6 Tensile Properties.	140
4-21	Effect of SPF Strain on 7475-T6 Notched Tensile Properties.	141
4-22	Effect of SPF Strain on 7475-T6 Compression Yield Strength.	142
4-23	Effect of SPF Strain on 7475-T6 Bearing Strength.	143
4-24	Effect of SPF Strain on 7475-T6 Shear Punch Strength.	144
4-25	Results of Smooth Fatigue Test on Post-SPF 7475-T6 Sheets	145

LIST OF ILLUSTRATIONS (Continued)

<u>FIGURE</u>		<u>PAGE</u>
4-26	Fatigue Crack Growth Rate of Post-SPF 7475-T6 Specimens in Laboratory Air.	147
4-27	Effect of SPF Strain on 7475-T6 Stress Corrosion Resistance	148
4-28	Climbing Drum Peel Test Specimen.	151
4-29	Weldbond Lap Shear Test Specimen.	153
4-30	Forming Cycle for SPF Pans.	158
4-31	Three Dimensional Microstructure of an As Received 0.090 Inch Thick Sheet of MD254	159
4-32	Microstructure Across the Thickness of an As Received 0.090 Inch Thick Sheet of MD254 Aluminum Alloy.	160
4-33	Variation of Percentage Elongation at Fracture With Strain Rate.	164
5-1	Original LEX Producibility Subcomponent	166
5-2	Original Avionics Deck Producibility Subcomponent	167
5-3	Avionics Deck Producibility Subcomponent Die.	168
5-4	LEX Subcomponent Cross Sectional View	169
5-5	Cavitation Measurements for LEX Subcomponent.	171
5-6	Modified LEX Producibility Subcomponent	172
5-7	Modified Avionics Deck Waffle Pan	173
5-8	Modified Avionics Deck Subcomponent Die	173
5-9	Modified Avionics Deck Producibility Subcomponent	174
5-10	Avionics Deck Producibility Subcomponent Microstructure . .	175
5-11	Cavitation Measurements for Avionics Deck Subcomponent. . .	177
6-1	LEX Corrugation Die	180
6-2	Avionics Deck Lower Skin Die.	184

LIST OF ILLUSTRATIONS (Continued)

<u>FIGURE</u>		<u>PAGE</u>
6-3	Avionics Deck Upper Skin Die.	185
6-4	Avionics Deck Waffle Pan Die.	186
6-5	Forming Cycle for IEX Corrugation	190
6-6	Superplastically Formed IEX Corrugations.	191
6-7	SPF IEX Corrugation Microstructure.	193
6-8	Forming cycle for Superplastic Forming of Avionics Deck Upper Skin.	196
6-9	Superplastically Formed Upper Skin Parts.	197
6-10	SPF Avionics Deck Upper Skin Microstructure	195
6-11	Forming Cycle for Superplastic Forming of Avionics Deck Lower Skin.	199
6-12	Superplastically Formed Lower Skin Parts.	200
6-13	Avionics Deck Lower Skin Microstructure	201
6-14	Forming Cycle for SPF of Waffle Pan	202
6-15	Avionics Deck Superplastically Formed Waffle Pan.	203
6-16	Waffle Pan Thicknesses Before Trimming.	204
6-17	Waffle Pan Thicknesses After Trimming	205
6-18	Avionics Deck Waffle Pan After Final Trimming	207
6-19	SPF Avionics Deck Waffle Pan Microstructure	209
7-1	Upper View of Assembled Deck Prior to Door Installation . .	217
7-2	Lower View of Assembled Deck Prior to Door Installation . .	218
7-3	Lower View of Assembled Deck After Door Installations . . .	219
7-4	F-5F Avionics Compartment Bending Moments (Cond. SAB13010, Symmetrical Pull-Up).	222

LIST OF ILLUSTRATIONS (Continued)

<u>FIGURE</u>		<u>PAGE</u>
7-5	F-5F Avionics Compartment Shear Loads (Cond. SAB13010, Symmetrical Pull-Up)	223
7-6	Avionics Deck Test Setup and Loading.	227
7-7	Avionics Deck Actual Test Setup	230
7-8	Location of Avionics Deck Internal Strain Gages	232
7-9	Locations of Avionics Deck External Strain Gages.	233
7-10	Avionics Deck Strain Survey Loading	235
7-11	Typical Block Designed for Constant Amplitude Fatigue Loading	239
7-12	Typical Fatigue Cycle Loading Versus Time	241
7-13	Initial Static Loading Versus Fatigue Loading Strain Response (Strain Gage No. 15, Lower Skin)	242
7-14	Initial Static Loading Versus Fatigue Loading Strain Response (Strain Gage No. 3A, Upper Skin)	243
7-15	Initial Static Loading Versus Fatigue Loading Strain Response (Strain Gage No. 26A, Waffle Pan).	244
7-16	Avionics Deck Left Hand and Right Hand Deflections for Residual Strength Testing	246

LIST OF TABLES

<u>TABLE</u>		<u>PAGE</u>
2-1	Three Shipset Hours Estimates.	44
2-2	300 Shipset Hours Estimates.	45
2-3	Variances and Slopes for Three Shipsets	47
2-4	Variances and Slopes for 300 Shipsets	47
2-5	Component Fastener Count Reduction.	51
2-6	Component Piece Count Reduction	51
2-7	Component Rating Chart.	52
3-1	LEX Maximum Major Principal Stresses.	86
4-1	Material Grain Geometry (As Received Condition)	102
4-2	List of Peak σ Values and Maximum Elongations in 7475, 7050 and P/M X7091 Alloys.	104
4-3	List of 7475 Cone Test Specimens Selected for Metallo- graphic Evaluation.	113
4-4	List of 7050 and P/M 7091 Cone Test Specimens Selected for Metallographic Evaluation	114
4-5	Forming Data for 7475 Aluminum Alloy Sheets	119
4-6	Task II - Test Matrix to Determine Post-SPF Properties of Selected Material	127
4-7	Task II - Evaluation of Secondary Processing.	128
4-8	Results of Room Temperature Tensile Tests on Mill-Produced SPF 7475 Aluminum Alloy Sheets (in T6 Condition) and the Conventionally Produced 7075-T6 Sheet	136
4-9	Test Matrix Used for Evaluation of Post-SPF Properties of a Fine Grain SPF 7475 Aluminum Alloy.	139
4-10	48-Hour Exco Ratings of Post-SPF 7475-T6 and Control Samples	149
4-11	Climbing Drum Peel Test Results	152

LIST OF TABLES (Continued)

<u>TABLE</u>		<u>PAGE</u>
4-12	Lap Shear Strength of Weldbonded Specimens in Cured Condi- tion.	153
4-13	Results of Secondary Processability Evaluation of Post-SPF 7475 Sheet.	154
4-14	Forming Condition for SPF Pans.	157
4-15	Room Temperature Tensile Tests on the Mill Produced SPF MD254 Aluminum and Conventionally Produced 7075-T6 Aluminum	161
4-16	Effect of SPF Strain on Cavitation in MD254 Alloy	162
5-1	Thickness Measurements for LEX Subcomponent	169
7-1	F-5F Avionics Compartment Loads	224
7-2	Avionics Deck Bending and Axial Loads (Condition SAB13010).	225
7-3	Strain Survey Testing, Maximum and Minimum Strain Values.	236
7-4	Strain Survey Testing, Maximum and Minimum Principal Stresses.	234
7-5	Avionics Deck Fatigue Loading Schedule.	238
7-6	Residual Strength Testing, Maximum and Minimum Strain Values	247
7-7	Residual Strength Testing, Maximum and Minimum Principal Stresses.	248
8-1	SPF Avionics Deck Design Benefits	252

1. INTRODUCTION

Superplasticity is a unique property exhibited by certain alloys having a characteristic microstructure which allows large uniform elongations without fracture when subjected to appropriate temperature and forming strain rates. The high elongations associated with the superplastic forming (SPF) process allow the design and fabrication of complex structures otherwise not possible with conventional methods. As a consequence the SPF process results in close tolerance parts with reduced piece count. This in turn, results in a reduction of machining and labor intensive assembly costs. In addition, a subsequent cost saving potential emerges since the reduced piece count is associated with reduced assembly details in the manufacturing area.

The bulk of superplastic forming work to date has concentrated on titanium. Until recently, the exploration of SPF aluminum has been rather limited. Superplastic forming of titanium has demonstrated significant cost, weight, and performance improvements for selected structural airframe parts. This program has exploited applications of SPF aluminum which developed and demonstrated the process as a viable means of producing structural airframe parts that are more efficient and cost effective than conventionally produced parts.

1.1 BACKGROUND

The feasibility to scale up the superplastic forming of aluminum to produce full scale structural parts was successfully demonstrated on Air Force Contract No. F33615-80-C-3240. During that program, the cost and weight savings along with the quality of the produced parts demonstrated the valuable potential of the SPF aluminum process. The ground work for that program was

accomplished under Air Force Contract No. F33615-79-C-3218, which demonstrated that high strength aluminum alloys, such as 7075 and 7475, were capable of being superplastically formed once their wrought forms had undergone a grain refinement. We achieved the grain refinement through a thermomechanical treatment (TMT) process which produced grain sizes in the $9\text{ }\mu\text{m}$ to $15\text{ }\mu\text{m}$ range. These fine grain sizes enabled the material to undergo tensile elongations near 400 percent in the 850°F to 900°F range. Other aluminum alloys, including powder alloys also have the potential to provide valuable cost and weight savings through superplastic forming.

1.2 OBJECTIVE

The overall objective of this program was to identify the best of three aluminum alloys, capable of superplastic formability, and two aircraft structural components where application of the SPF aluminum process would offer the maximum cost and weight savings potential. The program was divided into a five-task program; Part Selection and Design (Task I); Material Evaluation and Selection (Task II); Producibility Forming Tests (Task III); Part Fabrication (Task IV); and Part Evaluation and Structural Verification (Task V).

The objective of the first task was to select and design, from a number of Northrop F-5E/F aircraft structural assemblies, two components that most fully utilized the unique capabilities of SPF aluminum to provide significant cost and weight savings. The objective of the second task was to evaluate and select an aluminum alloy which represented the best combination of superplastic formability and post SPF mechanical properties. The third task's objective was to assure the forming feasibility of the components selected in Task I. The objective of the fourth task was to fabricate complete structural components using the SPF technology, and the objective of the fifth

task was to evaluate and verify the structural integrity of the SPF components through structural testing.

1.3 APPROACH

In Task I, design/producibility trade studies were conducted on several structural components from the Northrop F-5E/F aircraft to identify candidate SPF parts. The components were then rated against different factors such as recurring and non-recurring cost, weight impact on technology, forming risk, and assembly risk. Two components that rated the highest were selected, and their preliminary SPF designs were developed. The second task was conducted in two phases: (1) a preliminary evaluation of three candidate alloys representing the best combination of superplasticity and post SPF mechanical properties, followed by (2) an extensive evaluation of the final selected alloy. During the third task, the areas representing the most severe deformation on each component were fabricated in order to assess the forming feasibility of those areas. Tensile and fatigue tests on coupons excised from these critical areas were performed, and the microstructure of these areas was examined for cavitation. The fourth task involved the fabrication of the SPF parts for two components and the complete assembly of one component. The final task of the program consisted of a test plan development and verification of the structural integrity of the test component.

2. PART SELECTION

During this initial portion of the program, several structural components were selected and designed for superplastic forming. These parts were selected with an emphasis to provide significant cost and weight savings. Since the obvious areas of potential payoff for SPF parts are applications where labor-intensive subassemblies and extensive machining could be eliminated, the candidate components were selected so their SPF design would offer such a potential. The selected parts were designed as replacements for components of an existing baseline flight vehicle. This would provide the opportunity for cost and weight trade studies against existing baseline components. The Northrop F-5E/F aircraft was chosen as the baseline aircraft because it was the latest production version of Northrop aircraft, and it has a structure typical of air superiority fighters. The F-5E/F fuselage was of conventional frame and longeron construction, and secondary structures such as doors and fairings were a combination of waffle pans or honeycomb construction. Therefore, any structural component selected from F-5E/F would be an excellent generic example of a fighter aircraft structure. A spectrum of candidate parts representing both primary and secondary structures were considered to fulfill the objectives of this task. Once the candidate components were selected, they were redesigned as SPF assemblies. Layouts were prepared in sufficient detail to allow manufacturing plans to be generated and cost analyses to be completed. The design concepts for all SPF parts utilized the unique forming capabilities and configurations most readily achievable through the superplastic forming process.

2.1 SELECTION CRITERIA

During the selection of the candidate components, certain criteria were taken into consideration. Since the most

promising benefit of the SPF process was the cost saving associated with reduced piece count, the selection of the candidate components emphasized reduction of piece count. The manufacturing considerations also played an important role in order to take the most advantage from the close tolerances associated with the SPF part. Manufacturing plans were developed and used for cost analyses which later proved to be one of the governing factors in selection of the final components. Two other limiting factors considered in selection of the candidate components were the available raw stock size and press platten capacity. Arrangements were made with Reynolds aluminum to roll sheets with a maximum width of 36 inches as per Northrop specifications. Northrop's largest available heated platten press has a platten size of 36 by 60 inches. These factors defined the upper component size limits for the proposed program. Some of the other criteria considered during the selection of the final components were: the impact of the produced parts on SPF technology, the risk associated with forming of those parts and the risk associated with the final assembly to establish a thorough rating of the components based on criteria other than cost and weight.

2.1.1 Cost and Weight Considerations

As discussed earlier, establishment of cost data on the candidate components was the most emphasized criteria. Prior to generating the cost data, layouts of several components were prepared in sufficient details to allow the generation of manufacturing plans for the purpose of cost analyses. The objective of these cost activities was to provide cost profiles of the conceptual SPF aluminum candidate parts. A combination of two basic cost estimating methods at Northrop (detail and parametric estimating) was used to estimate the recurring production costs of the candidate parts. Once the cost figures were established, they were used in a rating matrix for the selection of the final SPF parts. This objective was accomplished by the performance of the following activities:

- (1) Estimation of standard fabrication and assembly selected.
- (2) Projection of the standard hours into production cost estimates for different production units.
- (3) Comparison of the production costs of the SPF parts with the respective existing baselines.

Working from detailed drawings and manufacturing plans, the detailed estimating method was used in setting time standards. This estimating technique employed time standards which were the result of time and motion studies and were incorporated into Northrop's Industrial Engineering Time Standards Book. Time standards were developed for those new and technically advanced processes where standards did not exist in the time standards book.

Time standards only accounted for the basic work content of operations and processes and did not allow for fatigue, delays or other variances that occur in the actual production environment. These variances were accounted for by the application of variance factors. These factors were taken from the cost history of a similar or related family of operations tracked and documented in the past.

The standards were then projected into production hours for the selected number of units using the appropriate learning curves which, similar to the variance factors, were based on history. The projected factory hours were then accounted and converted to factory labor costs using typical factory rates. Support labor hours were estimated based on an established direct/support factory labor estimating relationship. Basic material requirements were estimated from the detailed drawings and priced out. Allocated material was estimated as a percentage of the direct labor dollars. Assumed, but typical, burden rates and

factors were applied to the cost elements to estimate the total production costs at constant 1981 dollars. Costs were projected for the 1st, 30th, 500th and 1000th cumulative averages in order to determine the initial, near-term and long-term cost benefits of SPF aluminum parts over baseline parts. The detailed cost estimates are presented in Section 2.3.

Weight considerations were probably the second most important factor in selection of the candidate parts. Weights for the SPF design of the components were determined from the detailed drawings and the material requirements. Since the superplastic forming process involves forming of sheet material, the initial sheet material requirements were used to estimate the weight of the selected components. The baseline weights were available from previous weight data. Comparison of the baseline versus the SPF design weights provided a reasonable estimate of the potential weight savings.

2.1.2 Manufacturing Considerations

The manufacturing considerations in developing the manufacturing plans had a substantial contribution towards the generation of the cost and weight estimates. Both cost and weight estimates were prepared working from detailed drawings and manufacturing plans. In case of all candidate components, a full set of production manufacturing plans were provided. Subassemblies, were identified where necessary. Fabrication flow charts and tool lists were also generated. These plans always reflected a true production environment so that a realistic cost analysis would be possible. These preliminary manufacturing plans were also used to establish the assembly risk portion of the rating criteria. The manufacturing plans for all candidate components were carefully reviewed to assess the degree of difficulty associated with the assembly of each SPF design. Additionally, the plans provided an opportunity to assess the feasibility of using

any advanced joining techniques such as weldbonding and/or adhesive/rivetbonding. Detailed manufacturing plans for each candidate component is presented in Section 2.2.

2.2 SELECTED COMPONENTS

Based on the preliminary selection criteria discussed earlier, the following F-5E/F components were selected as candidates for SPF designs:

- (a) Forward Avionics Deck
- (b) Nose Gear Wheel Door
- (c) Trailing Edge Flap
- (d) Wing Leading Edge Extension

2.2.1 Description of Components

The following paragraphs describe the baseline and the SPF design of each component in detail:

Concept 1 - Forward Avionics Deck

As shown in Figure 2-1, the original assembly was comprised of a six-part split-level deck which was supported by eight frame segments and six beam segments, with their adjacent shear webs joined by separate shear clips. This structure was bounded by two machined bulkheads and left and right-hand long-rons which joined the deck to the outer skin providing lands for the avionics compartment access door. The parts count breakdown was as follows: 21 stretch-formed extrusions, 39 hydroformed sheet metal details, 2 flat sheet decks, and 1 stretch-formed outer skin, totalling 63 details in all.

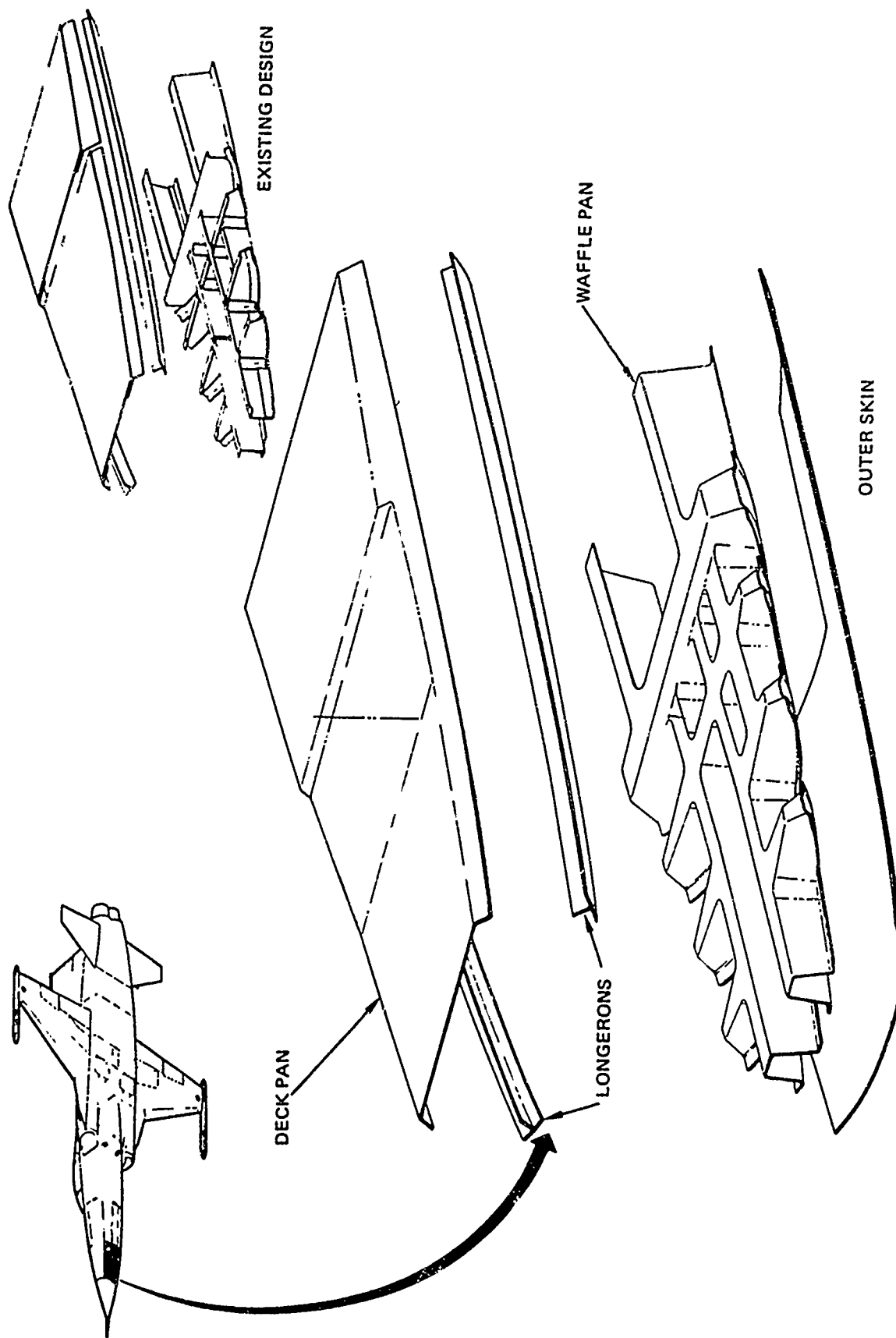


Figure 2-1. Baseline and Original SPF Avionics Deck

The original SPF assembly (Figure 2-1) was designed around five pieces, two of which were common to the original design. All of the substructure was combined into one waffled pan and upper deck skin was a one-piece pan. The outer skin was to be superplastically formed in a two-piece thermoform die. A waffle pattern insert and outer skin shim were added to the die so the waffle pan could be formed. Additional inserts and waffle pan shims were then added to the die so the inner deck pan could be formed. Multiple sheets were to be formed on both the waffle pan and inner skin to provide required doublers where necessary. All the parts were thus formed in one segmented die assuring proper fitup for the subsequent assemblies.

For the final assembly, the trimmed waffle pan and the existing longerons with adhesive applied to all faying surfaces were mated to the outer skin and clamped in place. This assembly was spot welded and oven cured. The inner skin would be adhesively bonded to the subassembly to complete the process. The manufacturing plans for the avionics deck is described in Section 2.2.2. The design modifications subsequent to this original SPF design are discussed in detail in Section 3.2.

Concept 2 - Nose Gear Wheel Door

The original baseline design was a simple honeycomb stiffened pre-warped door, supported on two hinges and articulated by an actuator attached to the left-hand forward corner (see Figure 2-2). The original design was complicated by a cooling air outlet vent located in the center of the door.

The SPF design (Figure 2-2) substituted a waffle pan for the honeycomb core and integrated several vent pieces into the door skin and inner pan. The previously separate louver details became integral features of the skins and pan. Only two angles and a louver cutout aft the edge fairing remained as separate details, which were required to maintain structural continuity between the inner skin pan and the outer skin.

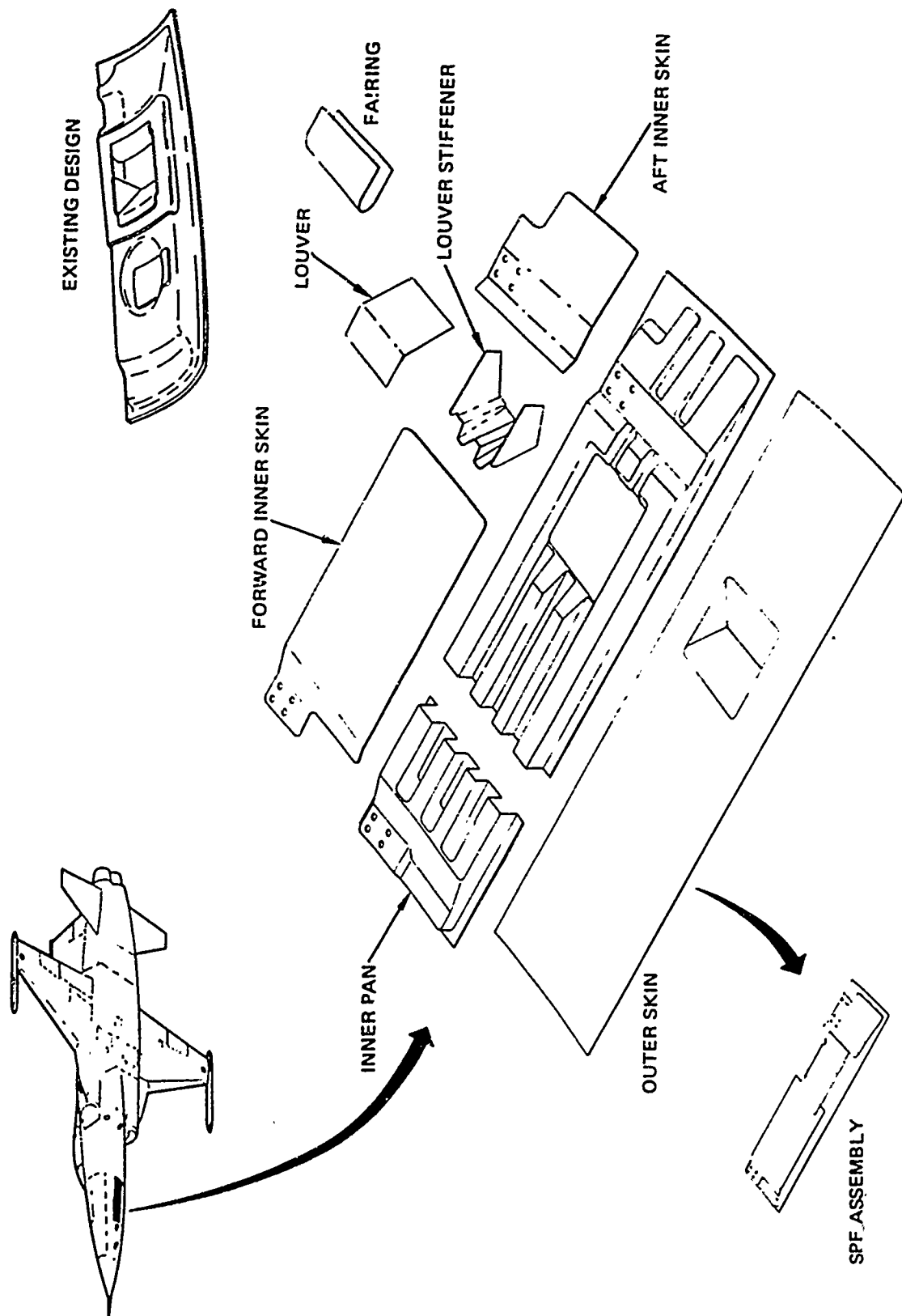


Figure 2-2. Baseline and SPF Nose Gear Wheel Door

Both the outer skin and the ribbed stiffening pan would be superplastically formed. The outer skin could be conventionally formed were it not for the portion of the air inlet duct incorporated into it. The louver stiffener would also be superplastically formed. The three doublers, the fairing, and the louver inner surface were to be formed conventionally. There were two machined aluminum back up ribs at the hinge locations which provided hinge support and transverse stiffness. Pilot holes would be drilled in these ribs and through both the outer skin and stiffening pan.

The SPF door was to be assembled in the following fashion. Adhesive would be applied to the outer skin, stiffening pan, and louver stiffener. The stiffening pan would be positioned on the outer skin using the pilot holes. The louver stiffener would be then positioned in the louver depression and clamped in place. The assembly would be then tack spot welded around the outer edge, at the depths of the stiffening pan ribbing and in the louver area. After oven cure, the doublers would be bonded in place and the fairing installed with blind rivets. This would complete the fabrication steps unique to the new design. All successive steps (e.g., door trim, hinge and name plate installation) would be common to both designs. The detailed Nose Gear Wheel Door manufacturing plans are described in Section 2.2.2.

Concept 3 - Trailing Edge Flap

The original design of the trailing edge flap consisted of ten two-piece ribs approximately equally spaced along a main spar at the 77 percent chord plane with leading and trailing edge spars as a closeout member for the separate bonded honeycomb trailing edge assembly. The two inboard most ribs were actually double ribs, strengthened to accept the concentrated loads introduced by the inboard hinge and actuator fittings. The outboard hinge support rib was a machined fitting. These last three

fittings would be common to both designs and their detail of costs were not included in the concepts, however, since they had to be installed before the flap assembly was complete, their assembly costs were included in the study results. Figure 2-3 contrasts the existing design with the SPF alternative.

The SPF design would substitute hat stiffened pans for all the intermediate ribs. Each trailing edge pan and skin would be symmetrical about the chord plane and could be used unchanged on the opposite hand flap. The two ribs at wing station (W.S.) 41.17 and 36.57 CANT would be similar to the existing ribs, which were extended at the trailing edge in an area formerly occupied by full depth honeycomb core. The outboard closing rib would be similar to the existing part but SPF formed and extended to the trailing edge. The forward rib at W.S. 74.75 would be unchanged from the original design as this was a machined fitting incorporating the outboard flap hinge.

The design approach investigated in the SPF design was basically the trading off of skin stiffening versus rib count and spacing. Every other rib was eliminated when spanwise beads were added as alternative skin stiffening. At the trailing edge, the stiffener pattern was designed as a waffle pattern and replaced the separate honeycomb bonded assembly of the original design. The spanwise skin stiffening eliminated the need for the forward spar. All the remaining ribs would be superplastically formed, eliminating the need for shear clips.

The outer skin pan combinations were contemplated as weldbonded assemblies. However, if the research efforts in welded two and three sheet panels were successful, the outer skins and stiffening would be formed similar to titanium SPF/DB two sheet panels.

The flap extended spanwise from the fuselage moldline to the inboard edge of the aileron and chordwise from the 70

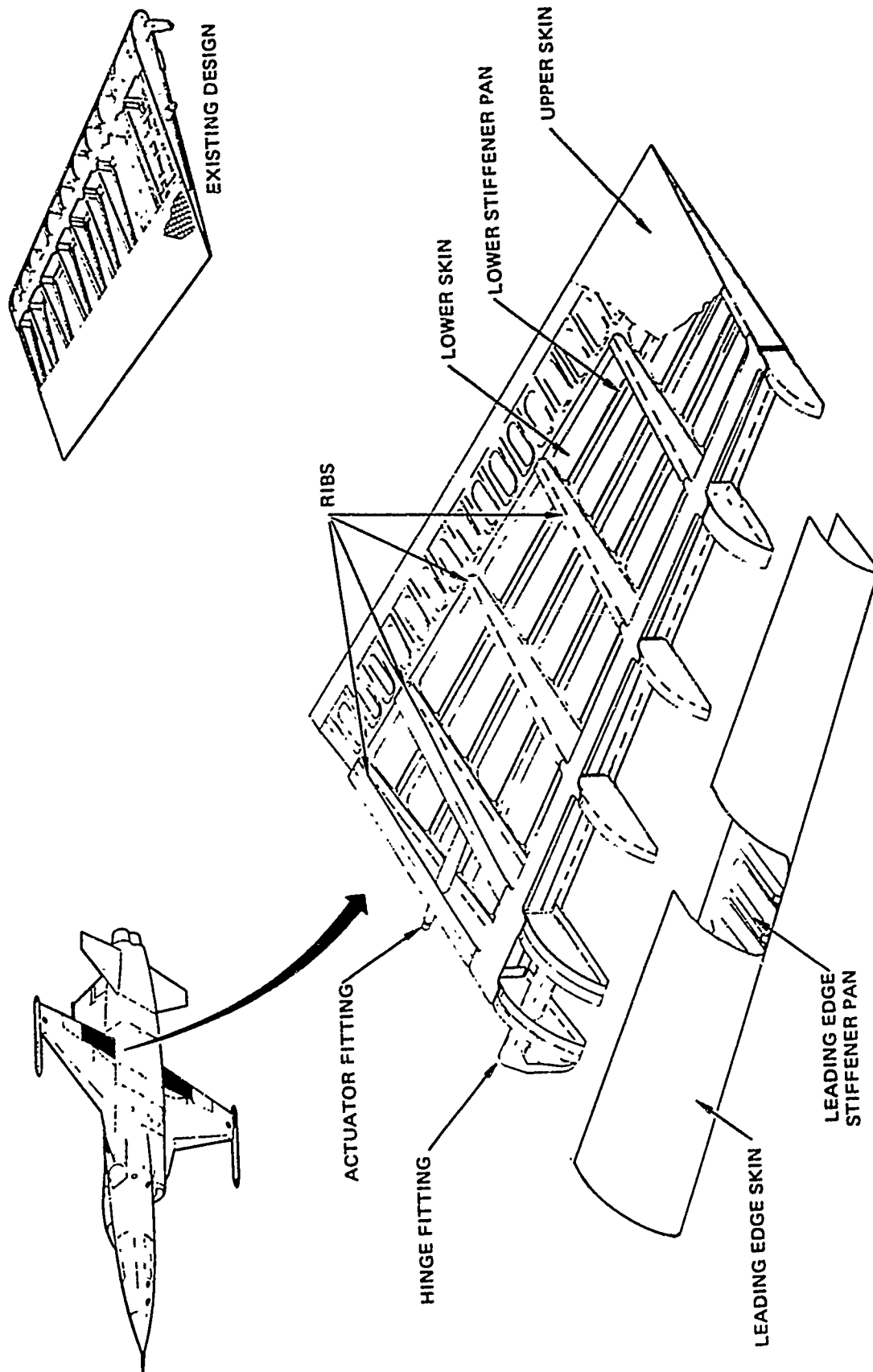


Figure 2-3. Baseline and SPF Trailing Edge Flap

percent wing chord to the trailing edge. The hinge line, along the 73.9 percent chord, was below the wing moldline. The inboard hinge would be supported by the fuselage and the outboard hinge by the wing rib at W.S. 74.75. The outboard hinge would be pinned to avoid inducing loads into the flap due to wing deflection. The flap, a conventional rib spar type, would be positioned by a fuselage mounted actuator operating a link attached to the actuator fitting. Air loads would be transferred to the ribs, carried forward to the main spar and then beamed out to the support points at the inboard hinge and at W.S. 74.75.

A variant of the illustrated design was also considered. This design incorporated symmetrical, about the chord plane, waffle pans with the corrugations running fore and aft in lieu of the spanwise stiffeners and ribs. These waffle pans were to be weldbonded to their respective skins and bonded together on final assembly. The leading edge remained unchanged.

Concept 4 - Wing Leading Edge Extension

The original leading edge extension (LEX) was of conventional rib and spar construction, containing four machined ribs, three machined spars, a machined leading edge insert, ten sheet metal rib and spar segments, a wing attach fitting and a one-piece skin (Figure 2-4). Two access panels were located on the under surface to provide access to the leading edge flap actuating edge spar, except for a shear pin at the fuselage station 299 bulkhead. The SPF design shown in Figure 2-4 replaced the internal ribs and spars with truss type corrugations running fore and aft, which reduced the piece count by five. Prior to making the decision to design the entire LEX, trade studies were conducted to determine if the entire LEX would be modified or the portion from the shear pin forward.

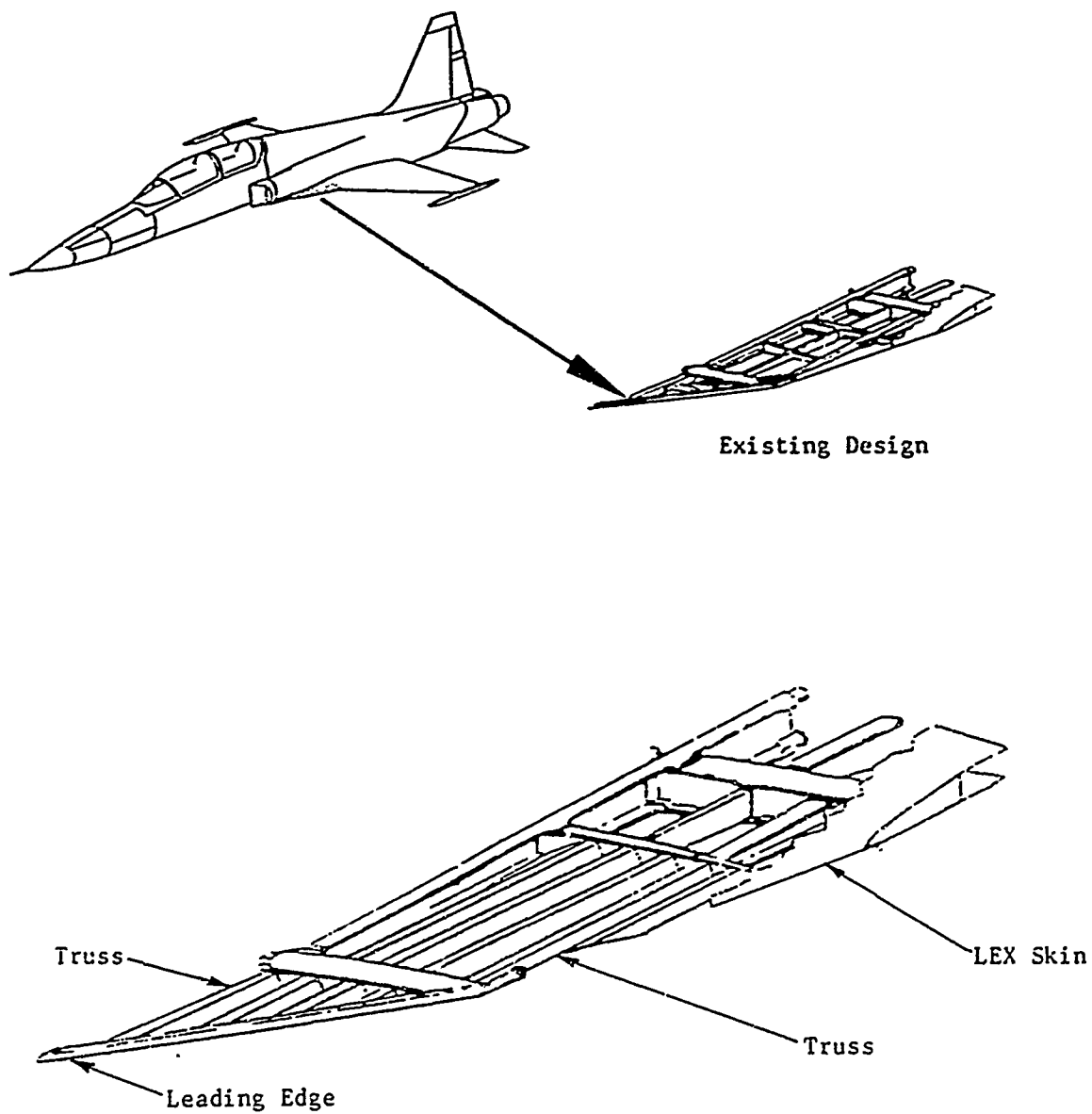


Figure 2-4. Baseline and Original SPF LEX

2.2.2 Manufacturing Plans

The following paragraphs describe the original manufacturing plans for each of the candidate components. These detailed manufacturing plans, as discussed earlier, were used to arrive at cost data for each of the components.

2.2.2.1 Forward Avionics Deck

The lower deck itself was of aluminum construction. It extended from Fuselage Station (F.S.) 47.50 aft to F.S. 87.50 and from the centerline of the airplane outboard to the lower longeron reference plane. The lower skin of the deck matched the lower moldline of the forward fuselage. The deck pan sat approximately four inches above the lower moldline at the centerline with a 0.75-inch joggle at F.S. 68.50.

The proposed SPF configuration consisted of the following superplastic-formed details:

- (1) Outer Skin
- (2) Waffle Pan
- (3) Inner Skin
- (4) L.H. and R.H. Bathtubs
- (5) L.H. and R.H. Channels
- (6) Z-stiffener at F.S. 68.50
- (7) Outboard Stiffener

The stiffeners, bathtubs, and channels provided the structural integrity required for continuity between the outer skin and the inner skin. The function of the existing lower longerons was performed by the bonded assembly of the outer skin, waffle pan and inner skin along the entire outboard edge on both sides of the lower deck.

The following is a detailed operational sequence for the fabrication and assembly of the above noted details:

Outer Skin, Waffle, and Deck Pan. Each detail was of 7475 fine grained aluminum alloy furnished by Reynolds. The outer skin was superplastically formed in a hot form die (SHFD) which consisted of a common two-piece cage with upper and lower cavities and removable inserts. The insert for the outer skin was tape cut to the outer moldline (OML) of the fuselage lower skin. The insert for the waffle was tape cut to the inner moldline (IML) of the fuselage lower skin and lower moldline of the inner skin. The insert for the inner skin was tape cut to the upper surface of the waffle.

Channels, Stiffeners and Bathtubs. These details were of the same material as the outer skin, waffle and inner skin and manufactured in the same manner. The SHFD used to fabricate these details contained a common upper and lower cavity with removable inserts. This allowed superplastic forming of one or more details at a time.

Each detail was of 7475 fine grained aluminum alloy sheet furnished by Reynolds. The production blank was cut to size, degreased, alkaline cleaned, given a uniform spray coat of forming lubricant and then air-dried. The SHFD had all foreign particles removed from the interior surfaces of the tool. The tool was then closed, with pressure applied on peripheral seals before the tool heat-up started.

After the tool was stabilized at operating temperature, it was opened and the production blank installed. The tool was then closed and the press loads applied to provide peripheral seal loads. Air pressure was maintained in the upper and lower tool cavities until all areas of the tool were within the forming temperature range. Air pressure was then increased in the upper cavity, and pressure maintained in the lower cavity during the

forming cycle. At the end of the forming cycle, the upper and lower cavities were vented to the atmosphere. The pressure load was then removed, the tool opened and the part removed. The details were heat-treated, placed in a trim fixture, routed net, wrapped and stored for use on the next assembly.

Weldbond Assembly. The first-stage details consisted of the outer skin, channels, bathtubs and stiffeners. They were processed for weldbond as follows:

The parts were vapor degreased, alkaline cleaned by immersing the parts in a non-silicated alkaline solution at 120 to 165°F for 12 to 15 minutes. They were then spray rinsed with deionized water for 5 to 6 minutes and inspected for a water-break-free surface. After inspection, the details were deoxidized by immersing in an agitated deoxidizer solution at 50 to 80°F for 6 to 8 minutes and spray rinsed with ambient temperature deionized water for 5 to 7 minutes. They were then immediately immersed in an anodized solution at 70 to 80°F for 18 to 22 minutes within the required voltage range, spray rinsed again with deionized water for 5 to 7 minutes and oven-dried in a recirculation air oven at 150 to 160°F for 30 to 60 minutes. The cleaned and anodized parts were handled with clean, cotton gloves and maintained in a clean room atmosphere until the weldbond adhesive was applied.

After anodizing, the parts were given a special surface treatment prime. The paste adhesive, warmed to room temperature, was applied to the faying surface of the details common to the outer skin within 120 hours from the time they were anodized. This would allow the film thickness to achieve a final glue line thickness of 0.005 to 0.012 inch. The outer skin was positioned in an assembly fixture that would index the details and hold them in position during the first-stage of weldbond operation.

The stiffener at F.S. 68.50 was positioned by nesting to the lower skin and a station jig locator. The left-hand channel was positioned by a station locator at buttock line (B.L.) +2.06 and nested against the stiffener at F.S. 68.50. The left-hand bathtub was positioned by butting against the left-hand channel and a station locator at F.S. 61.75. The right-hand channel was positioned by a station locator at B.L. -2.06 and nested against the stiffener F.S. 68.50. The right-hand bathtub was positioned by nesting against the right-hand channel and a station locator at F.S. 61.75. The right-hand outboard stiffener was positioned by nesting against the stiffener at F.S. 68.50, the bathtub at F.S. 61.75 and the channel at B.L. -2.06.

An electrode anti stick solution was then applied to the exterior surface in the areas to be weldbonded. Weldbonding was accomplished within 96 hours of the application of adhesive to the skin. After weldbonding, the assembly was removed from the assembly fixture and placed in an oven at 255 \pm 5°F for 90 minutes.

The second-stage of the assembly consisted of the waffle pan and first-stage weldbonded assembly. The details and subassembly was assembled and installed in the same assembly fixture as that used in the first-stage to control station location and moldline. The waffle pan was located in the first-stage assembly by indexing to the left-hand and right-hand edge trim. The balance of operations performed in the second-stage was the same as the first-stage.

Adhesive Bond Assembly. The third-stage details consisting of the second-stage assembly and the inner skin were processed for adhesive bonding as follows:

They were impression prefitted by assembling the inner skin and assembly in a female type bond fixture, indexing to the outer moldline of the fuselage lower skin. The impression fit

was accomplished by applying one ply of 0.015 inch thick FM643-2 mat verifilm in all metal-to-metal bondlines.

The bond fixture was placed in an autoclave with thermocouples, bleeder cloth and pressure membrane installed. A vacuum of 10 \pm 2 inches of mercury was applied and all significant leaks were checked and eliminated. An autoclave pressure of 30 to 100 psi was applied and the assembly vented to the atmosphere. The temperature was then raised from ambient to 225°F in a maximum of 120 minutes and then maintained at 225 to 250°F for a minimum of 90 minutes. It would then be cooled to 150°F or lower under pressure.

The bond fixture was removed from the autoclave, the details disassembled and the verifilm inspected. An acceptable fit indicated a metal-to-metal bondline of 0.015-inch maximum wherever one ply of verifilm was used. Within 72 hours prior to application of adhesive primer, the surfaces of the details were prepared by phosphoric acid anodizing prior to structural adhesive bonding.

After the surfaces of the details had been prepared, all traces of cured adhesive or other contaminations were removed from the bond tool surfaces and the tool would be wiped with solvent. A release agent was applied to the upper surfaces of the bonding tool at a temperature of 65 to 100°F and a relative humidity of 60 percent or less. It was then air-dried for a minimum of one hour and buffed to remove excess coating. The tool was air-dried an additional 24 hours or oven-dried at 225°F for one hour and then rebuffed.

The adhesives and adhesive primers were mixed and applied in enclosed areas with the temperature between 65 to 90°F and a relative humidity of 70 percent maximum. NAI-1412 type 2 adhesive primer was applied by spray to all surfaces of the deck pan within 72 hours following completion of the final drying

operation in the surface preparation of the details. The adhesive primer was thoroughly mixed for 15 minutes in a paint shaker immediately before pouring into a spray gun reservoir. The primer was applied in a uniform coat, air-dried for a maximum of 30 minutes and cured for 60 to 90 minutes at 225 to 250°F. NAI-1412 type I class C film adhesive was precut to size and applied to the bonding surfaces of all adhesive primed details.

The second-stage assembly was positioned in the bond fixture by locators. The inner skin was positioned over the second-stage assembly. The bond fixture was then installed in the autoclave with thermocouples, bleeder cloth and pressure membrane. A vacuum of 5 to 10 inches of mercury was applied and all leaks were checked and eliminated. Autoclave pressure was applied and the vacuum side of the pressure membrane vented to the atmosphere. The temperature was raised from ambient to 225°F in a maximum of 120 minutes and maintained at 225 to 250°F for a minimum of 90 minutes. After the cure cycle was completed, the autoclave was cooled to 150°F or lower under pressure.

The bond fixture was then removed from the autoclave. The pressure membrane, bleeder cloth, thermocouples and the final assembly was removed and cleaned up.

2.2.2.2 Nose Gear Wheel Door

The nose gear wheel door was of aluminum construction with the exception of three fiberglass laminates that were sandwiched between the inner and outer skins and acted as fillers and backup for the bracket and fore and aft hinges. The door extended from F.S. 87.50 to F.S. 126.50 and approximately 5.34 inches along each side of the aircraft centerline. It attached to the lower forward fuselage by means of the forward and aft hinges at F.S. 90.50 and F.S. 118.50.

The proposed configuration would consist of the existing hinges and brackets along with their respective hardware.

- (1) A SPF outer skin that formed the outer moldline of the door including the scoop.
- (2) A SPF inner skin that formed the inner moldline of the door and also included the scoop.
- (3) A SPF substructure made to the inner moldlines of both inner and outer skins.
- (4) Three fiberglass laminates made to the inner moldlines of both inner and outer skins. Each laminate acted as a filler and backup for the hinges and bracket.
- (5) A conventionally formed fairing that acted as a closeout at F.S. 113.35.
- (6) Two conventionally formed angles that nested against the outer skin and substructure along each side of the scoop.

The following was a detailed operational sequence for the fabrication of the inner skin, outer skin and substructure and assembly.

Outer Skin. The outer skin would be of 7475 fine grained aluminum alloy sheet furnished by Reynolds. The production blank would be cut to size, degreased, alkaline cleaned, given a uniform spray coat of forming lubricant and then air-dried. The SHFD would have all foreign particles removed from the interior surfaces of the tool. The tool would then be closed and pressure applied on peripheral seals. The heat-up of the tool would then be started. After the tool was stabilized at

operating temperature, it would be opened and the production blank installed.

The tool would then be closed and press loads applied to provide peripheral seal loads. Air pressure would be maintained in the upper and lower tool cavities until all areas of the tool were within the forming temperature range. Air pressure would be maintained in the lower cavity during the forming cycle. At the end of the forming cycle, the upper and lower cavities would be removed, the tool opened and the part removed. The skin would then be heat-treated, placed in a trim fixture, routed net and then wrapped and stored for use on the next assembly.

Inner Skin. The inner skin would be of the same material as the outer skin and would be manufactured in the same manner as the outer skin.

Substructure. The substructure would be of the same material as the outer skin and would be manufactured in the same manner as the outer skin.

The SHFD would use a common base or cage, with removable inserts for each skin and substructure.

Fiberglass Laminates. The laminates would be of pre impregnated fiberglass cloth. The material would be cut to size and laid up ply on ply in a pressure mold. After the layup was complete, the upper and lower sections of the die were to be clamped together and placed in an oven and cured. After cure, the part would be removed from the die, cleaned up and pilot holes drilled for tack rivets on the next assembly.

First-Stage Weldbond Assembly. The first-stage details which consisted of the outer skin and two angles would be processed for weldbond as follows:

They would be vapor degreased, then alkaline cleaned by immersing the parts in a non-silicated alkaline solution at 125 to 165°F for 12 to 15 minutes. They would then be spray rinsed with deionized water for 5 to 7 minutes and inspected for a water-break-free surface. After inspection, the details would be deoxidized by immersing in an agitated deoxidizer solution at 70 to 80°F for 18 to 22 minutes within the required voltage range and spray rinsed again with deionized water for 4 to 7 minutes and oven-dried in a recirculating air oven at 150 to 160°F for 30 to 60 minutes.

The cleaned and anodized parts would be handled with clean, cotton gloves and maintained in a clean room atmosphere until the adhesive for the weldbond was applied. After anodizing, the parts would be given a special surface treatment prime. The paste adhesive, warmed to room temperature, would be applied to the faying surface of the angles common to the outer skin within 120 hours from the time they were anodized, to a film thickness that would achieve a final glue line thickness of 0.005 to 0.012 inch.

The outer skin would be positioned in an assembly fixture that would index the details and hold them in position during the weldbond first and second-stage operations. The angles would be located on the outer skin and positioned by a locator simulating the substructure on both left and right-hand sides of the scoop. An electrode anti-stick solution would then be applied to the exterior surface in the areas to be weldbonded. Weldbonding would be accomplished within 96 hours of the application of adhesive to the angles.

Second-Stage Weldbond Assembly. The second-stage assembly, which consisted of the first-stage assembly and the substructure, would be processed for weldbond in the same manner as the first-stage assembly, except the adhesive would be applied to the faying surfaces of the substructure removed from the

assembly fixture and placed in an oven at 255 \pm 5°F for 90 minutes.

Third-Stage Adhesive Bond Assembly. The third stage assembly which consisted of the second-stage assembly, the inner skin and three fiberglass laminates would be processed for adhesive bonding as follows:

The assembly and details would be impression prefitted by placing them in a female type bond fixture, indexing to the outer moldline of the outer skin. The impression prefit would be accomplished by applying one ply of 0.015-inch thick FM643-2 mat verifilm in all metal-to-metal bondlines. The bond fixture would then be placed in an autoclave with thermocouples, bleeder cloth and pressure membrane installed. A vacuum of 10 \pm 2 inches of mercury would be applied and all significant leaks checked and eliminated. An autoclave pressure of 30 to 100 psi would be applied and the assembly vented to the atmosphere. The temperature would then be raised from ambient to 225°F in a maximum of 120 minutes and maintained at 225°F for a minimum of 90 minutes. It would then be cooled to 150°F or lower under pressure.

The bond fixture would then be removed from the autoclave, the details disassembled and the verifilm inspected. An acceptable fit would indicate a metal-to-metal bondline of 0.015-inch maximum wherever one ply of verifilm was used.

Within 72 hours prior to application of adhesive primer, the surfaces of the details would be prepared by phosphoric acid anodizing prior to structural adhesive bonding.

After the surfaces of the details had been prepared, all traces of cured adhesive or other contamination would be removed from the bond tool surfaces and the tool would be wiped with solvent. A release agent would be applied to the upper surfaces of the bonding tool at a temperature of 65 to 100°F and

a relative humidity of 60 percent or less. It would be air-dried for a minimum of one hour and then buffed to remove excess coating. The tool would be air-dried an additional 24 hours or oven-dried at 225 to 250°F for one hour and then rebuffed. The adhesives and adhesive primers would be mixed and applied in enclosed areas with the temperature between 65 to 90°F and a relative humidity of 70 percent maximum.

NAI-1412 type 2 adhesive primer would be applied by spray to all surfaces of all skins and details within 72 hours following completion of the final drying operation in the surface preparation of the details. The adhesive primer would be thoroughly mixed for 15 minutes in a paint shaker immediately before pouring into a spray gun reservoir. The primer would be applied in a uniform coat to an air-dry film thickness, then air-dried for a maximum of 30 minutes and cured for 60 to 90 minutes at 225 to 250°F. NAI-1412 type I class C film adhesive would be precut to size and applied to the bonding surfaces of all adhesive primed details.

The second-stage assembly would be positioned in the bond fixture by tool holes and by the scoop. The forward and aft fiberglass laminates would be positioned over the substructure and held in place with tack rivets. The inner skin would then be positioned over the substructure and outer skin. The bond fixture would be installed in the autoclave with thermocouples, bleeder cloth and pressure membrane.

A vacuum of 5 to 10 inches of mercury would be applied and all leaks checked and eliminated. Autoclave pressure would then be applied and the vacuum side of the pressure membrane vented to the atmosphere. The temperature would be raised from ambient to 225°F in a maximum of 120 minutes and maintained at 225 to 250°F for a minimum of 90 minutes. After the cure cycle had been completed, the autoclave would be cooled to 150°F or lower under pressure. The bond fixture would then be removed,

the pressure membrane, bleeder cloth, thermocouples, and the assembly removed from the bond fixture and cleaned up.

Structural Assembly. The door assembly would be placed in an assembly fixture and net trimmed. The hinges, brackets and their associated hardware would be installed as a final operation.

2.2.2.3 Trailing Edge Flap

The trailing edge flap SPF configuration would be manufactured utilizing the existing hinges and actuator rod with their respective brackets and hardware and the ribs forward of the front spar at W.S. 36.57, 41.17 and 74.75.

The new parts required would consist of the following:

- (1) A front spar assembly, located along the 77 percent plane, and made up of a web, an upper cap and a lower cap.
- (2) A leading edge skin assembly, extending from the 70.75 percent plane aft to the front spar and from W.S. 36.57 outboard to W.S. 84.36 and made up of a conventionally stretch formed and chem milled outer skin weldbonded to a SPF inner skin.
- (3) An upper trailing edge skin assembly extending from the front spar aft to the wing trailing edge and from W.S. 36.57 outboard to W.S. 84.36 and made up of a chem milled outer skin weldbonded to a SPF inner skin.
- (4) A lower trailing edge skin assembly extending from the front spar aft to the wing trailing edge and from W.S. 36.57 outboard to W.S. 84.36 and made up

of a chem milled outer skin weldbonded to a SPF inner skin.

- (5) A machined trailing edge wedge sandwiched between the upper and lower trailing edge skin assemblies at the extreme wing trailing edge and extended from W.S. 36.57 outboard to W.S. 84.36.
- (6) A SPF outboard rib at W.S. 84.36 extending from the 70.75 percent plane aft to the wing trailing edge.
- (7) Conventionally formed ribs at W.S. 36.57 and W.S. 41.17 that extended from the front spar aft to the wing trailing edge.

Other than the above mentioned weldbond skin assemblies, the balance of the flap would be mechanically fastened with the exception of the trailing edge wedge which would be bonded to the upper and lower trailing edge skins and the faying surfaces of the upper and lower trailing edge inner skins which would be foam bonded where they butt along the wing reference plane.

Trailing Edge Flap - Tooling Concepts. The assembly components that would be superplastically formed were: (1) leading edge inner skin, (2) trailing edge upper and lower inner skins, and (3) outboard rib. The leading edge inner skin tooling would be a self-contained tool, and the seal provided on the tool itself. The tool was to be machined to the inner moldline of the inner skin with approximately two inches excess on the periphery. One upper tool would have ends matching the bottom tool to obtain proper seal when closed. The sheet would be brake formed to the general contour of the tool. The preformed blank would be placed over the tool, seal obtained and superplastically formed to the tool geometry.

The trailing edge upper inner skin would be formed over a steel insert inside the universal cage. The trailing edge lower skin would be formed on another insert similar to the one used for the upper inner skin.

2.2.2.3.1 Spar Assembly

The spar assembly consisted of a web, and conventionally routed extruded upper and lower caps and also included the existing stiffeners for the leading edge ribs at W.S. 36.57 and W.S. 41.17 and the rib and outboard hinge at W.S. 74.75. The details would be positioned in an assembly jig and located to moldline and station locators.

A minimum number of fastener holes would be jig drilled to hold the moldline location. The balance of the holes would be located by a paint spot template for Drivmatic operations. The assembly would then be removed from the assembly jig and the fasteners installed by the Drivmatic. The stiffeners and fillers would be installed on the spar from predrilled pilot holes.

The outboard hinge and rib would be bolted together and forwarded along with the spar assembly as loose items to the next assembly station.

2.2.2.3.2 Leading Edge Skin Assembly

The leading edge skin assembly consisted of a wrap-around inner and outer skin. The outer skin would be stretch formed, chem milled and trimmed to detail allowing approximately 0.06 inch excess trim on the upper and lower aft edges. It would also have tool hole tabs for locating in the next assembly.

The inner skin would be of 7475 fine grained aluminum alloy sheet. It would be preformed in a V-shape configuration, degreased and alkaline cleaned, given a uniform spray coat of

forming lubricant and then air-dried. The SHFD would have all foreign particles removed from the interior surfaces of the tool. The tool would then be closed and pressure applied on peripheral seals. The heat up of the tool would then start. During the heat up, an air flow would be maintained through the upper and lower tool cavities until peripheral sealing occurred. Air pressure would be maintained in both tool cavities after peripheral sealing. After the tool was stabilized at operating temperature, the tool would be opened and the production part installed.

The tool would then be closed and press loads would be applied to provide peripheral seal loads. Air pressure would be maintained in the upper and lower tool cavities until all areas of the tool were within the forming temperature range. Air pressure would then be increased in the upper cavity with pressure maintained in the lower cavity during the forming cycle. At the end of the forming cycle, the upper and lower cavities would be vented to the atmosphere. The pressure load would be removed, the tool opened and the part removed. The skin would then be heat-treated, placed in a trim and drill fixture, routed net and tool holes drilled. The inner and outer skin would be processed for weldbond as follows:

They would be vapor degreased, alkaline cleaned by immersing the parts in a non-silicated alkaline at 125 to 165°F for 12 to 15 minutes. They would then be spray rinsed with deionized water for 5 to 7 minutes, and inspected for a water-break-free surface. After inspection the skins would be deoxidized by immersing in an agitated deoxidizer solution at 70 to 80°F for 6 to 8 minutes and spray rinsed with ambient temperature deionized water for 5 to 7 minutes. They would then be immediately immersed in an anodized solution to 70 to 80°F for 18 to 22 minutes within the required voltage range and spray rinsed again with deionized water for 5 to 7 minutes and oven-dried in a recirculating air oven at 150 to 160°F for 30 to 60 minutes. The

cleaned and anodized parts would be handled with clean, cotton gloves and maintained in a clean room atmosphere until the adhesive for the weldbond was applied.

After anodizing, the parts would be given a special surface treatment prime. The paste adhesive, warmed to room temperature, would be applied to the faying surface of the inner skin common to the outer skin, within 120 hours from the time they were anodized, to a film thickness that would achieve a final bondline thickness of 0.005 to 0.012 inch. The inner skin would be positioned in the assembly by locators indexing to the inner moldline. The outer skin would then be located over the inner skin and held in position by tool hole tabs in the excess trim area. An electrode anti-stick solution would then be applied to the exterior surface in the areas to be weldbonded. Weldbonding would be accomplished within 96 hours of the application of adhesive to the skin. After weldbonding, the assembly would be removed from the assembly fixture and placed in an oven at 255 \pm 5°F for 90 minutes.

2.2.2.3.3 Leading Edge Assembly

The leading edge assembly would consist of the new spar assembly, leading edge skin assembly, existing clips, fillers, ribs stiffeners and skins that were located at W.S. 36.57, 41.17 and 74.75. Also included would be the rib assembly and hinge assembly that were previously assembled with the spar and delivered as loose items. The details would be located in an assembly jig that would control wing station locations and inboard and outboard hinge points forward of the front spar.

2.2.2.3.4 Trailing Edge Skin Assemblies

The upper and lower trailing edge skin assemblies would consist of a SPF inner skin and a flat chem milled outer skin weldbonded together. The upper and lower assemblies would then

be bonded together on the next assembly. The inner skins would be fabricated the same as the leading edge inner skin with the exception that they would not require a preforming operation prior to SPF. A dummy blank would be used in the initial peripheral sealing operation prior to inserting the production blank for forming.

The outer skins would be fabricated the same as the leading edge outer skin with the exception that they would not require any forming. After the parts had been fabricated they would be processed, assembled and weldbonded in the same manner as the leading edge skin assembly.

2.2.2.3.5 Final Assembly

The flap final assembly would consist of the upper and lower trailing edge skin assemblies, trailing edge wedge, ribs at W.S. 36.57, 41.17 and 84.36, leading edge assembly, leading edge skin assembly, actuator rod and bracket, rub strips, markings and nameplate. The subassemblies and details would be assembled and installed in an assembly jig to control station location, moldline and hinge points. The leading edge assembly would be jig located by hinge points, tool holes and moldline locators. The inboard and outboard trailing edge rigs would be jig located by station locators and tool holes in the aft end. The bracket would be hand located on the rib at W.S. 41.17 and the actuator rod would be located between W.S. 36.57 and 41.17. Holes would be drilled full size through the ribs from holes in the bracket and actuator rod flange and the fasteners installed. The trailing edge wedge would be located by moldline and station locators and cleaned for adhesive bond. The spar assembly, the stiffeners at W.S. 36.57, and rib and hinge assembly at W.S. 74.75 would be jig located by tool holes and locators. The previously drilled pilot holes would be opened to full size and the fasteners installed. The inboard hinge would be jig located by hinge points and moldline locators.

The stiffeners at W.S. 41.17 would be located to the hinge and spar. The inboard and outboard ribs at W.S. 41.17 would be hand located and positioned against the hinge and jig locators. Pilot holes would be back drilled from the hinge assembly through both ribs. Holes would also be drilled in the spar web common to both ribs from pilots in the ribs. The inboard and outboard ribs at W.S. 36.57 would be installed by nesting to the hinge and jig locators and pilots would be back drilled from the hinge assembly. The outboard ribs at W.S. 36.47 and 41.17 would be located and holes drilled in spar webs common to all ribs and hinge assemblies. The remaining clips and fillers would be installed. Fastener holes, common to rib webs and hinge at W.S. 36.47 and 41.17, would be drilled and fasteners installed.

The new weldbonded leading edge skin assembly would be located on the structure by inserting the legs of the upper and lower spar caps between the outer and inner skins. Jig strap clamps would be used to hold the skin assembly to the structure. The existing structural pilot fastener holes would be marked on the outer skin and drilled in position. The edge trim of the skin would be marked from the spar for bench routing. The strap clamps would be released and the skin would be removed from the structure and trimmed net. After checking edge trim and marking fastener hole locations, the skin would be reinstalled on the structure and located by pilots. The remaining fastener holes would then be opened full size and countersunk. The skin would be removed for installation in the next sequence after the trailing edge skins had been installed.

The lower trailing edge skin assembly would be located by nesting against the spar assembly and lower moldline locators. Fastener holes would be drilled through the spar web common to the lower inner skin and through the lower outer skin common to the spar lower cap and ribs at W.S. 36.57 and 41.17. The forward

edge of the trailing edge skin would be trimmed next by temporarily installing the leading edge skin assembly to check skin gap. The upper trailing edge skin assembly would be located in the assembly in the same manner as the lower. After drilling and trimming, both upper and lower trailing edge skin assemblies and trailing edge wedge would be removed, deburred and hand cleaned on the inner surface in preparation for the foam bond application. After the skin assemblies and wedge had been cleaned, they would be reinstalled in the assembly with a layer of foam adhesive applied to the faying surface of the lower inner skin common to the upper inner skin. Also, a layer of film adhesive would be applied to both upper and lower surfaces of the trailing edge wedge. Blind fasteners would be installed in the spar assembly and trailing edge skin assemblies. The leading edge skin assembly would then be permanently installed and blind fasteners installed common to the upper and lower spar caps and leading edge ribs.

The flap assembly would then be removed from the assembly fixture, transported to an oven and cured. After cure, the rub strips, markings, and nameplate would be installed as the last operations.

2.2.2.4 Wing Leading Edge Extension

The two designs shown for the LEX are almost the same. They differed in that the first utilized a single SPF aluminum skin bonded to a SPF aluminum corrugated substructure, while the second utilized two SPF aluminum skins over a SPF aluminum corrugated substructure. The second design allowed one skin to be weldbonded and the other skin attached using blind fasteners. In both designs, a machined leading edge was weldbonded into the structure and the aft closing rib was mechanically attached.

These two design configurations of the LEX were proposed to provide manufacturing more flexibility in selection of a structure which would be easier and cheaper to fabricate.

The proposed configuration would consist of all new parts as follows:

- (1) A machined rib, located along the forward spar reference plane, with upper and lower caps machined to the inner moldline of the outer skins.
- (2) A machined "arrowhead" which extended from the nacelle moldline forward and outboard to the extreme leading edge reference plane. The arrowhead would contain a machined step on both upper and lower surfaces common to the inner moldline of the skins.
- (3) An upper outer skin which extended from the step in the arrowhead to the forward spar reference plane and from the nacelle moldline forward to approximately 0.50 inch aft of the extreme leading edge. The skin would be manufactured using conventional stretch forming and hydro forming methods.
- (4) A lower outer skin which extended from the machined step in the arrowhead to the forward spar reference plane and from the nacelle moldline out to the extreme leading edge where it wrapped around the machined rib and extended over the upper outer skin approximately 2.0 inches aft of the leading edge. This skin would also be manufactured using conventional stretch forming methods.
- (5) A SPF inner skin with ~~three~~ evenly spaced corrugations that paralleled the nacelle moldline and leading edge reference plane. The inner skin would be formed to the inner moldlines of the

upper and lower skins and would extend from the machined step of the arrowhead to the machined rib and from the nacelle moldline out to approximately 1.0 inch inside the extreme leading edge.

There were two assembly versions proposed for the LEX. One version was a two-stage operation that weldbonded the inner skin, upper outer skin and arrowhead in the first-stage. The second-stage assembled the lower outer skin, rib and first-stage assembly by means of blind fasteners. The other version was a two stage operation that used an adhesive bond method for assembling the inner skin, upper outer skin and arrowhead in the first-stage. The second-stage was identical to the second-stage of the other version. The following was a detailed operation sequence for the fabrication of the inner skin and for both versions of the assembly:

Inner Skin

The inner skin would be of 7475 fine grained aluminum alloy sheet furnished by Reynolds. The production blank would be cut to size, degreased, alkaline cleaned, given a uniform spray coat of forming lubricant and then air-dried. The SHFD would have all foreign particles removed from the interior surfaces of the tool. The tool would then be closed and pressure applied on peripheral seals. The heat-up of the tool would then start. After the tool was stabilized at operating temperature, it would be opened and the production blank installed.

The tool would then be closed and press loads applied to provide peripheral seal loads. Air pressure would be maintained in the upper and lower tool cavities until all areas of the tool were within the forming temperature range. Air pressure would then increase in the upper cavity with the pressure maintained in the lower cavity during the forming cycle. At the end of the forming cycle, the upper and lower cavities would be

vented to the atmosphere. The pressure load would be removed, the tool opened and the part removed. The skin would then be heat-treated, placed in a trim fixture, routed net, wrapped and stored for use on next assembly.

Weldbond Assembly

The first-stage details which consisted of the upper outer skin, inner skin and arrowhead would be processed for weldbond as follows:

They would be vapor degreased and alkaline cleaned by immersing the parts in a nonsilicated alkaline solution at 125 to 165°F for 12 to 15 minutes. They would then be spray-rinsed with deionized water for 5 to 7 minutes and inspected for a water-break-free surface. After inspection, the details would be deoxidized by immersing in an agitated deoxidizer solution at 70 to 80°F for 6 to 8 minutes and spray-rinsed with ambient temperature deionized water for 5 to 7 minutes. They would then be immediately immersed in an anodized solution at 70 to 80°F for 18 to 22 minutes within the required voltage range, spray-rinsed again with deionized water for 5 to 7 minutes and oven-dried in a recirculating air oven at 150 to 160°F for 30 to 60 minutes. The cleaned and anodized parts would be handled with clean, cotton gloves and maintained in a clean room atmosphere until the adhesive for the weldbond was applied.

After anodizing, the parts would be given a special surface treatment prime. The paste adhesive, warmed to room temperature, would be applied to the faying surface of the inner skin common to the upper outer skin and to the upper and lower machined steps of the arrowhead common to the inner skin and upper outer skin within 120 hours from the time they were anodized, to a film thickness that would achieve a final bondline thickness of 0.005 to 0.012 inch.

The upper outer skin would be positioned in an assembly fixture that would index the details and hold them in position during the weldbond operation and also during the second-stage operation for the installation of blind fasteners. The arrowhead would then be positioned and adjusted to maintain a proper gap between the edge of the skin and the step in the arrowhead. The inner skin would then be positioned by nesting to the lower outer skin and locators simulating the machined rib. The gap between the inner skin and arrowhead machined step would have to be maintained. An electrode anti-stick solution would then be applied to the exterior surface in the areas to be weldbonded. Weldbonding would be accomplished within 96 hours of the application of adhesive to the skin. After weldbonding, the assembly would be removed from the assembly fixture and placed in an oven at $255 \pm 5^{\circ}\text{F}$ for 90 minutes.

The second-stage of the assembly would consist of the lower outer skin, machined rib and first-stage weldbonded assembly. The details and subassembly would be assembled and installed in the same assembly fixture as that used in the first-stage to control station location and moldlines. The rib would be located in the assembly fixture by both station and moldline locators. The first-stage subassembly would be located in the fixture and nested against the rib. The lower outer skin would then be positioned and nested over the inner skin and machined rib.

Drill plate details and overlay would be installed, and fastener holes drilled through the rib common to the inner skin, and through the lower outer skin common to the inner skin, rib and upper outer skin. The details would then be removed from the assembly fixture, deburred, reinstalled and mechanical fasteners installed.

Adhesive Bond Assembly

The first-stage details which consisted of the upper outer skin, inner skin and arrowhead would be processed for adhesive bonding as follows:

They would be impression prefitted by assembling all details in a bond fixture which would be a female type indexing to the outer moldline of the upper skin and arrowhead. The bond fixture would simulate the machined rib and provide locators for positioning the inner and outer skin and arrowhead in position during the bonding cycle. The impression fit would be accomplished by applying one ply of 0.015-inch thick FM643-2 mat verifilm in all metal-to-metal bondlines. The bond fixture would then be placed in an autoclave with thermocouples, bleeder cloth and pressure membrane installed. A vacuum of 10 \pm 2 inches of mercury would be applied and all significant leaks checked and eliminated. An autoclave pressure of 30 to 100 psi would be applied and the assembly vented to the atmosphere. The temperature would then be raised from ambient to 225°F in a maximum of 120 minutes and then maintained at 225 to 250°F for a minimum of 90 minutes. It would then be cooled to 150°F or lower under pressure.

The bond fixture would then be removed from the autoclave, the details disassembled and the verifilm inspected. An acceptable fit would indicate a metal-to-metal bondline of 0.015-inch maximum wherever one ply of verifilm has been used. Within 72 hours prior to application of adhesive primer, the surfaces of the details should be prepared by phosphoric acid anodizing prior to structural adhesive bonding.

After the surface of the details had been prepared, all traces of cured adhesive or other contamination would be removed from the bond tool surface and the tool would be wiped with solvent. A release agent would be applied to the upper surfaces

of the bonding tool at a temperature of 65 to 100°F and a relative humidity of 60 percent or less. It would then be air-dried for a minimum of one hour and buffed to remove excess coating. The tool would then be air-dried an additional 24 hours or oven-dried at 225 to 250°F for one hour and rebuffed. The adhesive and adhesive primers would be mixed and applied in enclosed areas with the temperature between 65 to 90°F and a relative humidity of 70 percent maximum.

NA1-1412 type 2 adhesive primer would be applied by spray to all surfaces of all skins and details within 72 hours following completion of the final drying operation in the surface preparation of the details. The adhesive primer would be thoroughly mixed for 15 minutes in a paint shaker immediately before pouring into a spray gun reservoir. The primer would be applied in a uniform coat to an air dry film thickness, then air-dried for a maximum of 30 minutes and cured for 60 to 90 minutes at 225 to 250°F. NA1-1412 type 1 class C film adhesive would be pre-cut to size and applied to the bonding surfaces of all adhesive primed details.

The upper outer skin would be positioned in the bond fixture by tool holes and locators. The inner skin would be positioned over the upper outer skin and nested against the simulated machined rib bond fixture detail. The arrowhead would then be installed over the outer skin and underneath the inner skin and adjusted to hold skin gaps as before. The bond fixture would then be installed in the autoclave with thermocouples, bleeder cloth and pressure membrane.

A vacuum of 5 to 10 inches of mercury would be applied and all leaks checked and eliminated. Autoclave pressure would then be applied and the vacuum side of the pressure membrane vented to atmosphere. The temperature would be raised from ambient to 225°F in a maximum of 120 minutes and then maintained at 225 to 250°F for a minimum of 90 minutes. After the cure

cycle had been completed, the autoclave would be cooled to 150°F or lower under pressure. The bond fixture, pressure membrane, bleeder cloth and thermocouples would be removed. The assembly would then be removed and cleaned up. The assembly would be trimmed net to remove tool hole tabs and adhesive flash in preparation for the second-stage operation. The second-stage sequence of operations would be the same as that noted in the weldbond assembly.

2.3 COMPONENT RANKING

Upon the completion of the detailed drawings and the manufacturing plans, sufficient data was available to determine the cost and weight estimates for the selected components. Additionally, the manufacturing plans also provided an opportunity to assess the risk associated with fabrication and/or assembly of the SPF design of each component so that those factors could be considered in the ranking as well. Once these data became available, the components were ranked against these factors to determine the final candidates. This section contains the details of these studies.

The manufacturing hours estimates were generated on a 12-shipset/lot basis. The hours given were cumulative to the third shipset (Table 2-1) or 300 shipsets (Table 2-2). The hours shown in Table 2-1 represented the methods and tools employed in this program and did not necessarily reflect normal production practice. A number of hand trim and drilling operations were assumed rather than the fully tooled production approach. No such deviations, however, were made with regard to the SPF forming dies. Those tools were estimated as full production tooling. The tool design fabrication and planning hours estimates reflected program, not production practices, and were presented as a guide to expected program costs if their respective component was picked for full scale production.

TABLE 2-1. THREE SHIPSET HOURS ESTIMATES

	AVIONICS DECK			NOSE GEAR DOOR			TRAILING EDGE			LEADING EDGE EXTENSION #1			LEADING EDGE EXTENSION #2		
	BASE	SPF		BASE	SPF		BASE	SPF		BASE	SPF		BASE	SPF	
TOOL DESIGN	----	1478	----	----	1040	----	----	2346	----	----	516	----	----	1408	----
TOOL FAB	----	5060	----	----	1532	----	----	18524	----	----	5178	----	----	5027	----
PLANNING	----	148	----	----	193	----	----	200	----	----	209	----	----	209	----
TOOL SUB TOTL	----	6686	----	----	2765	----	----	21070	----	----	5903	----	----	6644	----
FABRICATION	725	394	-331	101	124	+ 23	993	1335	+342	383	379	- 4	383	379	- 4
ASSEMBLY	124	98	- 26	208	114	- 94	1942	1073	-869	82	100	+ 18	82	117	+ 35
FAB SUB TOTAL	849	492	-357	309	238	- 71	2935	2408	-527	465	479	+ 14	465	496	+ 31
TOTAL		7178			3003			23478			6382			7140	

Tooling hours are included to show program cost impact. Hours shown are cumulative hours to T3.

TABLE 2-2. 300 SHIPSET HOURS ESTIMATES

	AVIONICS DECK		NOSE GEAR DOOR		TRAILING EDGE		LEADING EDGE EXTENSION #1		LEADING EDGE EXTENSION #2					
	BASE	SPF	BASE	SPF	BASE	SPF	BASE	SPF	BASE	SPF				
FABRICATION	18848	12681	-6167	4530	+1863	27142	39738	12596	20714	15259	-5455	20714	15259	5455
ASSEMBLY	8045	5079	-2966	4792	-2135	67401	58381	-9020	2810	4168	+1358	2810	5228	+2418
TOTAL	26893	17760	-9133	9322	- 272	94543	98119	+3576	23524	19427	-4097	23524	20487	-3037

Tooling hours are not included. Baseline hours are estimated as a new vehicle (T1 to T300) not current production status (T1000+ to T1300+). Hours shown are cumulative to T300.

For the purpose of this study, all baseline component manufacturing hours were estimated as if the F-5F was just going into production of one shipset (T1) and not at the current production status of over 1000 shipset (T1000+). Overall, the following ground rules and assumptions were considered throughout the manufacturing cost estimates:

- (1) Baseline T1 F-5F component manufacturing hours were assumed as a new program and not at current production rates.
- (2) Standard and variances for organizations and/or operations were developed from history. Actual values used were representative of industry values.
- (3) Estimates were for Research and Development (R&D) type program of 3 shipsets and production program of 300 shipsets.
- (4) Standard variances and slopes were dependent on the operation.

The standard variances and slopes for 3 and 300 shipsets are shown in Tables 2-3 and 2-4, respectively. Figures 2-5 and 2-6 schematically represent the cumulative average hours comparison for each component. In addition, Figures 2-7 through 2-10 further describe the direct recurring labor hours comparison between the baseline and the SPF designs of each component. Also, these cost figures represent the projected comparison between T1 and T1000 shipset.

This section also includes the piece count and fastener count reduction data associated with each component. The piece

TABLE 2-3. VARIANCES AND SLOPES FOR THREE SHIPSETS

OPERATION	T1 VAR	% SLOPE
MACHINED PARTS	4	90
SHEET METAL FABRICATION	4	95
SUPERPLASTIC FORMING AL, DETAILS	6	87
WELDBOND ASSEMBLIES	6	95
SIMPLE SHEET METAL ASSEMBLY	20	78
CHEM MILLED DETAILS	2	95
ALL COMMON PARTS	2	95

TABLE 2-4. VARIANCES AND SLOPES FOR 300 SHIPSETS

OPERATION	T1 VAR	% SLOPE
MACHINED PARTS	5	90
SHEET METAL FABRICATION	4	85
SUPERPLASTIC FORMING AL, DETAILS	6	87
WELDBOND ASSEMBLIES	6	90
SIMPLE SHEET METAL ASSEMBLY	12	90
CHEM MILLED DETAILS	2	95
ALL COMMON PARTS	2	95

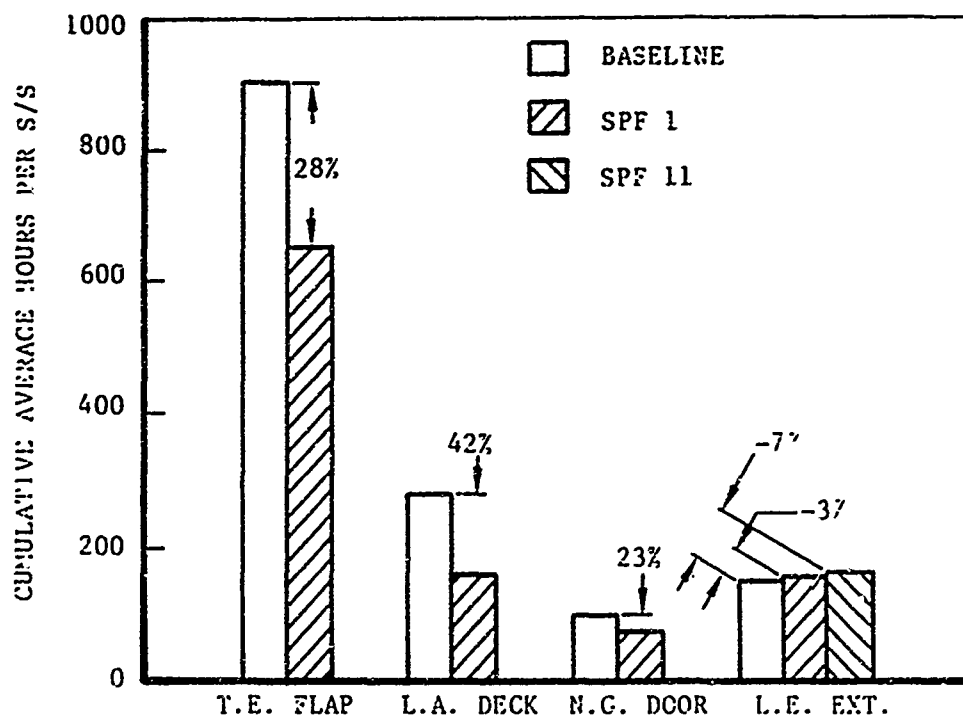


Figure 2-5. Cumulative Average Hours Comparison for Three Shipsets

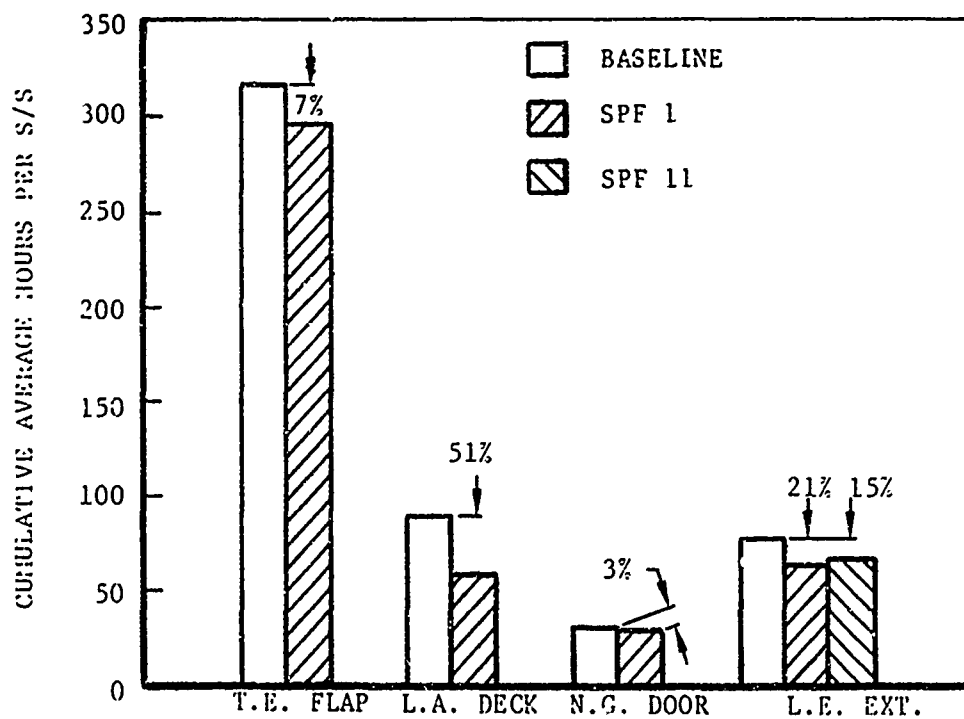


Figure 2-6. Cumulative Average Hours Comparison for 300 Shipsets

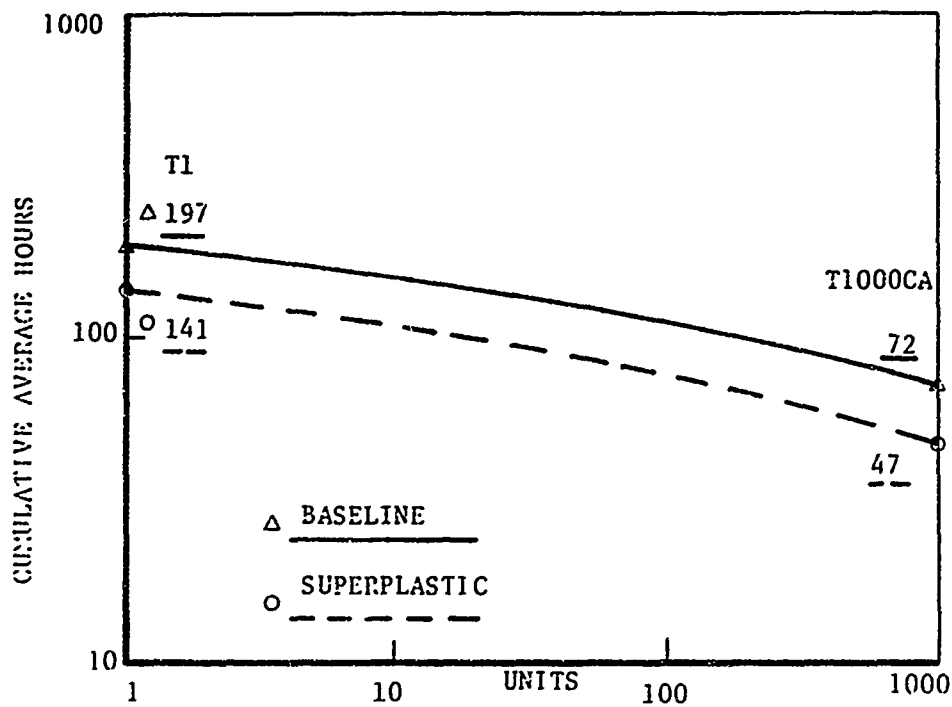


Figure 2-7. Direct Labor Hours Comparison (Avionics Deck)

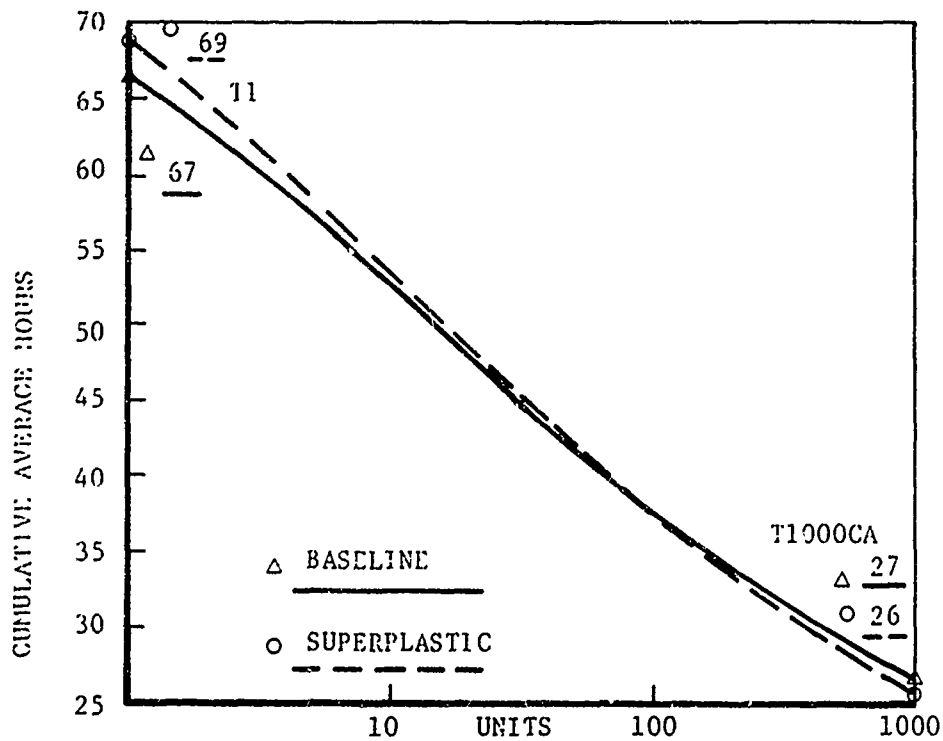


Figure 2-8. Direct Labor Hours Comparison (Nose Gear Door)

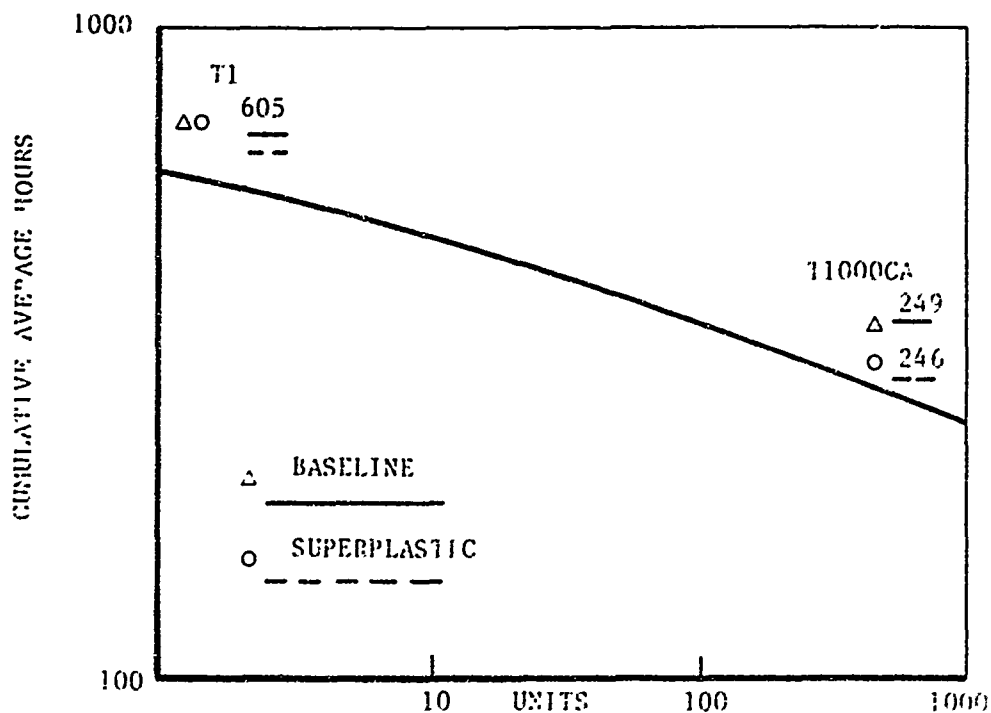


Figure 2-9. Direct Labor Hours Comparison (Trailing Edge Flap)

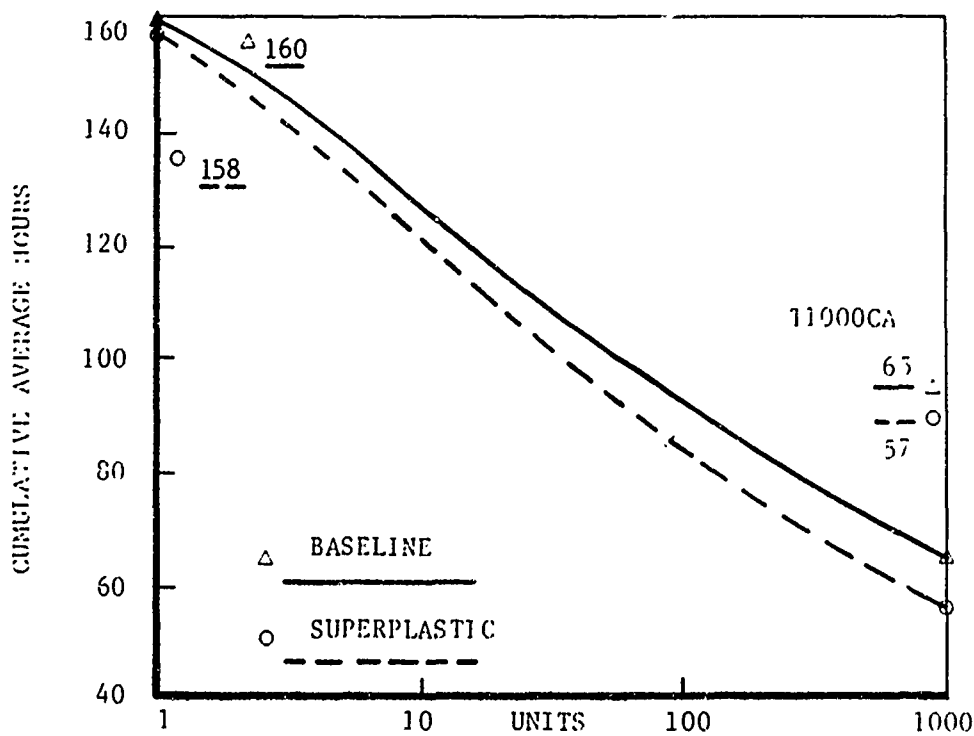


Figure 2-10. Direct Labor Hours Comparison (Leading Edge Extension)

count reduction was determined from the detailed drawings of each components SPF design. The fastener count reduction, on the other hand, was also a function of the assembly sequence scheduled through the manufacturing plans. These data give an indication of where the cost savings lie when applying the SPF technology. The fastener count and piece count reduction data are shown in Tables 2-5 and 2-6, respectively.

TABLE 2-5. COMPONENT FASTENER COUNT REDUCTION

COMPONENT	BASLINE	SPF DESIGN	DELTA
AVIONICS DECK	1009	---	-1009
NOSE GEAR WHEEL DOOR	27	---	- 27
TRAILING EDGE FLAP	1049	474	- 575
LEADING EDGE EXTENSION	63	18	- 45

TABLE 2-6. COMPONENT PIECE COUNT REDUCTION

COMPONENT	BASLINE	SPF DESIGN	DELTA
AVIONICS DECK	63	10	-53
NOSE GEAR WHEEL DOOR	21	9	-12
TRAILING EDGE FLAP	98	42	-56
LEADING EDGE EXTENSION	2	5	+ 3

The component rating chart (Table 2-7) ranked each component according to six significant attributes. The recurring cost savings and program cost ranking reflected the manufacturing hours estimates previously given.

TABLE 2-7. COMPONENT RATING CHART

RATING CRITERIA	AVIONICS DECK	NOSE GEAR WHEEL DOOR	TRAIL- ING EDGE FLAP	LEADING EDGE EXTEN- SION
RECURRING COST	1	9	10	5
WEIGHT	3	10	5	5
TECHNOLOGY	1	7	3	5
SPF RISK	10	5	3	2
ASSEMBLY RISK	7	4	5	2
TOTAL	22	35	26	19

COMPONENT RATING: SCALE 1 THROUGH 10, 1 = BEST

The weight savings potential was somewhat of a subjective evaluation as the lack of a complete stress analysis precluded a detailed weight analysis. However, the substitution of the sheet metal SPF leading edge extension for a heavy hogout part could not fail to reduce the component weight significantly, hence, effecting the ranking order of these components.

The avionics deck through large reductions in piece count and fastener count had significantly less linear inches of

lap joint and thus, achieved a modest weight savings. The trailing edge flap piece count reduction did not produce a clear weight savings, however, the stiffened pan design was lighter than the existing rib/honeycomb design. The nose gear wheel door SPF design replaced a bonded honeycomb structure and it was doubtful if any weight savings could be realized.

The risk and technology assessments were all highly subjective and required some explanation. The avionics deck contained areas with over 300 percent elongation and nested channels between closely held fuselage outer moldline and the deck reference planes. Because its design required the most accuracy and greatest superplastic deformation it, therefore, ranked highest in technology advancement and highest in risk.

The nose gear wheel door offered considerably less risk because of more modest forming requirements. It was similar in design to many honeycomb replacement schemes used in SPF titanium and advanced composites and therefore, rated lower on the technology advancement scale.

The leading edge extensions represented the least risk because of lower SPF deformations (150 percent maximum) and uncomplicated assembly. However, the skins required the development of dies capable of accepting preforms and thus, provided for significant technology advancement. The trailing edge flap required the same preform approach coupled with more severe deformations and showed somewhat greater technology advancement. However, simpler assembly procedures and a more accommodating design reduced the program risks.

The rating chart (Table 2-7) showed the LEX design ranking highest followed by the avionics deck with the trailing edge flap and the nose gear door a distant third and fourth respectively. The relatively poor showing of the trailing edge flap was the result of the large amount of remaining parts (42)

and fasteners (474) and its significantly larger size than any other component. The size and final piece count contributed greatly to the program tooling costs making it the most expensive of the components to make in the program. The reasons for the poor showing at the 300th shipset was caused by the long forming times of the many SPF details. Comparing the program quantity estimates with 300 shipset estimates showed the original hours saving turned into a loss at 300 shipsets because of inherently flatter learning curves of superplastic forming (fixed run times) and bonding.

2.4 FINAL SELECTION

Taking into account all of the foregoing factors and rankings, Northrop recommended that the best component candidates for full scale development were the avionics compartment lower deck assembly and the wing LEX. The avionics deck being the most cost effective and offering the most technology advancement was mainly due to the SPF waffle pan.

This superplastically formed substructure not only replaced a substantial number of details from the baseline design, but also offered the highest challenge toward forming of SPF aluminum. In certain areas of the pan the pockets were drawn as deep as 4 inches, which meant elongations in the range of 350-400 percent. The LEX was recommended for weight savings potential and the least risk involved in forming. A SPF LEX corrugation would also establish baseline cost and weight data for SPF corrugated structures. Even though the SPF design of the LEX increased the piece count over the baseline, the recurring cost and weight savings potential justified its selection over the nose gear wheel door and the trailing edge flap.

3. DESIGN AND ANALYSIS

This section contains a detailed description of the design and analysis of the selected components (Lower Avionics Deck and LEX). It will cover the preliminary design and analysis efforts conducted during the initial phase of part selection and the final design and analysis conducted on the selected components. The design process along with the design modifications and the reasons behind them will be discussed in detail.

3.1 PRELIMINARY PART DESIGN

Prior to the selection of two final F-5F candidate components, the preliminary design was initiated in order to generate the manufacturing plans. As a result, the baseline forward fuselage avionics deck and the wing LEX components were both redesigned as SPF assemblies. As discussed earlier, the major emphasis during the redesign was on reduction of piece count and associated assembly costs. For both components, the baseline moldlines and reference planes were maintained, and the key design issues became design parameters such as bend and corner radii, aspect ratio (width/depth), draft angles and the thickness profile. The structural description of the two components along with their preliminary SPF design approach are presented in the following paragraphs.

3.1.1 Forward Lower Avionics Deck

A detailed description of the avionics deck baseline design was given in Section 2.2.1. The original SPF design as discussed earlier was comprised of only five pieces, with the two side longerons common to the original design. All of the sub-

structure would be combined into one SPF waffle pan. Upper and lower SPF skins would cover the substructure waffle pan (Figure 2-1). However, clearance provisions for under deck equipment and exterior access and antenna mounting provisions created structural discontinuities and subsequently increased the piece count from the original estimates.

The later version of the avionics deck SPF design as shown in Figure 3-1, consisted of nine SPF details; a upper skin, a waffle pan, a lower skin, two left-hand (L.H.) and right-hand (R.H.) bathtubs, two L.H. and R.H. channels, a Z-stiffener at F.S. 68.50, and an outboard stiffener. The R.H. and L.H. side longerons were replaced by the overlapped outboard edges of the inner skin, waffle pan, and outer skin parts. The edges were flanged together to provide sufficient cross sectional area to function as longerons and provide the mounting flange for the avionics compartment access doors. This later version of the avionics deck was used to generate the manufacturing plans described earlier in Section 2.2.2.

Throughout the preliminary design stage, other design parameters such as material gage, corner radii, pocket aspect ratios, and draft angles were dictated by preliminary stress analysis, analytical thinning predictions, and data from previous studies on SPF aluminum.

3.1.2 Leading Edge Extension

A detailed description of the LEX baseline design was given in Section 2.2.1. The SPF design of the LEX was to replace the internal ribs and spars with truss type SPF corrugations running fore and aft. As discussed earlier, two different versions of the LEX were considered for redesign as an SPF assembly. The first version was the entire LEX, and the second version consisted of the portion forward of the shear pin.

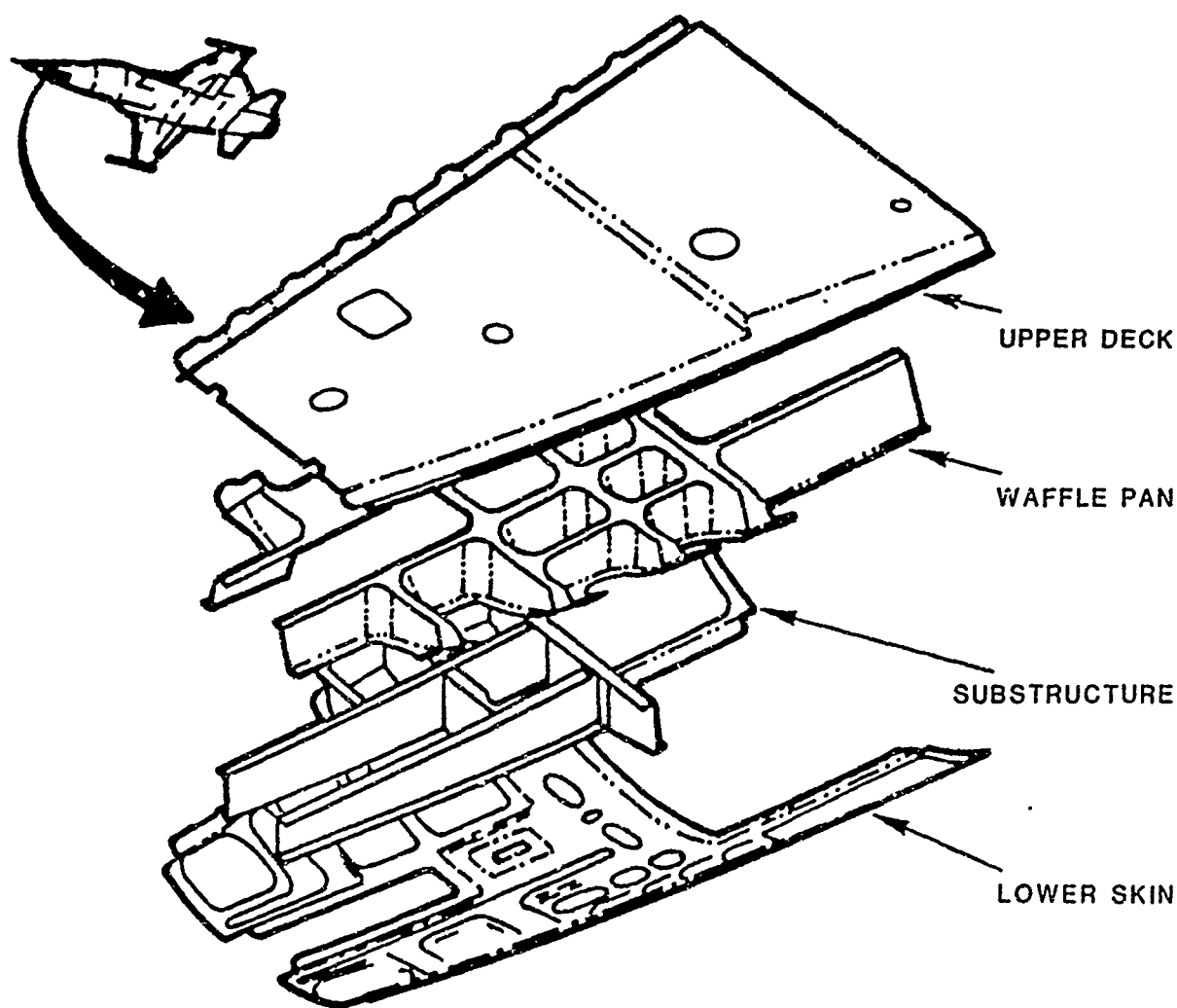


Figure 3-1. Modified Avionics Deck SPF Design

Trade studies were performed to determine which version of the LEX should be considered for a SPF design. Access requirements and load intensities required the retention of the existing fittings. Therefore, there was little advantage left in redesigning the entire LEX. As a result, only the forward portion of the LEX was redesigned as an SPF assembly. Two versions of the SPF LEX design were developed during the preliminary design stage. Both versions were similar except in the area of skins. The first version consisted of a single piece skin where the second version had upper and lower skins to provide manufacturing more flexibility in selection of a structure which would be easier and less costly to fabricate. Both versions consisted

of a SPF corrugated substructure which would be bonded to the SPF aluminum skins. The second version allowed one skin to be weld-bonded and the other skin attached using blind fasteners. In both designs, a machined leading edge would weldbond into the structure and the aft closing rib was mechanically attached. Conceptual sketches of the SPF designs for both versions are presented in Figures 3-2 and 3-3. A more detailed description of the LEX and its manufacturing plans was presented in Section 2.2.2.

3.2 PRELIMINARY ANALYSIS

A preliminary stress analysis based on computer predictions of structural element thinning and derived mechanical properties was undertaken. It was recognized that during the Task I trade studies and preliminary design phase, all of the necessary mechanical properties were not available in sufficient quantity for each of the candidate materials. Therefore, to provide the designer with the needed information in a timely manner, a set of preliminary allowables were projected from available data. SPF aluminum test data which had been developed at Northrop and elsewhere were used as the base. These values were reduced to a psuedo "A" basis (99 percent of the data expected to exceed the "A" basis allowable with a confidence of 95 percent) by assuming that, if a sufficient quantity of data were available, the same statistical reduction factors would be applied to the SPF aluminum as those used in MIL-HDBK-5D for a similar sheet material. It was further assumed that the same temperature reduction factors applied to both materials.

Further analysis of the selected components was conducted by finite element modeling (FEM) of each structure and the use of the NASTRAN analysis program. A finite element analysis was necessary because the unconventional structure in the SPF

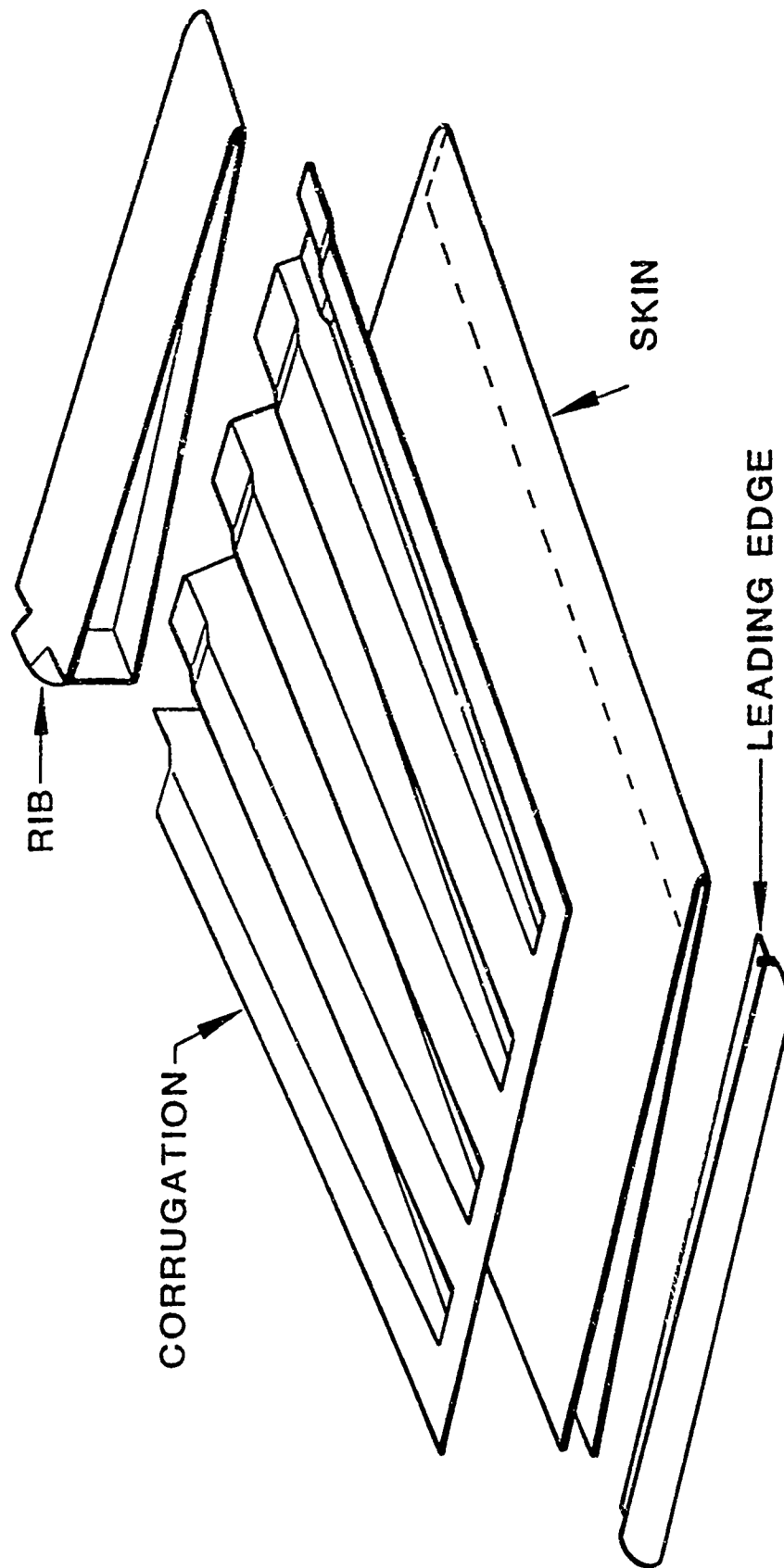


Figure 3-2. One Piece Skin SPF LEX Design

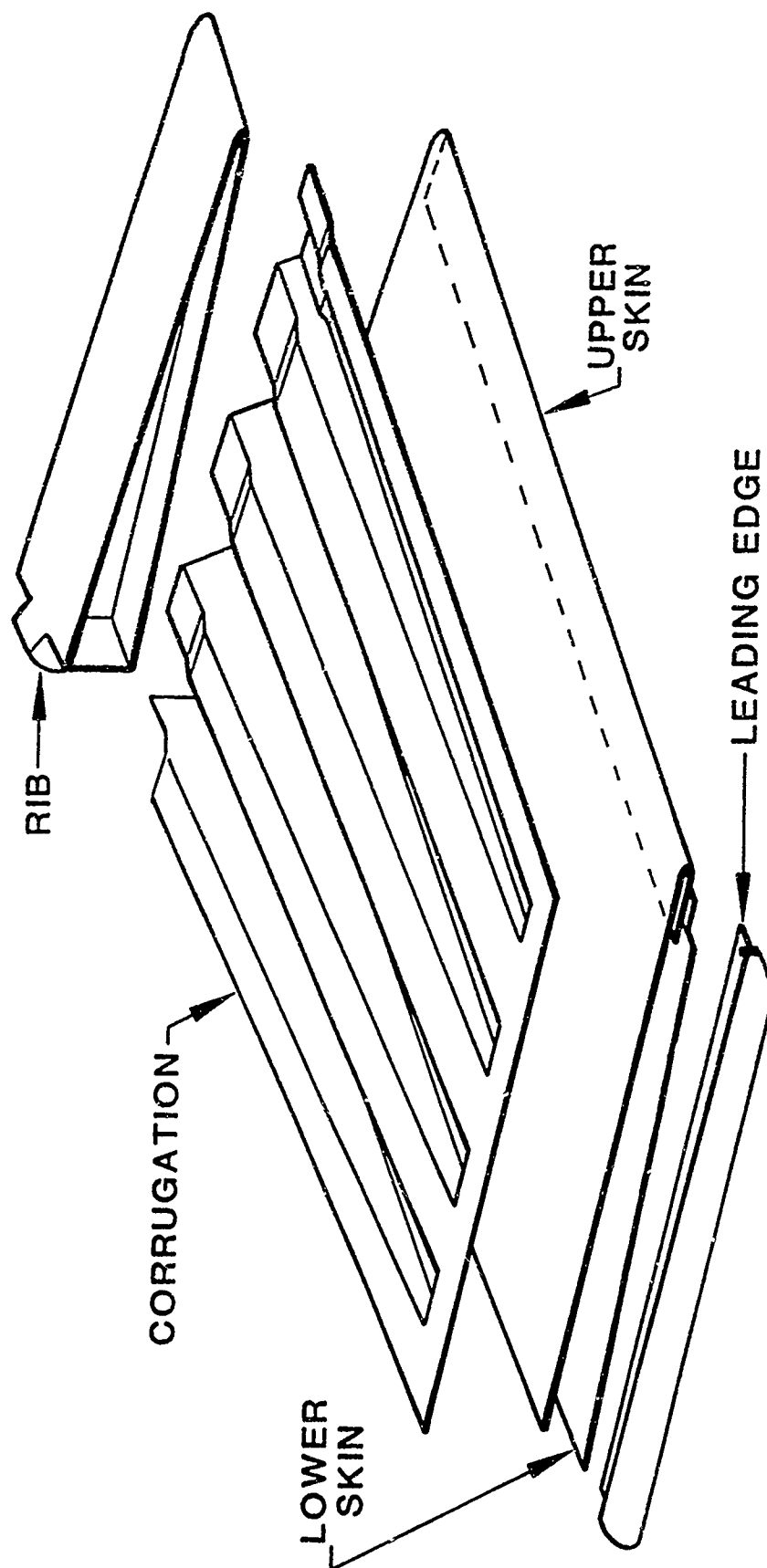


Figure 3-3. Two Piece Skin SPF LEX Design

configuration did not lend itself readily to conventional analysis due to the discontinuous load path in the parts. The avionics deck NASTRAN model, as shown in Figure 3-4, consisted of four separate submodels; FEM of the outer skin, waffle pan, substructural details, and inner skin. The avionics deck structure was modeled entirely of isoparametric flat shell elements (CQUAD4's and CTRIA3's). Care was taken to represent the pan stiffener intersection fillets. The loading on the structure came from inertia loads of installed equipment and the air loads on the structure and radome which attached to the bulkhead on the forward edge of the deck assembly. The avionics deck FEM was joined to the F-5F forward fuselage model at bulkheads at its front and rear and a partial web connected the upper nose structure to the deck. The rest of the fuselage model aft of F.S. 87.50 was not used, and the displacements and forces from the critical loads cases were applied to the F.S. 87.50 bulkhead.

The LEX was modeled mostly of CQUAD4's and CTRIA3's (Figure 3-5) except for a few solid elements to represent the leading edge arrowhead fitting, the lug and areas of the attached rib. Since the LEX FEM was of modest size, no truncation was required on this model. The LEX NASTRAN model was mated with the existing F-5F model. Material thicknesses were evaluated and included in the model. The upper and lower skin thicknesses were a constant 0.065 inch, and the rib web and flange thicknesses were 0.080 inch throughout. Corrugation thicknesses were acquired through an analytical computer SPF thinning analysis. This program calculated the thicknesses of a SPF structure at various locations given the sheet gage and properties and the dimensions of the corrugations. The corrugation thicknesses are shown in Figure 3-6.

Two load cases were performed as check on the validity of the NASTRAN results, a 10,000-lb tip shear load and a 100g gravity load. Since the results of the two check cases validated

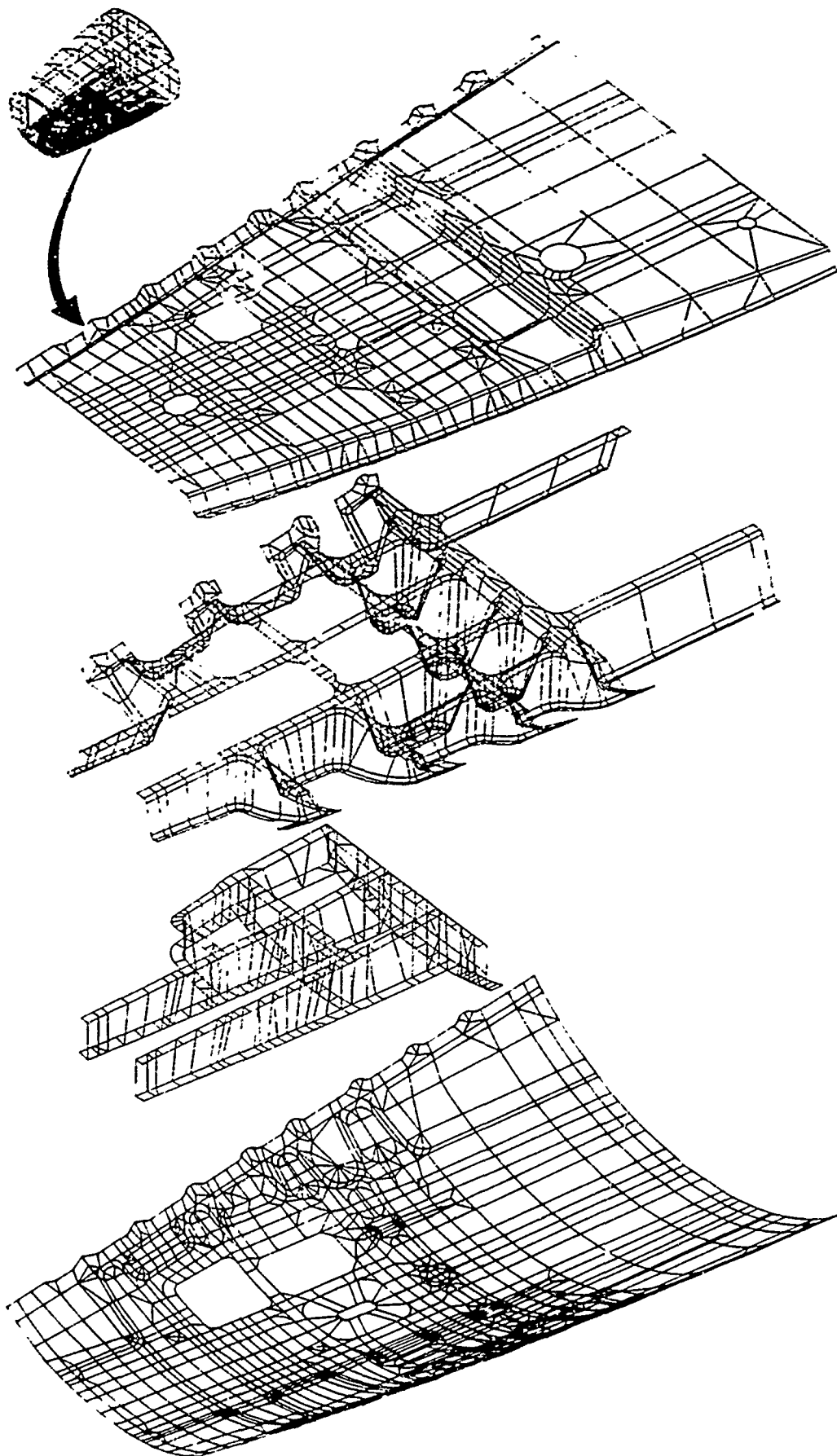


Figure 3-4. SPF Avionics Deck NASTRAN Model

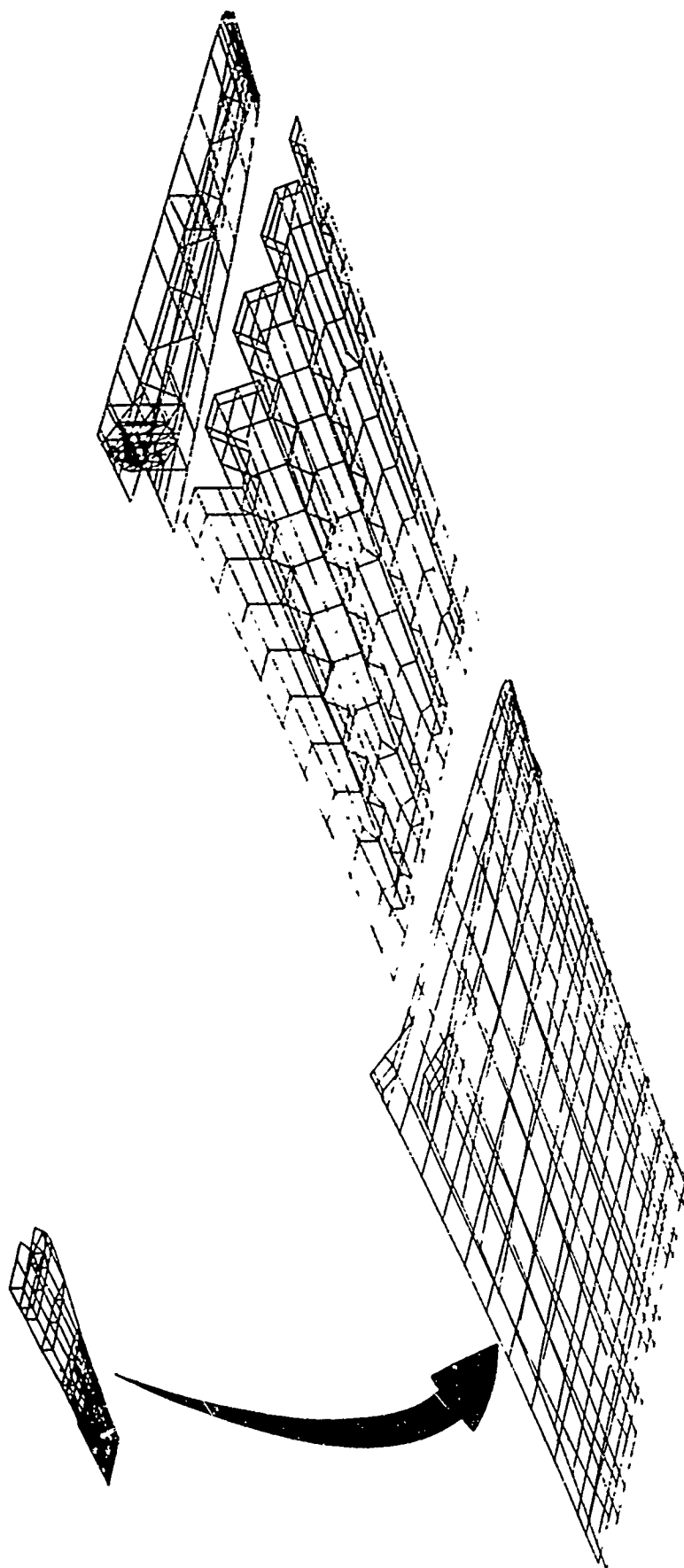


Figure 3-5. SPF Leading Edge Extension NASTRAN Model

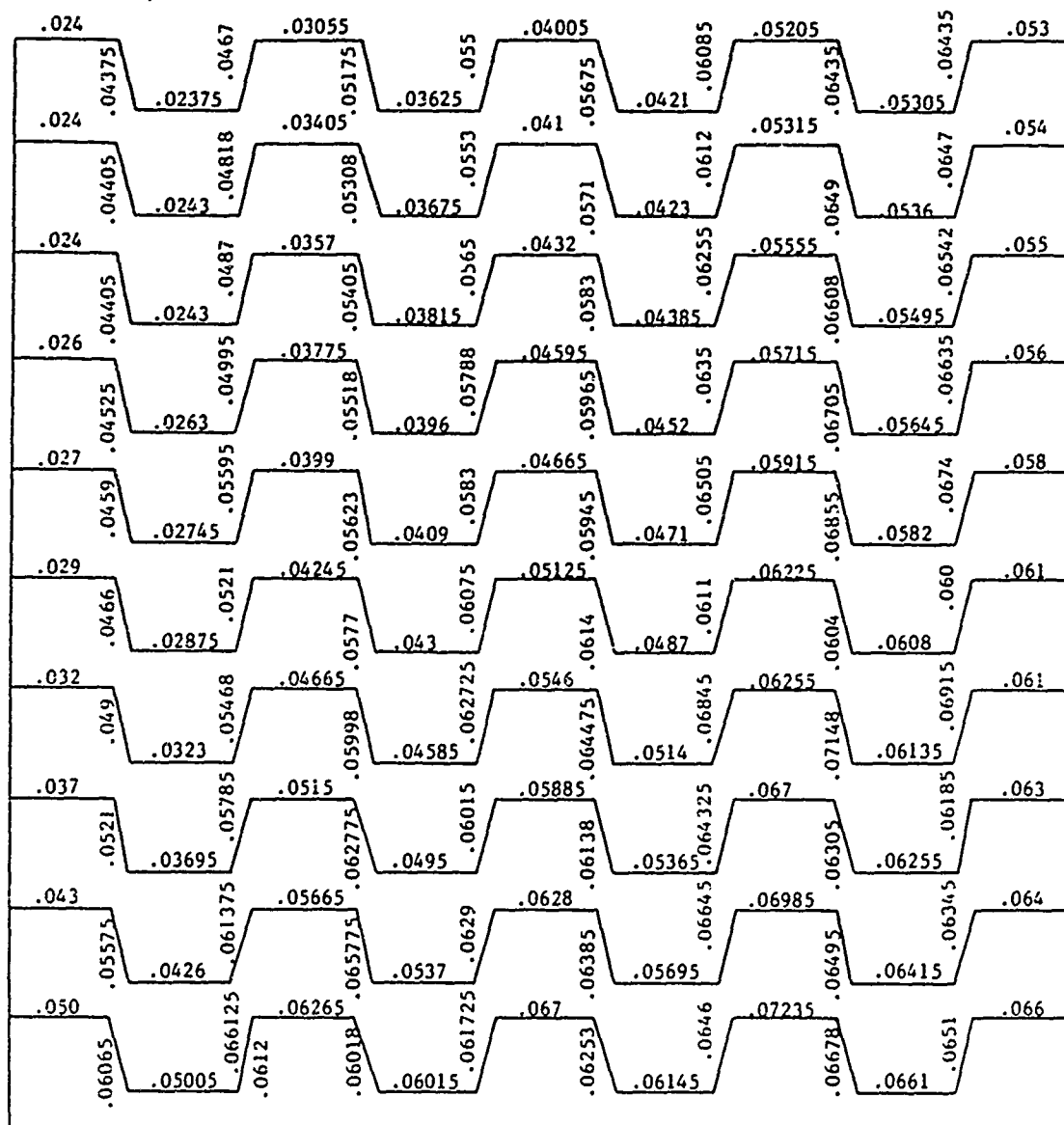


Figure 3-6. Leading Edge Extension Corrugation Thicknesses Variations

the structural behavior of the model, the third load case containing the actual flight pressure loads was run. The pressure loading on the LEX was a trapezoidal distribution running spanwise along the upper skin. The loads ranged from 9.97 to 18.02 psi, inboard to outboard respectively. The cross-sectional loading distribution is shown in Figure 3-7.

3.3 FINAL DESIGN

Since superplastically formed parts experience thinning reductions that are many times greater than what occurs in conventional forming, the geometry of the forming cavity and the relationship of the final part to this cavity had to be fixed before the final design and/or analysis. As a result, the final design of both candidate components was not completed prior to completion of Tasks II (Material Evaluation and Selection) and III (producibility Forming Tests). The findings of Task III in specific, were of great importance since they established the final design parameters such as cavity wall draft angles and edge and corner radii. The following paragraphs discuss the design modifications on both components and their final design.

3.3.1 Forward Avionics Deck

The final design of the avionics deck incorporated several changes. First, as discussed earlier, the major design revision was the elimination of the right- and left-hand side longerons and their replacement by overlapped edges of the upper skin, waffle pan, and lower skin. Secondly, since the original draft of the waffle pan depressions did not allow the pan's moldline flanges to match the existing antenna and door cutout flanges, the inboard side walls were eliminated and replaced by formers and intercostals, as shown in Figure 3-8. In addition, the aft center pocket on the waffle pan was eliminated, and the two narrow pockets of the left-hand side were joined to their neighboring pockets. The narrow pocket on the right-hand side was also joined to the neighboring pocket. These modifications

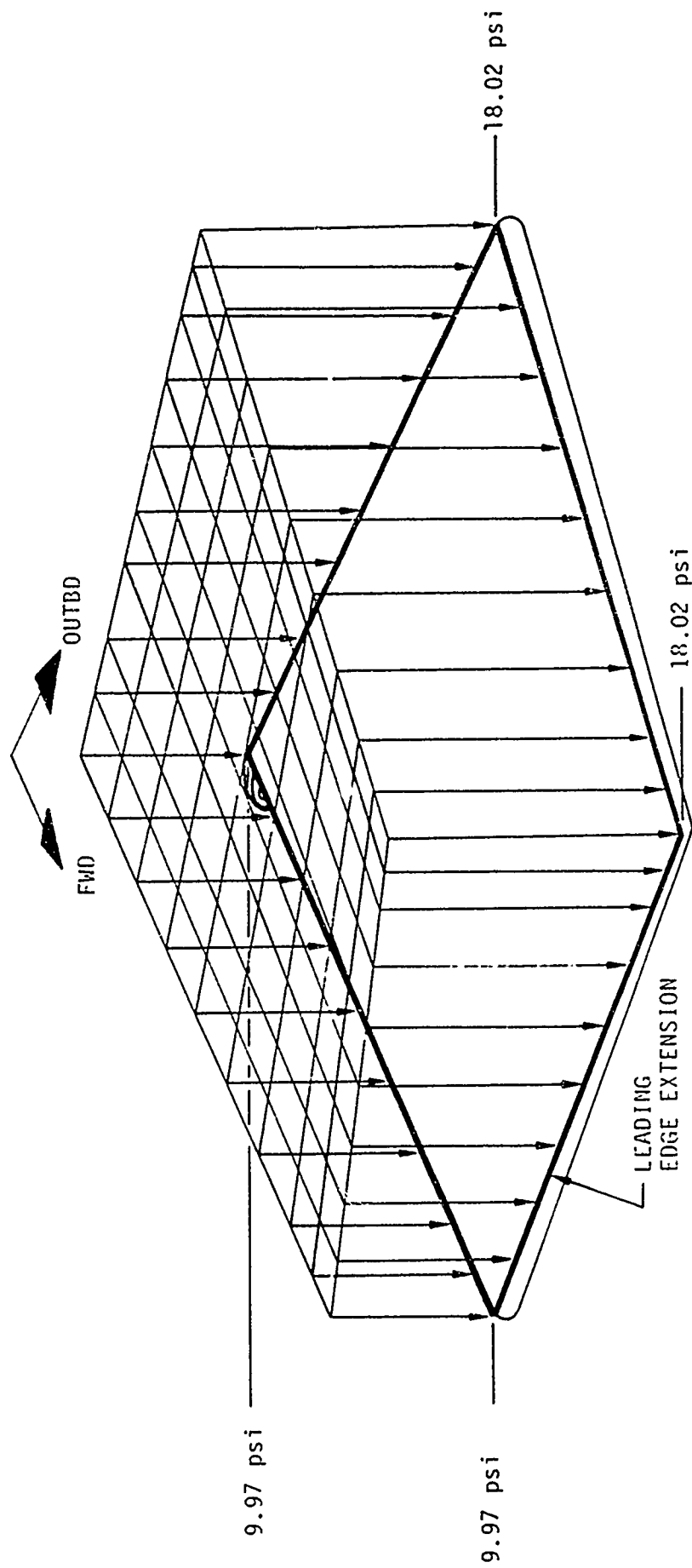


Figure 3-7. Leading Edge Extension Cross Sectional Pressure Loading

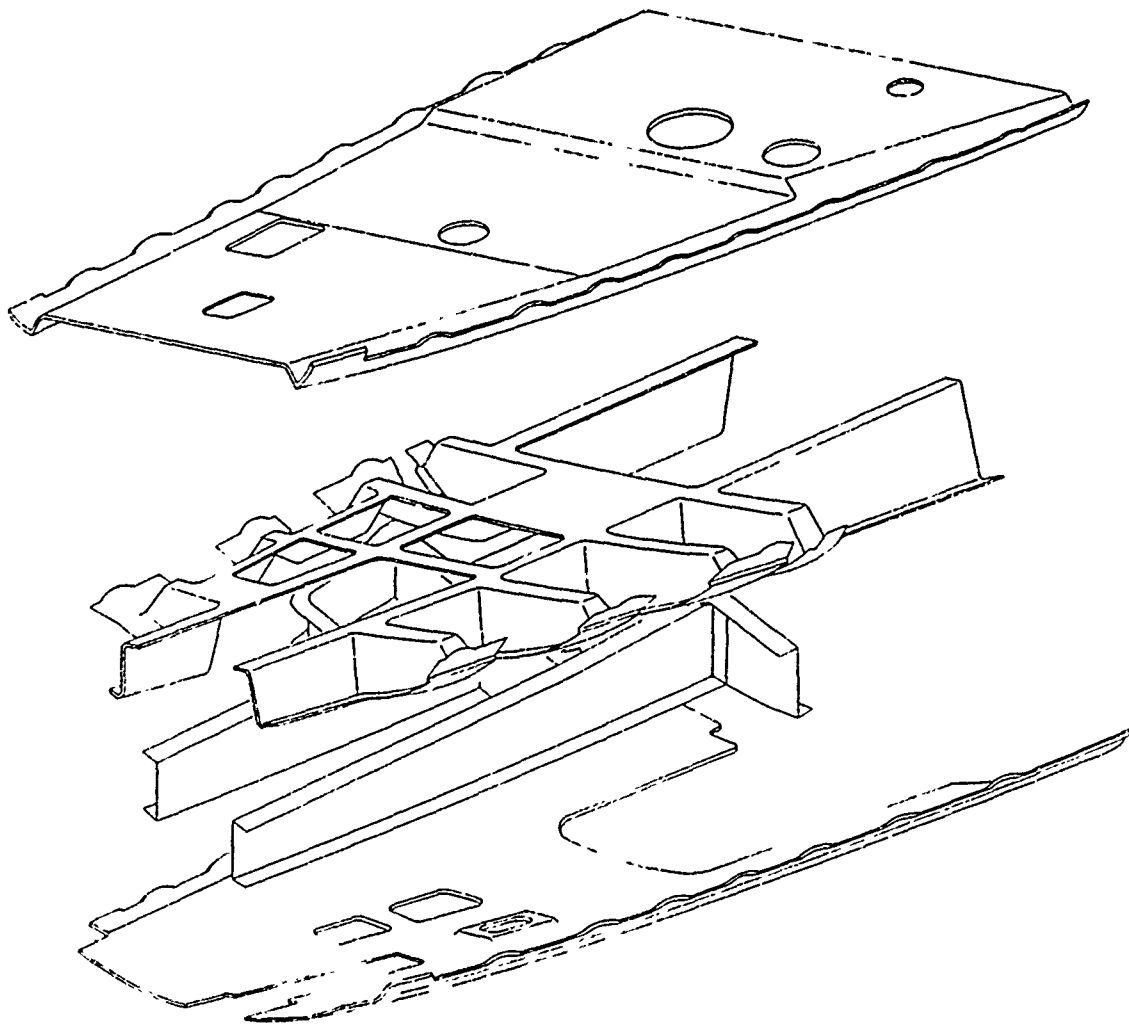
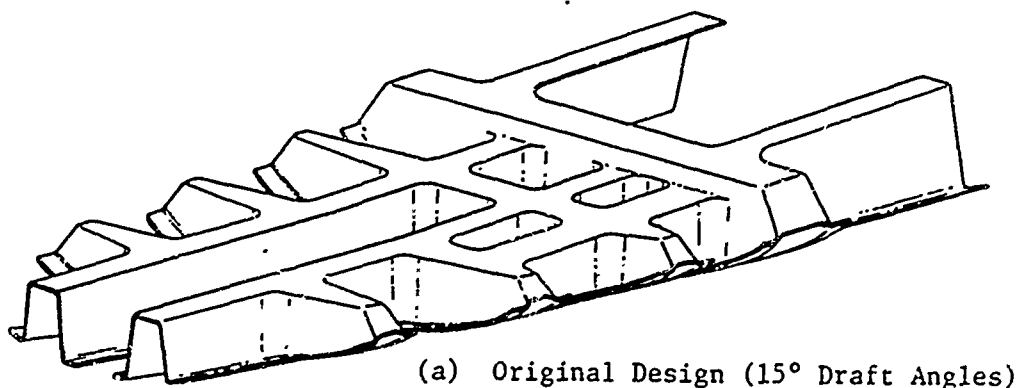
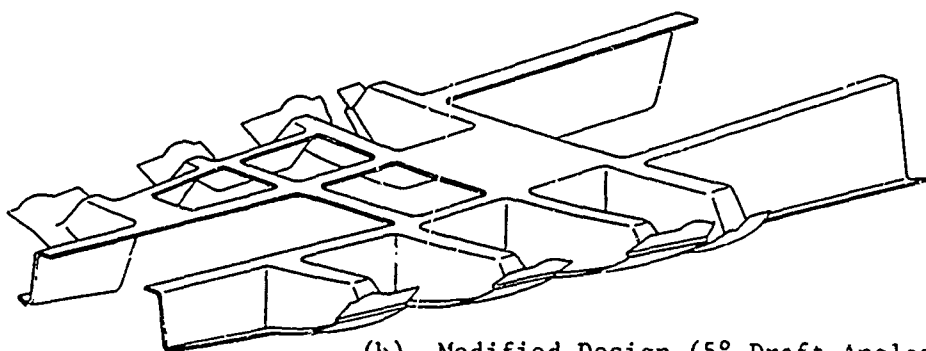


Figure 3-8. Final Avionics Deck SPF Design

were also in support of the producibility test results since the increased aspect ratio (width/depth) and slenderness ratio (length/depth) of the new pockets improved the thickness profile and provided a more uniform thinning. Figure 3-9 clearly represents the original and modified designs of the avionics deck waffle pan.



(a) Original Design (15° Draft Angles)



(b) Modified Design (5° Draft Angles)

Figure 3-9. Avionics Deck Waffle Pan Redesign

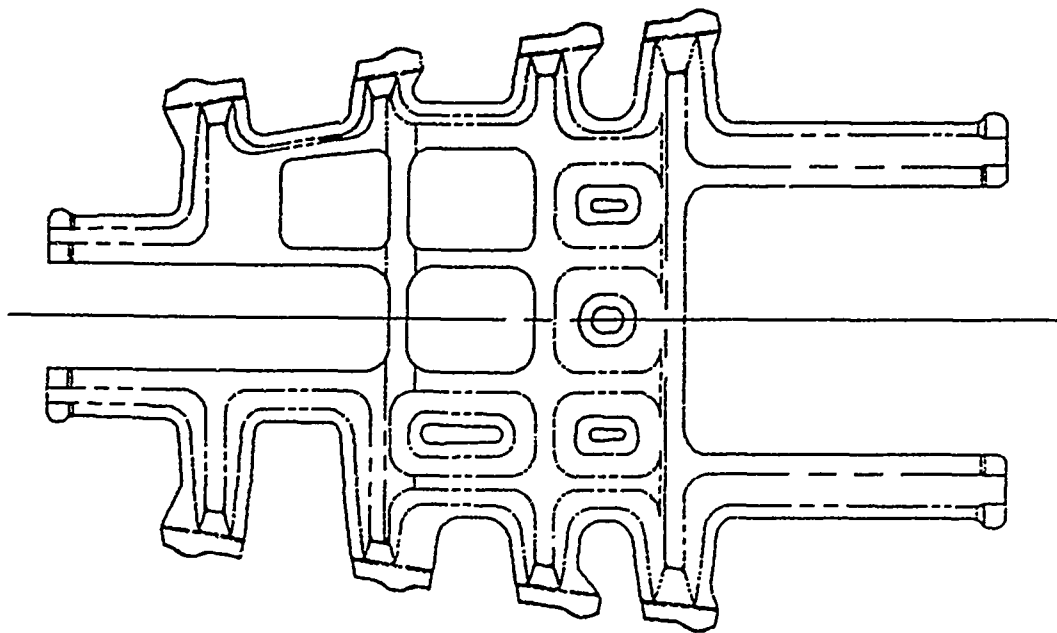
A third modification to the original design was the reduction of the waffle pan draft angles from 15 degrees to 5 degrees to further increase the uniform thinning. This change was also dictated by the producibility studies where forming of subcomponents with 15 degree draft angles showed excessive amounts of non-uniform thinning. The foregoing pan redesign indirectly influenced the upper skin design as the new draft angles shifted the pan flanges and consequently effected the skin trim pockets.

Finally, the lower flanges of the waffle pan, where the upper skin, waffle pan and lower skin joined, were modified to reduce the number of joggles on the lower skin flanges. All the joggles on the upper skin, waffle pan, and lower skin were eliminated at F.S. 47.50 and 87.50 for simplicity. This was done subsequent to a decision that the final avionics design would not be a flight article. The foregoing decisions were all made with the approval of the Air Force. The deck flange modifications are shown in Figure 3-10. As a result of the foregoing, the final SPF avionics deck design consisted of the following:

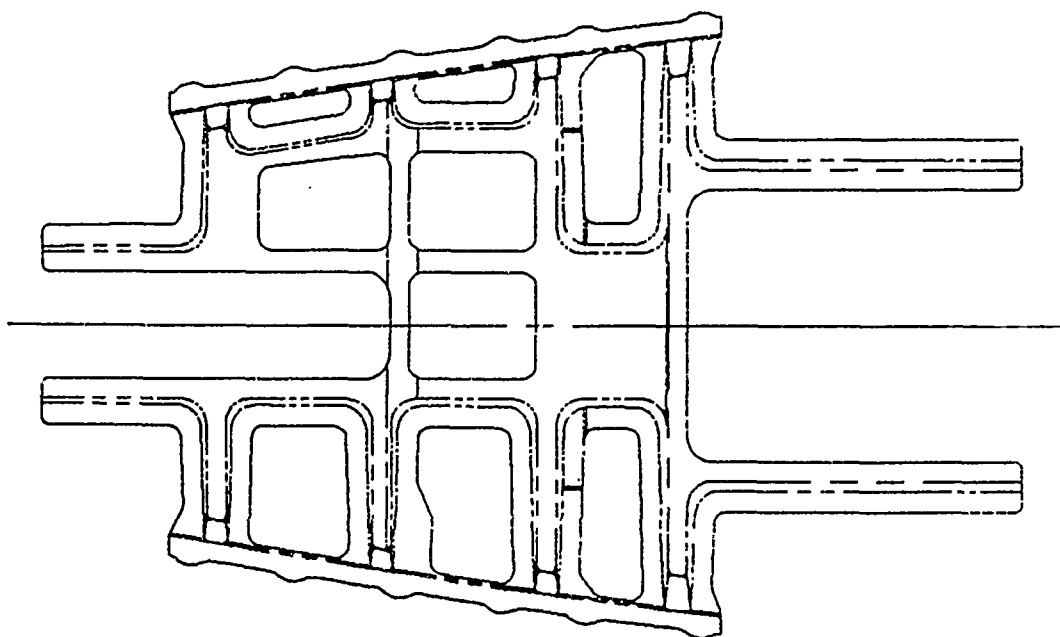
- (1) SPF Upper Skin
- (2) SPF Waffle Pan
- (3) SPF Lower Skin
- (4) Two Hydroformed Formers
- (5) Two Machined Formers
- (6) Three Hydroformed Intercostals

A total of ten structural details and the addition of the four access doors would increase the piece count to 14. However, when comparing the SPF to the baseline design, we could disregard the access doors which are common to both designs. The final detailed drawings of the SPF avionics deck are shown in Figures 3-11 through 3-14. These drawings were all generated by the CADAM (Computer Aided Design and Manufacturing) System.

The final LEX design was also modified due to the complexity involved in the fabrication of the original design. Further review of the original design showed that the outboard closeout skin could not withstand the crushing pressures during the welding process. Hence, as shown in Figure 3-15, the



(a) Old Design



(b) New Design

Figure 3-10. Avionics Deck Waffle Pan Flange Modifications

70 THRU 78
ARE FOLD OUTS

20003113

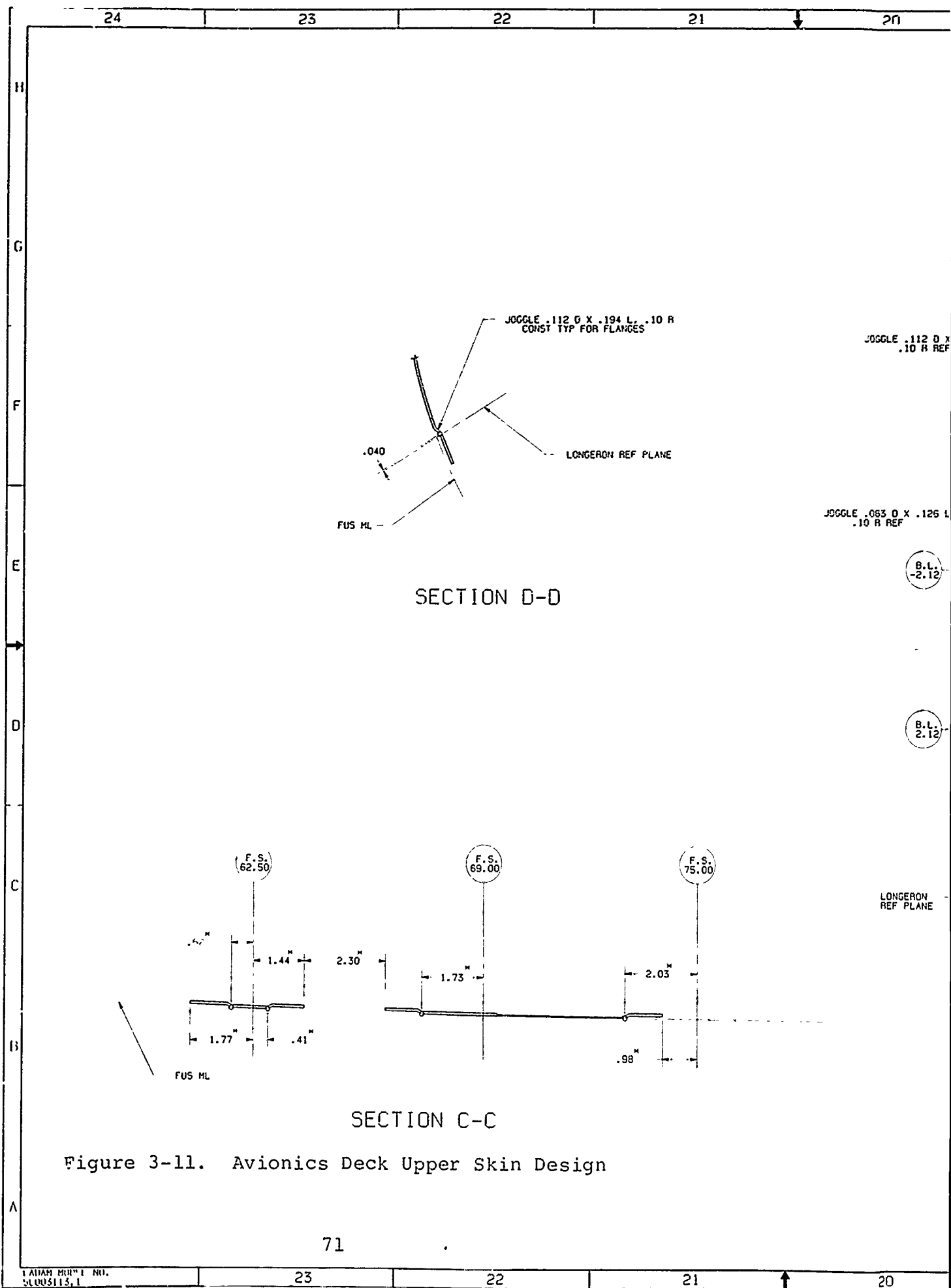
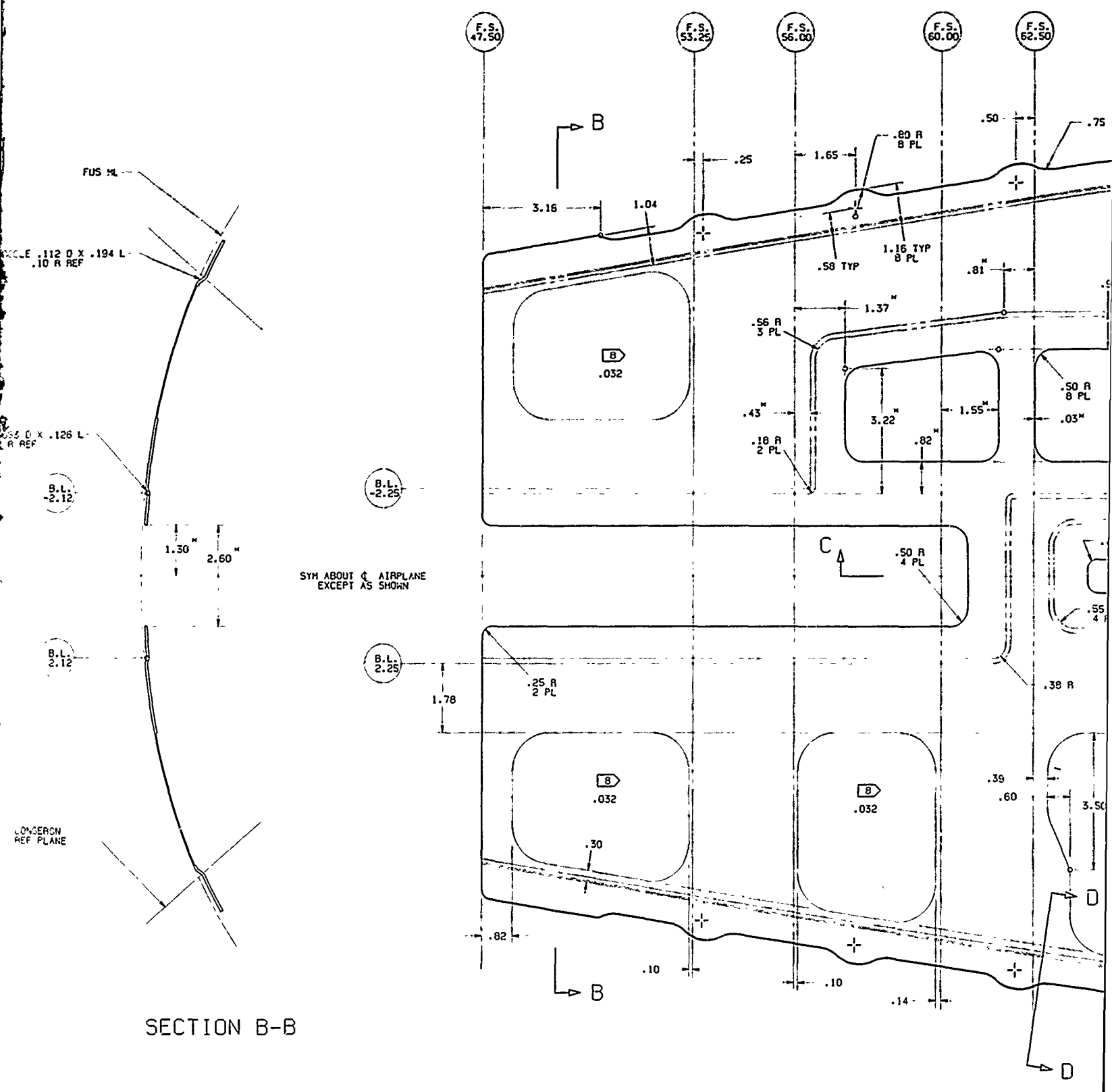


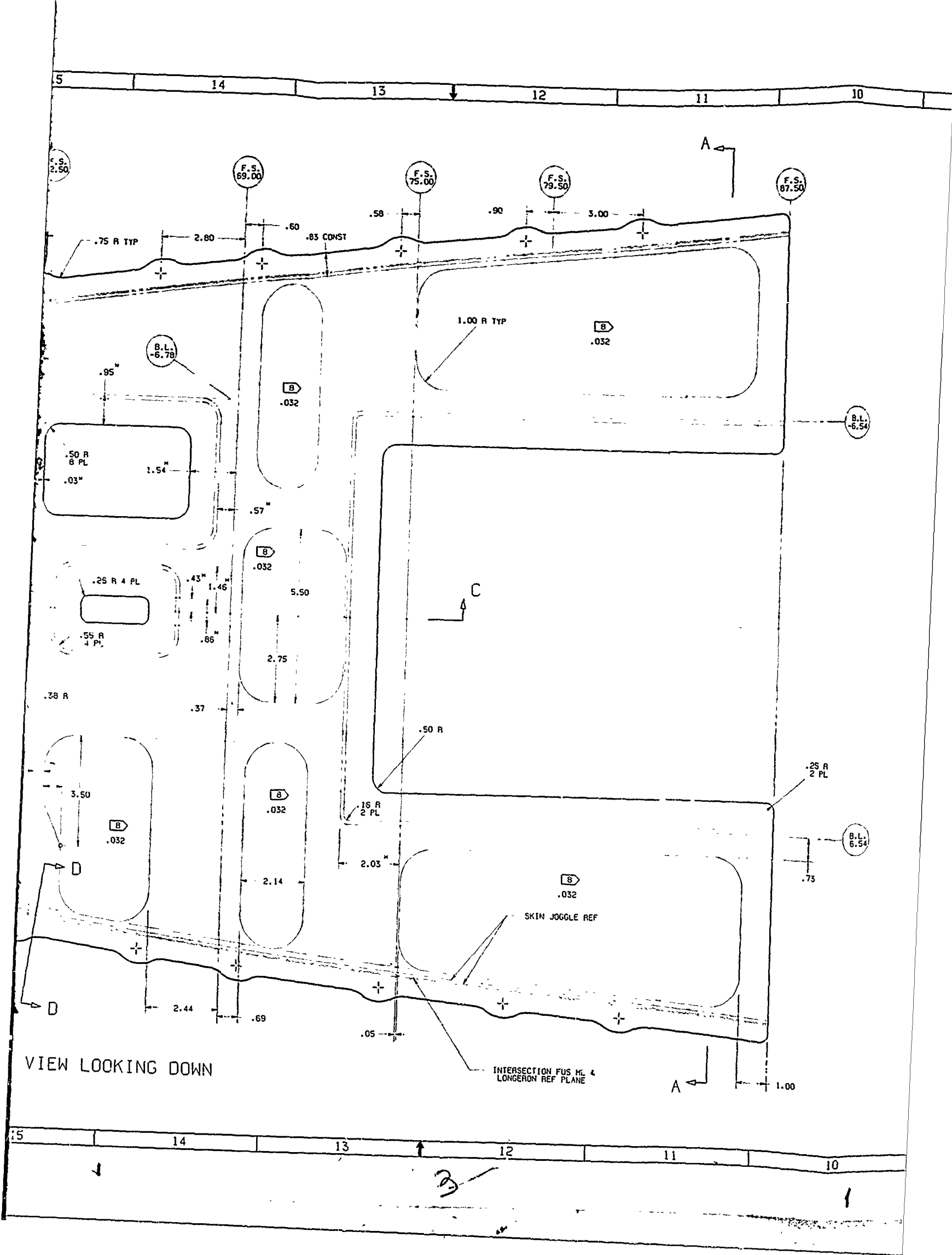
Figure 3-11. Avionics Deck Upper Skin Design

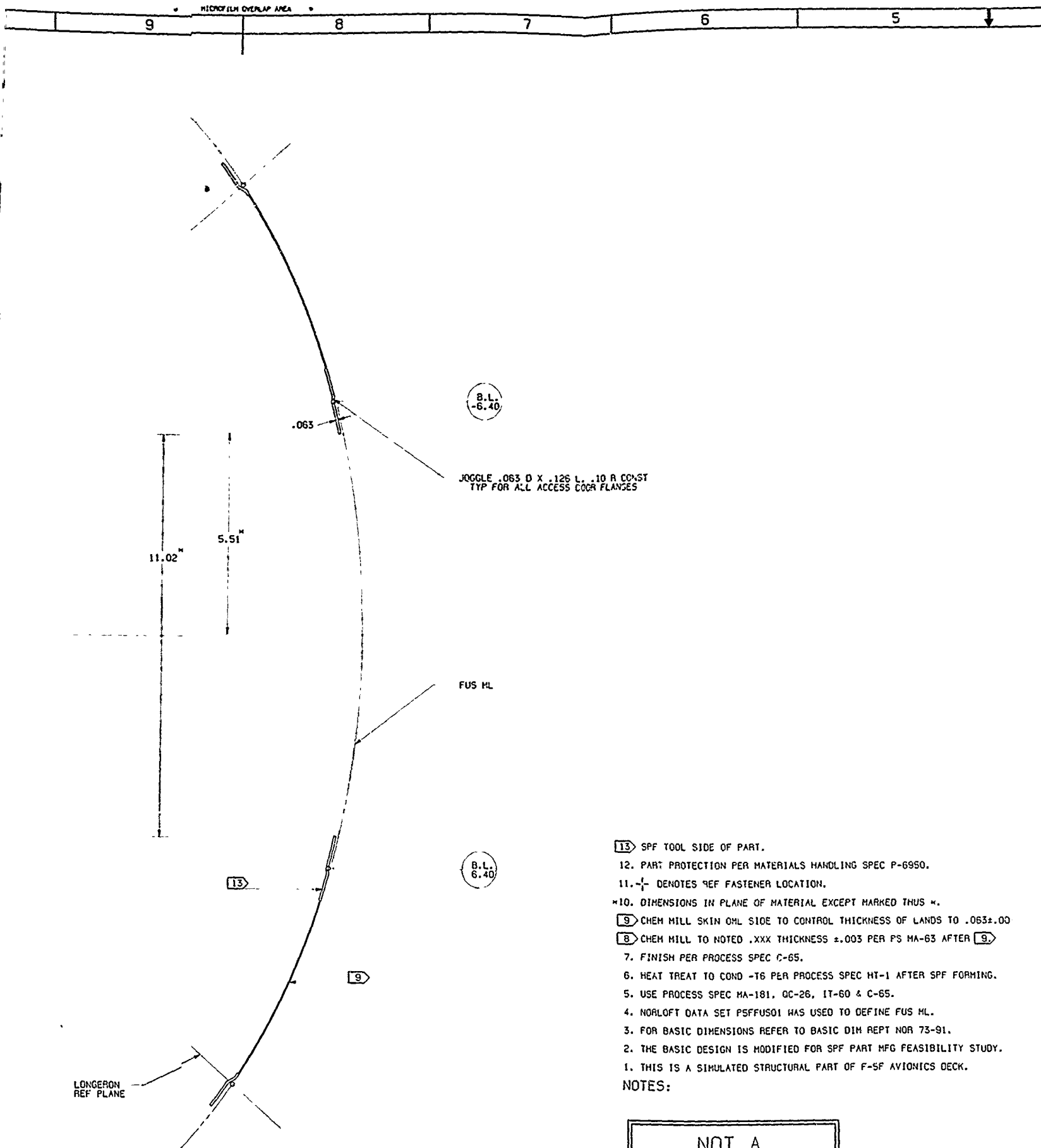


SECTION B-B

VIEW

SC003113 REV SH 1





13. SPF TOOL SIDE OF PART.
 12. PART PROTECTION PER MATERIALS HANDLING SPEC P-6950.
 11. -1- DENOTES REF FASTENER LOCATION.
 10. DIMENSIONS IN PLANE OF MATERIAL EXCEPT MARKED THUS.
 9. CHEM MILL SKIN OHL SIDE TO CONTROL THICKNESS OF LANDS TO .063±.00
 8. CHEM MILL TO NOTED .XXX THICKNESS ±.003 PER PS MA-63 AFTER 9.
 7. FINISH PER PROCESS SPEC C-65.
 6. HEAT TREAT TO COND -T6 PER PROCESS SPEC HT-1 AFTER SPF FORMING.
 5. USE PROCESS SPEC MA-181, QC-26, IT-60 & C-65.
 4. NORLOFT DATA SET PSFFUS01 HAS USED TO DEFINE FUS ML.
 3. FOR BASIC DIMENSIONS REFER TO BASIC DIM REPT NOR 73-91.
 2. THE BASIC DESIGN IS MODIFIED FOR SPF PART MFG FEASIBILITY STUDY.
 1. THIS IS A SIMULATED STRUCTURAL PART OF F-5F AVIONICS DECK.
- NOTES:

[illegible]

KEY TO BASIC CODES		CUSTOMER PROCESS SPEC.	
BASIC CODE		DASH NO. FOR DIA	
BASIC CODE FOR DIS-INSTALL		WANTED HEAD MEAS SIDE	
AL FOR PS		FOUND NO PAR SIZE	
		MANUFACTURED DRIVER HEAD	
WITH FLUSH COND ONLY		DASH NO. FOR LENGTH	
D-OMPLE		NOT SHOWN FOR ALL	
FIG -TIAL NO SHEETS		TYPES OF FASTENERS	
TO BE D-OMPLED			
C-COUNTDOWN			

[illegible]

2C003114

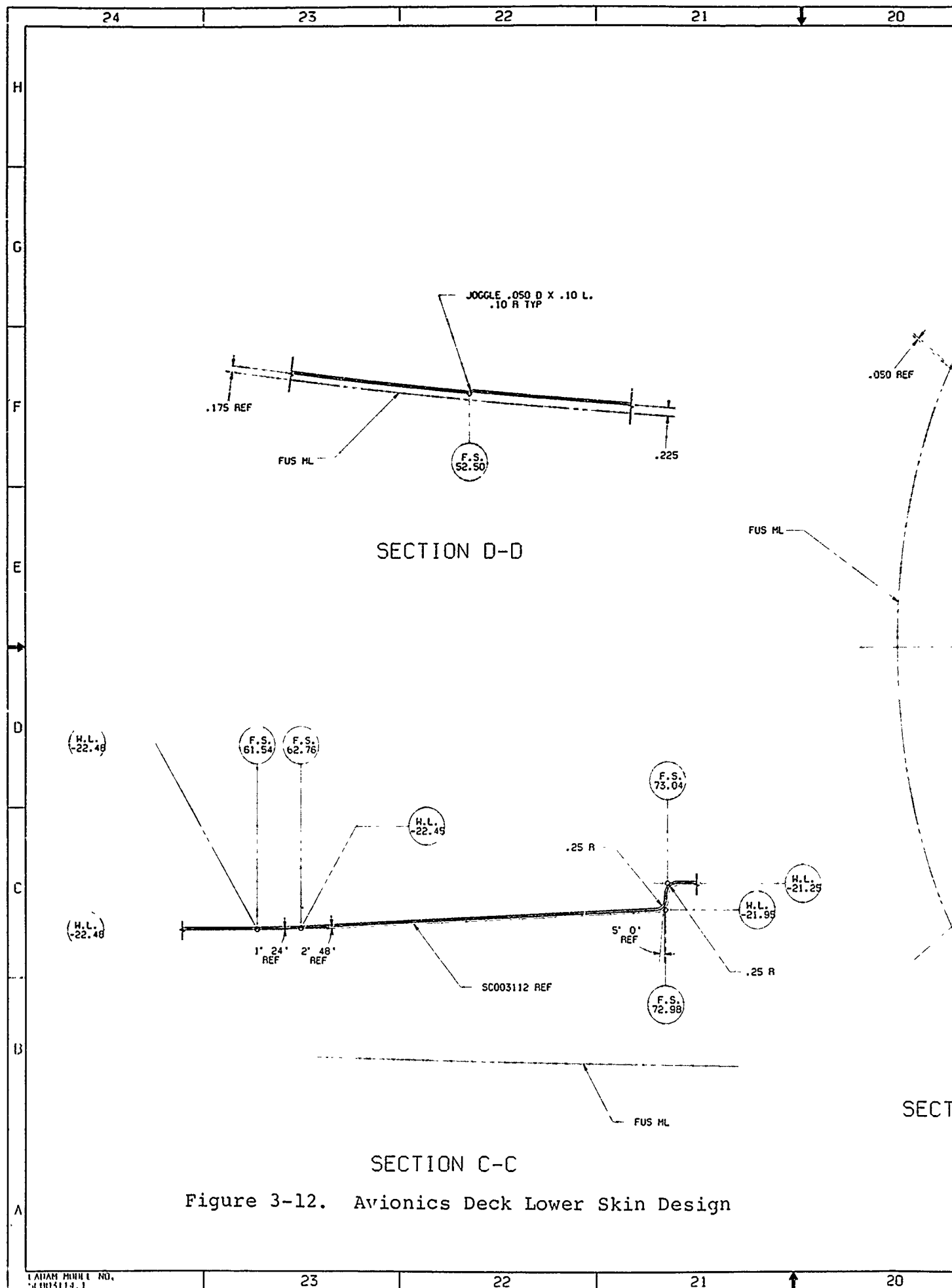


Figure 3-12. Avionics Deck Lower Skin Design

LAMAR MODEL NO.
SC003114.1

19

18

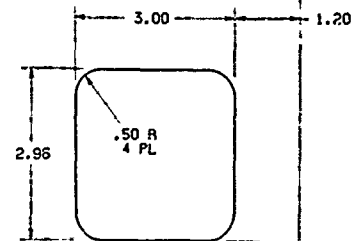
17

16

15

F.S.
47.50F.S.
52.50F.S.
61.54F.S.
62.76

B

II
X = -7.323
Y = 47.500
Z = -23.321II
X = -6.620
Y = 47.500
Z = -22.482SYM ABOUT C AIRPLANE
EXCEPT AS SHOWNFULL R
2 PL

C

.75 R

II
X = 6.620
Y = 47.500
Z = -22.482.25 R CONST
TYPII
X = 7.323
Y = 47.500
Z = -23.321

B

SECTION B-B

VIEW L

SC003114

REV
1

19

18

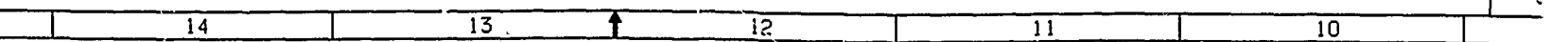
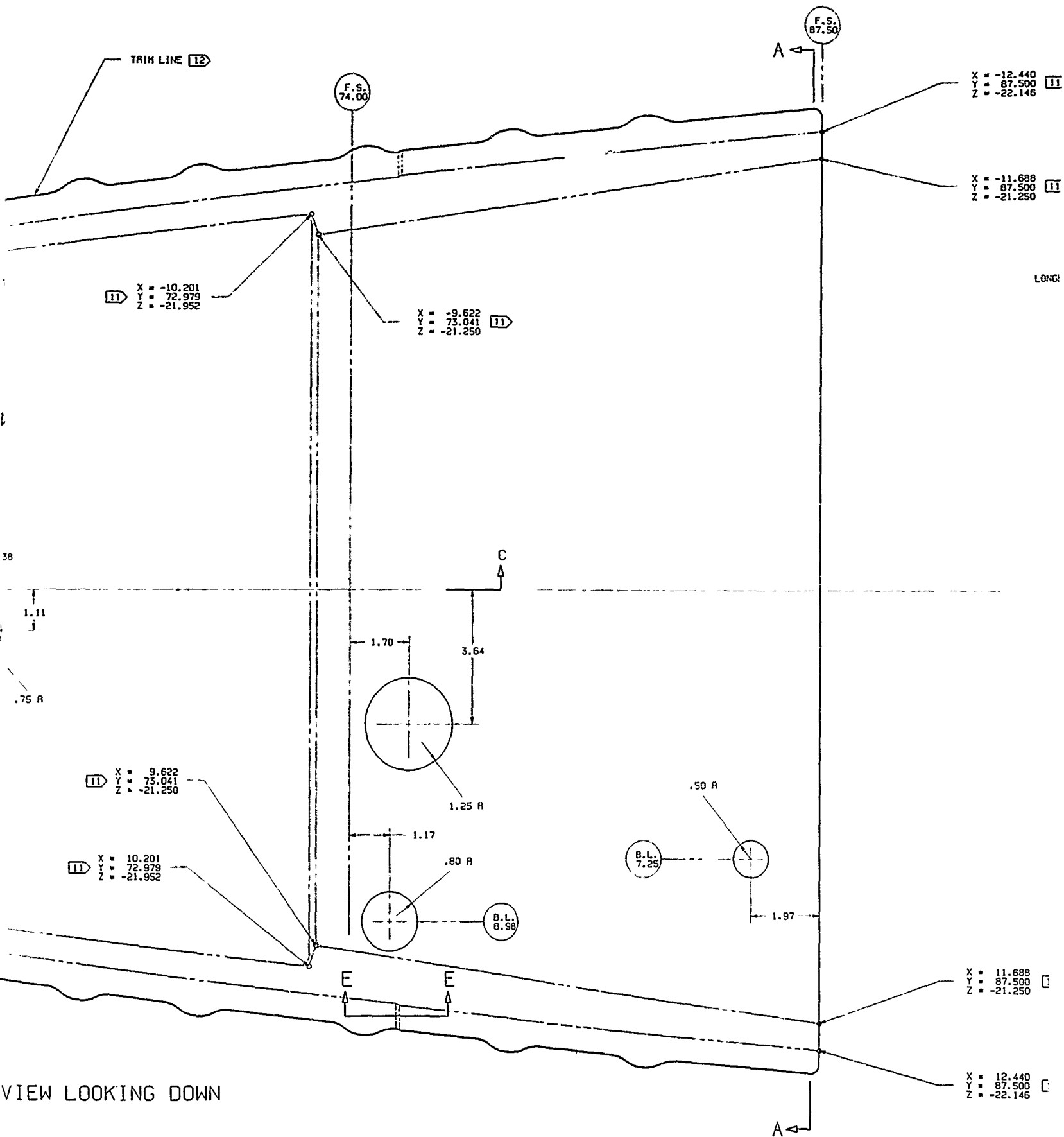
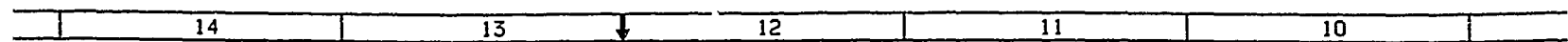
17

16

15

2

1



-12.440
87.500
-22.146

.175 TYP

.050 TYP

-11.688
87.500
-21.250

LONGERON REF PLANE

FUS ML

.050

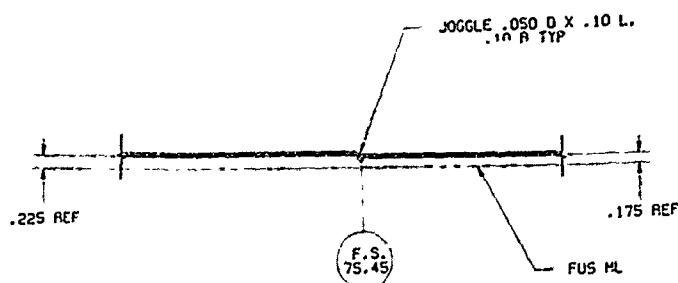
9

10 11

11.688
87.500
-21.250

12.440
87.500
-22.146

SECTION A-A



SECTION E-E

- 12 TRIM EDGES TO MATCH SC003113-1 SKIN.
- 11 ALL DEFINED PRINTS ARE ON THIS SIDE. (X = B.L. Y = F.S. Z = W.L.)
- 10 SPF TOOL SIDE OF PART.
- 9 CHEM MILL THIS SIDE TO CONTROL THICKNESS TO .050±.003.
8. PART PROTECTION PER MATERIALS HANDLING SPEC P-6950.
7. FINISH PER PROCESS SPEC C-65.
6. HEAT TREAT TO COND -T6 PER PROCESS SPEC HT-1 AFTER SPF FORMING.
5. USE PROCESS SPEC MA-SPF, OC-26, IT-60 & C-65.
4. NORLOFT DATA SET P5FFUS01 WAS USED TO DEFINE FUS ML.
3. FOR BASIC DIMENSIONS REFER TO BASIC DIM REPT NOR 73-91.
2. THE BASIC DESIGN IS MODIFIED FOR SPF PART MFG FEASIBILITY STUDY.
1. THIS A IS SIMULATED STRUCTURAL PART OF F-SF AVIONICS DECK.

NOTES:

NOT A
FLIGHT ARTICLE

REVISION	DATE	BY	CHKD
1	11/11/64	W. J. B. / J. W. B.	W. J. B. / J. W. B.
REVISIONS			
1. REVISED TO REFLECT CHANGES TO THE PART DUE TO THE RESULTS OF THE FEASIBILITY STUDY.			
2. REVISED TO REFLECT CHANGES TO THE PART DUE TO THE RESULTS OF THE FEASIBILITY STUDY.			
3. REVISED TO REFLECT CHANGES TO THE PART DUE TO THE RESULTS OF THE FEASIBILITY STUDY.			
4. REVISED TO REFLECT CHANGES TO THE PART DUE TO THE RESULTS OF THE FEASIBILITY STUDY.			
5. REVISED TO REFLECT CHANGES TO THE PART DUE TO THE RESULTS OF THE FEASIBILITY STUDY.			
6. REVISED TO REFLECT CHANGES TO THE PART DUE TO THE RESULTS OF THE FEASIBILITY STUDY.			
7. REVISED TO REFLECT CHANGES TO THE PART DUE TO THE RESULTS OF THE FEASIBILITY STUDY.			
8. REVISED TO REFLECT CHANGES TO THE PART DUE TO THE RESULTS OF THE FEASIBILITY STUDY.			
9. REVISED TO REFLECT CHANGES TO THE PART DUE TO THE RESULTS OF THE FEASIBILITY STUDY.			
10. REVISED TO REFLECT CHANGES TO THE PART DUE TO THE RESULTS OF THE FEASIBILITY STUDY.			
11. REVISED TO REFLECT CHANGES TO THE PART DUE TO THE RESULTS OF THE FEASIBILITY STUDY.			
12. REVISED TO REFLECT CHANGES TO THE PART DUE TO THE RESULTS OF THE FEASIBILITY STUDY.			

SC003114

REV SH
1

9

8

7

6

5

4

1

DATE 7/7	
CADAM DWG 1	

SECTION D-D



SECTION

F.S.
54.23

20	19	18	17	16	15
----	----	----	----	----	----

13 TRIM LINE

Technical drawing of a mechanical part, likely a bracket or arm. The drawing shows a horizontal base with a vertical section on the right. A dashed line indicates a fold or break in the part. Dimensions and labels are as follows:

- Top dimension: JOGGLE .050 D X .10 L.
- Below top dimension: .10 R TYP
- Label on the right: FUS ML
- Bottom left circular stamp: F.S. 69.62

SECTION F-F 13

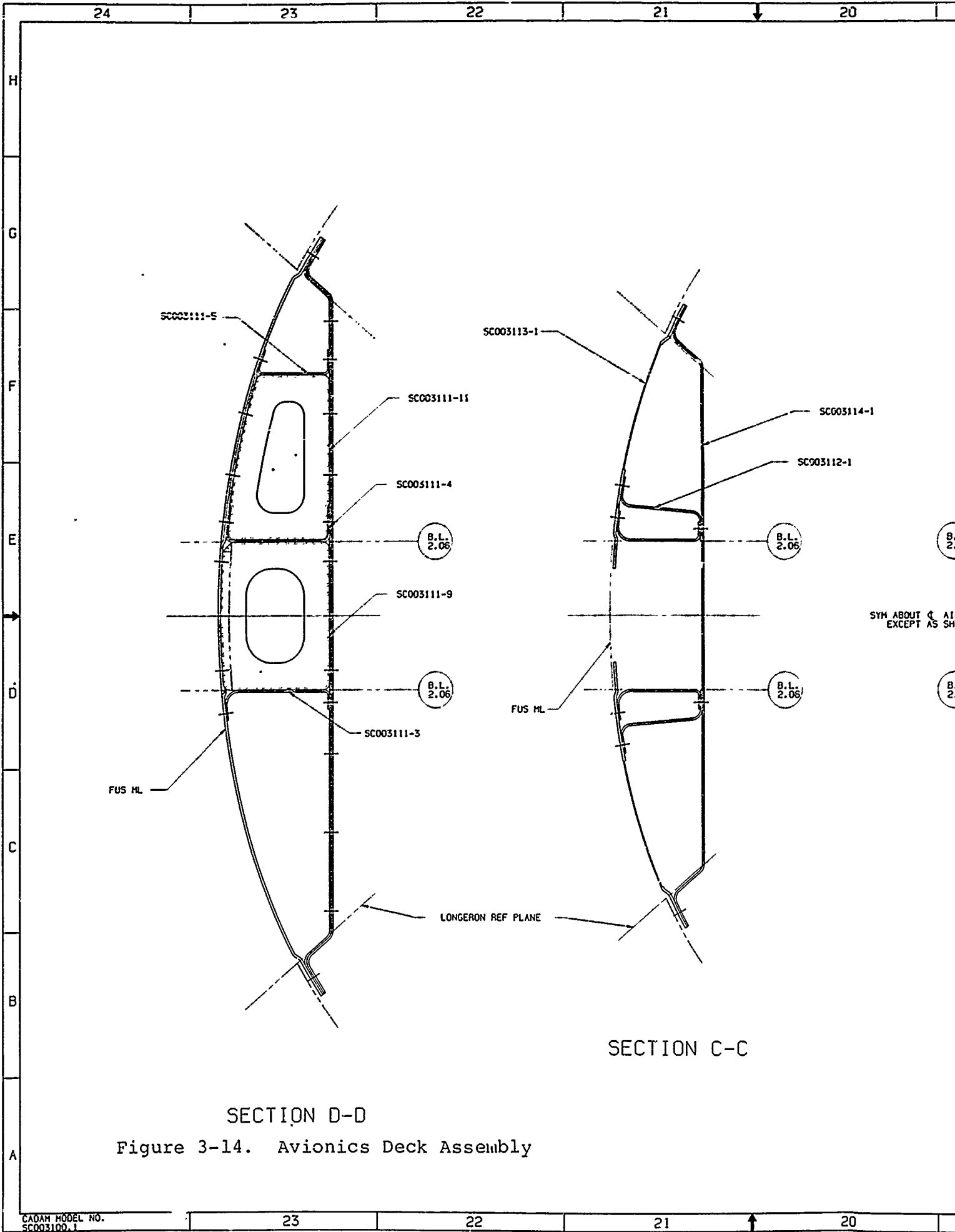
MATCH SC003113-1 SKIN.
 DIMENSIONS ARE ON THIS SIDE.
 OF PART.
 CONFORM PER MATERIALS HANDLING SPEC P-6950.
 INSURE THIS SIDE TO CONTROL THICKNESS TO .050±.003.
 DIMENSIONS MARKED THUS * ARE IN PLANE OF MATERIAL.
 PROCESS SPEC C-65.
 CONFORM TO T6 PER PROCESS SPEC HT-1 AFTER SPF FORMING.
 SPEC MA-SPF, QC-2E, IT-6Q & C-65.
 SET PSSFUS01 WAS USED TO DEFINE FUS HL.
 DIMENSIONS REFER TO BASIC DIM REPT NOR 73-91.
 DESIGN IS MODIFIED FOR SPF PART MFG FEASIBILITY STUDY.
 EVALUATED STRUCTURAL PART OF F-5F AVIONICS DECK.

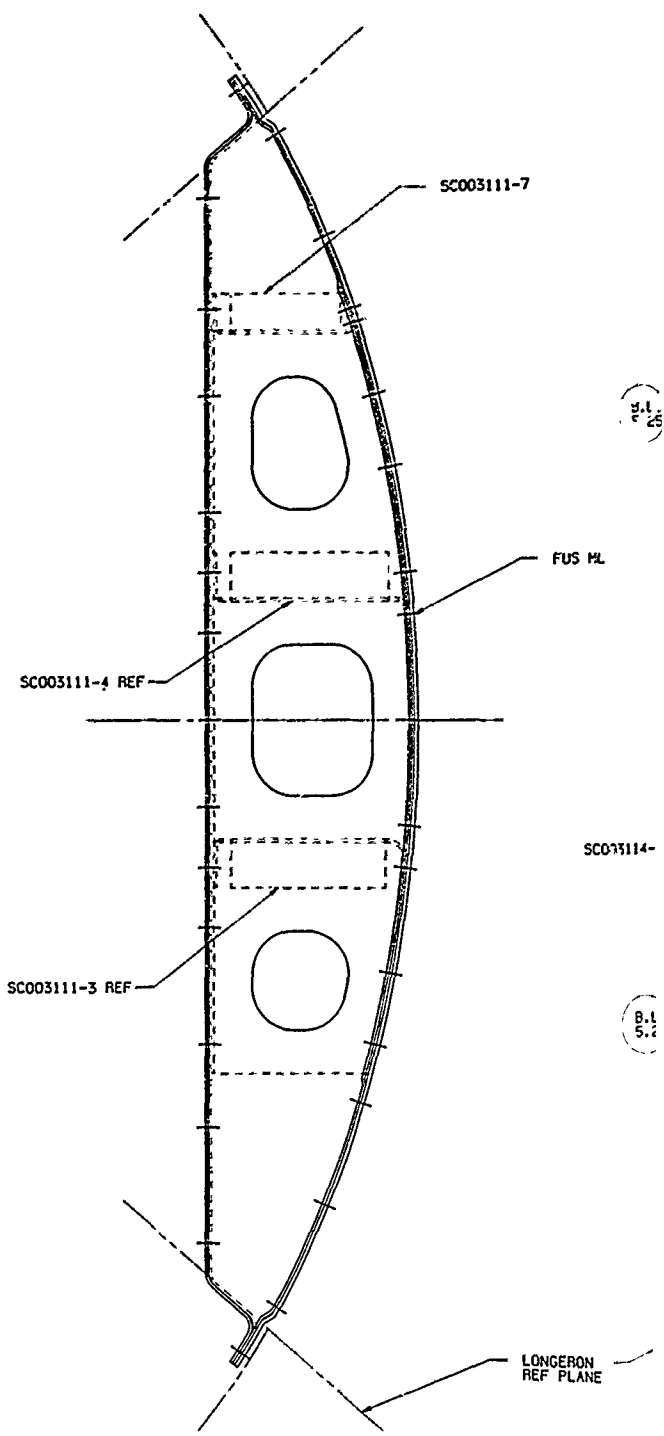
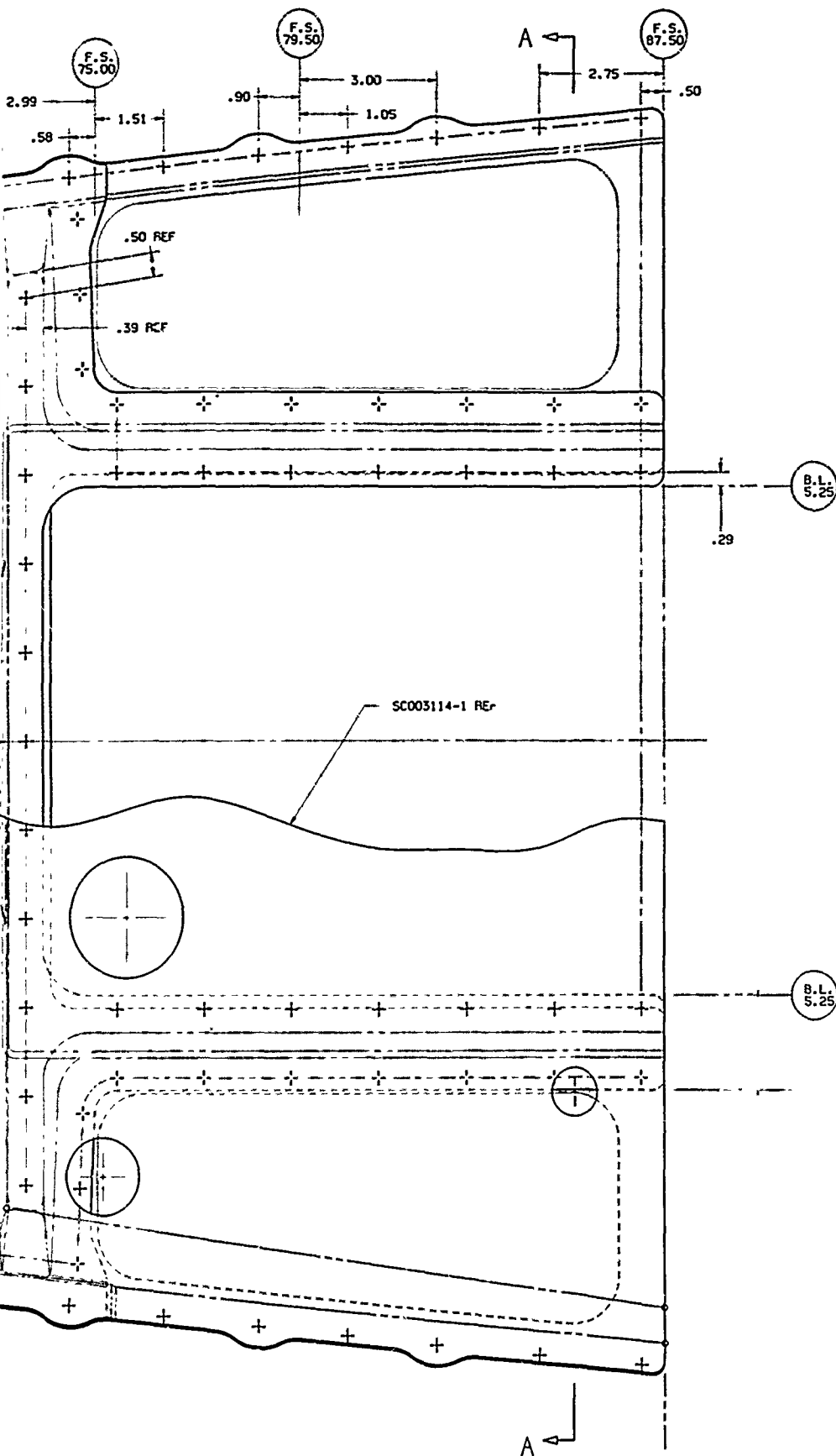
[illegible]

NOT A
FLIGHT ARTICLE

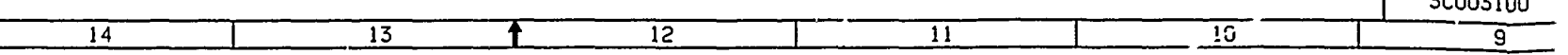
CADAM DWG, 1

SC003100





SECTION B-B



SC003100

3

1

MIDPOINT OVERLAP AREA

9

8

7

6

5

4

SC00311-7

SC003112-1 REF

B.L.
5.25

B.L.
5.51

FUS HL

SC003114-1 REF

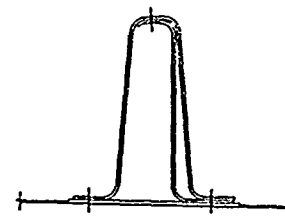
FUS HL

B.L.
5.25

B.L.
5.51

LONGERON
REF PLANE

SECTION A-A



SECTION E-E

11. USE HS20470AD4 FASTENER AT LWR FLANGE & REMOVE THE RIVETS AFTER CURE. MOUNT ACCESS DOOR USING EXISTING HOLES.
 10. + DENOTES FASTENER LOCATIONS AT UPR & LWR FLANGES.
 9. INSTALL RIVETS WITH FLUSH HEAD ON SKIN OHL SIDE & DECK UPR FLG SIDE.
 8. ALL FASTENERS EQUALLY SPACED BETWEEN LOCATED FASTENERS.
 7. BOND WITH A1444B ADHESIVE, AS MODIFIED AND CURED PER PROCESS SPEC XMS-HBA EXCEPT BONDING PRESSURE TO BE PROVIDED BY FASTENERS ONLY.
 6. USE HS20426AD4 FASTENER. IF NOT APPLICABLE, USE NAS1399-4 BLIND RIVET, GRIP LENGTHS TO BE DETERMINED ON ASSY.
 5. PART PROTECTION PER MATERIALS HANDLING SPEC P-6950.
 4. PRIOR TO ASSY, INSTALL STRAIN GAGES PER DEPT/3855 DIRECTION.
 3. DIMENSIONS MARKED THUS * ARE IN PLANE OF MATERIAL.
 2. FOR BASIC DIMENSIONS REFER TO BASIC DIM REPT NOR 73-91.
 1. THIS IS A SIMULATED STRUCTURAL PART OF F-5F AVIONICS DECK.
- NOTES:

NOT A
FLIGHT ARTICLE

XXCXXXX	XXXX
REF TO BASIC CODE	REF TO BASIC CODE
BASIC CODE	BASIC CODE
DATE CODE IN BOX-INSTALL	DATE CODE IN BOX-INSTALL
REF TO PL PL PL	REF TO PL PL PL
WITH FLUSH COND ONLY	WITH FLUSH COND ONLY
QUANTITY	QUANTITY
FIG-TOTAL NO SHEETS	FIG-TOTAL NO SHEETS
TO BE SIMPLY	TO BE SIMPLY
EXCERPTS	EXCERPTS

SC003100

REV SH
1

9

8

7

6

5

4

[illegible]

ASC .3855 01/28/85

2C003100

SC003100

1 A

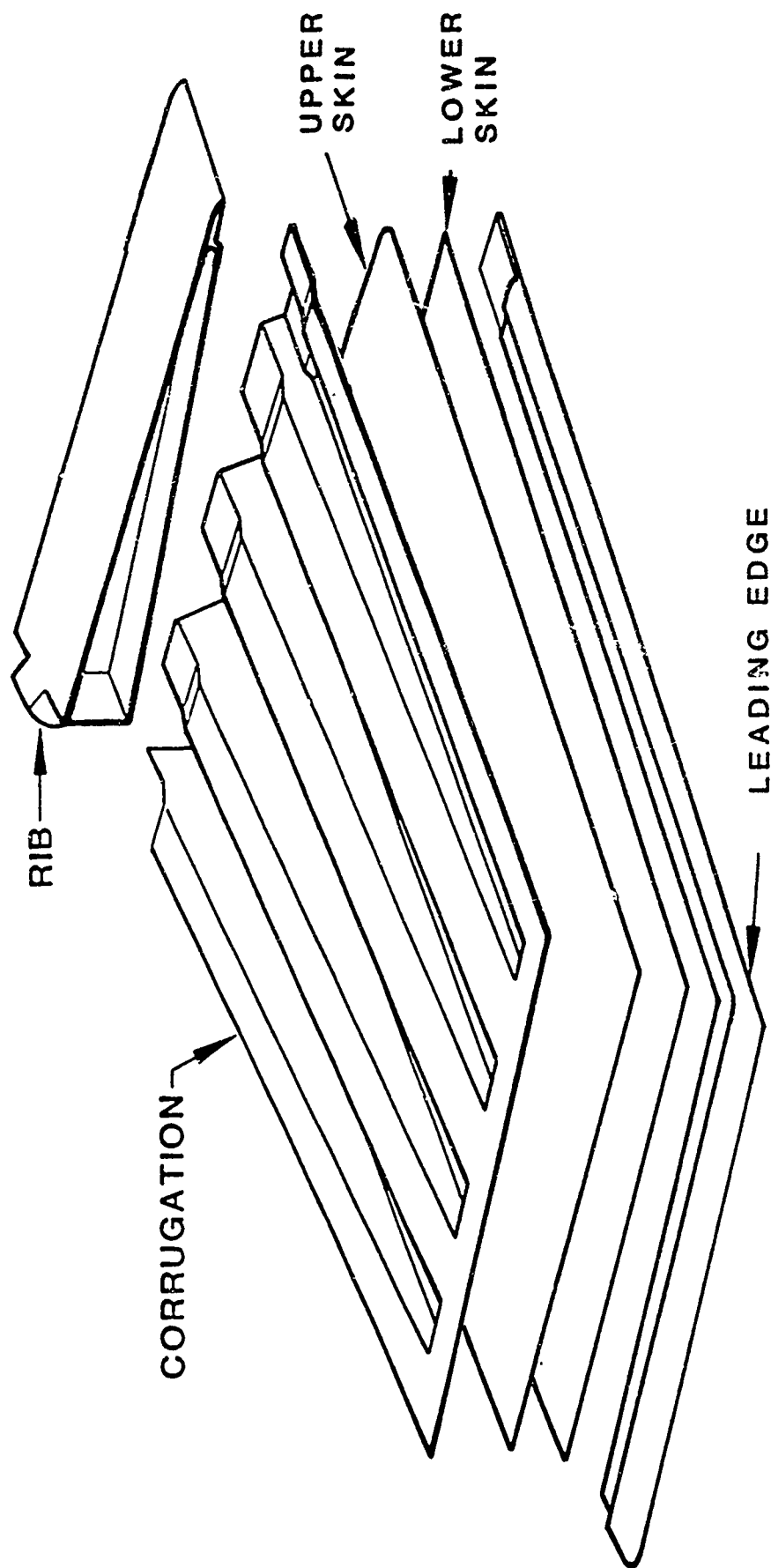


Figure 3-15. Modified Leading Edge Extension SPF Design

outboard closeout skin was made into one solid piece continuous with the leading edge. The new LEX design had a total of five parts, upper and lower skins, leading edge, corrugation and closeout rib. The machined leading edge was also modified in the area where it met the rib to allow for a smooth load transition.

Another design revision subsequent to producibility studies was the modification of the corner radii. Since thinning and cavitation measurements of the original LEX producibility subcomponent had shown unfavorable results, the corner radii were changed from 1/4 to 3/8 inch, to decrease the amount of thinning in that area.

3.4 DESIGN CONSIDERATIONS

The foregoing sections discussed the design modifications on both the avionics deck and the LEX. In order to arrive at the best design of a SPF structure, we need to consider several factors. Other than the geometry and the forming parameters of the selected material, the component forming feasibility needs to be investigated to avoid problems such as sub minimum thicknesses and/or cavitation.

As evidenced by the avionics deck and LEX redesign, most of the design modifications were dictated by the forming feasibility test results. These studies are perhaps the most important factor in the design of any complex SPF structure. During these studies, subcomponents representing the most severe areas of the component are fabricated and tested. This is done to assess the producibility of the component based on the assumed initial design parameters. In case the studies show unfavorable results, such as cavitation problems and/or undesirable sheet thicknesses, a modified design of the component is carried out. As a result, parameters such as material gage, draft angles, and edge and corner radii could all be modified.

It is important to note that these design parameters requiring modifications are in no way general to the SPF process. They are instead, a unique characteristic of the component under design. Furthermore, the producibility studies are not a general design requirement. In fact, once these studies have been conducted successfully on a particular material, the accuracy of the available analytical thinning prediction methods is assured for that material. However, since these semi-empirical techniques are not explicitly material dependent, the forming feasibility studies become a requirement when dealing with a new material system.

3.5 FINAL ANALYSIS

The final analysis of the avionics deck and LEX included a detailed review of the output loads and an assessment of their structural integrity after all design modifications. A rigorous finite element model was necessary because; (1) the thickness gradients due to the forming process and the discontinuous load paths were not easily evaluated by conventional analysis and (2) to ensure successful redistribution of the loads as compared to the baseline.

A total of nine loading conditions were evaluated for the avionics deck:

- (1) Two supersonic inflight conditions
- (2) Two subsonic maneuver conditions (yaw and roll)
- (3) Three taxiing conditions
- (4) Two miscellaneous pressurization conditions

The most critical loading condition was the supersonic symmetrical pull up at Mach 1.3 (SAB 13010), including internal pressure

and inertial loading performed at 7.33g's at an intermediate weight. The rigorous NASTRAN model and all of the loading conditions were used to represent the actual structure as accurately as possible.

The entire model of the nose, with an exploded view of the components of the deck, was shown in Figure 3-4. More than 3,000 elements composed the avionics deck model which included six degrees of freedom for each grid point; three in the rectangular coordinate system and three in the rotational coordinate system. The results gained from the model included the achievement of an acceptable convergence level and reasonable internal loading, deflections, and stresses.

Figure 3-16 shows a superimposed plot of the deformed and undeformed shapes of the deck and pan which were separated for clarity. The deformed shapes are a result of the most critical loading condition. These deflections have been scaled up many times so as to provide ease in viewing the overall bending from the cantilevered edge at the bulkhead at F.S. 87.50. The actual deflection was approximately 0.13 inch. Some localized twisting occurred at the access holes due to unsymmetrical characteristics of the substructure. The peak stresses ranged from 4,500 to 12,000 psi at the critical areas located about 1/3 the distance from the cantilevered edge. The critical areas were checked for buckling and crippling of the pan. In all instances, the margins of safety achieved were high. A thinning analysis was performed on the critical area of the pan. The results of this analysis showed the most critical web located at the same area could be thinned to 0.037 inch.

A post-NASTRAN program called NOR-POST was processed to generate the major principal stresses of all elements. A detailed review of the loading on all models showed the loading to be non critical factor in case of the avionics deck. In fact as review of the skin model indicated, the stress levels on three

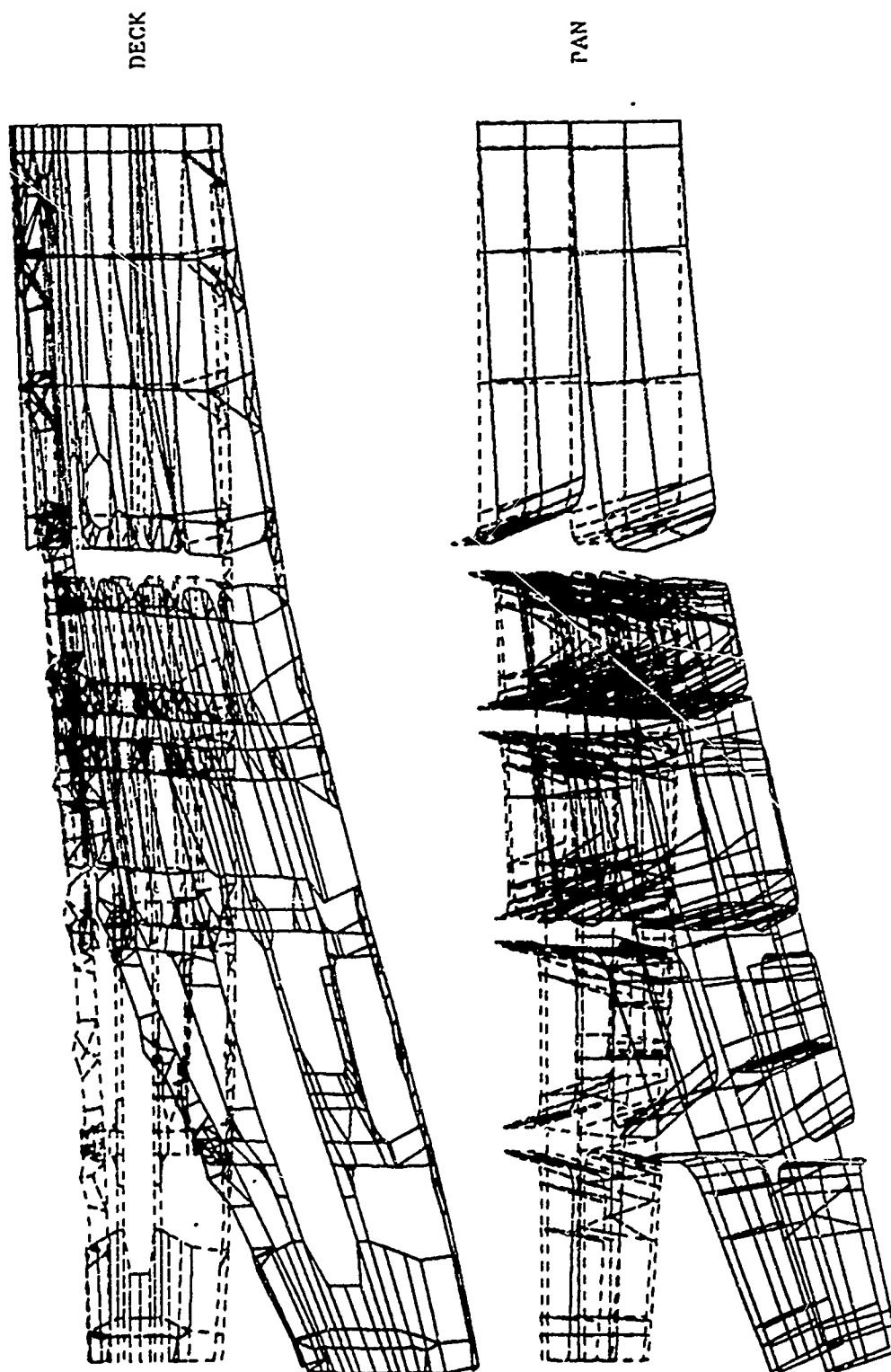


Figure 3-16. Superimposed Plot of the Deformed and Undeformed Avionics Deck

elements were in the area of 12,000 psi for the most critical loading condition (SAB 13010). These were element number 159509 with a stress of -11,596 psi, element number 160011 with a stress of -12,836 psi and element number 161709 with a stress of -12,200 psi. Review of the inner skin and pan models indicated similar results for all load conditions. Therefore, a secondary review of the model was conducted to assess the effects of all design modifications.

Figure 3-17 represents a comparison of two pan sections with the original and modified draft angles. As seen in the diagram, the actual shear load carried by the pan walls is: $V_1 = V/\cos \theta_1$ for case (1) and $V_2 = V/\cos \theta_2$ for case (2).

Assuming the vertical shear V remaining constant for both cases:

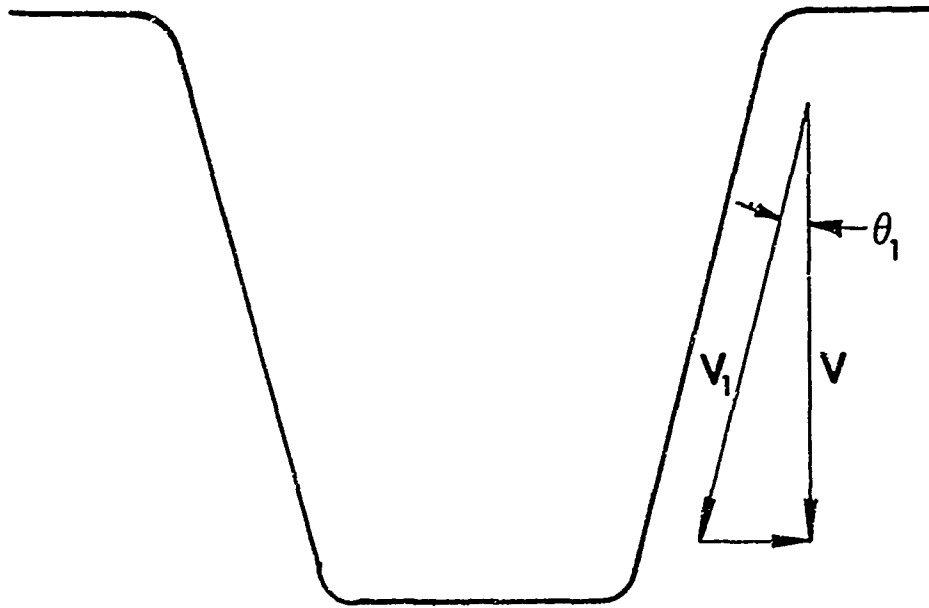
$$V_2/V_1 = \cos \theta_1 / \cos \theta_2$$

or in case of the waffle pan when θ_1 , (original draft angle) = 15° and θ_2 (modified draft angle) = 5°

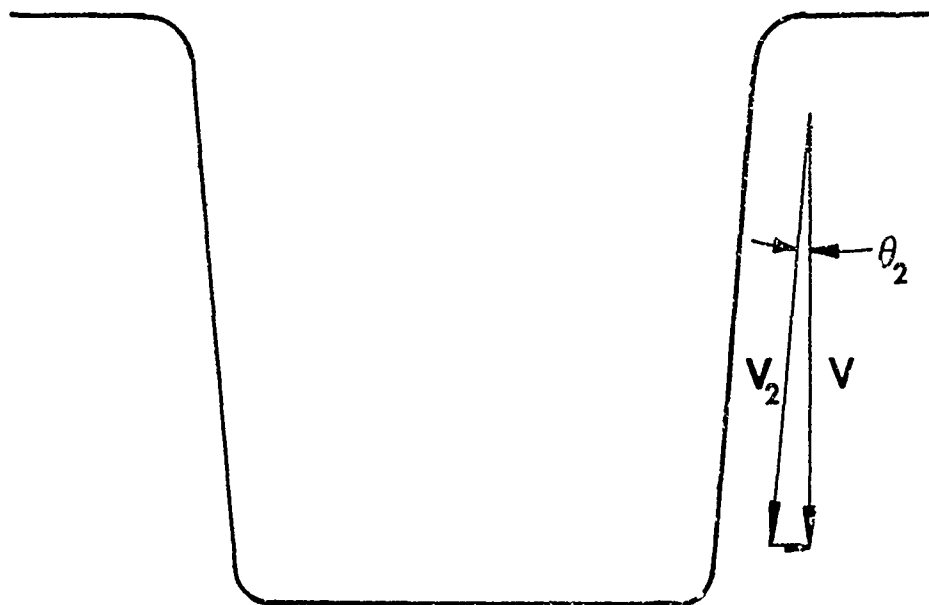
$$V_2/V_1 = \cos 15^\circ / \cos 5^\circ = 0.975$$

This indicates that a change in the wall draft angles does not change the shear loads substantially. Further reviews of the model also showed the stiffness of the modified deck to be sufficient for the prescribed loading. Overall, the NASTRAN model proved the validity of the design concept and it was concluded that the limiting factor of the design concept was the forming parameters rather than the stress levels.

In the case of the LEX, the original stress results from the flight pressure load case were low enough (less than 16 ksi) to allow the upper and lower skin to be thinned down from 0.065 inch to 0.050 inch. The results of the original NASTRAN



(a) TYPICAL PAN POCKET, OLD DRAFT ANGLE $\theta_1 = 15^\circ$



(b) TYPICAL PAN POCKET, NEW DRAFT ANGLE $\theta_2 = 5^\circ$

Figure 3-17. Comparison of Avionics Deck Waffle Pan Sections With Different Draft Angles

run yielded the maximum major principal stress of 35,565 psi located on the forward, inboard upper skin of the LEX (Element 22101). This stress was localized occurring in the area of the lug, a location which took the majority of the loading. The minimum major principal stress was -4,760 psi, located on the lower skin of the LEX in the same area as the maximum stress.

Overall, the stresses on the upper skin of the LEX were low (<10 ksi). The maximum major principal stresses (>10 ksi) are given in Table 3-1, and the locations of these stresses are shown in Figure 3-18. The stress plot of the major principal stresses on the upper skin of the LEX FEM are shown in Figures 3-19, 3-20 and 3-21 which show the chordwise and spanwise stress distribution. Further review of the NASTRAN loads showed the LEX redesign to have no significant effects on the structural adequacy of the part.

TABLE 3-1. LEX MAXIMUM MAJOR PRINCIPAL STRESSES

ELEMENT ID	STRESS (KSI)	ELEMENT ID	STRESS (KSI)
18101	11.55	21101	12.67
18151	12.20	21151	12.27
18171	10.83	22101	35.57
18181	11.37	22161	10.42
19101	15.16	22171	8.72
19151	16.90	23101	17.11
19171	13.00	24151	15.13
19181	12.71	24161	15.30
20101	16.78	24171	15.93
20151	16.75	24181	15.16
20152	15.36	24191	13.78
20171	11.96	24201	11.04
20172	10.82	25201	13.78
20181	10.26		

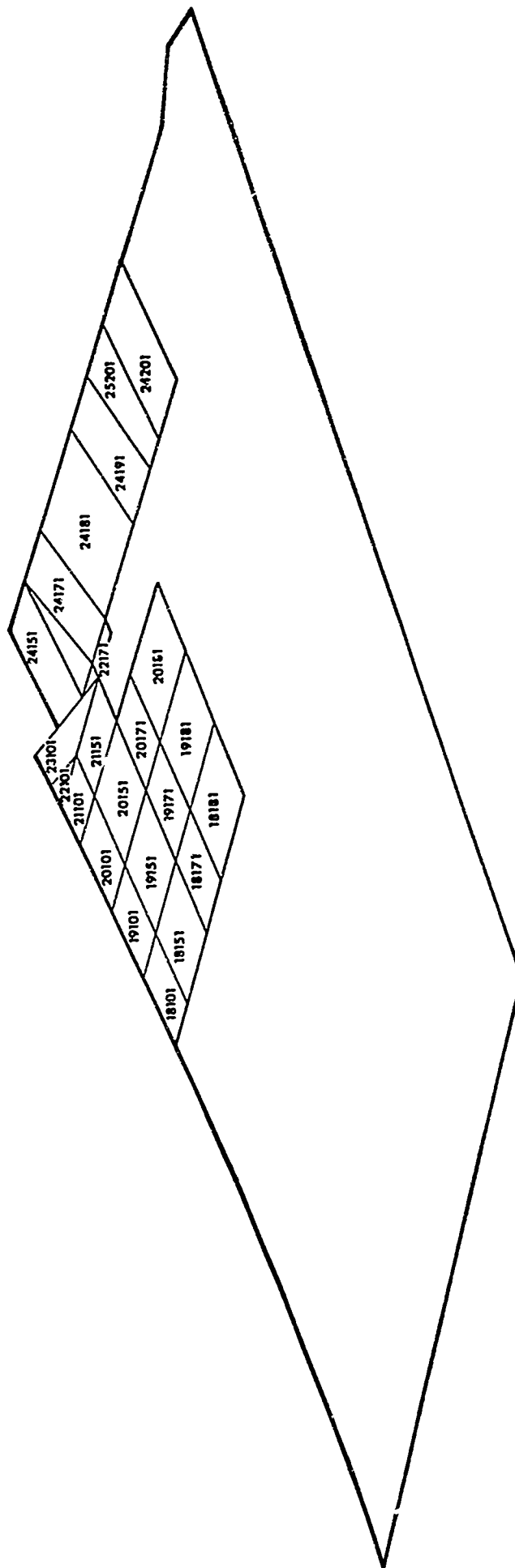


Figure 3-18. High Stress Element Locations (LEX)

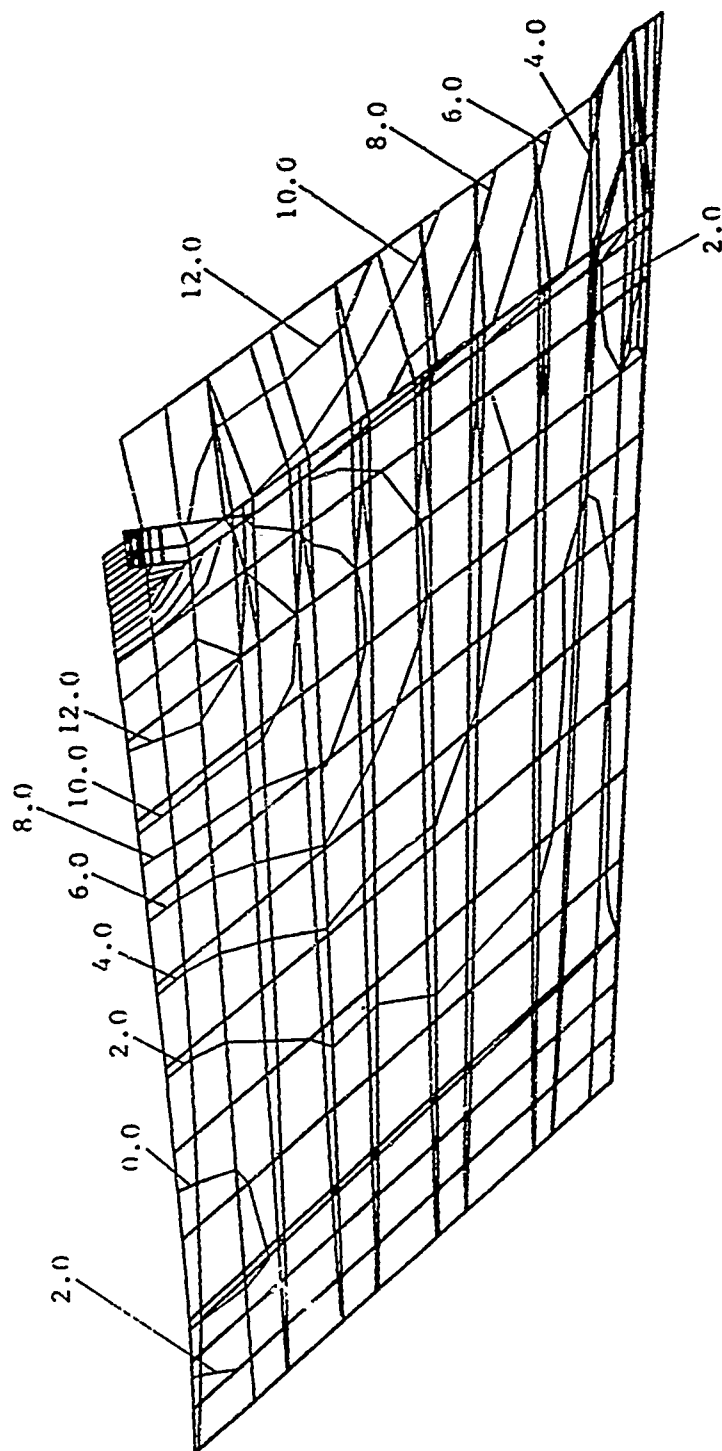


Figure 3-19. LEX Major Principal Stresses (Ksi)

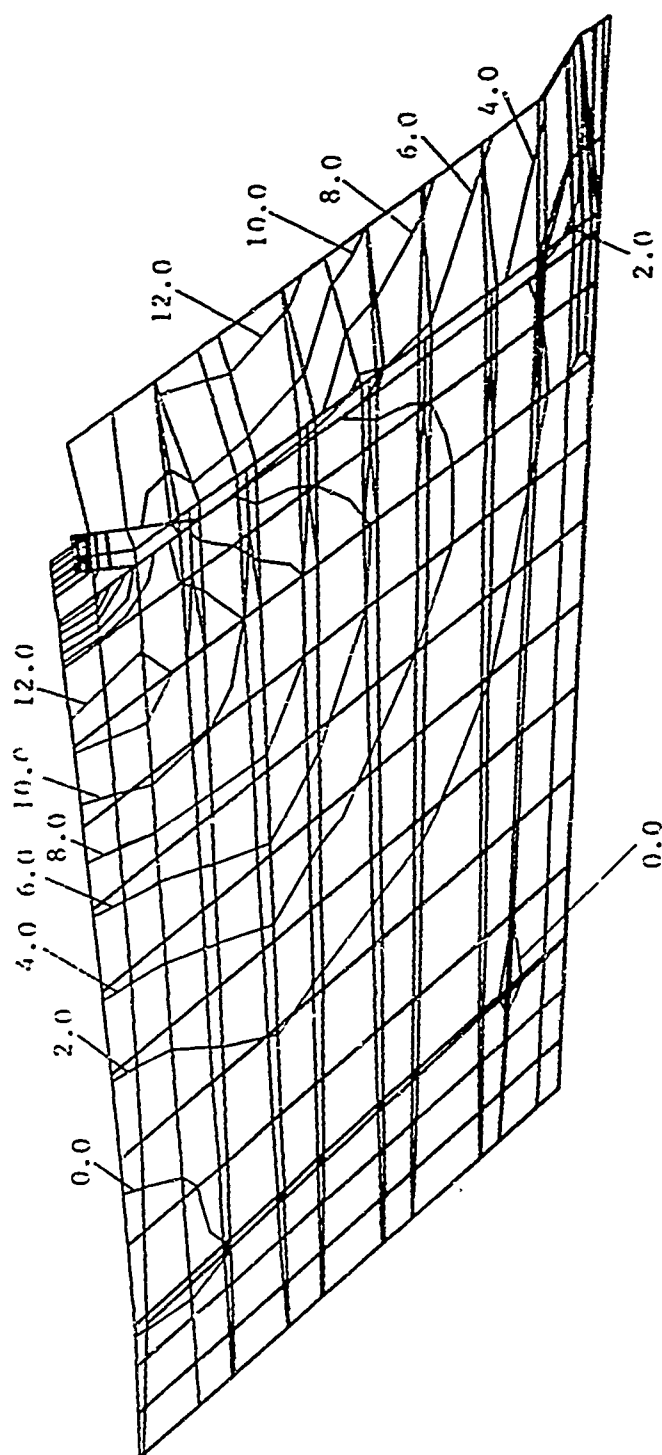


Figure 3-20. LEX Upper Skin Chordwise Stresses (Ksi)

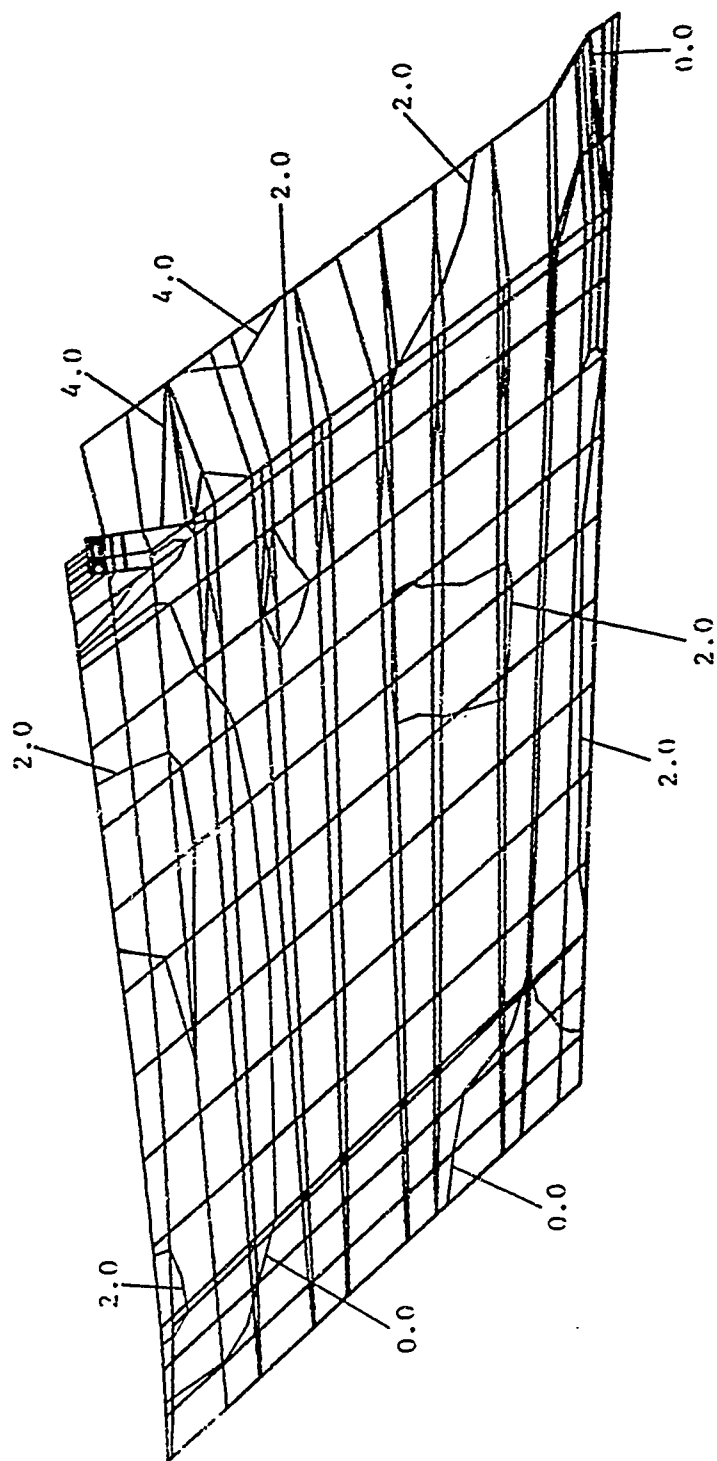


Figure 3-21. LEX Upper Skin Spanwise Stresses (Ksi)

Based on the final design of the components, several tooling concepts were studied to choose the most cost effective way of producing the SPF dies. There were two different methods of fabricating the SPF dies, conventional or numerical control (N/C) machining. In the conventional method, a plaster model of each part was generated using a number of templates and a steel die was machined by tracing the plaster model. For a part with simple geometry, this method might be faster than N/C machining, although the final die would be less accurate than a N/C machined die. The most time consuming task of the N/C machining method was to generate the N/C program tapes. Once the tapes were ready, the program would be checked by machining a soft foam block. Subsequently, the necessary modifications could be made on the N/C program. The N/C machining method was considered much more accurate than the conventional plaster method and made it easier to modify the tool. Since the LEX corrugation had a much simpler geometry than the avionics deck waffle pan, its corrugation die was decided to be fabricated by conventional machining. Due to the complexity of the avionics deck SPF dies, they were decided to be fabricated by N/C machining.

To reduce the tooling cost, it was determined to use the existing production titanium SPF cage die which required all SPF dies be designed to fit the cage. Since all SPF parts had been designed by the NCAD and/or CADAM computer systems, it was convenient to generate cross sectional views, key reference surfaces, and data points from those computer models. Tool designs were completed from the engineering designs considering a differential coefficient of thermal expansion (CTE) between the steel dies and the aluminum SPF parts. The direction of the tooling surface was also determined considering the assembly sequence and the tolerance build up problems. The required tool surface data were included in the engineering and tool drawings.

Based on the final design of the avionics deck, the tooling concepts for the SPF dies were examined for manufacturing tolerances, schedule and cost. The choice between conventional and N/C machining was decided based on a close tolerance accuracy and a faster schedule of completion. Conventional profile machining required a master tool to trace from, and the inaccuracies could be transferred directly into the production tool. In addition, the time required to fabricate the master combined with machining the dies proved to be longer than it would for the N/C method. The costs for both methods were relatively the same and only slightly higher for the conventional method. A lower risk was involved with the N/C method since the N/C tape check on scrap stock which reduced the possible fabrication errors involved in conventional machining.

With the concept methodology and parameters set, the dies for the avionics deck lower skin, upper deck and waffle pan were designed on CADAM. By having the design parts in CADAM and NCAD, the tool designs were completed by converting engineering part designs into tool designs. The tool designs were completed by incorporating the thermal expansion of the steel with the addition of four tool locating points.

Having completed the tool die designs on CADAM and NCAD, the surface data for N/C machining were down loaded for use in generating the N/C program tapes. The CADAM 2-D designs also served as dimensional aids for estimating and shop fabrication.

4. MATERIAL EVALUATION AND SELECTION

The objective of this task was to select and evaluate an aluminum alloy which represents the best combination of SPF and post-SPF mechanical properties for use in fabricating air-frame structures.

This task was conducted in two phases: (1) a preliminary evaluation of three candidate alloys to select one alloy representing the best combination of superplasticity and post-SPF mechanical properties, followed by (2) an extensive evaluation of the finally selected alloy.

4.1 MATERIAL SCREENING

A preliminary screening was conducted to pick three candidate alloys with the best SPF potential. These alloys were either procured in a fine-grained condition or were given a thermomechanical treatment (TMT) to refine their grain size. The superplastic response of each alloy was subsequently quantified, process parameters were defined and maximum useful superplastic elongations were determined. Cones were formed under biaxial tension at elevated temperatures to evaluate superplasticity and determine process parameters.

The results of preliminary evaluations were analyzed and the three alloys were rated for source, availability, SPF performance, useful elongation and structural properties.

4.1.1 Selection of Candidate Materials

The candidate materials included both ingot and powder metallurgy aluminum alloys and offered a broad range of service

properties including strength, damage tolerance and durability. Among the ingot alloys, 7475, 7075, 7050, 2024, Supral 100 and Alcan 08050 were considered; among the powder alloys, X7091 (formerly known as CT-91) was considered. The three alloys selected for preliminary evaluation and a brief rationale for their selection are as follows:

4.1.1.1 Characteristics of 7475 Alloy

It is a high strength aluminum alloy which offers strength equal to that of 7075, fracture toughness superior to 7075 and equivalent to 2024-T3, resistance to stress corrosion cracking comparable to 7075 and exfoliation resistance (in 7475-T61 condition) superior to 7075-T6. It has a relatively clean microstructure (fewer iron and silicon bearing inclusions than 7075, i.e., fewer natural sites for cavitation during the SPF deformation). It can be mill produced in fine grained condition, has demonstrated capabilities for large superplastic deformation, and can be procured from several sources in the U.S.

4.1.1.2 Characteristics of 7050 Alloy

It offers high strength and various other service properties characteristic of the 7XXX alloys. In addition, it has a lower sensitivity to the rate of quenching than other alloys in the same family. This property is considered very desirable because if optimum strength can be developed in an as-formed 7050 SPF component by a slower cool than water quench, (e.g., by air cooling after solution treatment and before aging). Problems associated with warpage due to thermal stresses induced during heat treatment would be significantly reduced. The presence of zirconium in the 7050 alloy also affords it more efficiency in grain refinement during mill processing. This alloy can also be easily procured from several domestic sources.

4.1.1.3 Characteristics of X7091 Alloy

This alloy was selected because of its high strength, high corrosion resistance and excellent toughness (without compromising strength). These superior properties are due to an inherently clean, fine grained and uniform structure in this alloy. The combination of the desirable service properties, typical of the 7XXX alloys and the fine microstructure inherent in the powder (P/M) alloys, in X7091 alloy is expected to result in a structural aluminum alloy with a high potential for SPF. All of the X7091 material used in the earlier portion of this program came from another AFWAL program, "High Strength P/M Aluminum Mill Products." This material was produced by Reynolds Metals Co., and the approval for its use was granted by the USAF Program Monitor of the said program.

4.1.2 Material Procurement

Mill stock of the three alloy plates of 7475 and 7050 and extruded bars of X7091 were thermomechanically processed (heat treated and rolled) into sheets with nominal gauge thicknesses of 0.060, 0.090 and 0.125 inch using the most desirable treatments investigated under a joint Northrop-Reynolds IR&D study. Specifically, two mill practices were used for producing these sheets. One was a "plate practice" wherein the material is warm rolled to an intermediate gauge after the thermal treatment, and then cold rolled to the finish gauge(s). The other was a "coil practice" in which the material was hot rolled prior to the thermal treatment and then cold rolled down to the finish gauge(s). The plate practice was used to produce sheets in all three gauges, 0.060, 0.090, and 0.125 inch. The coil practice was used to produce sheet in 0.060 inch gauge thickness only.

The reason for producing sheet in the 0.060-inch gauge thickness by both practices, "plate" as well as "coil", was to

provide the user an option to choose between the superior superplastic performance and the lower procurement cost. The sheet produced by the plate practice has better superplastic formability than a sheet of equivalent thickness produced by the coil practice. However, a sheet produced by the coil practice was expected to cost less than that produced by the plate practice. This is because in manufacturing production quantities of sheet by the coil practice rolling is done on five stand, irreversible mills and involves no hand operations. In manufacturing sheet by the plate practice, rolling is done on reversible, single stand mills and involves some hand work.

4.1.3 Preliminary Material Evaluation

The material evaluation prior to the final selection of the optimum alloy was primarily an assessment of the elevated temperature response of the three candidate alloys mill produced sheets. The SPF properties, service properties and microstructural observations on the three alloys were compared, along with their sources and availability, and the alloys ranked in order of desirability. A significant change from the classical approach to the evaluation of material superplasticity was incorporated in the test plan. Testing was done by biaxial forming of cone shaped specimens rather than by the uniaxial tension test of sheet coupons. The main reason for this was to ensure that the test methods employed could measure true material superplasticity in the high strength aluminum alloys without being affected by other phenomena occurring in these alloys which influence their superplastic ductility. It is well known that high strength aluminum alloys fail during the conventional SPF deformation by a mechanism involving cavity initiation and growth rather than by the classical mechanism of necking from strain localization as in Ti-6Al-4V and other titanium alloys. An elevated-temperature uniaxial tension test performed on the strips of these aluminum alloys without suppression of cavitation would result in a mixed mode failure that is due to necking as well as cavitation, and

would not measure true material superplasticity due to necking along with strain localization.

The biaxial tension SPF cone test procedure lends itself more readily to suppressing in situ cavitation during deformation than uniaxial tension test, and it also provides an opportunity to study the material behavior under conditions closer to those in manufacturing area. A biaxial-tension type test in which a sheet coupon is superplastically formed into a controlled geometry can be conducted in conjunction with a pressurization technique to suppress cavitation during deformation¹⁻³. This technique provides a better measure of superplasticity, since the effect of cavitation is minimized, even eliminated, so that the failure is expected to occur primarily by necking due to strain localization. Although the cone test has limitations⁴, primarily due to the effect of friction on strain and strain rate, the resulting errors due to this effect are believed to be considerably smaller than those due to cavitation. The close correspondence between the elevated-temperature uniaxial tensile test results and those obtained by the elevated-temperature biaxial tension cone forming method has been demonstrated previously in the non-cavitating titanium alloys⁵. The parameters measured from a cone test are the radius of curvature and sheet thickness at the pole and the height of the cone formed. Material flow stress, total strain and strain rate, can be computed by measuring the applied gas pressure and the time allowed to form the cone, as shown by Mackay, et al. on a previous AFWAL program⁵.

Dies to form cone shaped specimens were plumbed for gas introduction and exit during SPF, and were checked out by trial runs. It was determined that the cone test results could be reasonably well translated into the elevated temperature flow parameters (σ , m , $\dot{\epsilon}$) of the candidate materials.

Typical three dimensional microstructures of the three test alloy sheets, 0.125 inch thickness, are shown in Figures 4-1 through 4-3. A generally fine grain structure with relatively small aspect ratios is apparent in most cases. Using a linear intercept method on a Bausch and Lomb FAS-II image analyzer, grain size and aspect ratios were determined on each sheet in the longitudinal short transverse (L-ST) plane near the sheet surface, as well as near the centerline of sheet thickness. The average grain diameter along the rolling direction and that normal to it, together with the respective values of the standard deviation and the aspect ratio are shown in Table 4-1. Each value of the grain diameter represents an average of 200 line counts (ten different fields on the specimen L-ST plane with 20 lines on each field).

This technique was utilized on all of the samples except the X7091. The X7091 samples did not etch properly to allow for the grain boundary intercepts to be measured with the image analyzer. To determine grain diameter of the X7091, five photomicrographs of each sample were taken and the grain boundary intercepts were manually measured on the photomicrographs.

The 7475 sheet material exhibited the finest grain structure of the three alloys examined. The average grain diameter for the plate rolled samples was between 8.3 and 9.1 μm , measured in the direction transverse to the sheet rolling direction. The standard deviations for these measurements were also the lowest. The average grain diameters in the direction parallel to the sheet rolling direction ranged between 13.0 and 16.3 μm . The grain diameters of the coil rolled sheet samples were slightly higher.

The grain structure of the 7050 material was slightly coarser than that of 7475, however, there was very little difference in the grain diameter of the coil rolled 7050 -IV sample compared to the specimens from the other sheets of this alloy.

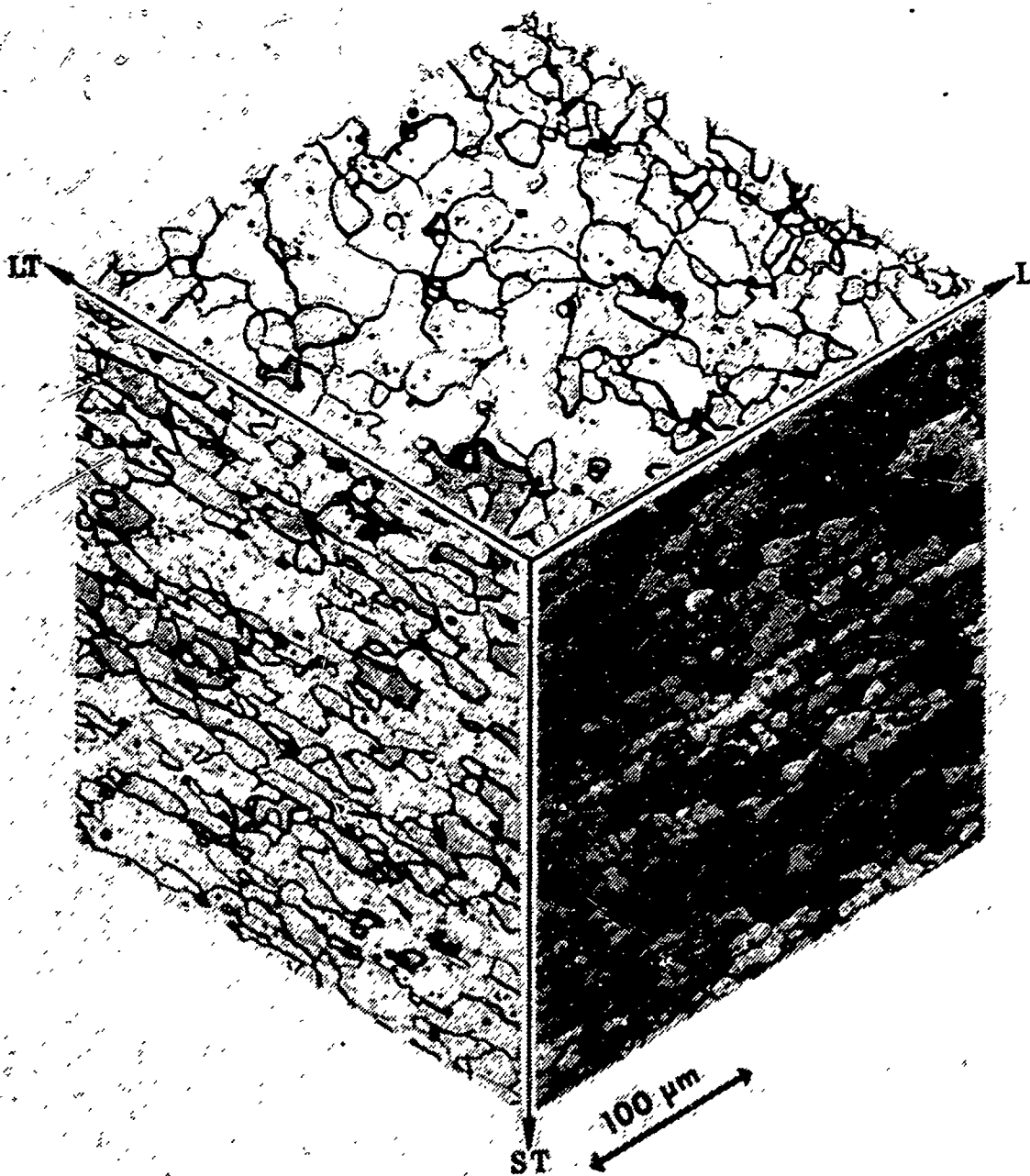


Figure 4-1. As Received Microstructure of SPF Aluminum Alloy Sheet 7475-I (0.125 Inch Thickness)

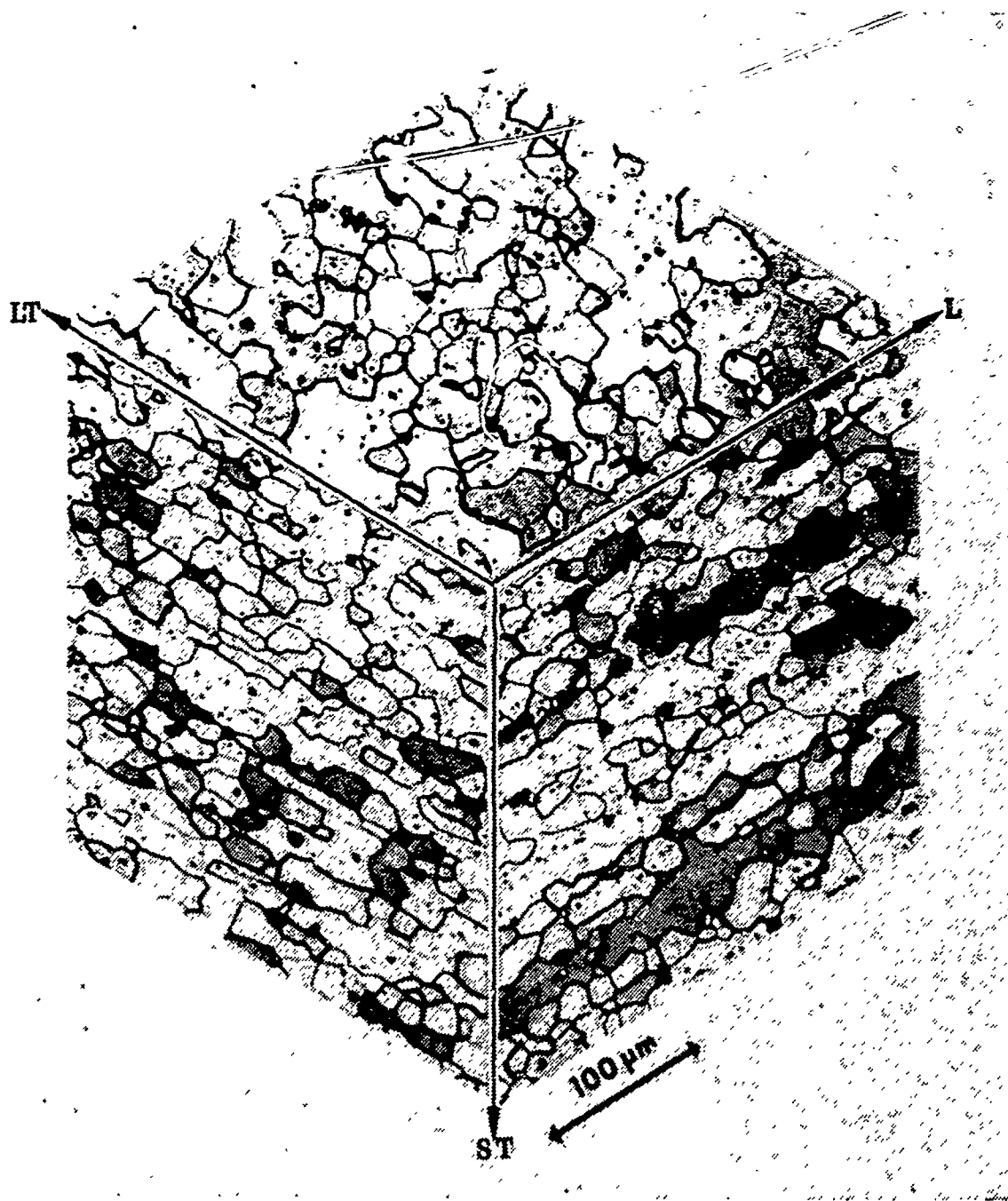


Figure 4-2. As Received Microstructure of SPF Aluminum Alloy Sheet 7050-I (0.125 Inch Thickness)

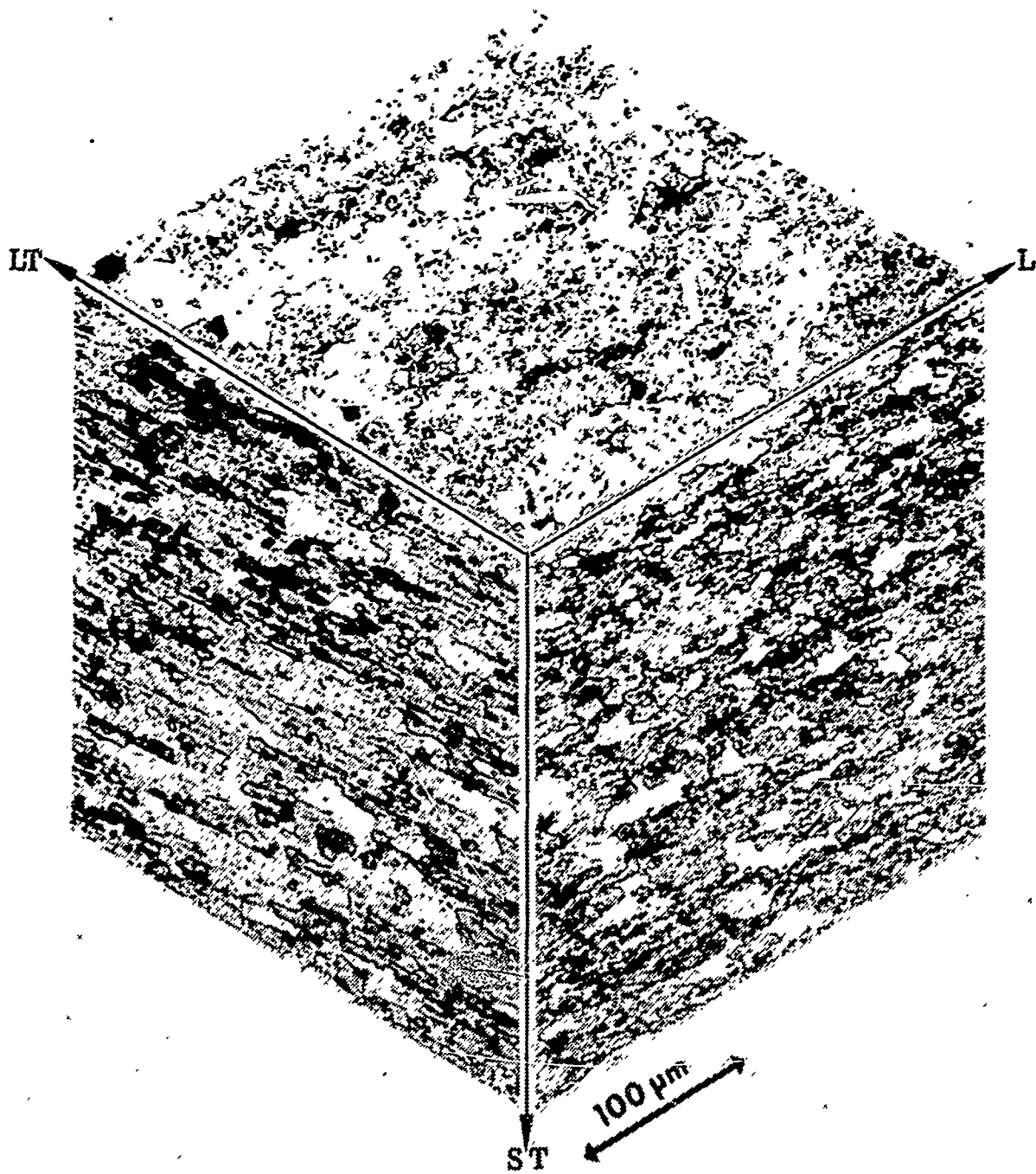


Figure 4-3. As Received microstructure of SPF Aluminum Alloy Sheet X7091-I (0.125 Inch Thickness)

TABLE 4-1. MATERIAL GRAIN GEOMETRY (AS RECEIVED CONDITION)

SAMPLE ID	SHEET THICK- NESS (INCH)	ROLLING METHOD	MEASUREMENT POSITION										
			CENTERLINE					SURFACE					
			LONGITUDINAL a (2) (M)	STD DE- VIATION (M)	TRANSVERSE b (2) (M)	STD DE- VIATION (M)	ASPECT RATIO (a/b)	LONGITUDINAL a (2) (M)	STD DE- VIATION (M)	TRANSVERSE b (2) (M)	STD DE- VIATION (M)	ASPECT RATIO (a/b)	
7475	-I	0.125	PLATE	16.3	4.1	8.7	1.3	1.9	15.4	3.5	8.8	1.4	1.7
	-II	0.090	PLATE	13.6	3.1	9.1	1.4	1.5	13.4	2.6	8.7	1.2	1.6
	-III	0.060	PLATE	13.0	2.5	8.4	1.3	1.5	13.0	2.5	8.3	1.2	1.6
	-IV	0.060	COIL	15.7	4.8	10.1	1.9	1.5	15.4	3.5	9.5	1.4	1.6
7050	-I	0.125	PLATE	17.0	3.8	11.3	1.9	1.5	15.4	2.7	11.5	2.0	1.3
	-II	0.090	PLATE	17.7	3.7	11.9	2.0	1.5	15.5	2.7	11.8	2.1	1.3
	-III	0.060	PLATE	15.4	3.4	11.0	1.8	1.4	14.6	2.7	10.7	1.7	1.4
	-IV	0.060	COIL	15.2	2.9	10.2	1.7	1.5	15.6	3.0	11.3	1.8	1.4
X7091	-I	0.125	PLATE	22.1	4.5	9.3	1.4	2.4	58.2	25.6	38.7	25.2	1.5
	-II	0.090	PLATE	21.1	7.9	11.9	1.4	1.8	47.2	12.2	23.4	4.0	2.0
	-III	0.060	PLATE	14.2	2.4	7.8	0.9	1.8	36.3	13.6	19.6	6.6	1.9
	-IV	0.060	COIL	27.6	5.6	13.1	1.9	2.1	54.0	30.2	23.9	4.2	2.3

NOTES: 1. All measurements were obtained by a linear-intercept method. Measurements on 7475 and 7050 samples were made by an automatic image analyzer: measurements on X7091 were done manually on photomicrographs.

2. a = Average grain diameter along sheet rolling direction.
b = Average grain diameter transverse to sheet rolling direction.

The microstructure of the X7091 material varied widely depending upon where the measurements were made. The grain structure in the center of the sheet was generally finer than away from it. The grains near the sample surface were very coarse with some of the average diameters exceeding 50 micrometers. These large grains were observed in all of the X7091 sheets produced by the various processes.

Elevated temperature cone tests were conducted on the three alloys for determination of their superplastic formability. Test temperatures in the range of 840 to 980°F were used for the 7475 sheets. Similar temperatures were used for testing the X7091 alloy sheets. Temperatures for 7050 sheets were slightly lower, 840 to 945°F, due to a lower solvus temperature. Constant gas pressures in the range of 100 to 150 psi were used to impose several nearly constant strain rates to SPF a given cone geometry.

Results obtained from the elevated temperature tests are listed in Table 4-2. Typical results are also shown as log flow stress (σ) versus log true strain rate ($\dot{\epsilon}$) curves in Figures 4-4 through 4-6. The corresponding strain rate sensitivity (m) versus log true strain rate curves are shown in Figures 4-7 through 4-9.

The shapes of the two types of curves shown in Figures 4-4 through 4-9 are those normally expected. The $\log \sigma - \log \dot{\epsilon}$ curves are generally sigmoidal, a stretched S-shape, with segments of lower values of slope in regions of high and low strain rates flanking a nearly linear segment of higher slope in region of intermediate strain rate. The $\sigma - \dot{\epsilon}$ relationship in this intermediate region is described by the equation.

$$\sigma(\dot{\epsilon}, T) = k\dot{\epsilon}^m(\dot{\epsilon}) \quad (1)$$

TABLE 4-2. LIST OF PEAK m VALUES AND MAXIMUM SPF STRAINS IN 7475, 7050 AND P/M X7091 ALLOYS (a)

MATERIAL ID	TEST TEMPERATURE (F)	PEAK m (± 0.05)	STRAIN RATE AT PEAK m (SEC^{-1})	MAXIMUM SPF STRAIN (%)	STRAIN RATE CORRESPONDING TO MAXIMUM STRAIN (SEC^{-1})	APPROXIMATE m CORRESPONDING TO MAXIMUM STRAIN (± 0.05)
7475	-I	970	1.6×10^{-4}	448	2.0×10^{-4}	0.70
	-II	970	2.4×10^{-4}	304	4.9×10^{-4}	0.45
	-III	970	9.5×10^{-4}	1425	8.7×10^{-5}	0.60
	-IV	970	8.5×10^{-4}	920	6.0×10^{-5}	0.35
7050	-I	935	7.5×10^{-4}	301	1.1×10^{-4}	0.60
	-II	900	1.2×10^{-4}	306	3.3×10^{-4}	0.50
	-III	935	2.0×10^{-4}	408	7.8×10^{-4}	0.40
	-IV	935	4.6×10^{-4}	178	4.8×10^{-4}	0.36
X7091	-I	(b)				0.60
	-II	(b)				
	-III	970	3.2×10^{-4}	320	5.4×10^{-4}	0.37
	-IV	970	4.0×10^{-4}			

NOTES: (a) All data were obtained from cone tests.
 (b) These materials were not tested.

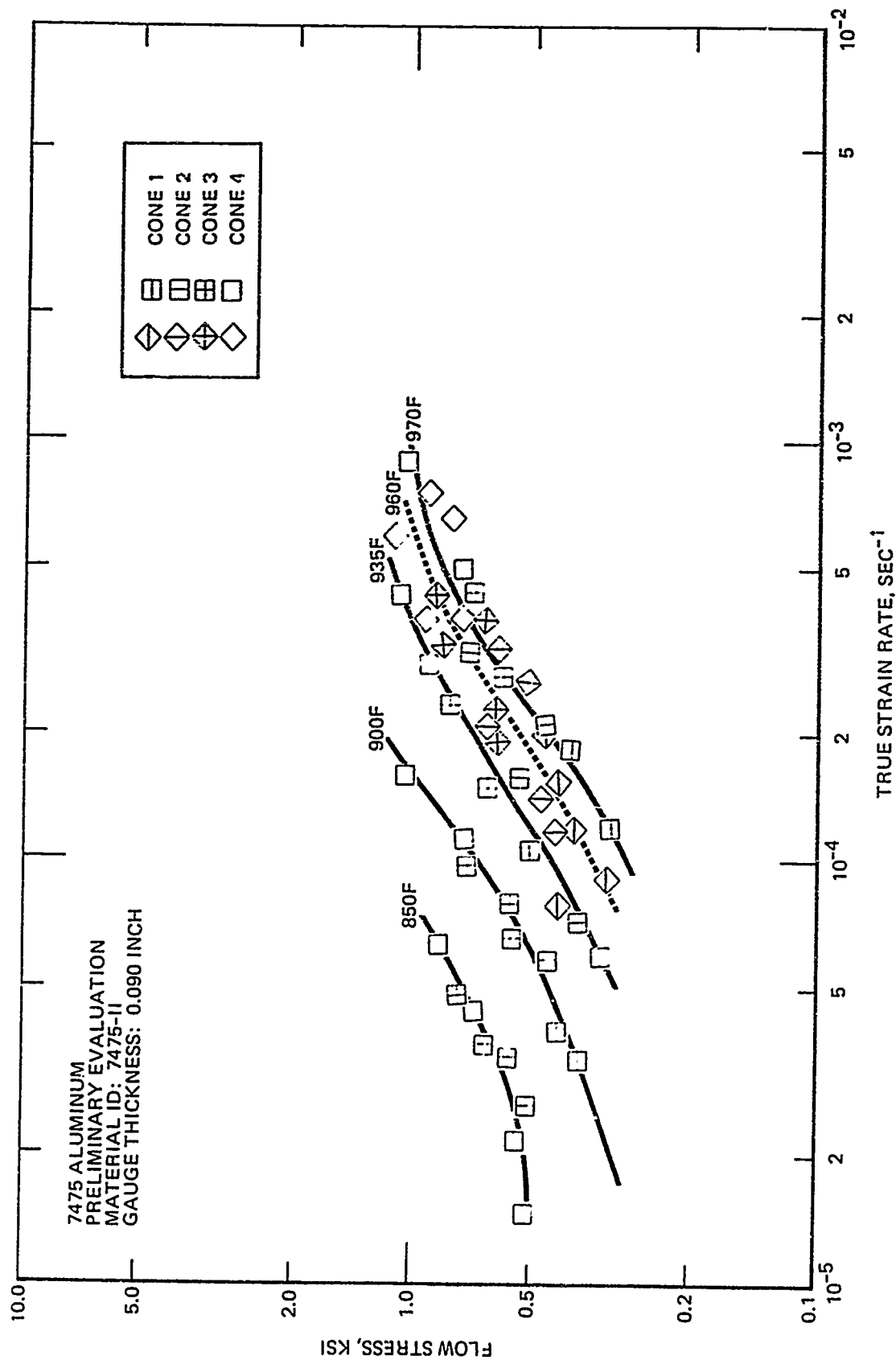


Figure 4-4. Plots of Log Flow Stress Versus Log True Strain Rate for 7475-II Material at Various Temperatures

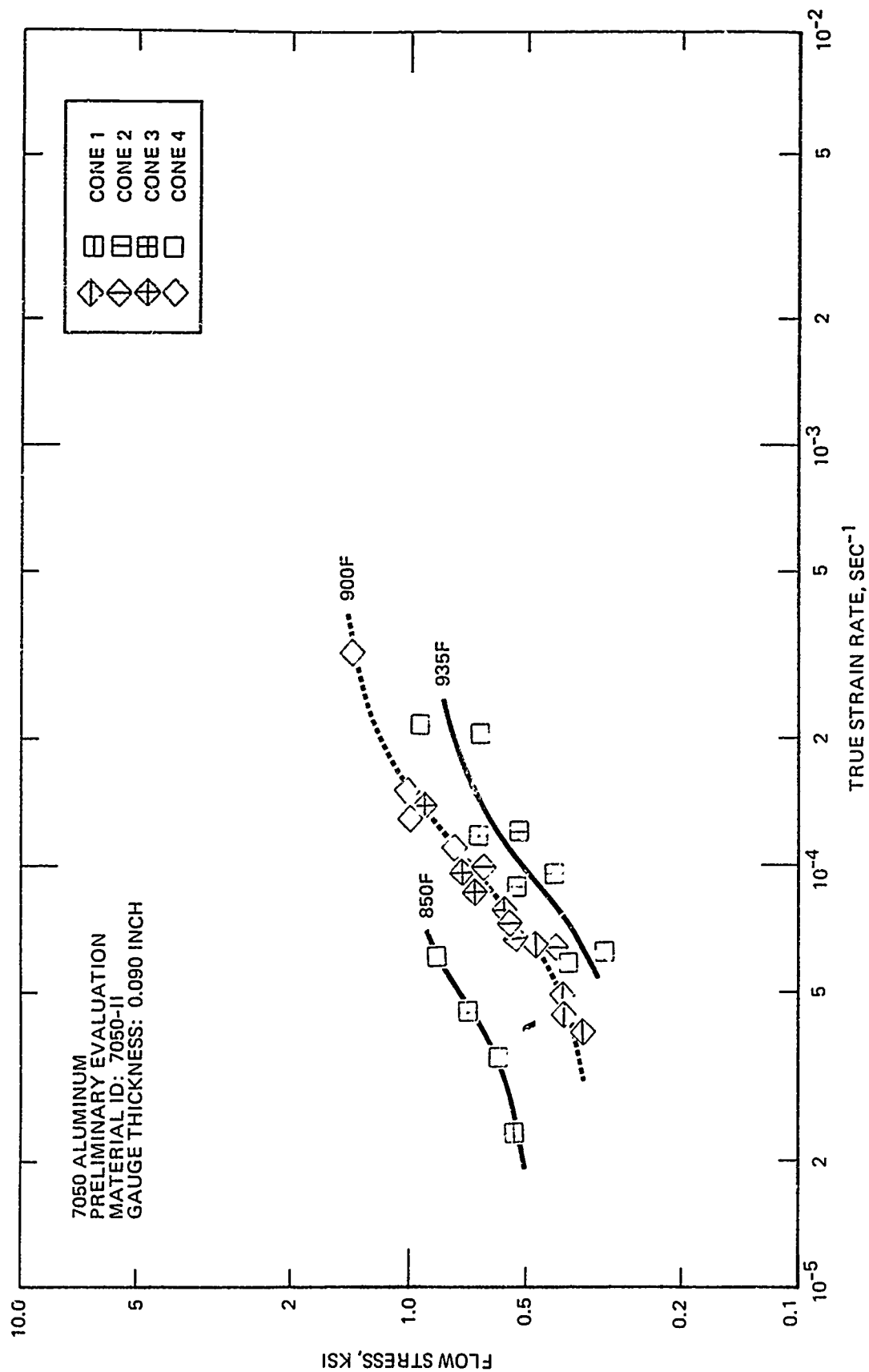


Figure 4-5. Plots of Log Flow Stress Versus Log True Strain Rate for 7050-II Material at Various Temperatures

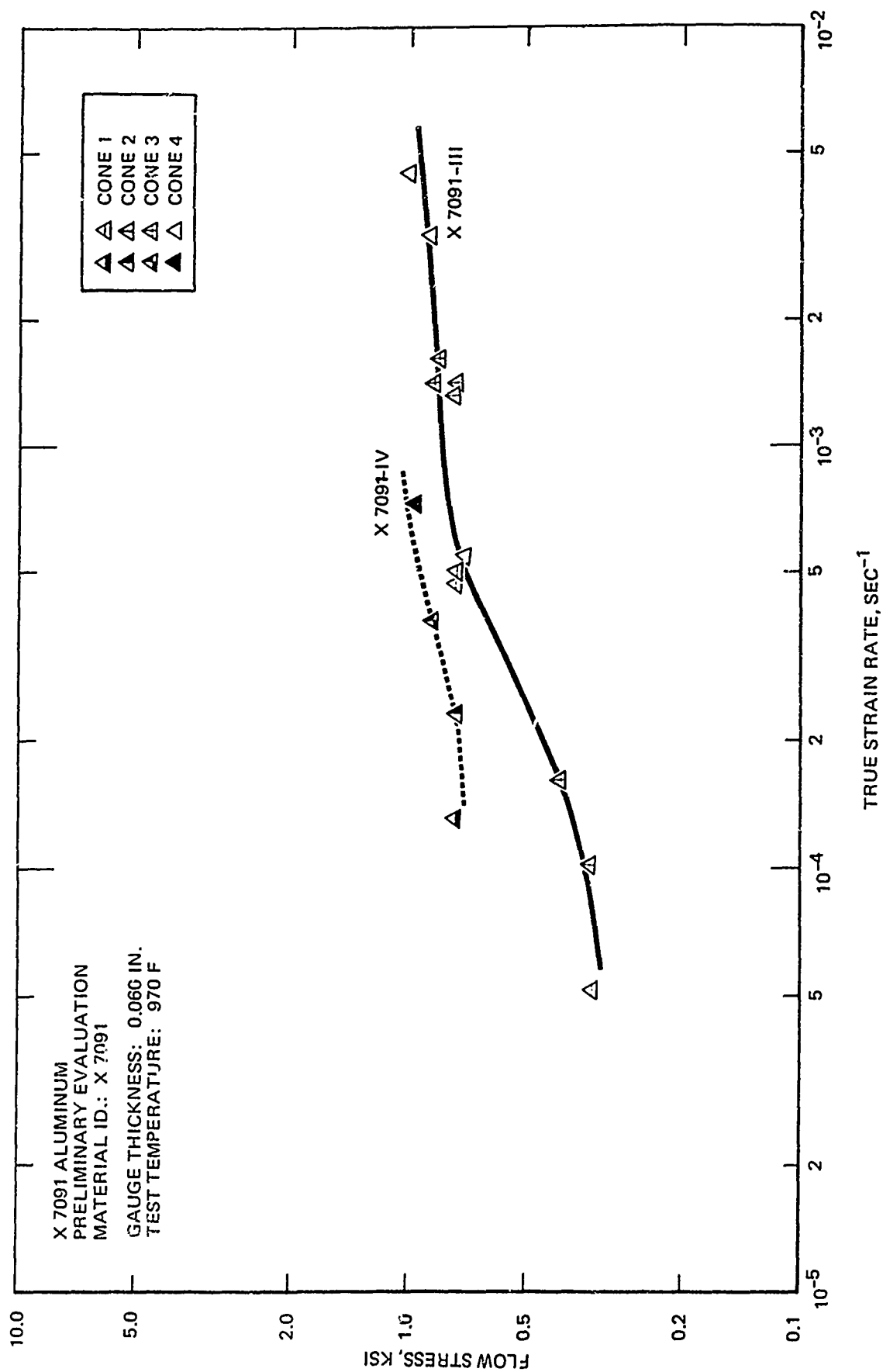


Figure 4-6. Plots of Log Flow Stress Versus Log True Strain Rate for P/M X7091-III and X7091-IV Materials at 970°F Temperature

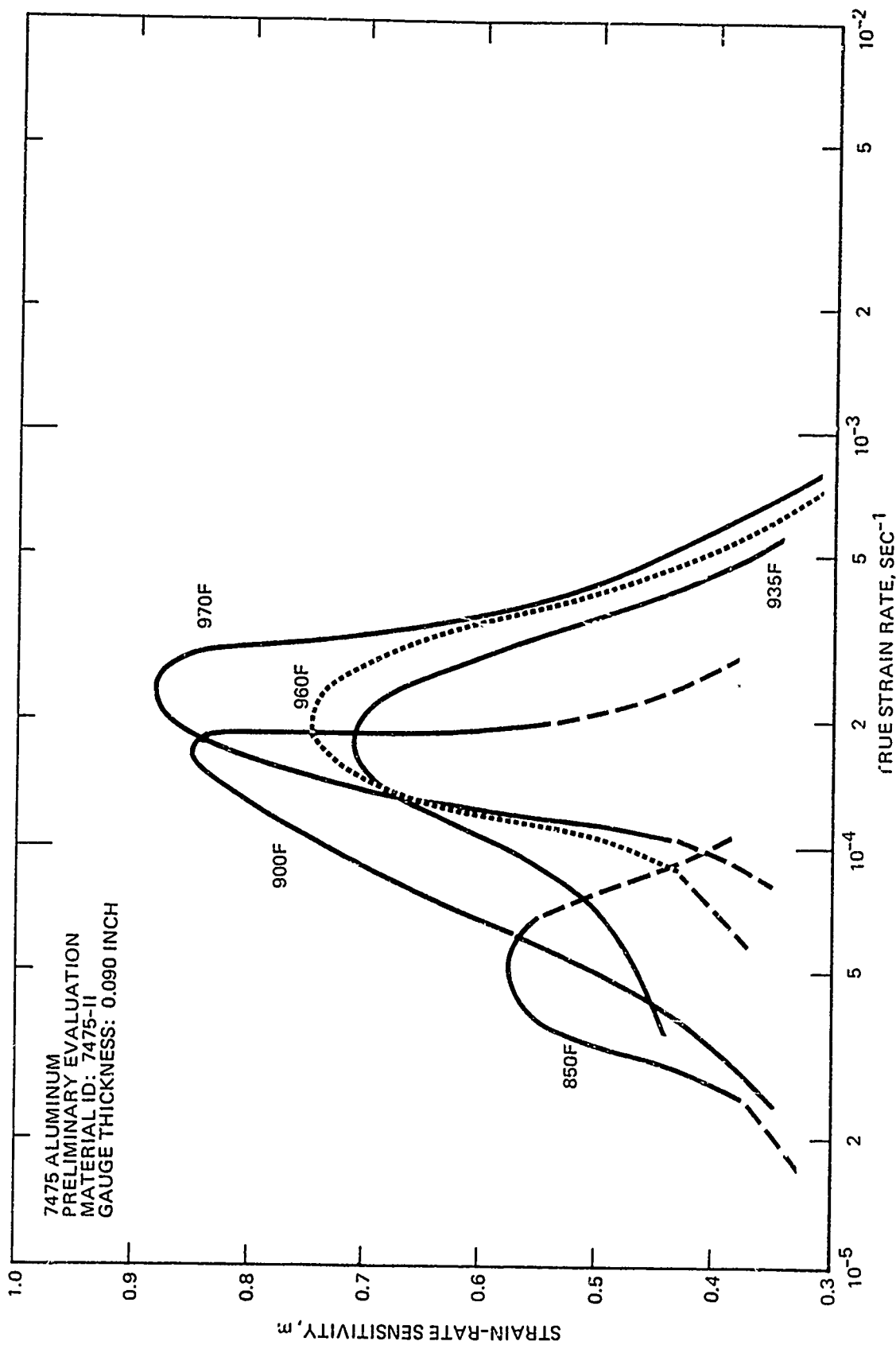


Figure 4-7. Plots of Strain-Rate Sensitivity (m) Versus Log True Strain Rate for 7475-II Material at Various Temperatures

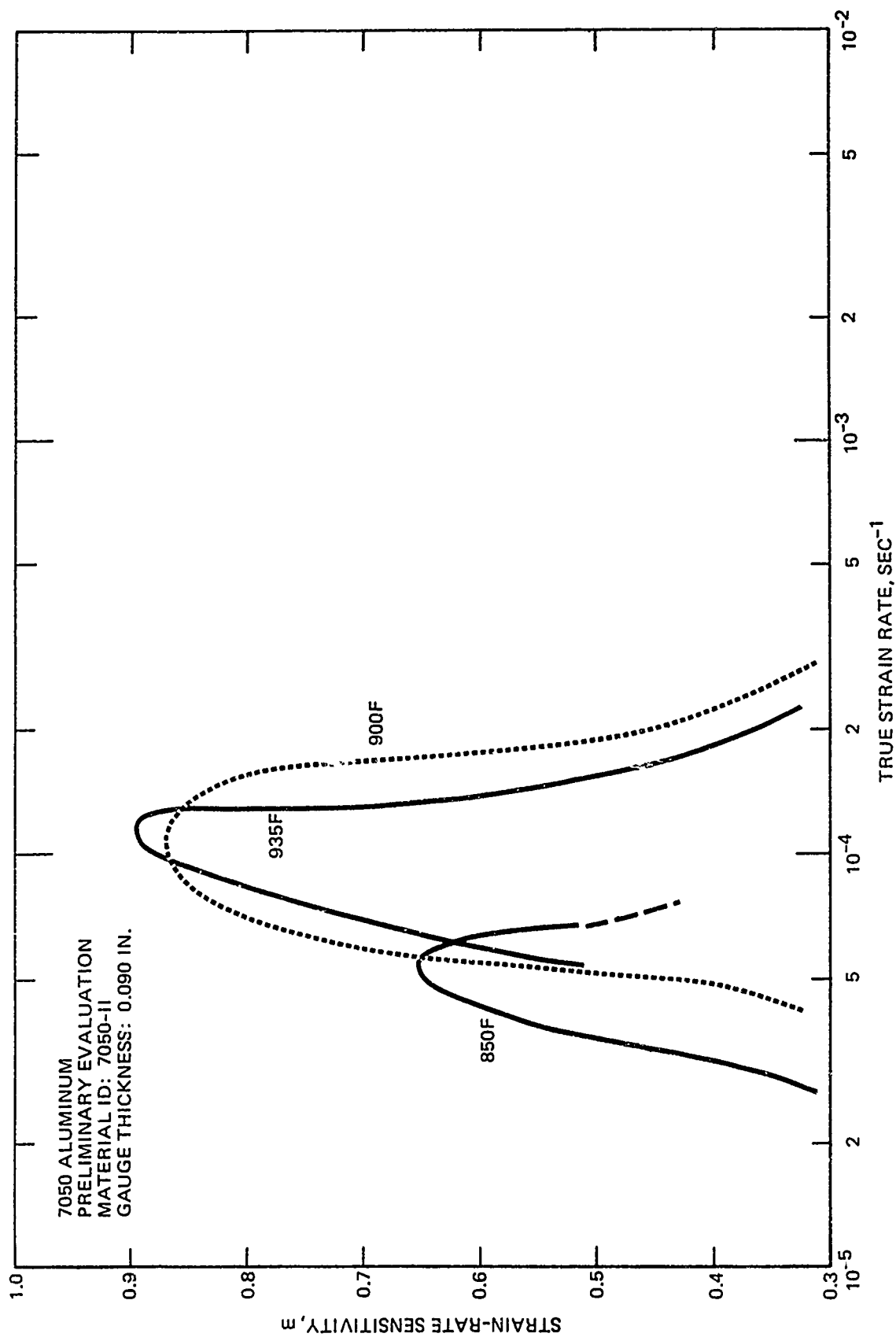


Figure 4-8. Plots of strain-Rate Sensitivity (m) Versus Log True Strain Rate for 7050-II Material at Various Temperatures

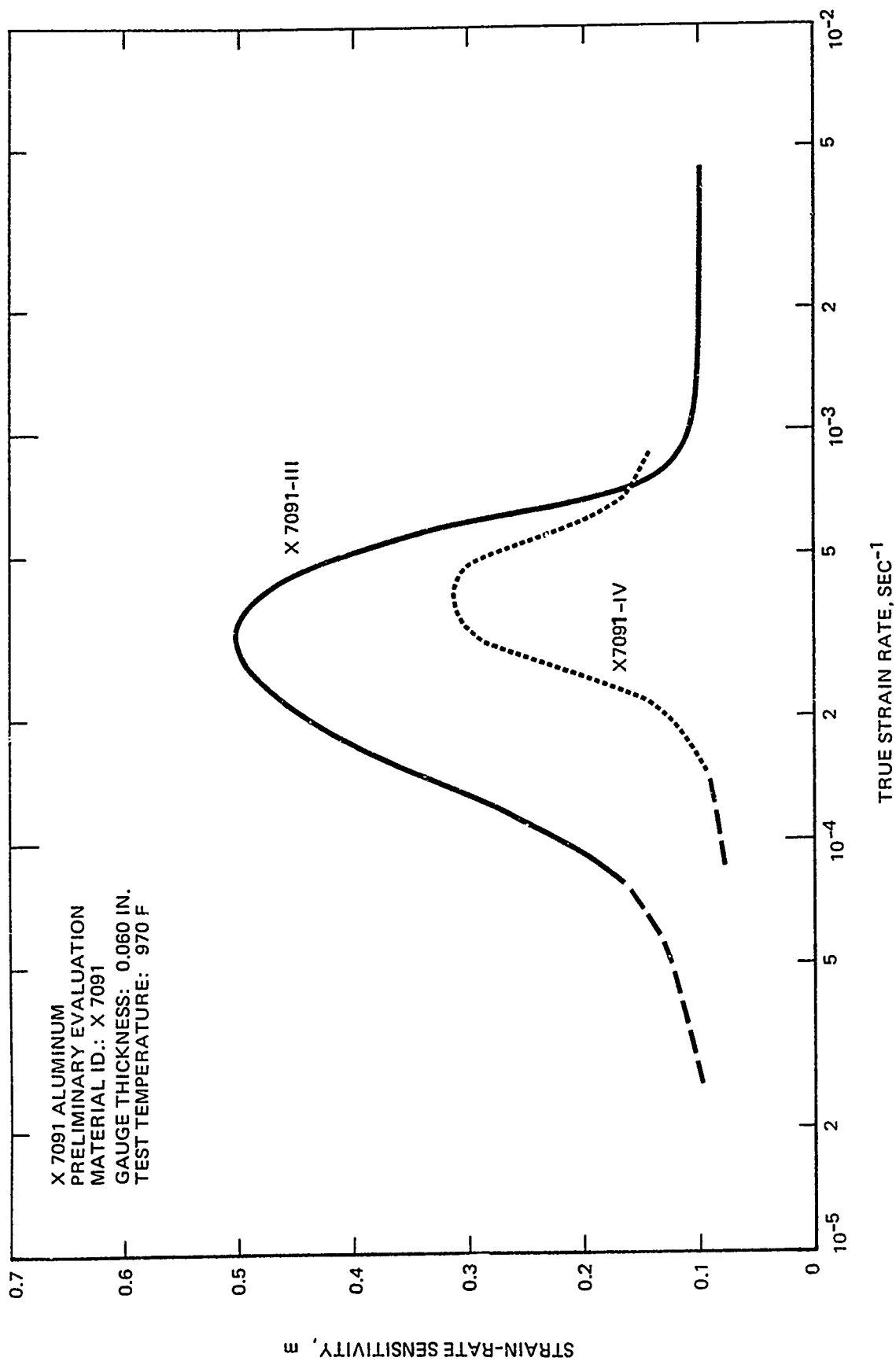


Figure 4-9. Plots of Strain-Rate Sensitivity (m) Versus Log True Strain Rate for P/M X7091-III and X7091-IV Materials at 970°F Temperature

where T is the test temperature and k a material constant. The $m - \log \dot{\epsilon}$ curves, calculated from the slope of the $\log \sigma - \log \dot{\epsilon}$ curves ($m = \partial \log \sigma / \partial \log \dot{\epsilon}$), usually have a bell shape with a peak value lying in the intermediate strain rate range and significantly lower values obtained in regions of high and low strain rates.

These results show that 7475 alloy had the highest peak m values. The range of peak m values for the various sheet gauges of this alloy evaluated over the temperatures of 900 to 970°F was 0.64 to 0.88. The corresponding peak m values were in the range of 0.59 to 0.89 over the temperatures of 900 to 935°F for 7050 alloy and 0.3 to 0.5 at 970°F for X7091 alloy. Since peak m values in a variety of superplastic materials have been shown to be related to the fracture strain^{6,7}, the higher the peak m value of an alloy, the higher is its projected superplastic strain. The strain rates corresponding to the peak m were also in a higher range for 7475 alloy than for the other alloys, 1.5×10^{-4} to $1 \times 10^{-3} \text{sec}^{-1}$ for 7475, compared to 7×10^{-5} to $5 \times 10^{-4} \text{sec}^{-1}$ for 7050 alloy and 3×10^{-4} to $4 \times 10^{-4} \text{sec}^{-1}$ for X7091. The differences in the strain rates are important, since the higher strain rates would result in shorter fabrication time and, therefore, lower cost for a given component. Finally, of the three alloys evaluated, the flow stresses corresponding to the peak m values were the lowest for 7475, approximately 350 psi at $1.5 \times 10^{-4} \text{sec}^{-1}$ and 1,000 psi at $1 \times 10^{-3} \text{sec}^{-1}$ for 7475, compared to 400 to 500 psi at $7 \times 10^{-5} \text{sec}^{-1}$ and 1,000 to 1,200 psi at $5 \times 10^{-4} \text{sec}^{-1}$ for 7050, and 550 to 800 psi at $3 \times 10^{-4} \text{sec}^{-1}$ and 650 to 900 psi at $4 \times 10^{-4} \text{sec}^{-1}$ for X7091. The lower flow stresses are advantageous, since they translate into lower gas pressure requirements during forming and, due to the lower resultant stress concentrations, result in reduced incidence of cavitation.

4.1.4 Post-SPF Microstructural Evaluation

The primary purpose of this evaluation was to determine the effect of superplastic deformation on the microstructure of these alloys. The microstructural features examined were those most closely related to the service properties, namely cavitation voids and grain size.

Table 4-3 presents a description of the alloy 7475 specimens selected for the metallographic evaluation. These specimens were selected to determine the effect of SPF strain, the forming temperature and the strain rate on cavitation and grain size. The 0.090-inch thick 7475 material was chosen for this evaluation because the 0.090-inch sheet thickness is intermediate between 0.060 and 0.125 inch thickness. Therefore, the observations made with the 0.090 inch thick material may be extrapolated to the 0.060-inch thick as well as the 0.125-inch thick material.

Table 4-4 presents a similar description of the selected cone specimens of alloys 7050 and P/M 7091.

A pie shaped section was excised from each of the cones selected for metallographic evaluation. It was mounted to reveal the cross section of the thickness plane, and prepared for optical metallography using the standard procedures. As polished samples were examined to determine cavitation in four locations along the specimen cross section. These locations represented regions of four different SPF strains in the cone, including the region of minimum strain (designated as Area 1), maximum strain (Area 4), region of strain at or near the onset of cavitation (Area 2, onset being defined as ≤ 0.5 percent areal cavitation), and a region of intermediate strain between onset of cavitation and maximum cavitation (Area 3). All measurements of cavitation were performed using a Bausch and Lomb FAS II image analysis system interfaced to a Leitz MM5 metallograph. In measuring

TABLE 4-3. LIST OF 7475 CONE TEST SPECIMENS SELECTED FOR METALLOGRAPHIC EVALUATION

SPECIMEN ID	CONE NUMBER	TEST TEMPERATURE (°F)	INITIAL SHEET THICKNESS (IN)	MAXIMUM STRAIN ACHIEVED (1) (%)	TRUE STRAIN RATE (2) (SEC ⁻¹)
7475-II-E5	2	850	0.090	17	2.9×10^{-5}
7475-II-E1	2	850	0.090	21	3.5×10^{-5}
7475-II-E5	4	850	0.090	22	3.7×10^{-5}
7475-II-E1	4	850	0.090	41	6.4×10^{-5}
7475-II-E7	2	935	0.090	46	9.9×10^{-5}
7475-II-E3	2	935	0.090	50	1.7×10^{-4}
7475-II-E7	4	935	0.090	193 *	2.8×10^{-4}
7475-II-E3	4	935	0.090	193 *	4.5×10^{-4}
7475-II-P7	2	970	0.090	87	2.2×10^{-4}
7475-II-P6	2	970	0.090	61	3.0×10^{-4}
7475-II-P7	4	970	0.090	316 *	5.0×10^{-4}
7475-II-P6	4	970	0.090	285 *	8.6×10^{-4}

(1) Measured from a photograph of the cross section of the cone specimen.

(* Indicates that the specimen ruptured.)

(2) Calculated by dividing the maximum true strain by the total forming time of the test.

TABLE 4-4. LIST OF 7050 AND P/M 7091 CONE TEST SPECIMENS
SELECTED FOR METALLOGRAPHIC EVALUATION

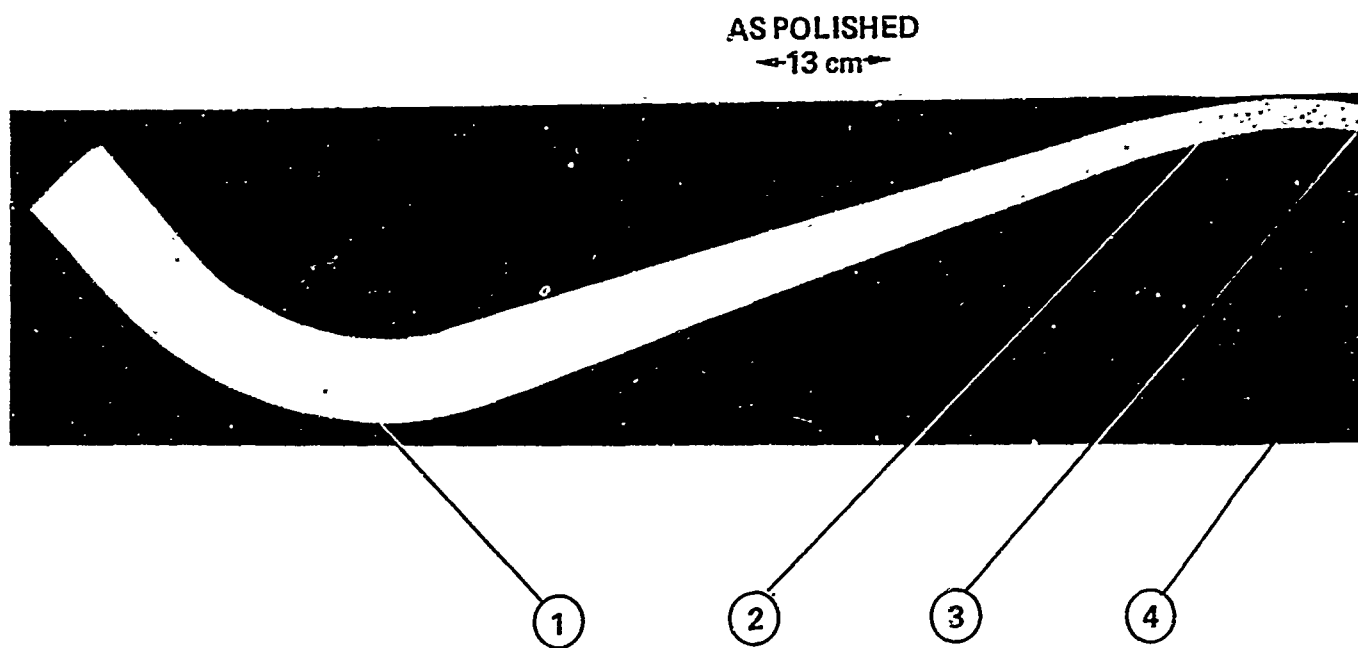
SPECIMEN ID	CONE NUMBER	TEST TEM- PERATURE (°F)	INITIAL SHEET THICKNESS (IN)	MAXIMUM STRAIN ACHIEVED (1) (%)	TRUE STRAIN RATE (2) (SEC ⁻¹)
7050-II-E1	4	850	0.090	39	6.1×10^{-5}
7050-II-E2	2	900	0.090	45	6.8×10^{-5}
7050-II-P4	3	900	0.090	56	8.3×10^{-5}
7050-II-E3	3	900	0.090	83	1.4×10^{-4}
7050-II-P6	1	935	0.090	33	5.0×10^{-5}
7050-II-P6	3	935	0.090	91	1.1×10^{-4}
7050-IV-P5	4	970	0.090	38	6.2×10^{-4}
7050-III-P6	4	970	0.090	320 *	5.4×10^{-4}

- (1) Measured from a photograph of the cross section of the cone specimen.
(* Indicates that the specimen ruptured.)
(2) Calculated by dividing the maximum true strain by the total forming
time of the test.

cavitation, it was of critical importance to distinguish between cavities and constituent particles. This was done by ensuring surface flatness during specimen preparation, so that the particles would not be pulled out of the matrix leaving "cavities" behind, and by a careful adjustment of the threshold setting for cavity detection. The error in resultant measurements was within ± 5 percent of the measured value when cavitation was in excess of 1 percent. The error rose to within ± 10 percent when cavitation was between 0.5 to 1 percent, and was approximately ± 15 percent when cavitation was very small (< 0.5 percent).

Subsequent to the determination of the areal cavitation, these samples were etched to reveal the grain boundaries for determination of grain size and grain shape in these regions. A linear intercept method was used manually for measuring all grain sizes. Five neighboring fields of view were first photographed at 250 magnification at each location of a given specimen. Five lines, each 100 mm long, were then inscribed on each of these photographs along the sheet rolling direction. The number of intercepts was counted on each of these lines and average longitudinal grain diameter (\bar{a}) was determined at that location. Five similar lines were subsequently inscribed on duplicate prints of the same photomicrographs in a direction transverse to the sheet rolling direction. Intercepts were counted as before, and the transverse grain diameter (\bar{b}) was determined at each specimen location. The grain aspect ratio, a measure of grain shape, was calculated as the ratio (\bar{a}/\bar{b}).

Figure 4-10 shows an example of the results of metallographic evaluation on a 7475 alloy specimen. The photomicrograph on the top left shows the cross section of the specimen and identifies the four selected areas representing different SPF strains. The values of local strain in each of these areas, measured directly on the photomicrograph, and the \bar{a} and \bar{b} grain sizes as well as the area cavitation corresponding to each of these four areas are tabulated below the photomicrograph. A complete set of data for the various specimens of 7475 alloy is presented in Table 4-5. The corresponding photomicrographs at these locations, both as polished to reveal cavitation and as etched to reveal grain boundaries, are shown at the right. An increase in cavitation with increasing strain, i.e., as one moves from area 1 to area 4 along the specimen cross section, is apparent in this figure. No change in the grain size with increasing SPF strain is apparent at first sight.

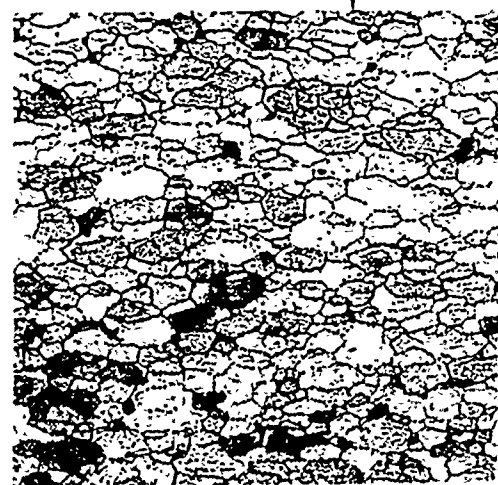
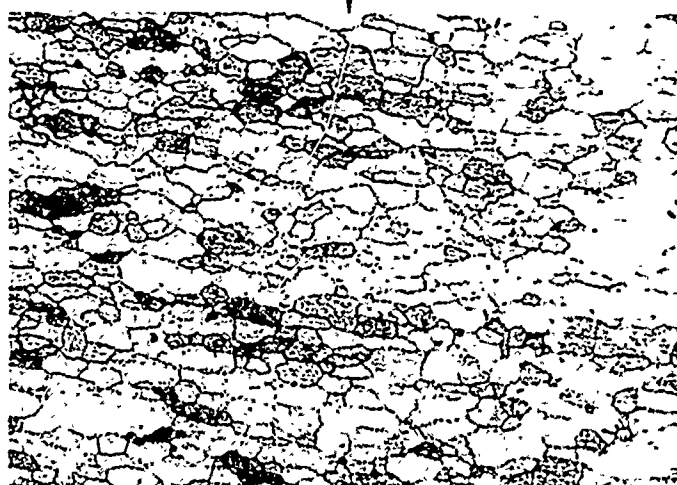
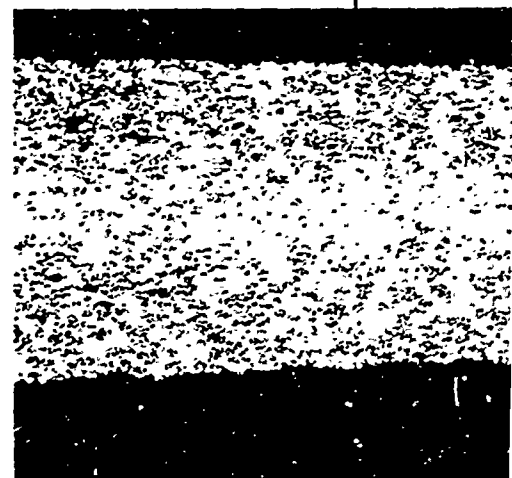
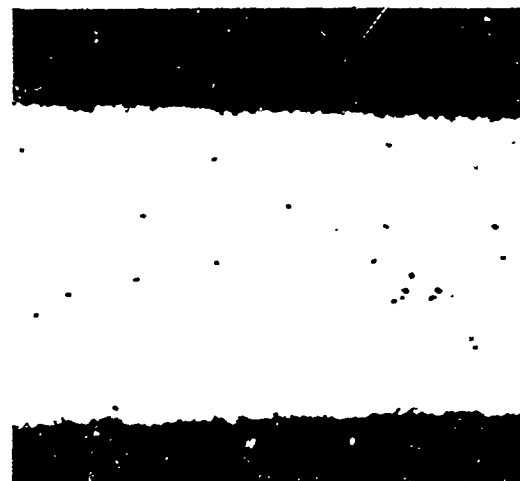
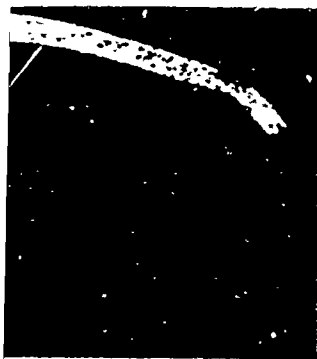


STRAIN (%)	50.6	122.0	262.0	316.0
GRAIN SIZE (\bar{a}) (μm)	19.6	18.3	17.8	16.7
GRAIN SIZE (\bar{b}) (μm)	9.4	9.3	9.6	10.0
AREAL CAVITATION (%)	>0.01	0.1	4.3	12.8

Figure 4-10. Microstructure of a 7475 Alloy Cone Specimen (ID 7475-II-P₇, Cone 4) at Various Strain Locations, Initial Sheet Thickness 0.090 Inch, Test Temperature 970 F

①

②



2 ✓

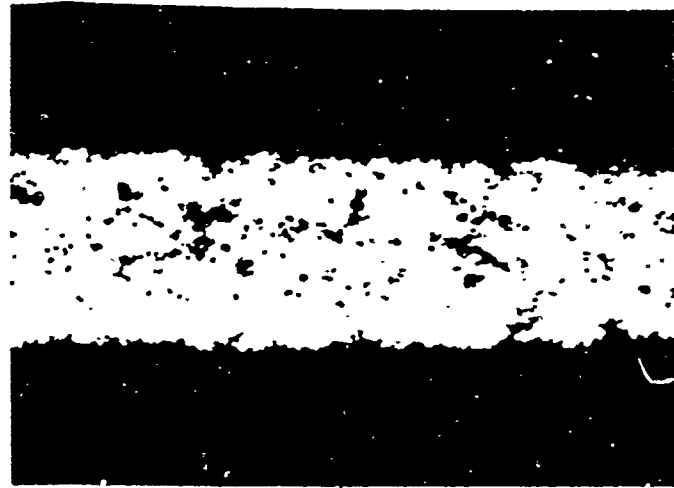
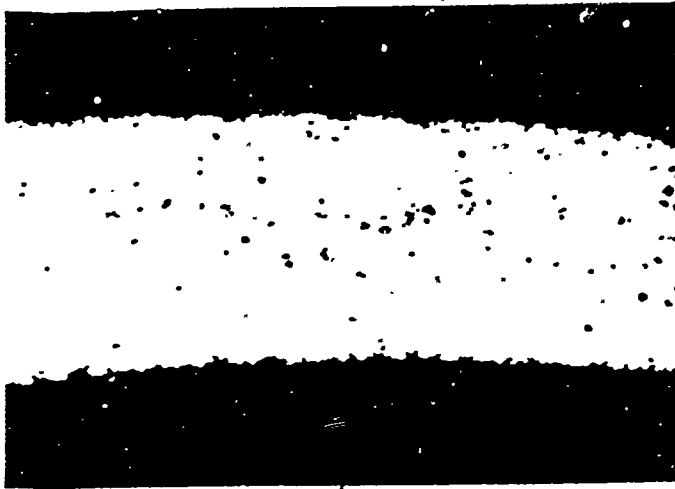
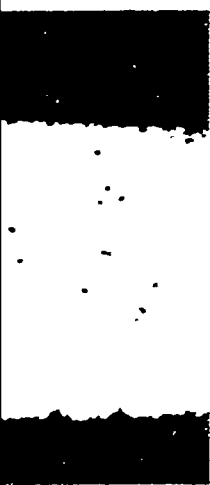
1

7475 ALUMINUM ALLOY
7475-II-P7, CONE 4

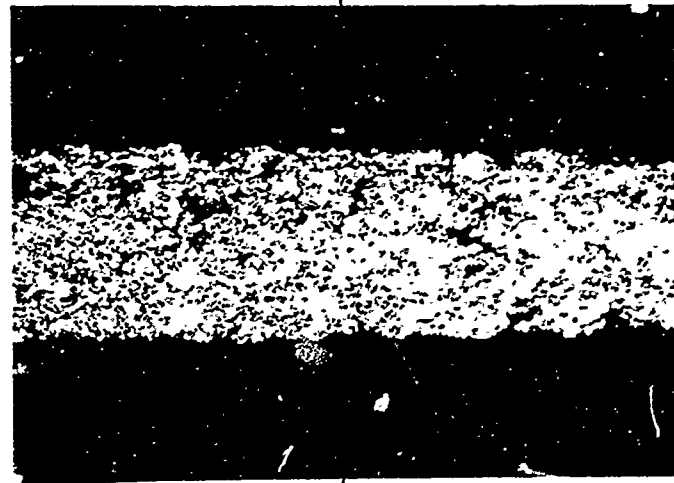
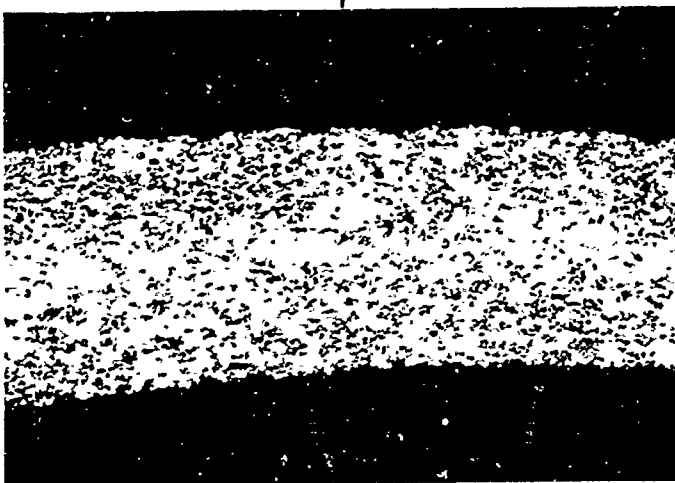
AS POLISHED
→ 500 μm →

3

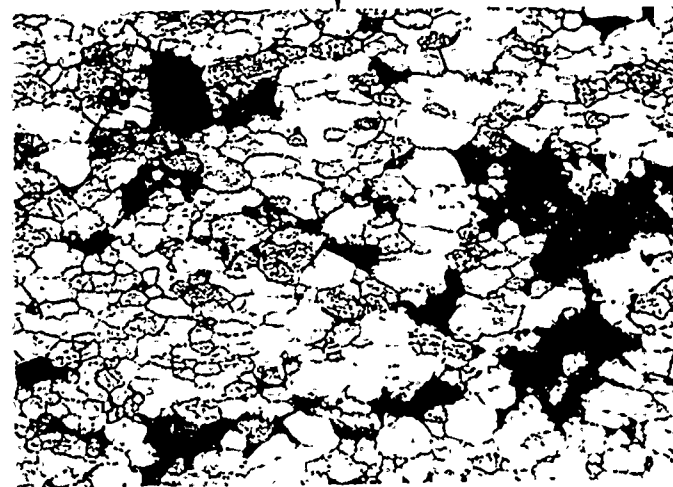
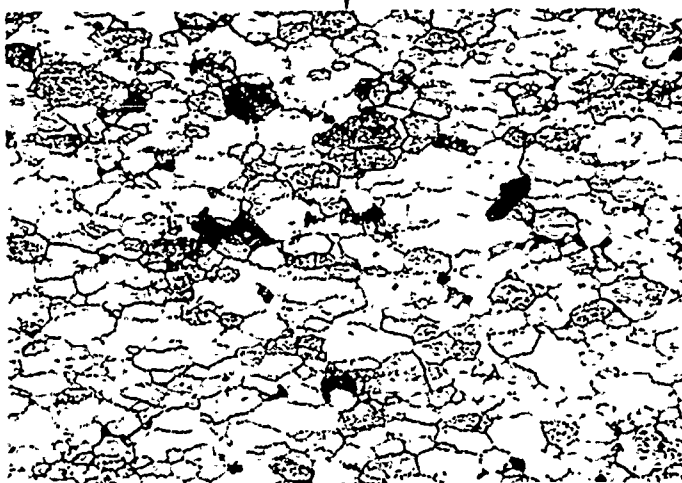
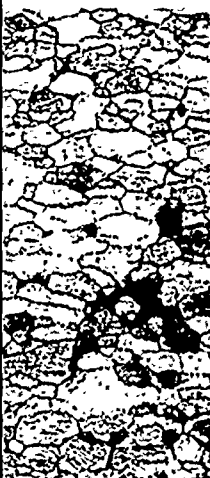
4



ETCHED
→ 500 μm →



ETCHED
→ 100 μm →



118

3

1

TABLE 4-5. Fo

SPECIMEN IDENTIFICATION	FORMING TEMPERATURE (F)	TOTAL FORMING TIME (SEC)	AREA 1							
			ϵ (%)	$\dot{\epsilon}$ (SEC ⁻¹)	GRAIN SIZE (μm)		$\frac{\bar{a}}{\bar{b}}$	AREAL CAVITATION (%)	ϵ (%)	(
					\bar{a}	\bar{b}				
7475-II - E5 - CONE 2	850	5400	4.6	8.3×10^{-6}	15.2 ± 1.0	7.5 ± 0.3	2.03	0	8.4	1.
E1 - CONE 2	850	5400	7.2	1.3×10^{-5}	17.7 ± 1.0	8.7 ± 0.4	2.03	0	15.7	2.
E5 - CONE 4	850	5400	8.4	1.5×10^{-5}	20.1 ± 0.4	9.1 ± 0.4	2.20	<0.01	17.0	2.
E1 - CONE 4	850	5400	11.2	2.0×10^{-5}	13.2 ± 0.5	7.1 ± 0.2	1.56	0	31.5	5.
E7 - CONE 2	935	3856	12.5	3.0×10^{-5}	18.5 ± 0.9	10.0 ± 0.5	2.11	0	32.9	7.
E3 - CONE 2	935	2376	12.5	5.0×10^{-5}	20.5 ± 0.8	9.8 ± 0.3	2.09	0	42.8	1.
E7 - CONE 4	935	3856	20.8	4.9×10^{-5}	17.8 ± 0.6	10.1 ± 0.2	2.09	0	72.1	1.
E3 - CONE 4	935	2376	17.0	6.6×10^{-5}	22.7 ± 1.1	10.0 ± 0.5	2.27	0	72.1	2.
P7 - CONE 2	970	2878	15.7	5.1×10^{-5}	19.4 ± 1.0	9.2 ± 0.4	2.11	0	56.4	1.
P6 - CONE 2	970	1569	11.2	6.8×10^{-5}	18.6 ± 0.9	9.3 ± 0.3	2.00	0	44.7	2.
P7 - CONE 4	970	2878	50.6	1.4×10^{-4}	19.6 ± 0.9	9.4 ± 0.8	2.09	<0.01	122.0	2.
P6 - CONE 4	970	1569	18.0	1.0×10^{-4}	18.3 ± 0.9	9.1 ± 0.3	2.01	0	163.0	6.

119

TABLE 4-5. Forming Data for 7475 Aluminum Alloy Sheets

LOCATION														
			AREA 2						AREA 3					
i)	$\frac{\bar{a}}{\bar{b}}$	AREAL CAVITATION (%)	ϵ (%)	$\dot{\epsilon}$ (SEC ⁻¹)	GRAIN SIZE (μm)		$\frac{\bar{a}}{\bar{b}}$	AREAL CAVITATION (%)	ϵ (%)	$\dot{\epsilon}$ (SEC ⁻¹)	GRAIN SIZE (μm)		$\frac{\bar{a}}{\bar{b}}$	AREAL CAVITATION (%)
					\bar{a}	\bar{b}					\bar{a}	\bar{b}		
0.3	2.03	0	8.4	1.5×10^{-5}	16.6 ± 0.9	7.8 ± 0.3	2.00	<0.01	12.5	2.2×10^{-5}	15.6 ± 0.9	7.7 ± 0.3	2.03	0.01
0.4	2.03	0	15.7	2.7×10^{-5}	16.8 ± 0.8	7.8 ± 0.2	2.15	0	20.6	3.5×10^{-5}	15.7 ± 0.9	7.6 ± 0.3	2.07	0
0.4	2.20	<0.01	17.0	2.9×10^{-5}	20.4 ± 2.0	9.0 ± 0.4	2.27	0.02	21.9	3.7×10^{-5}	19.0 ± 0.9	8.0 ± 0.2	2.38	0.02
0.2	1.56	0	31.5	5.0×10^{-5}	13.9 ± 1.0	7.0 ± 0.2	1.53	0	37.8	5.9×10^{-5}	13.4 ± 0.8	6.9 ± 0.2	1.94	0
0.5	2.11	0	32.9	7.4×10^{-5}	21.4 ± 1.0	9.7 ± 0.4	2.01	0	46.3	9.9×10^{-5}	20.7 ± 1.0	10.0 ± 0.5	2.09	0.01
0.3	2.09	0	42.8	1.5×10^{-4}	19.8 ± 1.0	9.2 ± 0.3	2.15	0	50.0	1.7×10^{-4}	19.5 ± 0.8	9.0 ± 0.3	2.17	0
0.2	2.09	0	72.1	1.4×10^{-4}	17.3 ± 1.0	10.0 ± 0.5	1.96	1.2	166.0	2.5×10^{-4}	16.1 ± 1.0	10.3 ± 0.4	1.85	5.2
0.5	2.27	0	72.1	2.3×10^{-4}	18.4 ± 1.2	8.7 ± 0.3	2.10	0.5	166.0	4.1×10^{-4}	17.0 ± 1.0	9.4 ± 0.3	1.81	2.8
0.4	2.11	0	56.4	1.5×10^{-4}	17.9 ± 0.6	8.9 ± 0.3	2.01	0.055	80.8	2.1×10^{-4}	18.6 ± 0.9	8.9 ± 0.3	2.09	0.05
0.3	2.00	0	44.7	2.3×10^{-4}	18.2 ± 0.9	8.8 ± 0.3	2.07	0	52.1	2.7×10^{-4}	16.4 ± 0.8	8.6 ± 0.2	1.90	0
0.8	2.09	<0.01	122.0	2.8×10^{-4}	18.3 ± 0.8	9.3 ± 0.3	1.96	0.1	262.0	4.5×10^{-4}	17.8 ± 0.6	9.6 ± 0.4	1.85	4.3
0.3	2.01	0	163.0	6.2×10^{-4}	14.7 ± 0.7	8.4 ± 0.3	1.75	0.4	221.0	7.4×10^{-4}	14.1 ± 0.7	8.7 ± 0.3	1.60	3.6

AREA 4							
$\frac{\bar{a}}{\bar{b}}$	AREAL CAVITATION (%)	ϵ (%)	$\dot{\epsilon}$ (SEC ⁻¹)	GRAIN SIZE (μm)		$\frac{\bar{a}}{\bar{b}}$	AREAL CAVITATION (%)
				\bar{a}	\bar{b}		
0.03	0.01	17.0	3.0×10^{-5}	16.6 ± 1.0	8.1 ± 0.3	2.05	0.01
0.07	0	20.6	3.5×10^{-5}	16.6 ± 1.0	7.8 ± 0.2	2.13	<0.01
0.38	0.02	21.9	3.7×10^{-5}	18.6 ± 1.0	8.1 ± 0.2	2.30	0.01
1.94	0	41.3	6.4×10^{-5}	13.0 ± 0.5	6.8 ± 0.2	1.91	0.02
2.09	0.01	46.3	9.9×10^{-5}	20.7 ± 0.9	9.7 ± 0.4	2.16	0.1
2.17	0	50.0	1.7×10^{-4}	18.1 ± 0.8	8.8 ± 0.3	2.06	0.2
1.85	5.2	193.0	2.8×10^{-4}	16.5 ± 0.8	11.6 ± 0.5	1.67	12.7
1.81	2.8	193.0	4.5×10^{-4}	17.3 ± 0.9	9.5 ± 0.6	1.82	4.4
2.09	0.05	86.6	2.2×10^{-4}	18.4 ± 1.0	8.5 ± 0.4	2.16	0.08
1.90	0	60.6	3.0×10^{-4}	16.2 ± 1.0	8.5 ± 0.3	1.90	0.01
1.85	4.3	316.0	4.9×10^{-4}	16.7 ± 0.8	10.0 ± 0.5	1.67	12.8
1.60	3.6	285.0	8.6×10^{-4}	13.7 ± 0.7	8.8 ± 0.4	1.60	7.2

The cavitation measurements of Table 4-5 for the 7475 alloy sheet are plotted as a function of the SPF strain in Figure 4-11. The data obtained at all three temperatures are presented in this figure. Several observations made from the plots in this figure are summarized in the following paragraphs.

Virtually no cavitation, < 0.5 areal percent, was observed up to 60 percent SPF strain at all three temperatures. Beyond this strain, cavitation began to increase with increasing strain. Up to 100 percent strain was achieved with a cavitation level of < 1 percent at 935°F temperature. This value of strain, with cavitation < 1 percent, increased to 150 percent when the temperature was raised to 970°F. Beyond 100 percent strain at 935°F and 150 percent strain at 970°F, cavitation increased dramatically with the increasing strain. Values of areal cavitation in excess of 12 percent were obtained with strains of 320 percent. As expected, the effect of temperature was to suppress cavitation. This is evidenced by the fact that the 970°F curve is to the right of the 935°F curve, i.e., larger SPF strain is attained at the higher temperature for a given level of cavitation. However, from the slopes of the curves at these two temperatures, it is noted that the effect of temperature is to delay cavitation, perhaps due to a more efficient accommodation of cavities by the faster diffusion at the higher temperatures, rather than to retard its rate. Thus, a higher temperature serves to delay the onset of cavitation but does not significantly influence the rate of cavitation, i.e., the rate of nucleation and growth of cavities. Strain rate showed a similar effect on cavitation as the temperature. For the levels of strain achieved in these specimens, Table 4-5, virtually no cavitation was observed up to strain rates of $1.5 \times 10^{-4} \text{ sec}^{-1}$. Beyond this strain rate, cavitation rose rapidly with the rise in strain rate and strain. Again, the effect of a higher temperature was to shift the cavitation curve to the right on the strain rate axis, i.e., at higher temperature the onset of cavitation occurred at a faster strain rate than at lower temperature.

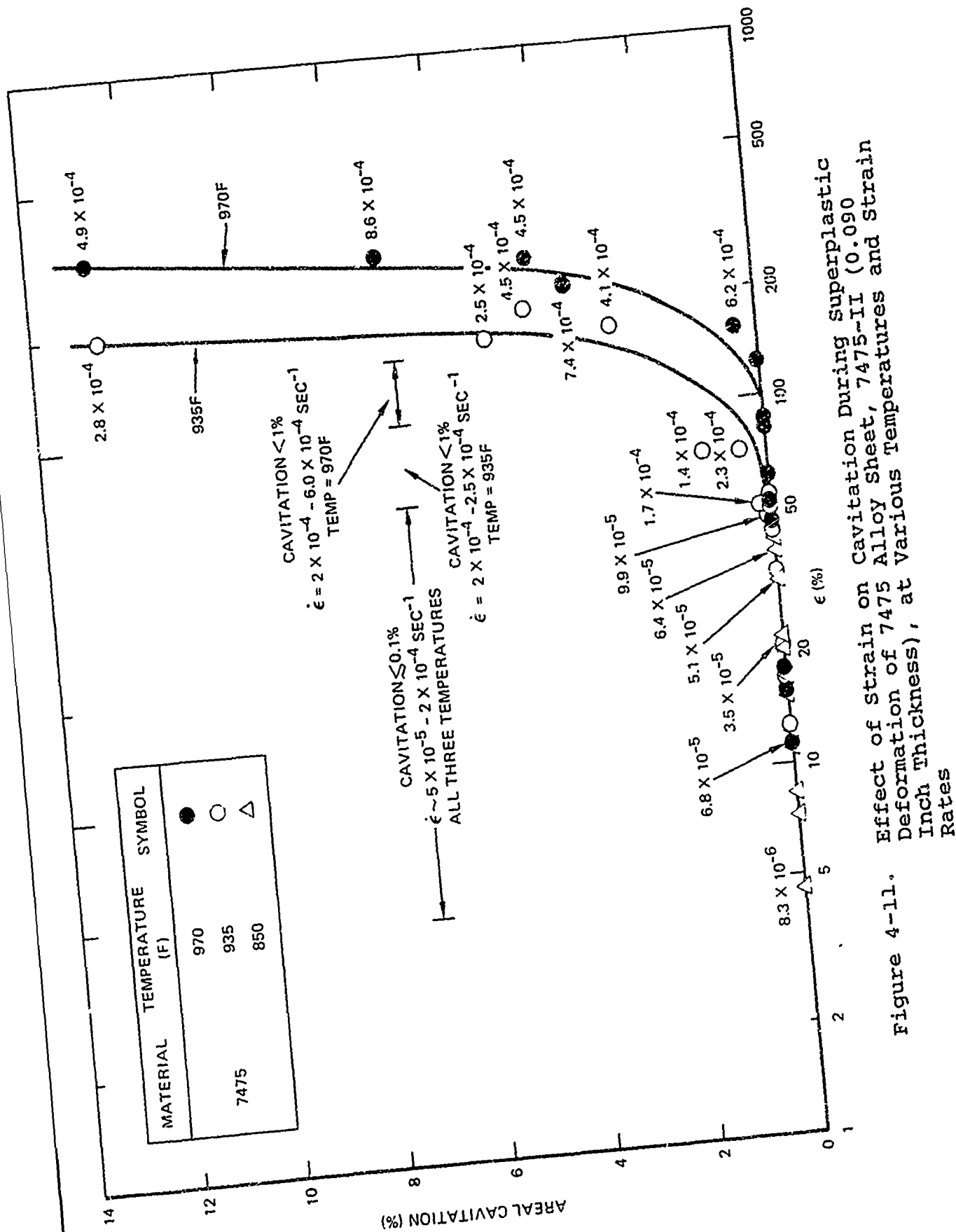


Figure 4-11. Effect of Strain on Cavitation During Superplastic Deformation of 7475 Alloy Sheet, 7475-II (0.090 Inch Thickness), at Various Temperatures and Strain Rates

The longitudinal and transverse grain size measurements, \bar{a} and \bar{b} , for the 7475 alloy sheet were examined as a function of the SPF strain, Table 4-5. A slight grain refinement with increasing SPF strain was noted in these specimens, Figure 4-12. This is in contrast to the predominant grain growth observed in Ti-6Al-4V alloy as a result of the exposure to SPF process conditions^{8,9}, but is possible due to a dynamic recrystallization effect at the higher strain rates¹⁰. The transverse grain size, \bar{b} , showed very little change with strain, Figure 4-13. Thus, the net result due to a slight refinement in the \bar{a} dimension and little or no change in the \bar{b} dimension was to reduce the \bar{a}/\bar{b} aspect ratio, i.e., the grains were a little more equiaxed after SPF deformation than in the initial mill produced sheet material.

Microstructural observations similar to those shown in Table 4-5 and Figures 4-12 and 4-13 for 7475 were also made for 7050 and P/M 7091 alloys. Trends observed in the SPF behavior of alloys 7050 and P/M 7091 were similar to those noted in 7475. However, the overall strains attained in these alloys prior to onset of cavitation, as well as when cavitation becomes significantly large, were considerably smaller than those attained in 7475.

4.2 FINAL MATERIAL SELECTION AND EVALUATION

The second phase of this task included an extensive evaluation of the finally selected alloy. The foregoing observations regarding the preliminary evaluation of the superplastic performance of the three alloys, in addition to the considerations of their source and availability, led to the choice of 7475 as the most suitable of the three alloys for use in this program. Subsequent to selection of 7475 for fabrication of the program components it was thoroughly characterized. This characterization included fabrication of SPF pans with varying levels of strains from which test specimens were excised, determination of

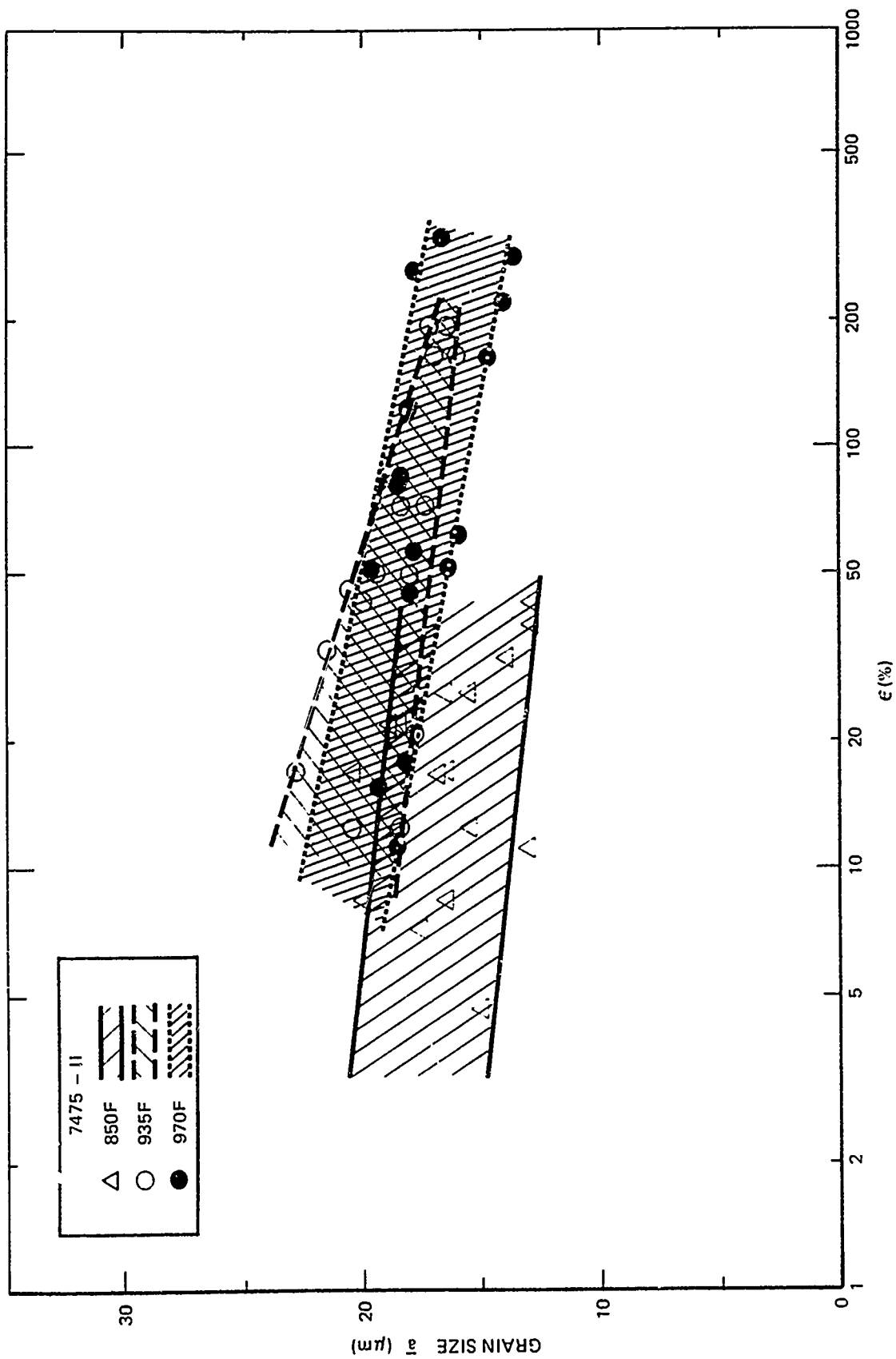


Figure 4-12. Effect of SPF Strain on Grain Size (a) in a 7475 Alloy Sheet, 7475-II (0.090 Inch Thickness), at Various Temperatures

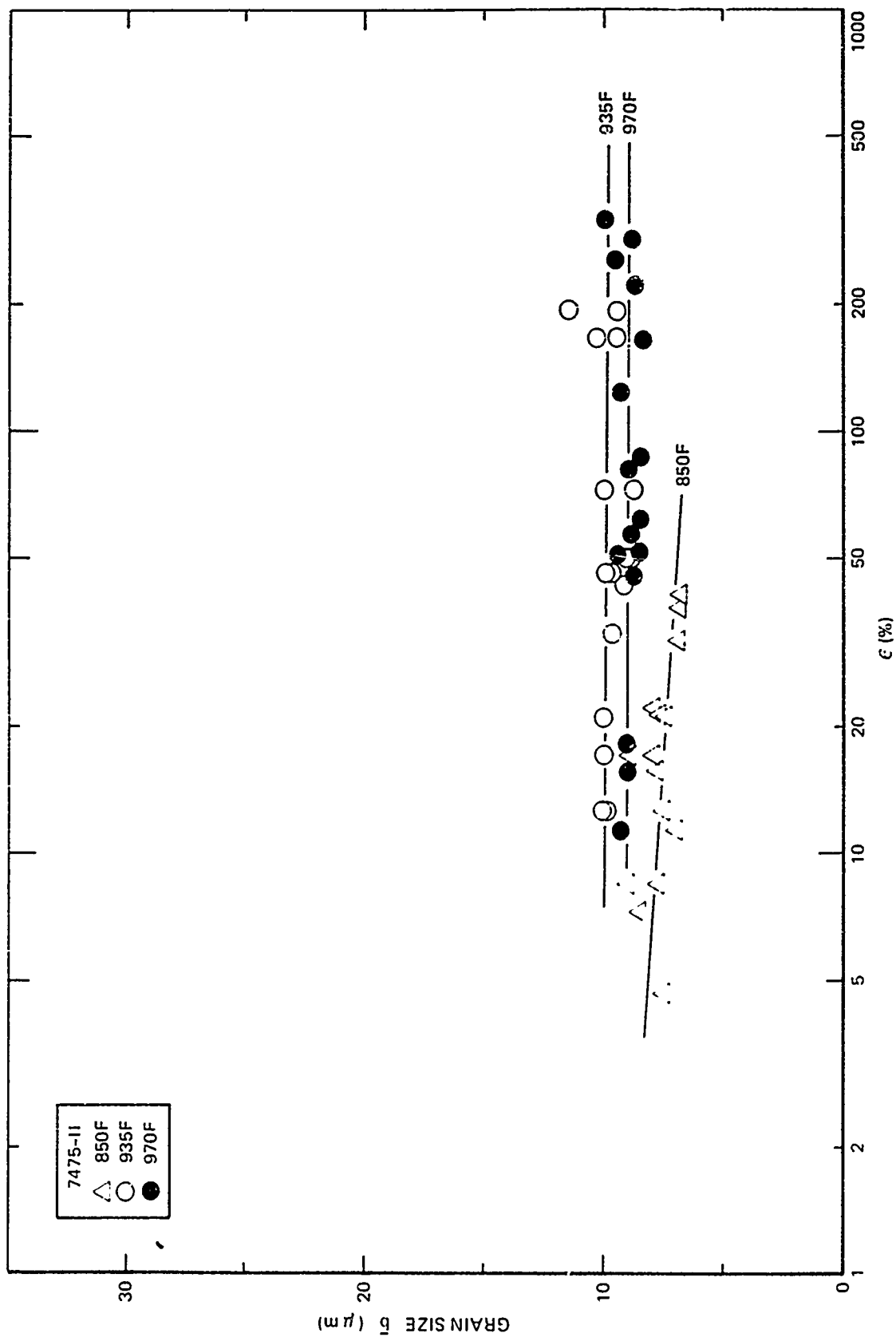


Figure 4-13. Effect of SPF Strain on Grain Size (b) in a 7475 Alloy Sheet, 7475-II (0.090 Inch Thickness), at Various Temperatures

the mechanical and structural properties of the post-SPF material, examination of microstructure of the formed material, and correlation of microstructural features with the observed properties of material formed to different SPF strain levels and loading conditions. The approved plan for the test matrices to determine post-SPF properties of the finally selected material, and evaluation of its secondary processability after SPF is shown in Tables 4-6 and 4-7, respectively.

4.2.1 Material Evaluation

The test plan described in Tables 4-6 and 4-7 represents a systematic and thorough approach to help meet Task II goals. As shown in the tables, comprehensive post-SPF static and fatigue mechanical property data were obtained on the finally selected alloy. Static properties were generated for longitudinal and transverse orientations from two initial sheet thicknesses and three SPF strains. Selected combinations of three variations were used for fatigue and environmental tests. Stress corrosion, exfoliation corrosion and fatigue crack growth in salt water were also tested.

In addition, secondary processing factors were examined. The ability of the SPF material to accept paint, adhesives, and anodic coatings was tested as well as the spot and seam weld quality. Chemical milling was also evaluated. Appropriate microstructural evaluations were performed to verify the results obtained in the material testing effort.

Subsequent to the selection of 7475 as the final alloy sheets of this alloy were mill produced in two gauges, 0.090 and 0.125 inch, at Reynolds' mill production facilities at McCook, Illinois and Richmond, Virginia. Efforts were concentrated on spot checking this mill produced material to ascertain its SPF potential, and the as produced microstructure and room-temperature mechanical properties.

TABLE 4-6. TASK II - TEST MATRIX TO DETERMINE POST SPF PROPERTIES OF SELECTED MATERIAL.

TEST	MECHANICAL PROPERTY DATA REQUIRED	TEST METHOD	NUMBER OF SPECIMENS	
			EACH COMBI-NATION ¹	TOTAL
TENSION	F_{tu} , F_{ty} , e , E	ASTM E 8	1	12
SHARP-NOTCH TENSION	SNS, SNS/ F_{ty}	ASTM E 388	1	12
COMPRESSION	F_{cy} , E_c	ASTM E 9	1	12
BEARING	F_{bru} , F_{bry} ($e/D = 2.0$)	ASTM E 238	1	12
SHEAR	F_{su}	PUNCH-TYPE	1 ²	6
FATIGUE, $K_t=1.0$, $R=0.1$	STRESS-LIFE (10^4 TO 10^6 CYCLES)	ASTM E 466	10 ³	20
FATIGUE, $K_t=3.0$, $R=0.1$	STRESS-LIFE (10^4 TO 10^6 CYCLES)	ASTM E 466	10 ³	20
FATIGUE CRACK GROWTH, $R=0.1$, AIR	da/dN VS ΔK	ASTM E 647	2 ³	4
FATIGUE CRACK GROWTH, $R=0.1$, SALT WATER	da/dN VS ΔK	ASTM E 647	1 ³	2
STRESS CORROSION, ALTERNATE IMMERSION	NO STRESS CORROSION CRACKING IN 84 DAYS AT 75% MINIMUM YIELD	ASTM G 44 ASTM G 39	1 ³	6
CONSTANT-IMMERSION CORROSION	EXFOLIATION RESISTANCE	ASTM G 34	1 ^{2,3}	6

¹ Combinations: 3 SPF strain levels (1, 2, 3), 2 orientations initial stock (L,T)

² L and T orientations of starting stock (t_1 , t_2)

³ Two combinations will be selected.

TABLE 4-7. TASK II - EVALUATION OF SECONDARY PROCESSING

PROCESS	TEST	NUMBER OF SPECIMENS
ANODIZING	SALT FOG	1 QUARTER PAN, LOW SPF STRAIN 1 QUARTER PAN, HIGH SPF STRAIN
PAINTING	IMPACT	2 LOW SPF STRAIN 2 HIGH SPF STRAIN
		1 QUARTER PAN, LOW SPF STRAIN 1 QUARTER PAN, HIGH SPF STRAIN
CHEM MILLING	CHEM MILL RATE SURFACE ROUGHNESS	1 QUARTER PAN, LOW SPF STRAIN 1 QUARTER PAN, HIGH SPF STRAIN
	FATIGUE-S/N SMOOTH	2 EACH L & T, LOW SPF STRAIN 2 EACH L & T, HIGH SPF STRAIN
ADHESIVE BONDING	LAP SHEAR	3 EACH L & T, NO SPF STRAIN 3 EACH L & T, HIGH SPF STRAIN
	T-PEEL	3 EACH L & T, NO SPF STRAIN 3 EACH L & T, HIGH SPF STRAIN
RESISTANCE WELDING (SEAM)	PEEL TEST RADIOGRAPHY	3 EACH L & T 3 EACH L & T
WELDBONDING	LAP SHEAR - UNCURED ADHESIVE	3 EACH L & T, NO SPF STRAIN 3 EACH L & T, HIGH SPF STRAIN
	LAP SHEAR - CURED ADHESIVE	3 EACH L & T, NO SPF STRAIN 3 EACH L & T, HIGH SPF STRAIN
	WEDGE TEST	3 EACH L & T, NO SPF STRAIN 3 EACH L & T, HIGH SPF STRAIN

The constant-strain-rate cone tests with the dual pressurization approach used for spot checking the SPF potential of the mill produced material, was the same as that used previously with the lab produced material. A set of test conditions approximating the expected forming conditions, 970°F test temperature and strain rates in the range of 5×10^{-5} to $5 \times 10^{-4} \text{ sec}^{-1}$ were employed. One cone test using four cones, each forming at a different, although nominally constant strain rate was made for each of the two sheet materials tested. The SPF parameters determined in this manner are shown as log flow stress (σ) vs. log strain rate ($\dot{\epsilon}$) plots in Figures 4-14 and 4-15, respectively, for the 0.125-inch and the 0.090-inch material. The results of the present tests are shown as solid points in these figures. The average curves, previously obtained from several tests on the lab produced material using similar testing procedures are also presented in these figures for comparison. The elongation obtained at the pole of each of the four cones, calculated from the reduction in thickness, is indicated on these plots by a number adjacent to each solid point. The number in parentheses is the corresponding value obtained with the laboratory material under comparable conditions.

The following observations were made from these results:

- (1) For both sheet gauges produced at the mill, the $\log \sigma - \log \dot{\epsilon}$ values were very close to those predicted by the average curves corresponding to the lab produced material. The data for the mill produced material could be directly superimposed on the prior curve for the lab material. Consequently, the resultant m values or slopes of these curves at various strain rates, were also the same as those obtained before, both in their absolute magnitude and in the range of strain rates for the peak m .

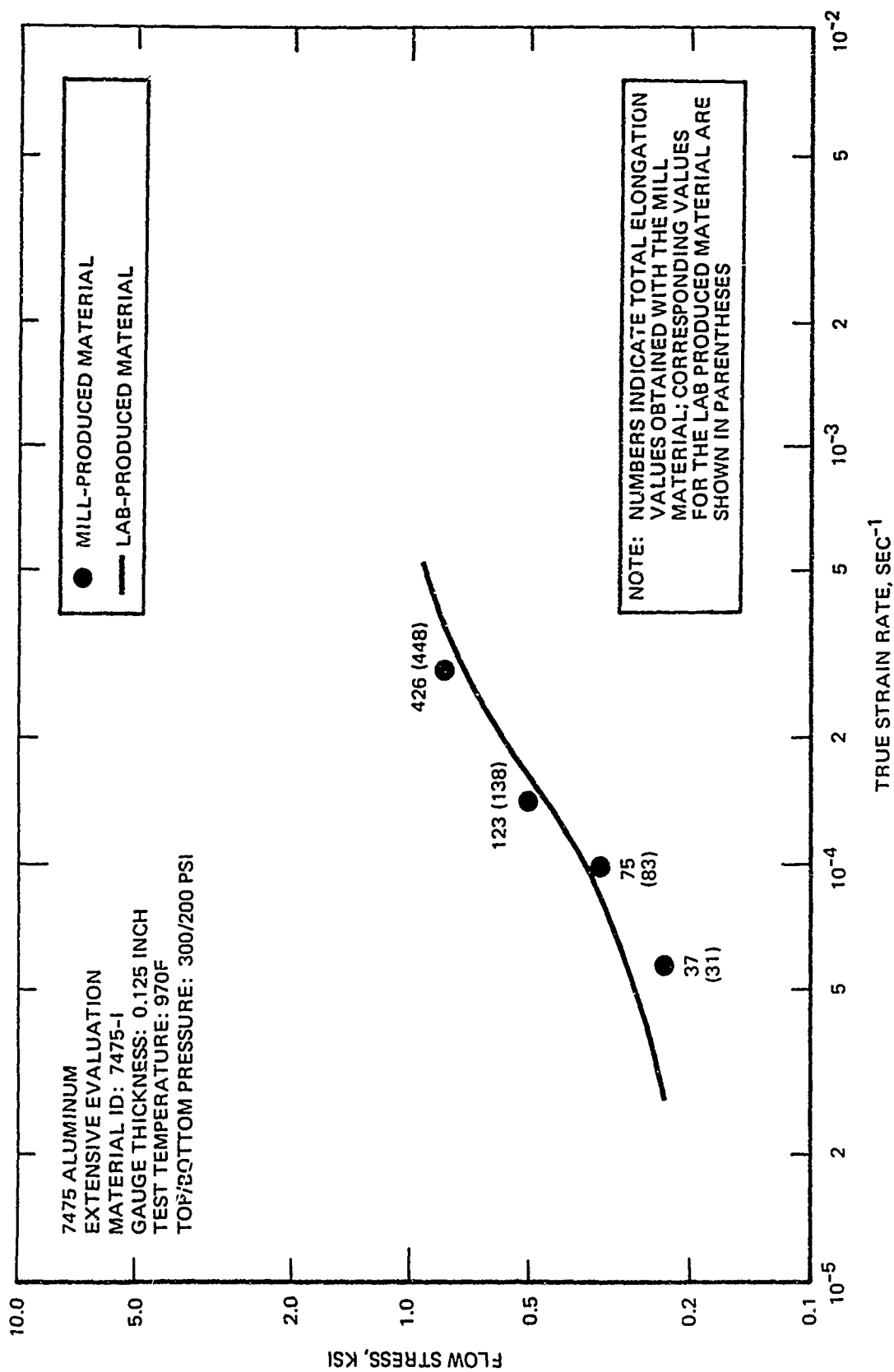


Figure 4-14. Log Flow Stress Versus Log True Strain Rate Plot for the Laboratory and Mill Produced 7475 Aluminum Alloy Sheets (Gauge Thickness 0.125 Inch)

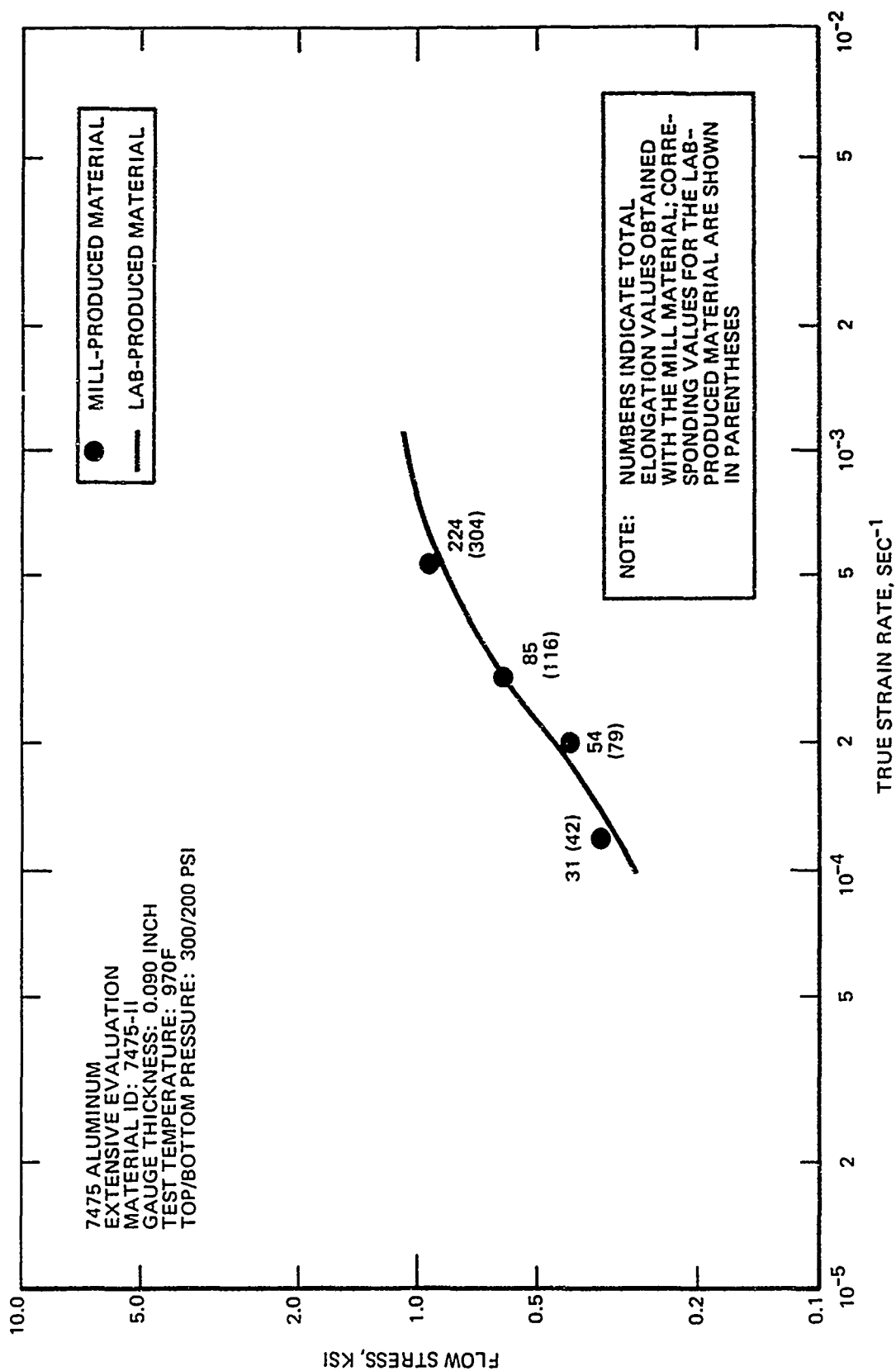


Figure 4-15. Log Flow Stress Versus Log True Strain Rate Plot for the Laboratory and Mill Produced 7475 Aluminum Alloy Sheets (Gauge Thickness 0.090 Inch)

- (2) It was noted from the thickness strain values at the poles of various cones that the mill produced material showed slightly lower strains than the laboratory produced material for both material thicknesses. This could be due to several reasons, including a possible difference in the chemistries of the laboratory and the mill materials, which would influence the cavitation response, and thereby their SPF strains. However, the relative difference in strain to fracture (largest strain number on each plot) between the mill and the laboratory produced versions of the two gauges of sheets was large only in the case of the 0.090-inch thick material (224 percent vs. 304 percent). The difference in the 0.125-inch thick material was only 5 percent (426 percent vs. 448 percent).

Based upon the foregoing, it was concluded that the SPF potential of the two mill materials was comparable to that of the laboratory produced materials.

4.2.2 Microstructural Evaluation

The three dimensional microstructures of these materials are shown in Figures 4-16 (7475-I, 0.125 inch thick) and 4-17 (7475-II, 0.090 inch thick). A slight surface to center variation in the grain size and morphology was noted in both sheet gauges. However, it was believed to be too small to appreciably influence the SPF behavior of these materials. The average values of grain size in the longitudinal and short transverse directions were 22 ± 1.8 and $8.8 \pm 0.4 \mu\text{m}$, respectively, for the 0.125-inch thick sheet, and 18.4 ± 1.3 and $8.3 \pm 0.4 \mu\text{m}$, respectively, for the 0.090-inch thick sheet. The aspect ratios were 2.5 and 2.2, respectively, for the 0.125- and 0.090-inch thick

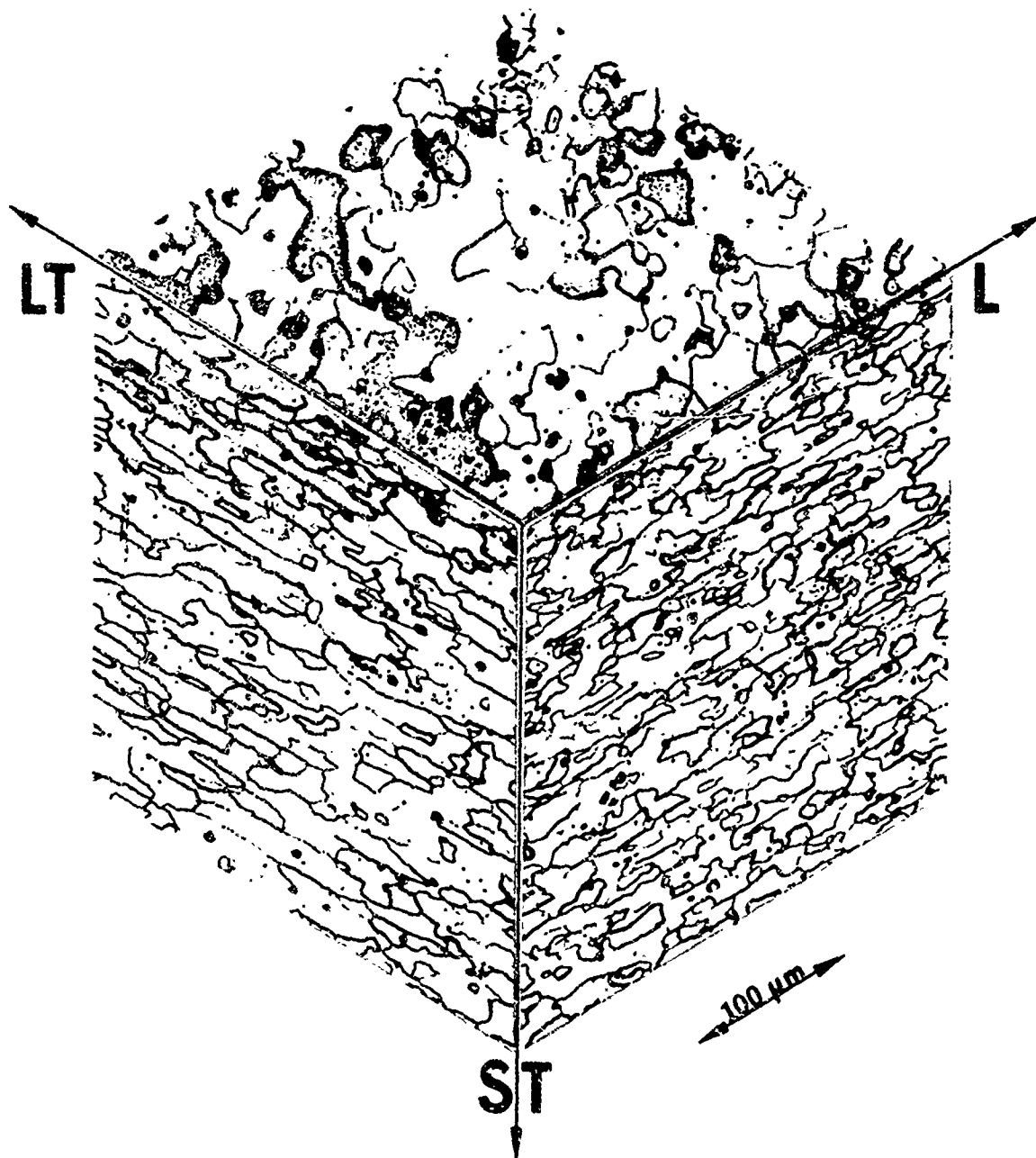


Figure 4-16. Microstructure of the Mill Produced SPF Aluminum Alloy Sheet M7475-I (0.125 Inch Thickness)

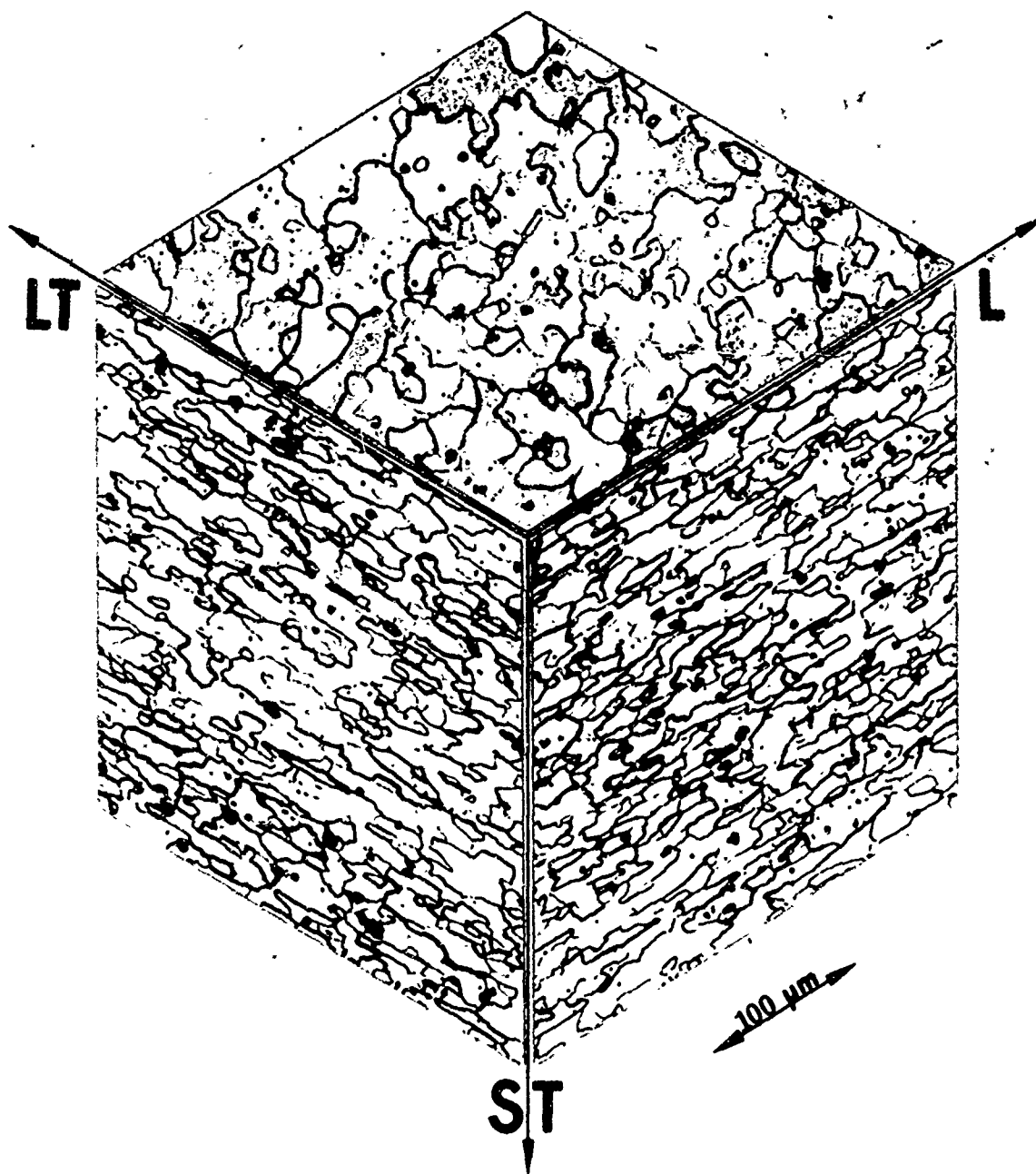


Figure 4-17. Microstructure of the Mill Produced SPF Aluminum Alloy Sheet M7475-II (0.090 Inch Thickness)

sheets. The corresponding values of grain size for the laboratory produced material in the longitudinal and short transverse directions, respectively, were 15.3 ± 4.1 and $8.7 \pm 1.3 \mu\text{m}$, for the 0.125-inch thick sheet, and 13.6 ± 3.1 and $9.1 \pm 1.4 \mu\text{m}$ for the 0.090-inch thick sheet. The aspect ratios were 1.9 and 1.5, respectively, for the 0.125- and 0.090-inch thick sheets.

4.2.3 Property Evaluation

The room temperature mechanical properties of the two SPF aluminum mill materials, M7475-I and M7475-II in the T6 condition, are listed in Table 4-8. Also shown for comparison in this table are similar properties for the conventionally produced 0.090-inch thick 7075 sheet. It is apparent from these data that some of the properties of the mill produced 7475 material in both gauges were comparable, and in some instances superior, to those of the conventional 7075 material. An important observation to be made here is that the SPF mill material is more isotropic in the plane of the sheet than the conventional 7075 material. This is consistent with the less elongated, more equiaxed grain structure in the SPF material than in the conventional 7075 material.

The post-SPF property evaluation task consisted of SPF pans to obtain specimens for post-SPF evaluations and determining the post-SPF mechanical properties and secondary processing parameters. The type of tests and the results obtained are described in the following paragraphs.

4.2.3.1 Superplastic Forming of Pans

Trough shaped pans of different geometries, representing different magnitudes of maximum superplastic strain, were fabricated using the superplasticity parameters determined earlier. The pressure-time profiles (forming cycles) for fabricating these pans and a photograph of typical pans are shown in Figures 4-18 and 4-19, respectively¹¹. All of these pans were formed at

TABLE 4-8. RESULTS OF ROOM TEMPERATURE TENSILE TESTS ON THE MILL-PRODUCED SPF 7475 ALUMINUM ALLOY SHEETS (IN T6 CONDITION) AND THE CONVENTIONALLY PRODUCED 7075-T6 SHEET

MATERIAL IDENTIFICATION	ORIENTATION	YIELD STRENGTH (KSI)	ULTIMATE STRENGTH (KSI)	ELONGATION (%)	MODULUS (10 ⁶ PSI)
M-7475-I	LONGITUDINAL	74.4	83.8	14.5	11.9
		75.0	84.6	15.3	11.4
		AVERAGE	74.7	84.2	14.9
M-7475-I	TRANSVERSE	74.5	83.9	19.1	11.3
		74.3	83.7	15.5	11.9
		74.3	83.7	14.8	12.4
		AVERAGE	74.4	83.8	16.5
M-7475-II	LONGITUDINAL	76.0	84.7	13.9	11.4
		76.1	84.7	14.2	11.1
		76.0	84.6	15.5	10.8
		AVERAGE	76.0	84.7	14.5
M-7475-II	TRANSVERSE	73.7	84.4	15.5	11.2
		73.4	83.9	14.7	11.4
		73.9	84.2	14.9	12.0
		AVERAGE	73.7	84.2	15.0
7075-T6	LONGITUDINAL	73.5	79.4	14.6	10.3
		72.8	78.9	14.1	10.4
		73.5	78.3	15.3	10.3
		AVERAGE	73.3	78.9	14.7
7075-T6	TRANSVERSE	73.4	82.7	15.5	10.5
		73.1	82.0	14.5	10.4
		78.4	80.3	14.9	10.5
		AVERAGE	75.0	81.7	15.0

NOTE: M-7475-I Sheet is 0.125 inch thick.

M-7475-II and 7075-T6 Sheets are 0.090 inch thick.

Modulus values were measured from the load-displacement curves.

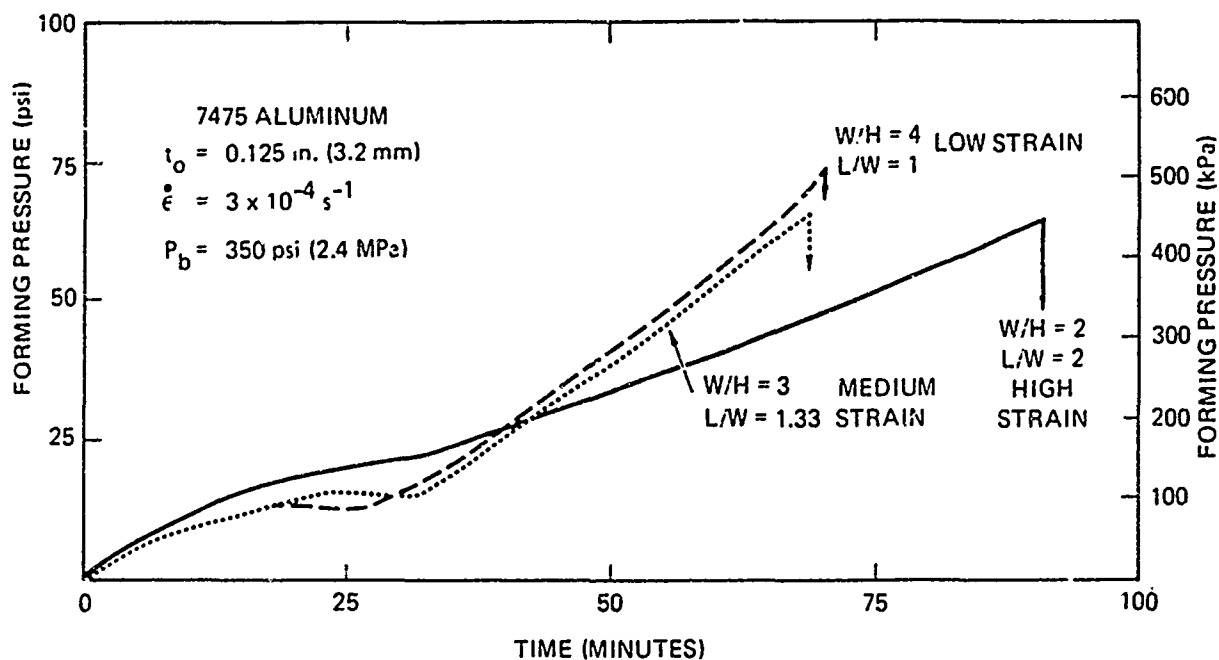


Figure 4-18. Pressure-Time Profiles (Forming Cycles) Used for Fabricating SPF Pans of Three Geometries

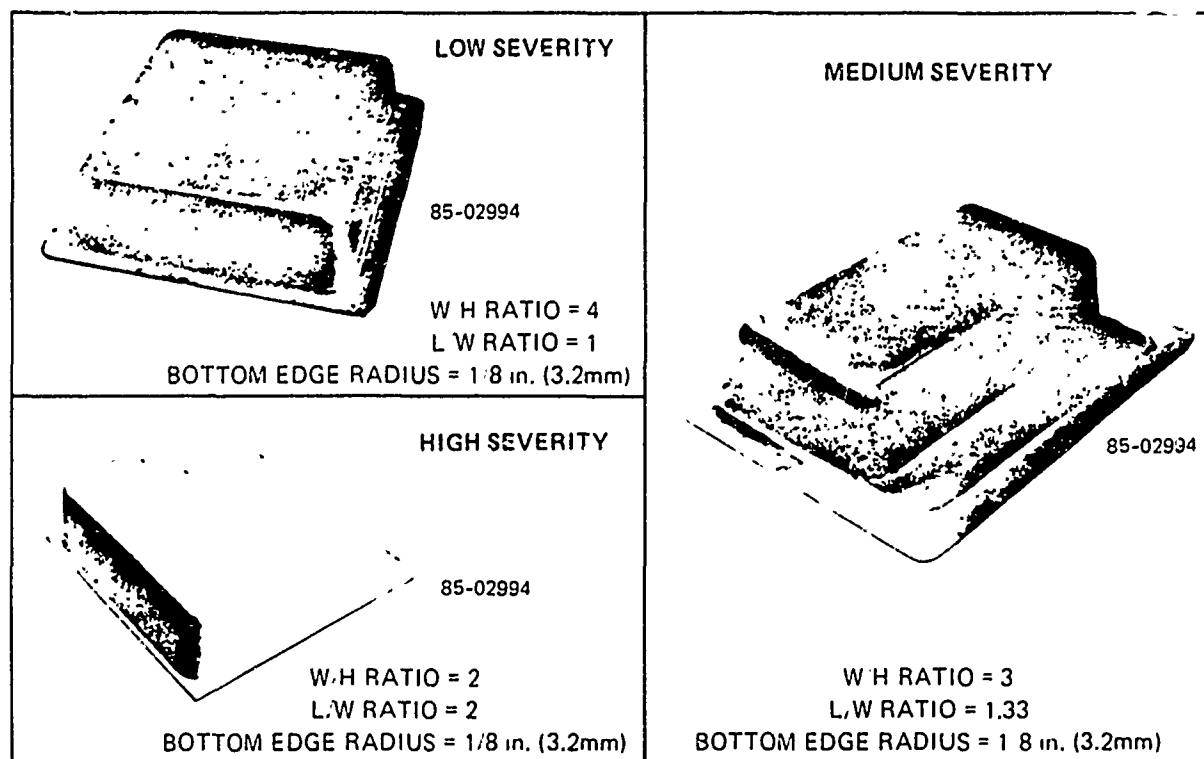


Figure 4-19. SPF Pans of Aluminum Alloy 7475 With Varying Severity of Forming

temperatures in the range of 960 to 970°F using a dual pressurization technique, i.e., a compressive hydrostatic pressure, in addition to the normal tensile pressure for cavity suppression³. The maximum strains in the flat bottom region of these pans were approximately 50 percent (low severity pan, Figure 4-19), 100 percent (medium severity), and 150 percent (high severity).

4.2.3.2 Post-SPF Evaluations

The SPF pans were air cooled and heat treated to a peak age (T6) condition by solution treating, water quenching and a long time low temperature aging. Specimens were subsequently excised for post-SPF material property and secondary processability evaluations. Most of the specimens were obtained from the bottom flat portion of the pans, although some of the tests also utilized specimens from other sections of the pans.

4.2.3.3 Post-SPF Material Properties

Sections obtained from the SPF pans of the type shown in Figure 4-19 were tested for the various room temperature properties in accordance with the test matrix shown in Table 4-9. As mentioned previously, all specimens were in a T6 condition. Results of these were presented at international conference on superplasticity in aerospace aluminum¹² and are described in the following paragraphs.

4.2.3.3.1 Tensile Tests

Typical results of tensile tests conducted on the post-SPF coupons are shown in Figure 4-20. It is evident that the ultimate and yield strengths do not depend upon the amount of prior SPF strain over the present range of strain. It is also noted that the strength values are substantially higher than the MIL-Handbook 5 minimum requirements. The elongation is also independent of SPF strain, and is greater than the MIL-Handbook 5

TABLE 4-9. TEST MATRIX USED FOR EVALUATION OF POST SPF PROPERTIES OF A FINE GRAIN SPF 7475 ALUMINUM ALLOY

TEST	MECHANICAL PROPERTY DATA REQUIRED	TEST METHOD
TENSION	F_{tu} , F_{ty} , e , E	ASTM E 8
SHARP-NOTCH TENSION	SNS , SNS/F_{ty}	ASTM E 388
COMPRESSION	F_{cy} , E_c	ASTM E 9
BEARING	F_{bru} , F_{bry} ($e/D = 2.0$)	ASTM E 238
SHEAR	F_{su}	PUNCH-TYPE
FATIGUE, $K_t=1.0$, $R=0.1$	STRESS-LIFE (10^4 TO 10^6 CYCLES)	ASTM E 466
FATIGUE, $K_t=3.0$, $R=0.1$	STRESS-LIFE (10^4 TO 10^6 CYCLES)	ASTM E 466
FATIGUE CRACK GROWTH, $R=0.1$, AIR	da/dN VS ΔK	ASTM E 647
FATIGUE CRACK GROWTH, $R=0.1$, SALT WATER	da/dN VS ΔK	ASTM E 647
STRESS CORROSION, ALTERNATE IMMERSION	NO STRESS CORROSION CRACKING IN 84 DAYS AT 75% MINIMUM YIELD	ASTM G 44 ASTM G 39
CONSTANT-IMMERSION	EXFOLIATION RESISTANCE	ASTM G 34

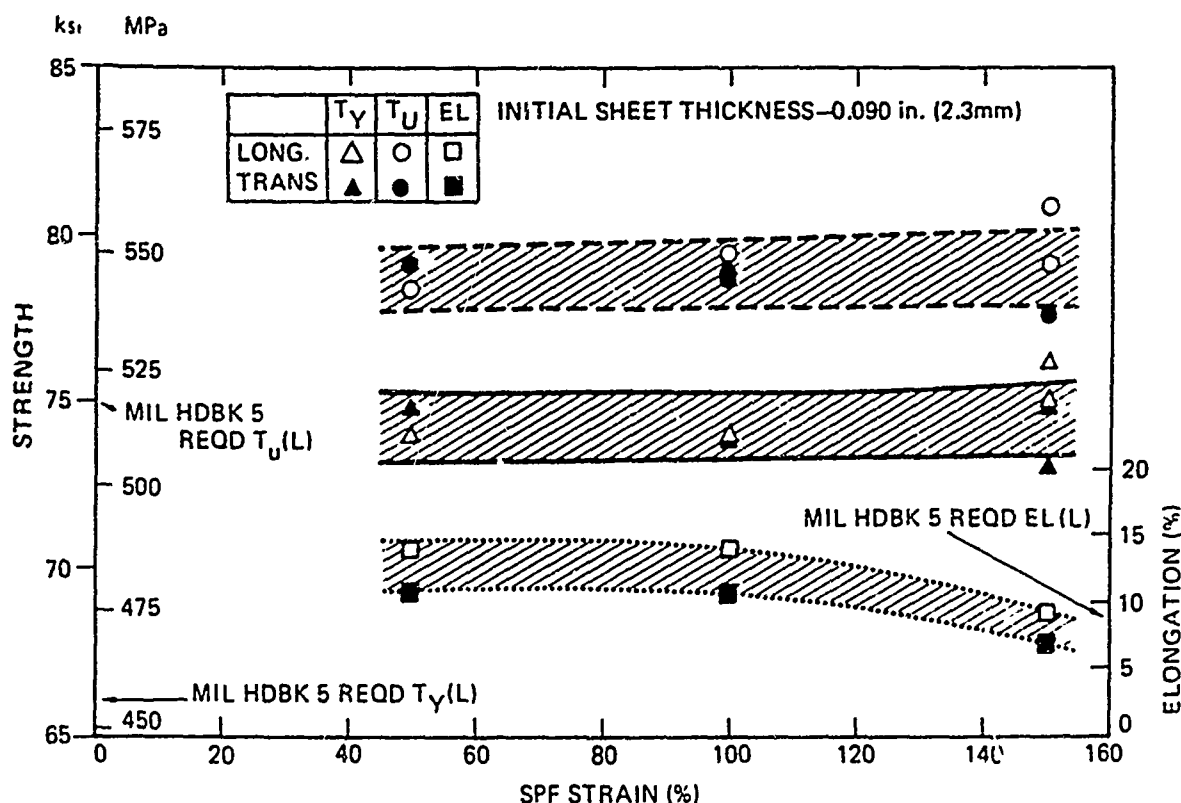


Figure 4-20. Effect of SPF Strain on 7475-T6 Tensile Properties

requirement, up to a value of 100 percent SPF strain. Beyond that, the elongation shows a slight loss with increasing SPF strain.

To date, very little published data are available in the literature showing the effect of SPF strain on the post SPF room temperature properties of high strength aluminum alloys. The only available results of this nature on a similar alloy¹³ support the aforementioned observations, i.e., yield and ultimate strength values are not influenced by the SPF strains of these magnitudes and the elongations shows a drop beyond 100 percent SPF strain.

4.2.3.3.2 Notched Tensile Tests

Figure 4-21 shows the results of notched tensile tests on the post SPF 7475 material representing various SPF strains. It is seen here that after a slight initial loss in the notched tensile strength (NTS), below approximately 100 percent SPF strain, the value remains steady and becomes independent of strain. Accordingly, the notched tensile strength-to-yield (NTS/T_y) ratio also shows some dependence on SPF strain at the lower strain values and none at the higher strains.

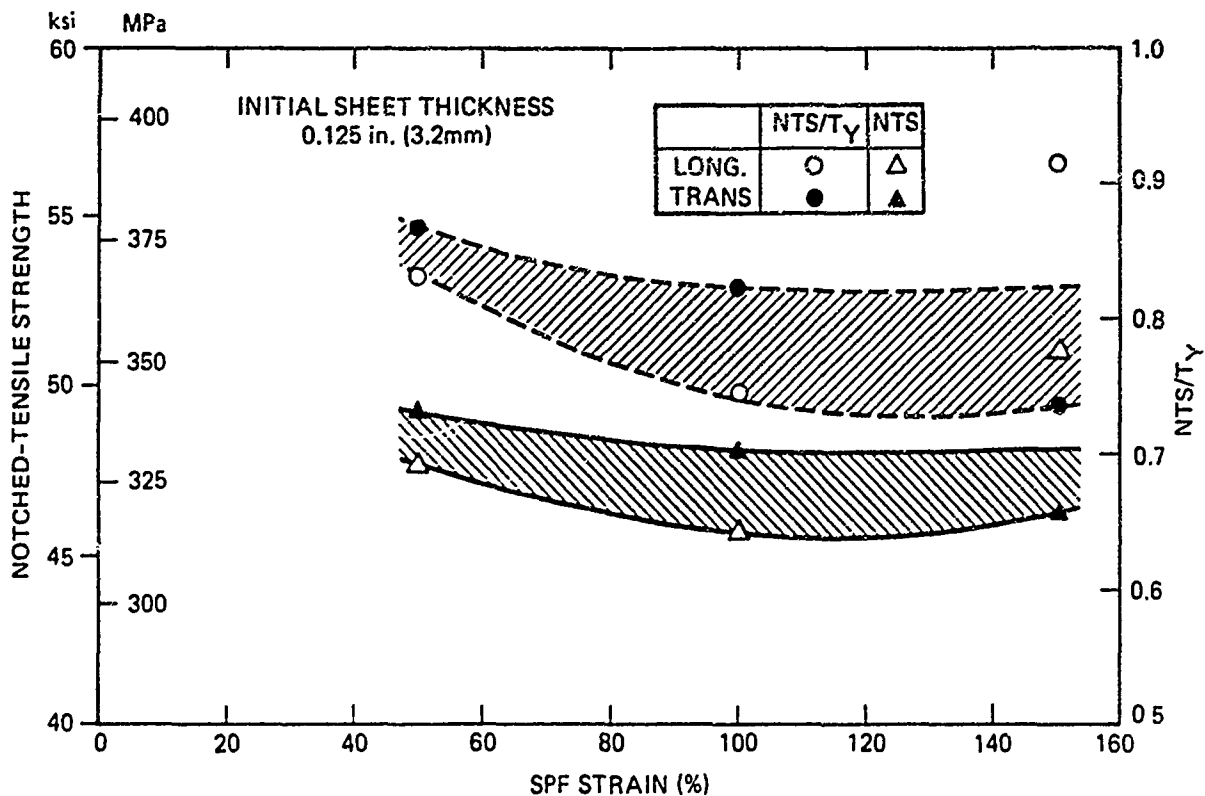


Figure 4-21. Effect of SPF Strain on 7475-T6 Notched Tensile Properties

4.2.3.3.3 Compression Tests

Compression yield strength of the post SPF specimens of 7475 is shown in Figure 4-22 as a function of SPF strain. After

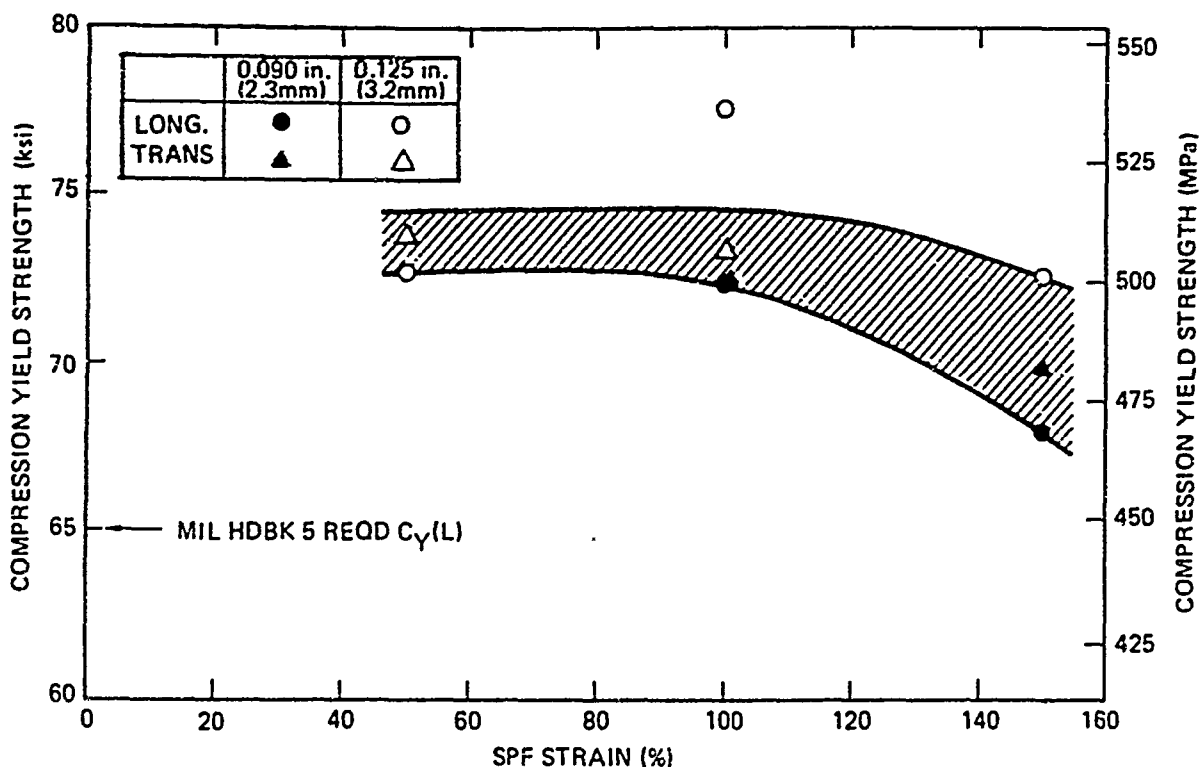


Figure 4-22. Effect of SPF Strain on 7475-T6 Compression Yield Strength

a flat response up to 100 percent strain, the results show 3 to 4 percent reduction in strength at 150 percent SPF strain. However, the measured values of the compression yield strength in the entire range of SPF strains remain higher than the MIL-Handbook 5 required values.

4.2.3.3.4 Bearing Tests

Typical results of these tests are shown in Figure 4-23 as plots of bearing yield and ultimate strength versus SPF strain. Similar to the compression yield strength, the bearing strength is independent of the SPF strain up to 100 percent strain. At 150 percent strain, a slight loss of 5 percent is observed in the bearing strength values. It is however, of concern to note that the present values are similar in magnitude to those required by the MIL-Handbook 5. Thus, it is possible

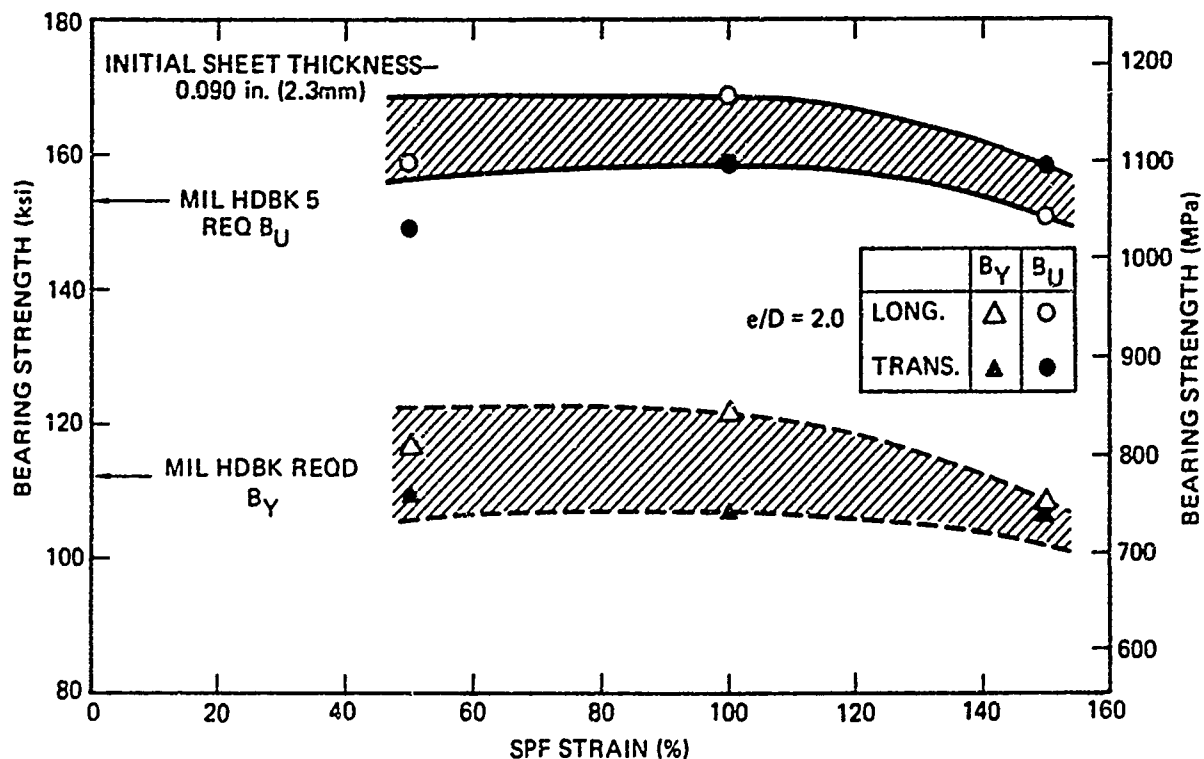


Figure 4-23. Effect of SPF Strain on 7475-T6 Bearing Strength

that the statistically arrived design allowable bearing strength values of the post-SPF material may lie lower than the handbook requirements. This could impact the design philosophy in those instances where bearing strength is of concern.

4.2.3.3.5 Shear Punch Tests

Results of these tests, as presented in Figure 4-24, show a slight decrease in the shear punch strength at the higher end of the SPF strain. The specimens corresponding to the 0.125-inch initial sheet thickness, i.e., prior to pan forming, tended to retain their strength at the higher SPF strains much better than those corresponding to the 0.090-inch initial sheet thickness. This would suggest that the lower shear punch strength values at the higher SPF strains are related to a thickness effect. Present results are too limited to establish that trend clearly.

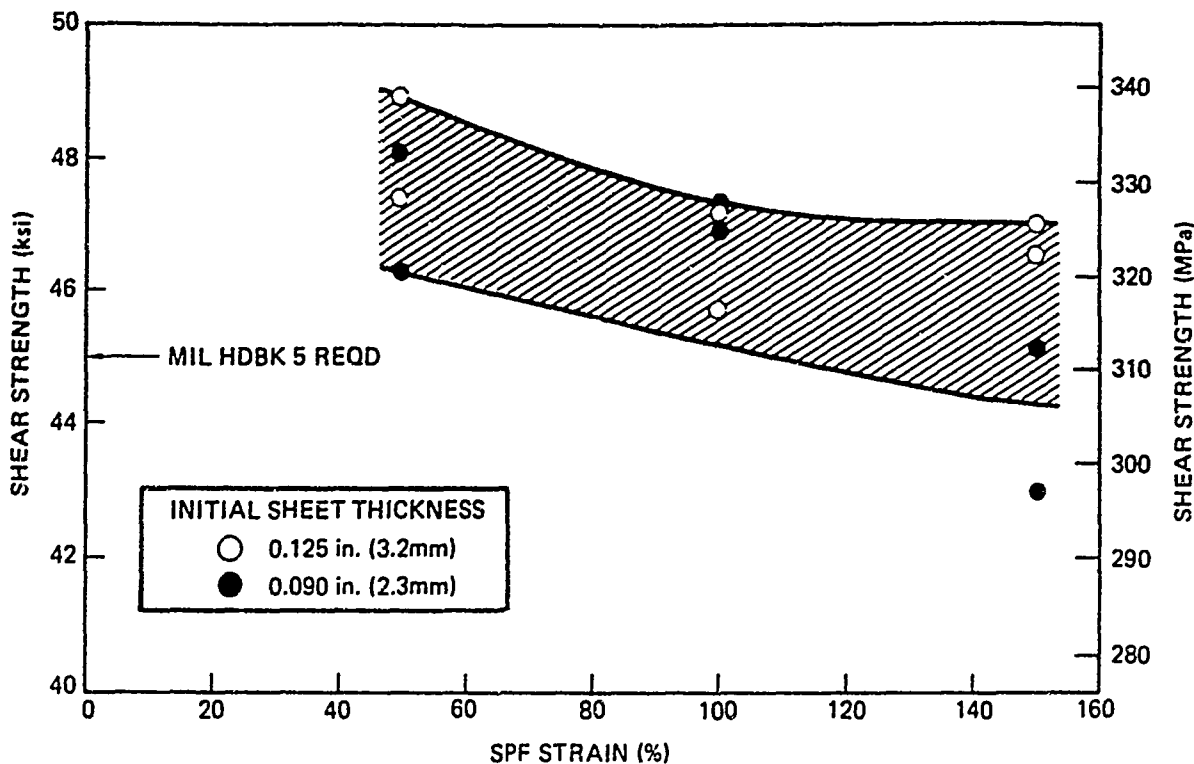


Figure 4-24. Effect of SPF Strain on 7475-T6 Shear Punch Strength

We see from the foregoing discussion of the results of the mechanical tests above that in most instances the properties of the post-SPF material exceeded the MIL-Handbook 5 requirements by a significant margin. Only two tests, bearing and shear punch, gave results which were only slightly above, or sometimes below, the MIL-Handbook 5 requirements. Although a detailed investigation to explain these observations was not undertaken, it is postulated that the present results indicate a tendency for loss in shear strength of the material after SPF. It would be of interest in future investigations to confirm this and to determine the effect of specimen thickness and the magnitude of cavitation on the shear strength of the post-SPF material.

4.2.3.3.6 Fatigue Tests

Smooth fatigue tests were conducted by applying maximum stresses in the range of 30 to 50 ksi at a stress ratio (R) of 0.1. The specimens were in a T6 condition and chemically milled. The results are shown as open and closed symbols and a solid line in Figure 4-25. The available data on conventionally processed commercial material^{14,15} and on a thermomechanically processed fine grain material¹³, similar to the present as-received material, are also shown for comparison. Differences in surface conditions of the test specimens from these materials, present material was chemically milled, the other fine grain material¹³ was surface ground to 600 grade emery, and the conventionally processed commercial material^{14,15} had an unspecified surface condition, presumably representing an aggregate of normal mill-processed sheet surfaces, are ignored since these were the only available results.

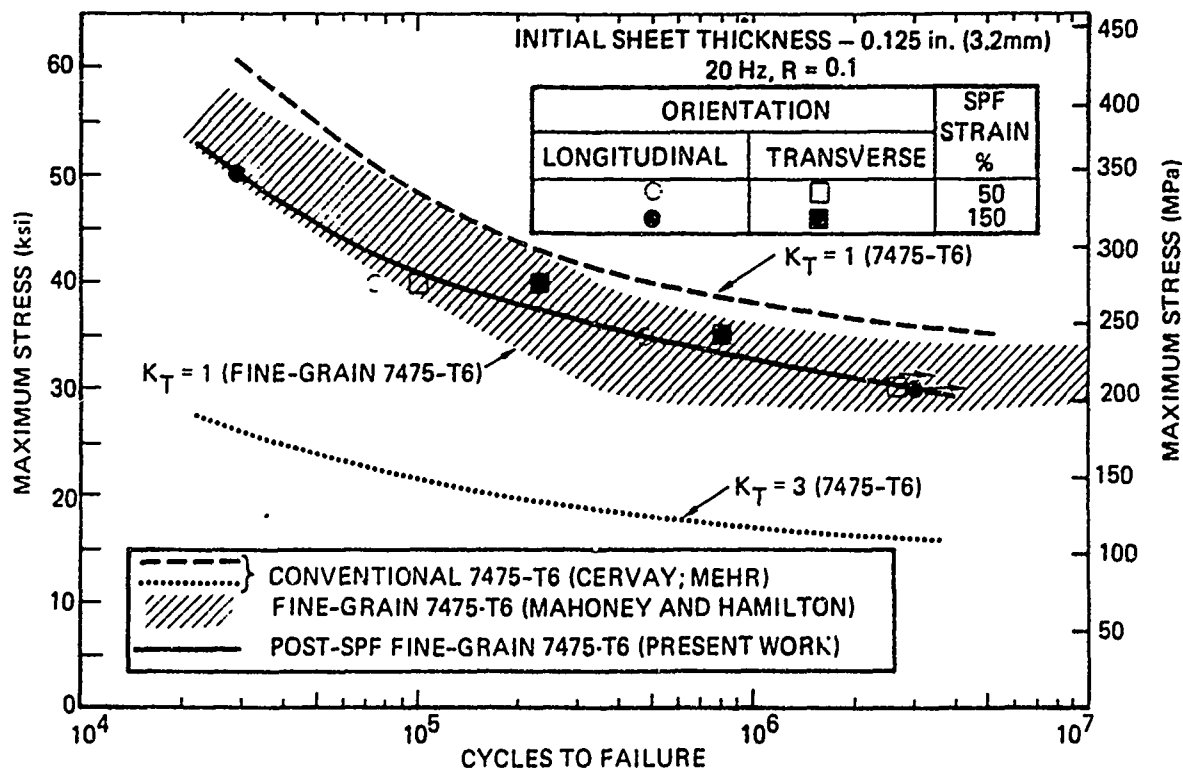


Figure 4-25. Results of Smooth Fatigue Test on Post SPF 7475-T6 Sheets

It is seen in Figure 4-25 that the fatigue behavior of the post-SPF material in both orientations (solid line), is within the band obtained for an equivalent pre SPF material (hatched region). This is particularly true at the lower stresses, or longer lives. This observation suggests that the fatigue response of the post-SPF material is independent of the prior SPF strain, within the range tested, and the specimen orientation. It is possible that when higher SPF strains are achieved in the sheet, or if cavitation is not adequately suppressed, the fatigue response of the post-SPF material may not remain independent of the SPF strain.

While the results of Figure 4-25 do not show any dependence of the fatigue life of post-SPF sheet on the prior SPF strain, they do show that the whole band of performance of the fine grain SPF material¹³ lies just below the mean curve obtained for the conventionally processed material, corresponding to the stress concentration factor (K_t) of 1. This anomaly was not pointed out in the earlier work¹³. Differences in the surface conditions of the various materials of Figure 4-24 could help explain this difference in the fatigue performance, however, a complete description of the materials used in References 14 and 15 will be needed to fully understand the reason for this discrepancy. A more encouraging observation to be made from the results of Figure 4-25 is that the performance of the two fine grain materials, hatched region representing results of Reference 13 and the solid line from the present work, is substantially above that of the commercially processed material for a K_t of 3. The importance of this observation lies in the fact that a K_t of 3 corresponds to the stress concentration due to a round hole, such as that used for mechanical fastening of sheet metal parts in aircraft. Until an integral advanced joining technology, such as diffusion bonding, becomes available for manufacturing applications, holes and fasteners will continue to be utilized to fasten the SPF aluminum parts. Therefore, these holes, K_t of 3, will predominantly control the overall fatigue performance of a

given component. The inherent performance of the fine grain material, i.e., without holes, will be substantially above this level.

4.2.3.3.7 Fatigue Crack Growth Tests

The results of fatigue crack growth tests in air on the post SPF 7475-T6 material at room temperature are shown in Figure 4-26. Specimens representing prior SPF strains of 50 to 150 percent fell in a narrow band on the crack growth rate (da/dN) versus stress intensity factor (ΔK) plot. These results represent normal performance for this class of alloys. For example, the da/dN versus ΔK line for a conventionally processed 7075 plate in T73 temper¹⁶, shows a dashed line in Figure 4-26, falls within the band of the present results.

No measurable effect of the magnitude of the prior SPF strain is noted on the crack growth rate, in air, in these results. The crack growth rates in salt water were eight to ten times faster than those in air, albeit these rates were also independent of the prior SPF strain.

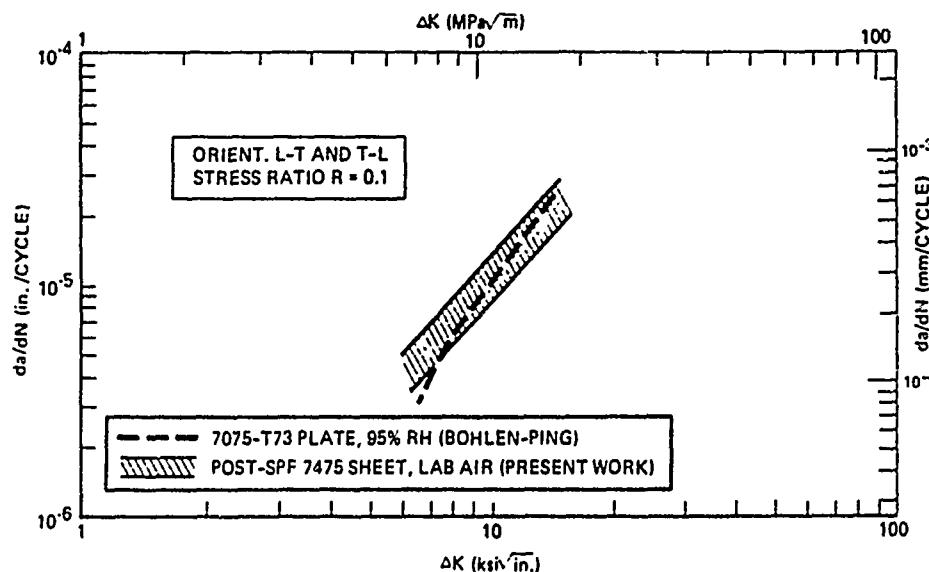


Figure 4-26. Fatigue Crack Growth Rate of Post SPF 7475-T6 Specimens in Laboratory Air

4.2.3.3.8 Stress Corrosion Tests

Stress corrosion tests were conducted on the post-SPF 7475-T6 specimens in accordance with ASTM G44 specifications. A stress equivalent to approximately 74 percent of the yield strength of the 7475-T6 was applied on each specimen which was alternately immersed in a 3.5 percent salt water at room temperature. Only specimens having an initial sheet thickness of 0.125 inch and superplastically deformed to 50 and 150 percent strains were tested. Results are shown in Figure 4-27. Note that the average failure time was about 60 days, regardless of the magnitude of SPF strain, as compared to the required minimum failure time of 30 days.

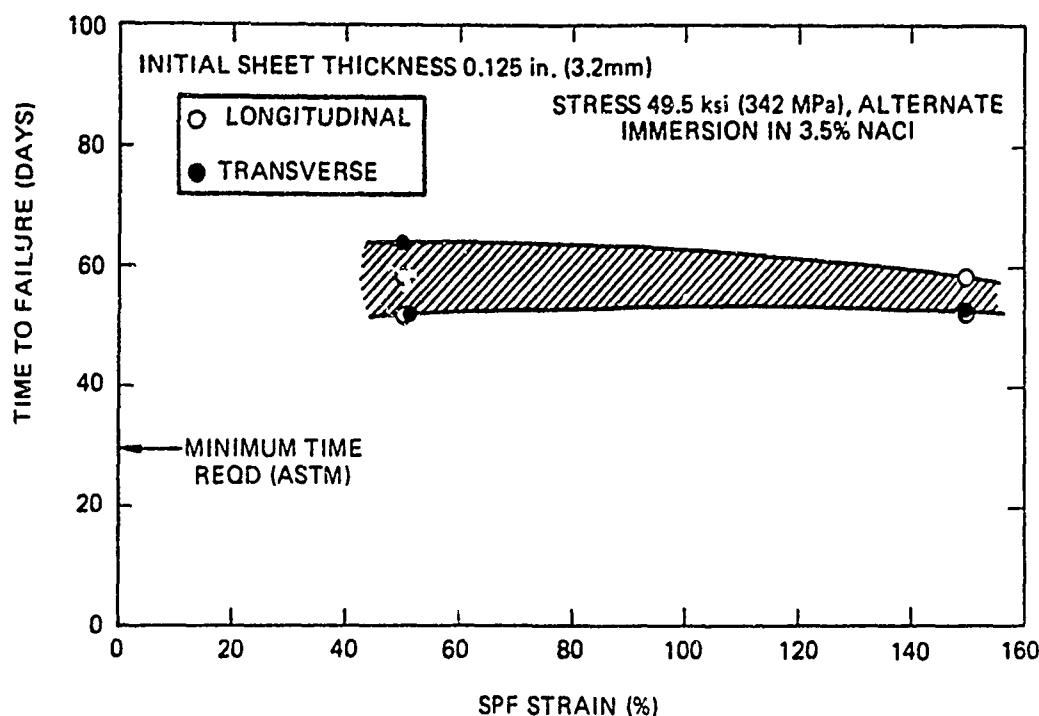


Figure 4-27. Effect of SPF Strain on 7475-T6 Stress Corrosion Resistance

4.2.3.3.9 Exfoliation Corrosion Tests

Several post-SPF 7475-T6 samples were tested by the EXCO test method per ASTM G34-79 and rated per ASTM G34-79 and G34-72. Duplicate specimens of 7475-T6 and 7475-T73 were run as controls, along with aged and underaged 7021 controls. The 7021 specimens were tested by the SWAAT method per ASTM G85-Annex A3 and rated according to the above scheme. The ratings are shown in Table 4-10.

The 7475-T6 and -T73 control samples were rated EA by the G34-79 method, PB and P by G34-72. The post-SPF samples were slightly more resistant with G34-79 ratings of PB and G34-72 ratings of P. All the post-SPF samples thus showed high exfoliation resistance which is consistent with their fine grain structure.

TABLE 4-10. 48-HOUR EXCO RATINGS OF POST-SPF 7475-T6 AND CONTROL SAMPLES

MATERIAL	SAMPLE ID	SPF STRAIN (%)	EXCO RATING		CONDUCTIVITY (% IACS)
			G34-79	G34-72	
POST-SPF 7475-T6	7475 NO. 2	50	PB	P	32.0
	7475 NO. 3	50	PB	P	32.0
	7475 NO. 5	50	PB	P	31.5
	7475 NO. 6	50	PB	P	31.2
	7475 NO. 15	150	PB	P	32.2
	7475 NO. 16	150	PB	P	32.2
	7475 NO. 21	150	PB	P	32.0
	7475 NO. 27	150	PB	P	32.2
CONTROL MATERIALS	7475-T6 NO. 1	---	EA	PB	32.2
	7475-T6 NO. 2	---	EA	PB	32.2
	7475-T73 NO. 1	---	EA	P	35.6
	7475-T73 NO. 2	---	EA	P	38.0
	7021-6 *	---	EA	PB	---
	UNDERAGED 7021 **	---	ED	EA	---

* GOOD SWAAT RESULTS

** BAD SWAAT RESULTS

4.2.3.4 Secondary Processability Evaluations

In addition to the various mechanical and service property evaluations, several tests were conducted to evaluate the secondary processability of the superplastically deformed material. The secondary processes selected were typical of routine operations in manufacturing airframe components. Results of these tests are described in the following paragraphs.

4.2.3.4.1 Anodizing Test

The post-SPF material in the T6 type temper was observed to be identical to 7075-T6 in its response to the anodizing treatment.

4.2.3.4.2 Painting Test

Using the standard procedures, no difference was observed in the paint adhesion characteristics of the post-SPF 7475 material and the conventional 7075 sheet. The post-SPF material also successfully met the impact and wet tape strength requirements in accordance with the Northrop specifications NAI 1269/NAI 1278.

4.2.3.4.3 Chem Milling

Chem milling tests were conducted using Northrop's production facilities. The following results were obtained with regard to the rate of chem milling and the subsequent fatigue tests.

- (1) Chem Milling Rate. Thickness measurements were taken after submerging samples in the milling solution for one minute; this process was repeated five times and a cumulative metal removal in 5 minutes was calculated. The average chem milling

rate in the post-SPF 7475-T6 was approximately 0.006 inch/minute, which is higher than 0.002 to 0.004 inch/minute for the conventional 7075-T6 sheet.

- (2) Fatigue Test. Smooth fatigue tests were conducted by applying maximum stresses in the range of 30 to 50 ksi at $R = 0.1$. It was seen that the fatigue life of the post-SPF 7475 after chem milling is slightly lower than that of the conventional 7475-T61 sheets. It is believed that this difference may be related to some surface effects in the post-SPF material. The total SPF strain appeared to make no difference in the fatigue performance of the material.

4.2.3.4.4 Adhesive Bonding

Post-SPF 7475 sheets were anodized in phosphoric acid, sprayed with BR127 primer, and bonded with FM-73 film adhesive per Northrop Specification MA108. The average lap shear strength of six tests was 5400 lbs compared to the minimum strength of 4200 lbs required by the Northrop specification NAI 1286.

4.2.3.4.5 Climbing Drum Peel Test

The geometry of the peel test specimens is shown in Figure 4-28. The base plate was 0.125 inch thick 7075 aluminum, and the thin sheet was post-SPF 7475, which was milled to the

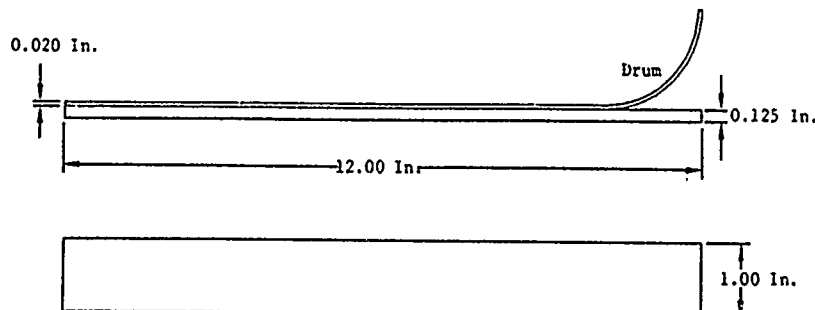


Figure 4-28. Climbing Drum Peel Test Specimen

closest possible thickness of 0.020 inch. Table 4-11 shows the peel test strength of nine post-SPF specimens which were adhesively bonded in a T6 temper. Even the lowest value of strength obtained, 108 lbs/inch, is considered excellent when compared to the conventional high strength aluminum alloy sheets. It was noted, however, that the samples with low SPF strain had higher strength, 144 and 153 lbs/inch, than that with high SPF strain, 108 lbs/inch.

TABLE 4-11. CLIMBING DRUM PEEL TEST RESULTS

SPECIMEN I.D.	14 ABC-1XL	25 ABC-1XH	13 ABC-1XL
STRENGTH	153 LB/IN	108 LB/IN	144 LB/IN

4.2.3.4.6 Resistance Seam Welding

Consistently defect free, reproducible resistance seam welds were obtained in the post-SPF 7475-T6 sheet specimens using the normal welding parameters for 7075-T6 sheets of equivalent thickness. X-ray radiography indicated no internal defects in the weld zone. Peel tests resulted in material failing outside the fusion zone, indicating the high strength of the seam welds.

4.2.3.4.7 Weldbonding

It was determined that the welding parameters established for 7075-T6 sheets can be reliably used to weld the post-SPF 7475-T6 sheets of comparable thickness. Uncured joint strength values of 600 to 850 lbs were obtained, depending upon the welding current used. These values are the same as those normally obtained for the conventional 7075-T6 sheets. Surface treatment was based on the Northrop process specification C-65.

Cured test specimens had a 1 x 1 inch overlap area, as shown in Figure 4-29. A temperature of 225°F for 90 minutes was

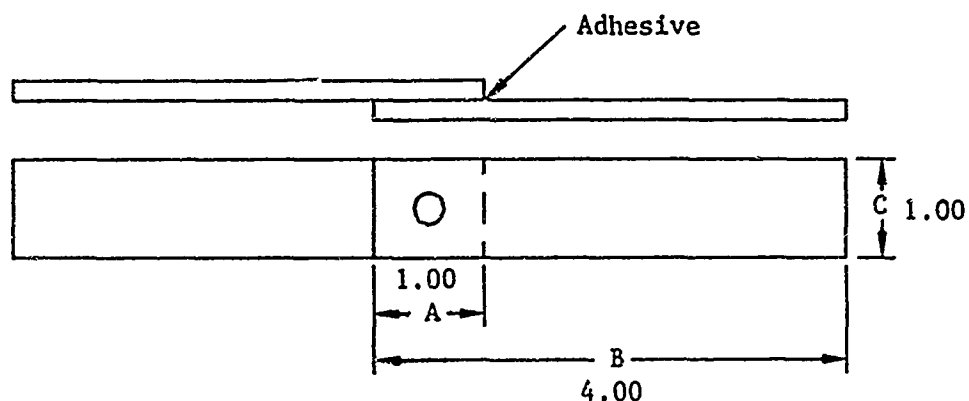


Figure 4-29. Weldbond Lap Shear Test Specimen

used as the curing treatment after welding. The results of the lap shear strengths of the weldbond specimens in cured condition are listed in Table 4-12.

TABLE 4-12. LAP SHEAR STRENGTH OF WELDBONDED SPECIMENS IN CURED CONDITION

SPECIMEN NO.	FAILURE LOAD (LBS)	FAILURE MODE
34-WBC-1X0	3900	BM
17-WBC-1X0	4950	J
28-WBC-1X0	4900	J
28-WBC-1X0	4850	J
31-WBC-1X0	3950	BM
17-WBC-1XH	5050	J
28-WBC-1XH	3950	BM
17-WBC-1XH	5250	BM
28-WBC-1XH	3850	BM
AVERAGE	4520	

NOTE: BM = Represents failure in the base metal.
J = Represents failure in the joint.

Specimens which failed in the joint (J) represented the true joint strength of the weldbond specimens. Specimens with thicknesses less than 0.063 inch failed in the base metal (BM), because these sheets were too thin for the specimen overlap geometry used. The average lap shear strength of 4940 lbs for the specimens failing in the joint exceeds the required weldbonded joint strength of 4800 lbs in 7075-T6 sheet per Northrop specifications.

Table 4-13 shows a summary of results obtained on the secondary processability evaluations of the post SPF 7475-T6

TABLE 4-13. RESULTS OF SECONDARY PROCESSABILITY EVALUATION OF POST-SPF 7475 SHEET

PROCESS	RESULTS	CONCLUSIONS
ANODIZING	NORMAL BEHAVIOR; MET ALL VISUAL REQUIREMENTS	GOOD ANODIZING RESPONSE; SAME AS 7075
PAINTING	MET ALL PAINT STRENGTH TEST REQUIREMENTS	GOOD PAINT ADHESION RESPONSE; SAME AS 7075
ADHESIVE BONDING	AVERAGE JOINT STRENGTH: 5400 psi (37.3 MPa) MINIMUM DESIGN REQUIREMENT: 4200 psi (29.0 MPa)	GOOD BONDABILITY; SAME AS 7075
WELDBONDING	AVERAGE JOINT STRENGTH: 4950 psi (34.1 MPa) MINIMUM DESIGN REQUIREMENT: 4800 psi (33.1 MPa)	GOOD WELDABILITY AND BONDABILITY; SAME AS 7075
CHEM MILLING (C/M)	NORMAL C/M RESPONSE: AS RECD 7075 C/M RATE: 0.002-0.004 IN/MIN (847-1694 NM/SEC) POST-SPF 7475 C/M RATE: 0.006 IN/MIN (2540 NM/SEC)	C/M BEHAVIOR COMPARABLE TO 7075

material as well as a comparison with the counterpart 7075-T6 material. It is noted that the post SPF material displayed a response similar to the baseline material in its anodizing, painting, adhesive bonding, and weldbonding characteristics. The chem milling rate of the post SPF fine grain material was slightly faster than that of the conventionally processed material.

4.2.4 Development of Forming Parameters

Preliminary SPF runs were made on a smaller tool (Length = 12 inches, Width = 4 inches, Height = 2 inches). Cone test data reported earlier¹ was used to select temperature, strain rate and corresponding flow stress. The forming conditions were as follows:

$$T = 970^{\circ}\text{F}$$

$$\dot{\epsilon} = 3.7 \times 10^{-4} \text{ sec}^{-1} \text{ for } 0.090 \text{ inch thick 7475 aluminum}$$

$$\sigma = 720 \text{ psi}$$

The forming cycle was determined using constant flow stress. Forming under these conditions resulted in rupture at the die entry radius in the very early stage of the forming. The cause was attributed to the faster rate of forming initially if constant stress is used in computing the forming cycle. Therefore, in all subsequent formings variable flow stress was utilized. The semi-empirical relationship between flow stress, strain rate and strain was derived for the present material based on the results obtained from a Northrop manufacturing technology program.

Two material gages, 0.125 and 0.090 inch, were superplastically formed into 3 tooling geometries to obtain low,

medium and high SPF strain levels in the formed pans. The forming conditions are listed in Table 4-14. The forming cycles for 0.125 gage aluminum sheet are shown in Figure 4-30(a) to (c) for the forementioned tool geometries. They were computed using variable flow stress and a forming rate of $3 \times 10^{-4} \text{ sec}^{-1}$ at 960 to 970°F.

4.3 MATERIAL SUBSTITUTION TO MD254

Concurrent with this AFWAL program, Northrop had been conducting an extensive IR&D program to further develop and optimize high strength SPF aluminum alloy sheets. A recommendation was made to the Air Force program monitor to substitute the present program material, 7475, with a more advanced version of this alloy, developed jointly by Northrop and Reynolds Metals Company under their joint IR&D programs. The new material, MD254, represented a highly superplastic and commercial form of the conventional alloy 7475. In Northrop's evaluation, this material had been superplastically deformed to over 1,000 percent strain without appreciable, <0.5 percent area, cavitation. Following Air Force approval of this substitution, full-size production sheets of this material were procured in 0.090 and 0.160 inch gauges.

The as-received grain structure of the 0.090 inch thick material is shown in three dimensions in Figure 4-31. The average longitudinal and transverse grain sizes, measured on two randomly selected sheets, were 17.0 and 8.5 μm , respectively. The grains had an aspect ratio of 2.0. These values compared well with Reynolds' measurements of 16.9 μm longitudinal, 10.0 μm transverse grain sizes and 1.7 aspect ratio. No significant surface-to-center variation was observed in this material (see Figure 4-32).

Table 4-15 shows the results of room temperature tensile tests on these materials in a T6 temper. Also listed in

TABLE 4-14. FORMING CONDITION FOR SPF PANS

STRAIN LEVEL DESIGNATION	PAN GEOMETRY	INITIAL SHEET	PAN NUMBER	FORMING PARAMETERS
LOW	WIDTH = 12 INCHES LENGTH = 12 INCHES DEPTH = 3 INCHES	0.125	01 THRU 06, & 35	T = 960 - 970°F = $3 \times 10^{-4} \text{ s}^{-1}$ BACK PRESSURE = 400 PSI
		0.090	07 & 08	
MEDIUM	WIDTH = 9 INCHES LENGTH = 12 INCHES DEPTH = 3 INCHES	0.125	09 & 10	T = 960 - 970°F = $3 \times 10^{-4} \text{ s}^{-1}$ BACK PRESSURE = 350 PSI
		0.090	11 & 12	
HIGH	WIDTH = 6 INCHES LENGTH = 12 INCHES DEPTH = 3 INCHES	0.125	13 THRU 28	T = 960 - 970°F = $3 \times 10^{-4} \text{ s}^{-1}$ BACK PRESSURE = 350 PSI
		0.090	29 THRU 34	

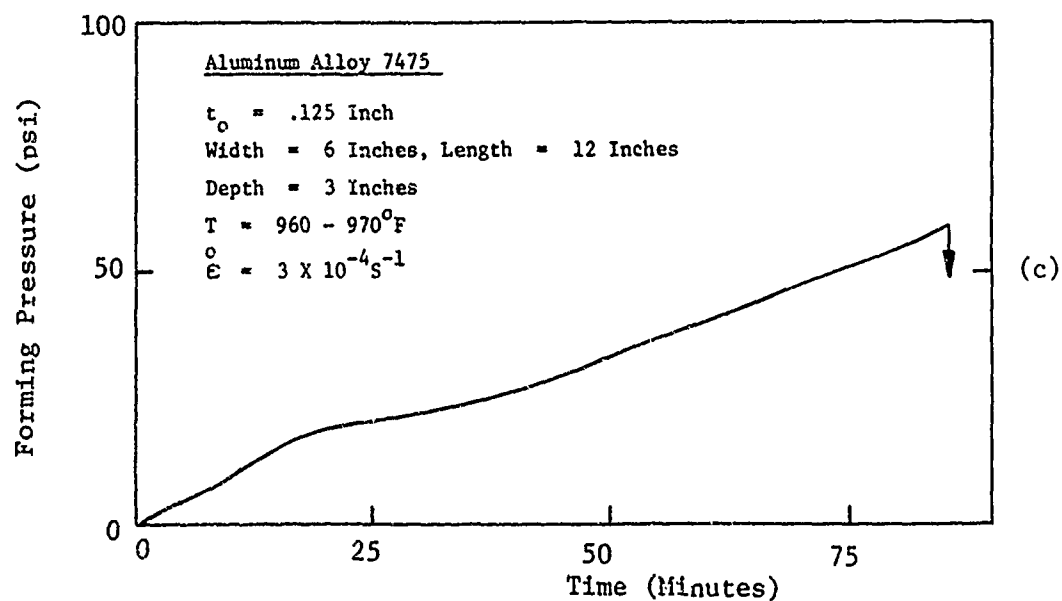
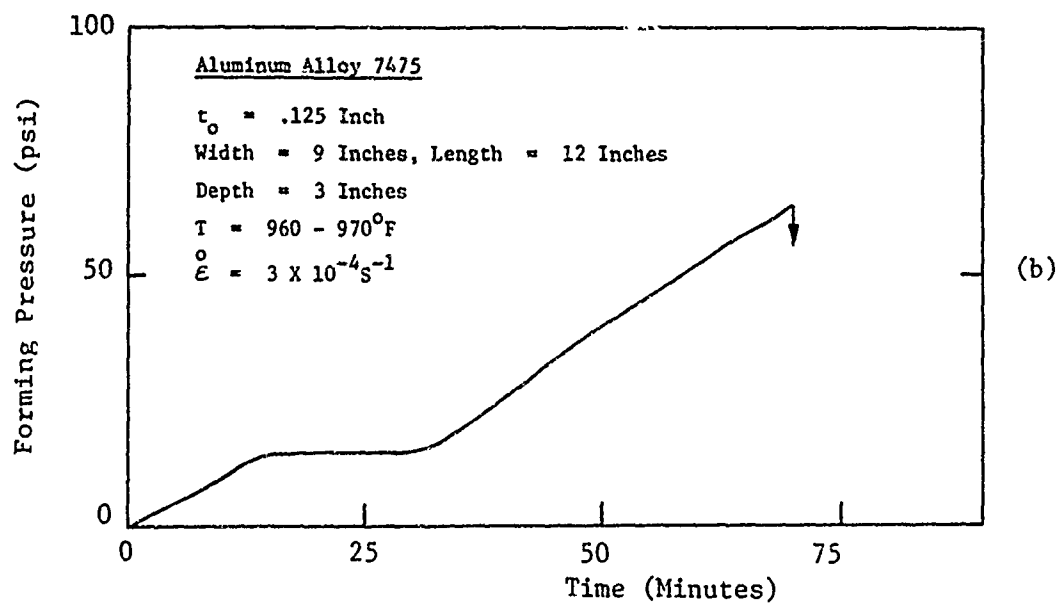
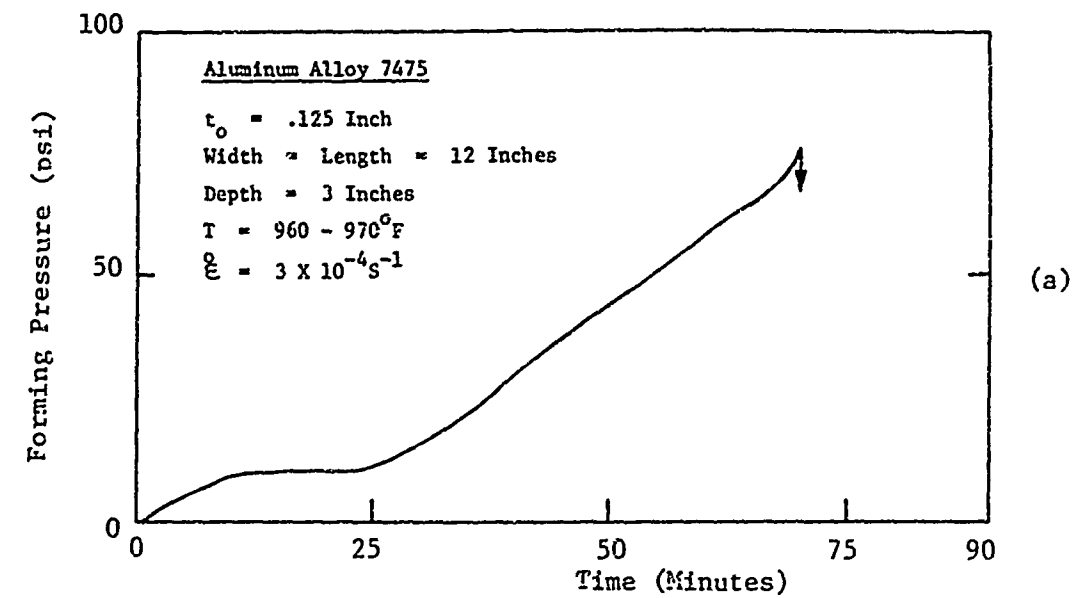


Figure 4-30. Forming Cycle for SPF Pans

Al Alloy 7475
MD-254-090-1

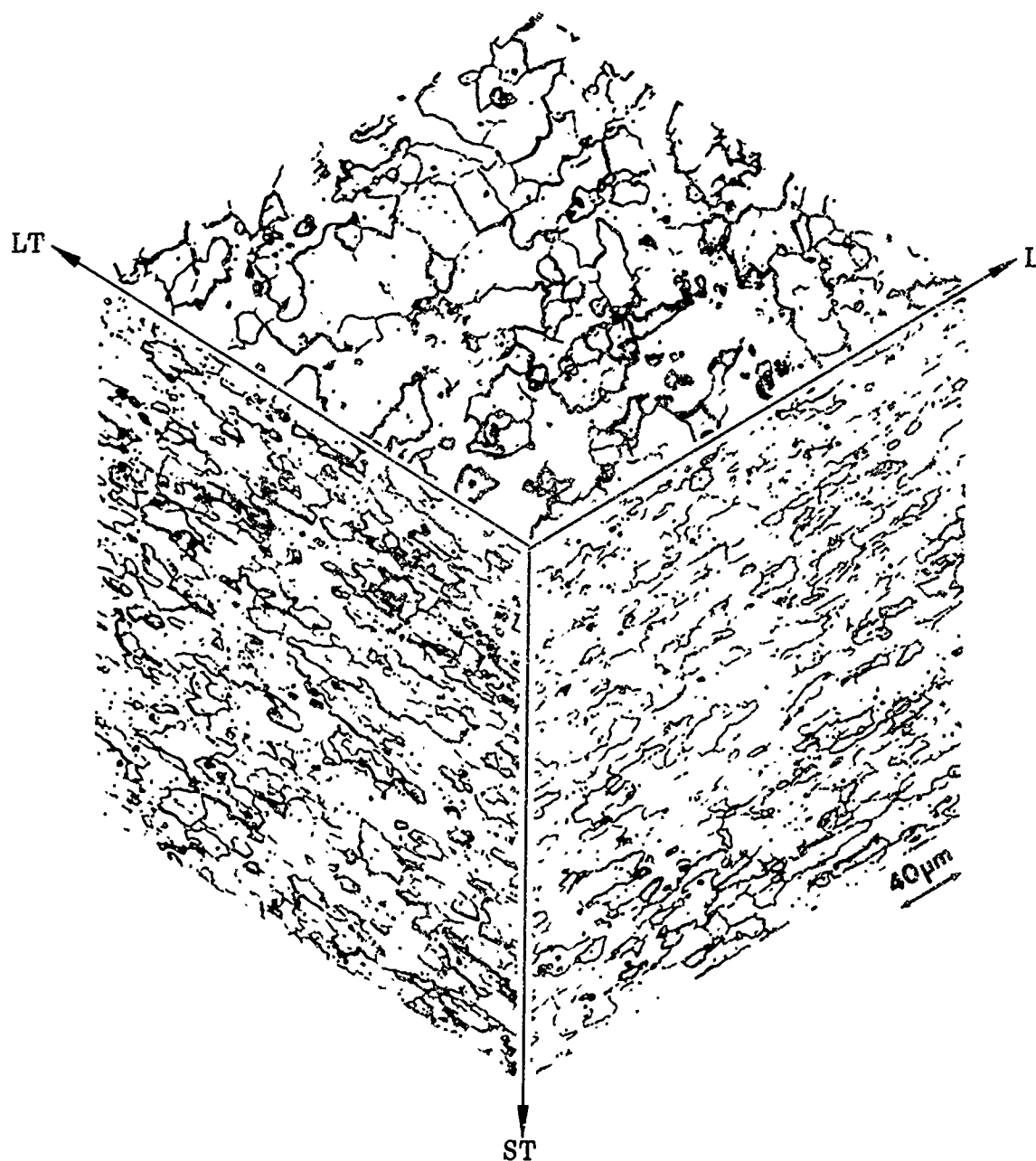


Figure 4-31. Three Dimensional Microstructure of an As Received 0.090 Inch Thick Sheet of MD254

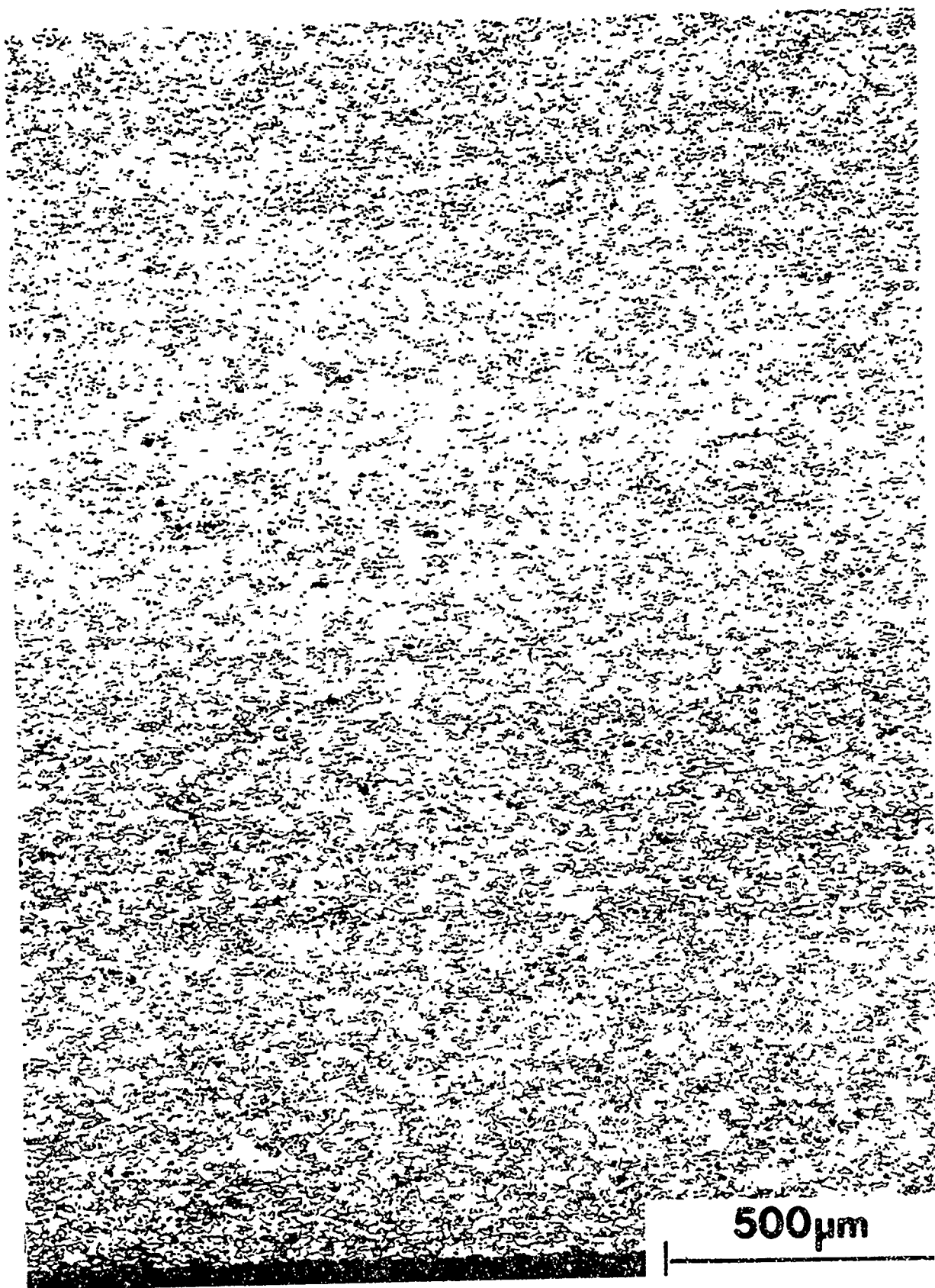


Figure 4-32. Microstructure Across the Thickness of an As Received 0.090 Inch Thick Sheet of MD254 Aluminum Alloy

TABLE 4-15. ROOM TEMPERATURE TENSILE TESTS ON THE SPF MD254* ALUMINUM AND CONVENTIONALLY PRODUCED 7075-T6 ALUMINUM

MATERIAL IDENTIFICATION	ORIENTATION	YIELD STRENGTH (KSI)	ULTIMATE STRENGTH (KSI)	ELONGATION (%)	MODULUS (10 ⁶ PSI)
MD254 (0.090 IN)	LONGITUDINAL	76.0	84.3	14.0	10.2
		76.3	84.7	14.0	10.5
		76.8	84.9	13.0	11.4
	AVERAGE	76.4	84.6	13.7	10.7
MD254 (0.090 IN)	TRANSVERSE	75.2	84.1	13.0	11.2
		74.7	83.6	13.0	11.3
		74.2	83.3	16.0	11.0
	AVERAGE	74.7	83.7	14.0	11.2
MD254-1 (0.160 IN)	LONGITUDINAL	71.5	79.5	14.0	11.3
		71.9	79.7	16.0	11.8
		71.4	79.5	15.0	11.0
	AVERAGE	71.6	79.6	15.0	11.4
MD254-1 (0.160 IN)	TRANSVERSE	69.8	78.8	16.0	10.9
		69.2	78.8	16.0	10.9
		69.2	79.0	15.0	10.6
	AVERAGE	69.4	78.9	15.7	10.8
MD254-2 (0.160 IN)	LONGITUDINAL	71.6	80.0	15.0	11.3
		71.8	80.0	16.0	11.3
		71.3	79.5	15.0	10.7
	AVERAGE	71.6	79.8	15.3	10.8
MD254-2 (0.160 IN)	TRANSVERSE	69.7	79.0	16.0	11.5
		69.5	79.0	17.0	10.2
		69.7	78.9	16.0	12.4
	AVERAGE	69.6	79.0	16.3	11.4
7075-T6 (0.090 IN)	LONGITUDINAL	74.3	80.4	11.0	11.5
		74.4	80.4	10.0	9.9
		74.5	80.2	11.0	11.5
	AVERAGE	74.4	80.3	10.7	11.1
7075-T6 (0.090 IN)	TRANSVERSE	74.3	84.0	11.0	10.5
		74.8	84.3	11.0	11.3
		74.9	84.3	10.0	11.4
	AVERAGE	74.7	84.2	10.7	11.1

* PRODUCED USING PRODUCTION FACILITIES

this table for comparison are the results obtained on a conventional 7075-T6 sheet of 0.090 inch thickness. While the 0.090 inch MD254-T6 sheet properties compared quite favorably with the 0.090 inch 7075-T6 properties, the 0.160 inch MD254-T6 strength properties were somewhat lower. The ductility of MD254-T6 sheets in both thicknesses was considerably higher than that of 0.090 inch 7075-T6.

The SPF evaluation of these sheets was done by biaxial cone tests at 970°F. The dual pressurization approach³ was utilized for suppression of cavitation during SPF. Strains of over 1,000 percent were achieved in the 0.090-inch thick sheet. A significant fraction of these strains was found to be without much cavitation. In one test, 1430 percent strain was obtained prior to rupture, at a strain rate of $1.3 \times 10^{-4} \text{ sec}^{-1}$, and virtually all of it was with <0.2 percent cavitation. These results are shown in Table 4-16.

TABLE 4-16. EFFECT OF SPF STRAIN ON CAVITATION IN MD254 ALLOY

ALLOY	SHEET	FORM-	LOCATION OF SPECIMEN*								APPROXIMATE SPF
	THICK-	ING	AREA 1		AREA 2		AREA 3		AREA 4		STRAIN AT ONSET
	NESS	TEMP	SPF	AREAL	SPF	AREAL	SPF	AREAL	SPF	AREAL	(<0.5%) OF CAVI-
	(IN)	(°F)	SIRAIN	CAVITA-	SIRAIN	CAVITA-	SIRAIN	CAVITA-	SIRAIN	CAVITA-	
			(%)	TION(%)	(%)	TION(%)	(%)	TION(%)	(%)	TION(%)	
MD254	0.090	970	28	0	84	0	311	0	1430	0.02	1430
	0.160	970	12	0	770	0.1	1520	0.6	>1520	3.0	>1000

*Results were obtained from biaxial SPF cone tests. Area 1 is near the die entry, Area 2 is where the cavities are first observed, Area 3 is intermediate to Area 2 and a region near the final failure (Area 4).

The 0.160-inch thick sheets also developed similarly high strains prior to rupture and much of the total strain was without cavitation. In the test specimen examined for cavitation, the thickness strain obtained at rupture was 1925 percent. At a section representing 770 percent strain cavitation was 0.1 percent, and at 1520 percent strain the cavitation was 0.6 percent. The strain corresponding to 0.2 percent cavitation, 0.5 percent defined as the onset of cavitation, is estimated to be approximately 1000 percent. The influence of SPF strain on cavitation is also shown in Table 4-16.

Uniaxial tension tests were also conducted on these sheets at the same temperature, 970°F, as the biaxial cone tests. These tests were performed without the use of hydrostatic compression for cavity suppression. The 0.090-inch sheet was tested in a strain rate range of 7.4×10^{-5} to $1.3 \times 10^{-2} \text{ sec}^{-1}$. The maximum ductility, uniform elongation, of 900 percent was obtained at $7.4 \times 10^{-5} \text{ sec}^{-1}$. Approximately 700 percent elongation was obtained at $1.3 \times 10^{-4} \text{ sec}^{-1}$ strain rate, compared to a thickness strain of 1430 percent in the cone test on this material at the same strain rate using cavity suppression methods. The 0.160-inch thick sheet was tested in the range of 2.2×10^{-4} to $1.3 \times 10^{-2} \text{ sec}^{-1}$ strain rates. The maximum elongation in this range was 700 percent and was obtained at a strain rate of $2.2 \times 10^{-4} \text{ sec}^{-1}$. Approximately 600 percent elongation was obtained at $3.9 \times 10^{-4} \text{ sec}^{-1}$ strain rate, compared to a thickness strain rate of 1925 percent in the cone test on this material at the same strain rate using cavity suppression methods. Figure 4-33 shows the plot of percentage elongation at fracture as a function of the strain rate.

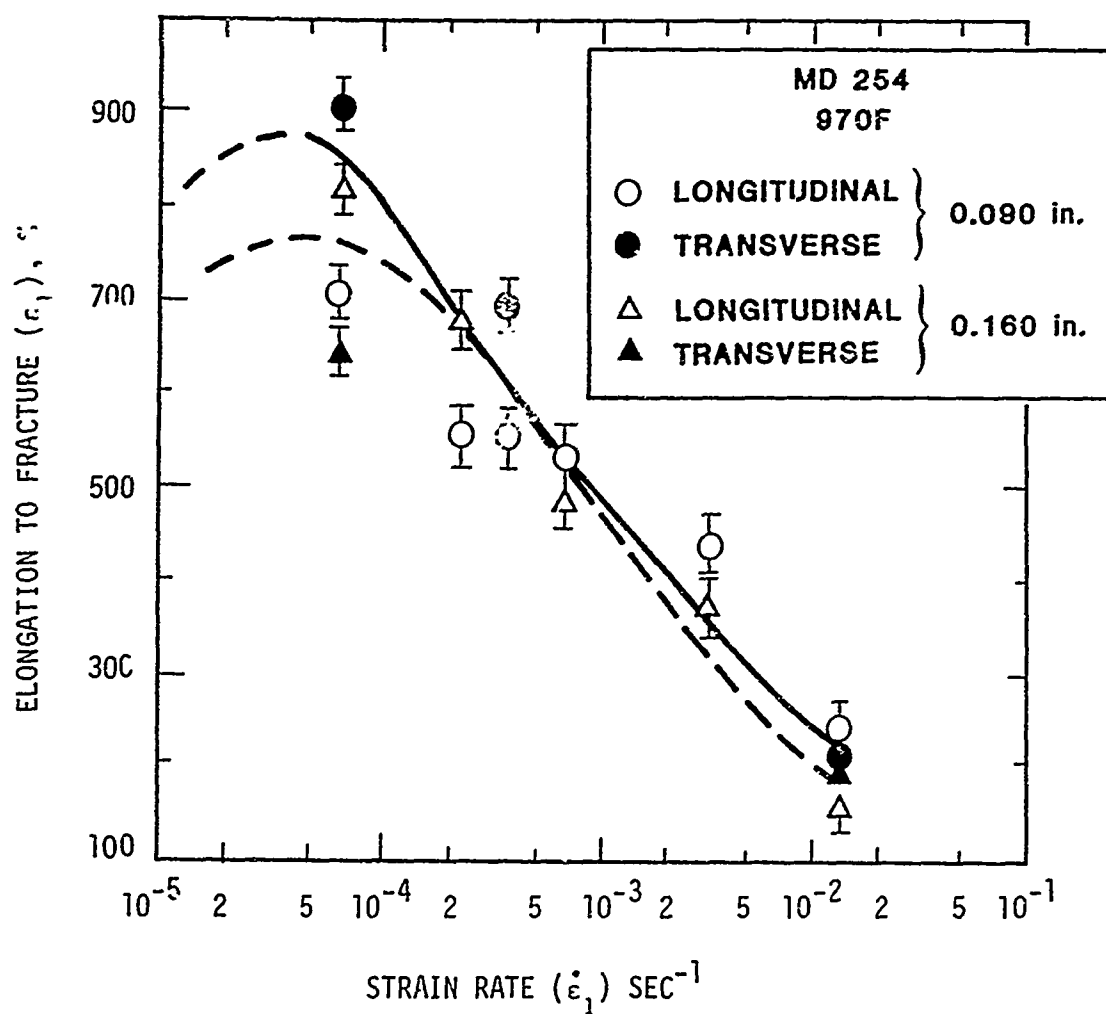


Figure 4-33. Variation of Percentage Elongation at Fracture With Strain Rate

5. PRODUCIBILITY FORMING TESTS

The objective of this task was to assure the producibility of the selected components. This was accomplished through forming and testing of subcomponents representing the most severe areas of the parts from the design and fabrication point of view. These studies also referred to as forming feasibility studies, are perhaps the most important factor in design of a complex SPF structure.

The forming of subcomponents which is done under the same processing conditions as the actual component will assess the forming feasibility of the component based on the assumed initial design parameters. In case these studies show unfavorable results such as cavitation problems and/or undesirable sheet thicknesses, a new, modified design of the component is carried out. As a result, parameters such as material gage, draft angles, and edge and corner radii could all be modified.

Once the forming of the subcomponents are completed, tests are conducted to validate the parts integrity. Microstructural tests are conducted to assure the formed subcomponents are free of cavitation, and static and fatigue tests are performed to assure the structural integrity of the formed subcomponents.

5.1 PRODUCIBILITY SUBCOMPONENT SELECTION

Producibility subcomponents were selected for both the LEX and the avionics deck. The subcomponents were selected based on geometric configuration, predicted thinning and generally represented areas of greatest elongation.

5.1.1 Leading Edge Extension

The substructure on the SPF design of the LEX was a one-piece corrugation of varying depth and compound curvature. Geometry of the most severe section of these corrugations was selected for the subcomponent design. The LEX producibility subcomponent, as shown in Figure 5-1, represented the deepest of the substructure corrugations to simulate the maximum material elongation.

The subcomponent design was 2 inches wide, 1.75 inches deep, had 15 degree draft angles on side walls, 0.25 inch corner and edge radii, and a dihedral angle of 59 degrees at the closed end. An aluminum insert was machined to this geometry to act as the tool, the length was kept such that slenderness ratio was not a significant factor.

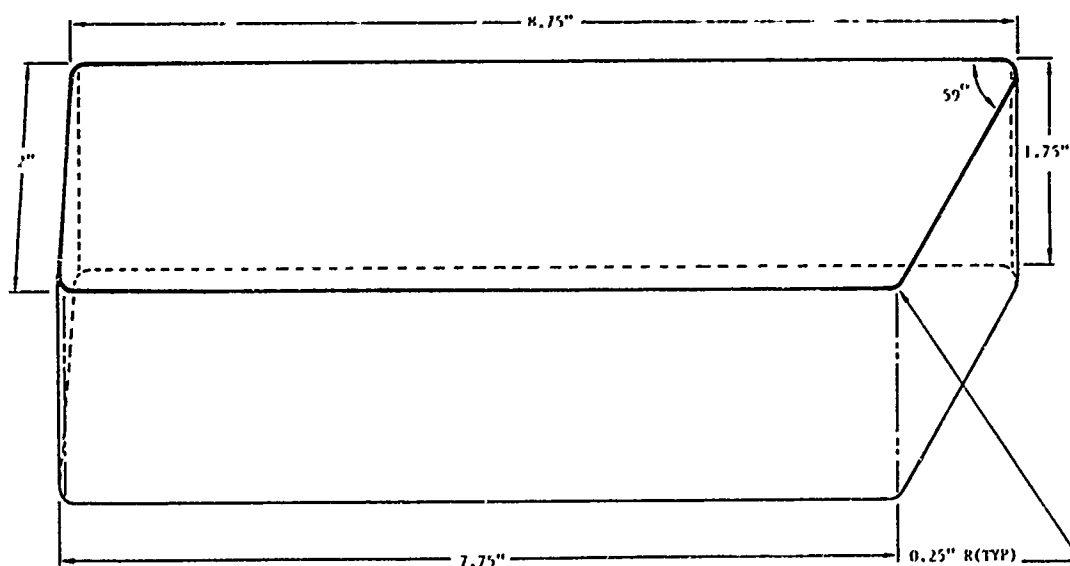


Figure 5-1. Original LEX Producibility Subcomponent

5.1.2 Avionics Deck Lower Compartment

The original avionics deck substructure was a waffle pan consisting of deep and almost square pockets with 15 degree draft angles on the walls. The producibility subcomponent for the avionics deck consisted of a single depression pan representing a typical aft pocket of the waffle pan, Figure 5-2. The pan

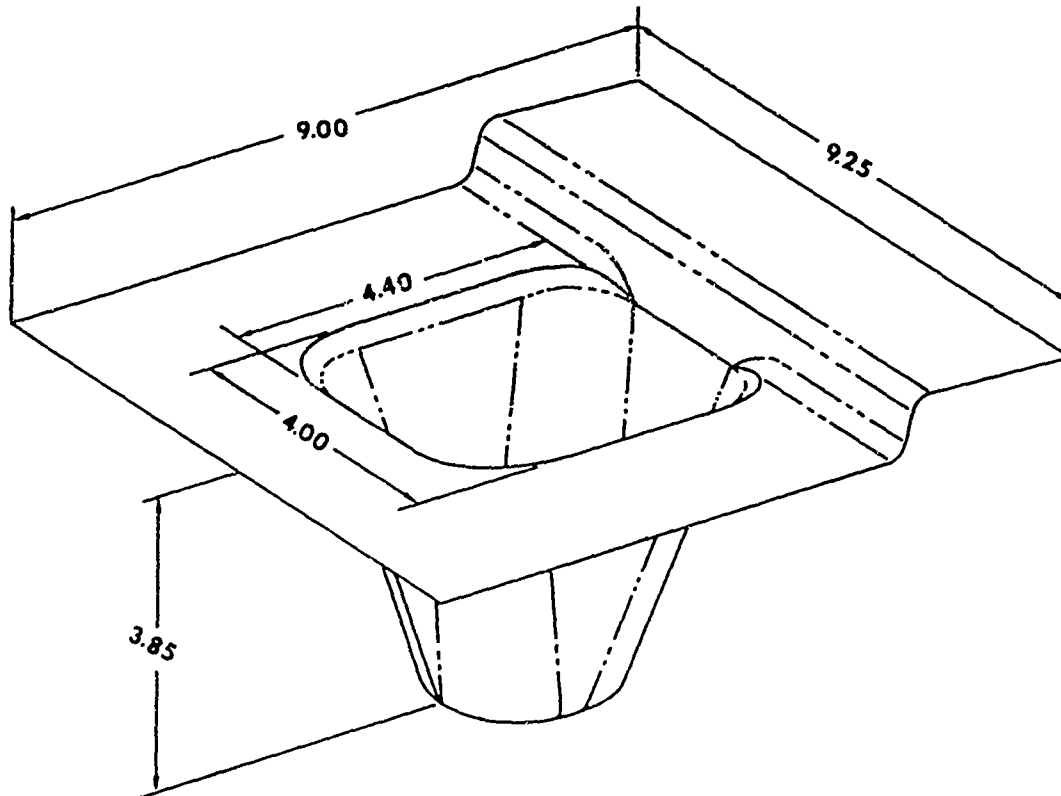


Figure 5-2. Original Avionics Deck Producibility Subcomponent

represented the area of the deck where the material was subjected to the largest elongation. As shown in Figure 5-2, the square shaped subcomponent had a length of 4.4 inches, a width of 4 inches and a depth of 3.85 inches. This would result in an aspect ratio (width/depth) of approximately 1 and a slenderness ratio (length/depth) of 1.1, with bottom edge radii of 0.25 inch. The tool for this subcomponent was machined from 4340 steel and is shown in Figure 5-3. It was a self-contained tool with inlets and outlets for gas introduction.



Figure 5-3. Avionics Deck Producibility Subcomponent Die

5.2 PRODUCIBILITY FORMING

The forming of the subcomponents was carried out based on the material characteristics of 7475 and MD254 aluminum found in Task II (Section 4.0). All forming was carried out in the temperature range of 960 to 980°F with a back pressure of 400 psi to suppress cavitation. This pressure was the maximum attainable on the laboratory press. The strain rates were also selected from the studies of Task II to correspond to maximum elongations without any cavitation problems.

5.2.1 LEX Producibility Subcomponent Forming

Reynolds superplastic aluminum alloy, MD254, was utilized for forming of the LEX subcomponent. The starting sheet thickness was 0.090 inch, and the forming was carried out at a strain rate of $2 \times 10^{-4} \text{ sec}^{-1}$ to achieve maximum elongations prior to fracture. The actual forming rate measured was $1.4 \times 10^{-4} \text{ x sec}^{-1}$.

The subcomponent was fully formed and the minimum thickness, as expected, occurred at the acute angled corner radius and was measured to be 0.016 inch. Thinning and cavitation analysis were conducted on the LEX subcomponent. Figure 5-4

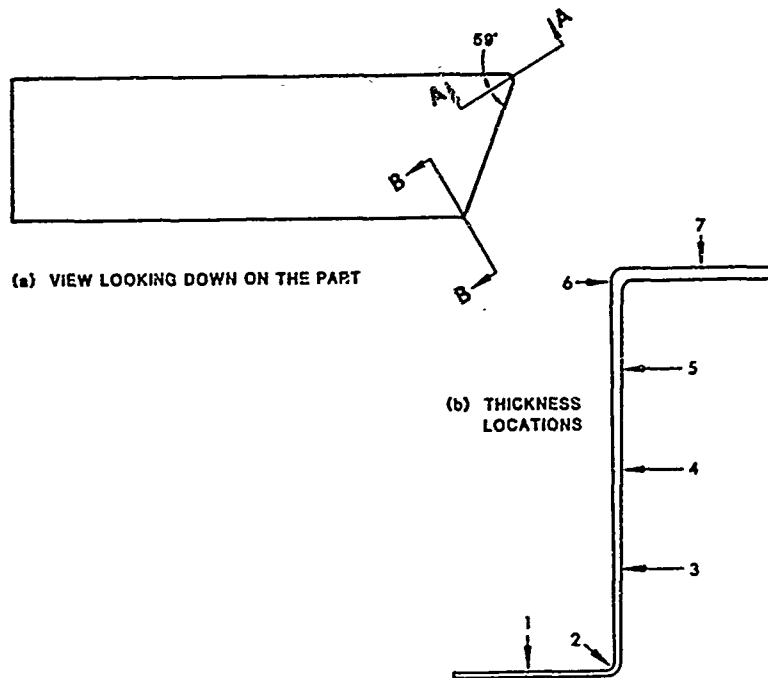


Figure 5-4. LEX Subcomponent Cross Sectional View

shows the cross section through the acute and obtuse angled corners of the subcomponent, and the measured thicknesses are shown in Table 5-1.

TABLE 5-1. THICKNESS MEASUREMENTS FOR LEX SUBCOMPONENT

SECTION	PART THICKNESS IN INCHES AT LOCATIONS						
	1	2	3	4	5	6	7
A-A	0.021	0.016	0.027	0.071	0.078	0.085	0.086
B-B	0.025	0.022	0.030	0.043	0.032	0.085	0.078

The formed part was sectioned through the acute angle for optical microscopy. Figure 5-5 shows this section along with optical micrographs of three different locations. Area fraction of cavities were measured at three strain values by optical microscopy using an image analyzer. Cavitation at thickness strain of 350 percent was measured to be 0.8 percent, whereas at strains of 157 and 260 percent, the area fraction of cavities was less than 0.1 percent. The excessive cavitation at the corner radius indicated that a redesign of that area was in order.

5.2.2 Avionics Deck Producibility Subcomponent Forming

The avionics deck producibility subcomponent forming was carried out at $970 \pm 10^\circ\text{F}$, at a strain rate of $3 \times 10^{-4} \text{ sec}^{-1}$ with a 400 psi back pressure. Two runs, one from 0.125-inch thick 7475 sheet and one from 0.090-inch thick MD254 were made. During forming, the 7475 sheet ruptured at a true thickness strain, ϵ , of 1.43 which corresponds to the maximum elongation attainable from 7475. It was decided that the high draft angles on the cavity were producing an accelerated thinning gradient and the final formed subcomponents minimum thickness would fall below the minimum gage of 0.020 for bare aluminum alloys. These unfavorable results indicated that a redesign of the subcomponent and avionics deck waffle pan was in order.

5.3 SUBCOMPONENT MODIFICATIONS

The subcomponent producibility tests for both the LEX and the avionics deck showed unfavorable thickness and cavitation results. As a consequence, a redesign of both components became necessary. However, in order to verify the validity of the redesigned component, a second set of subcomponents were fabricated to investigate the forming feasibility with the modified design parameters.

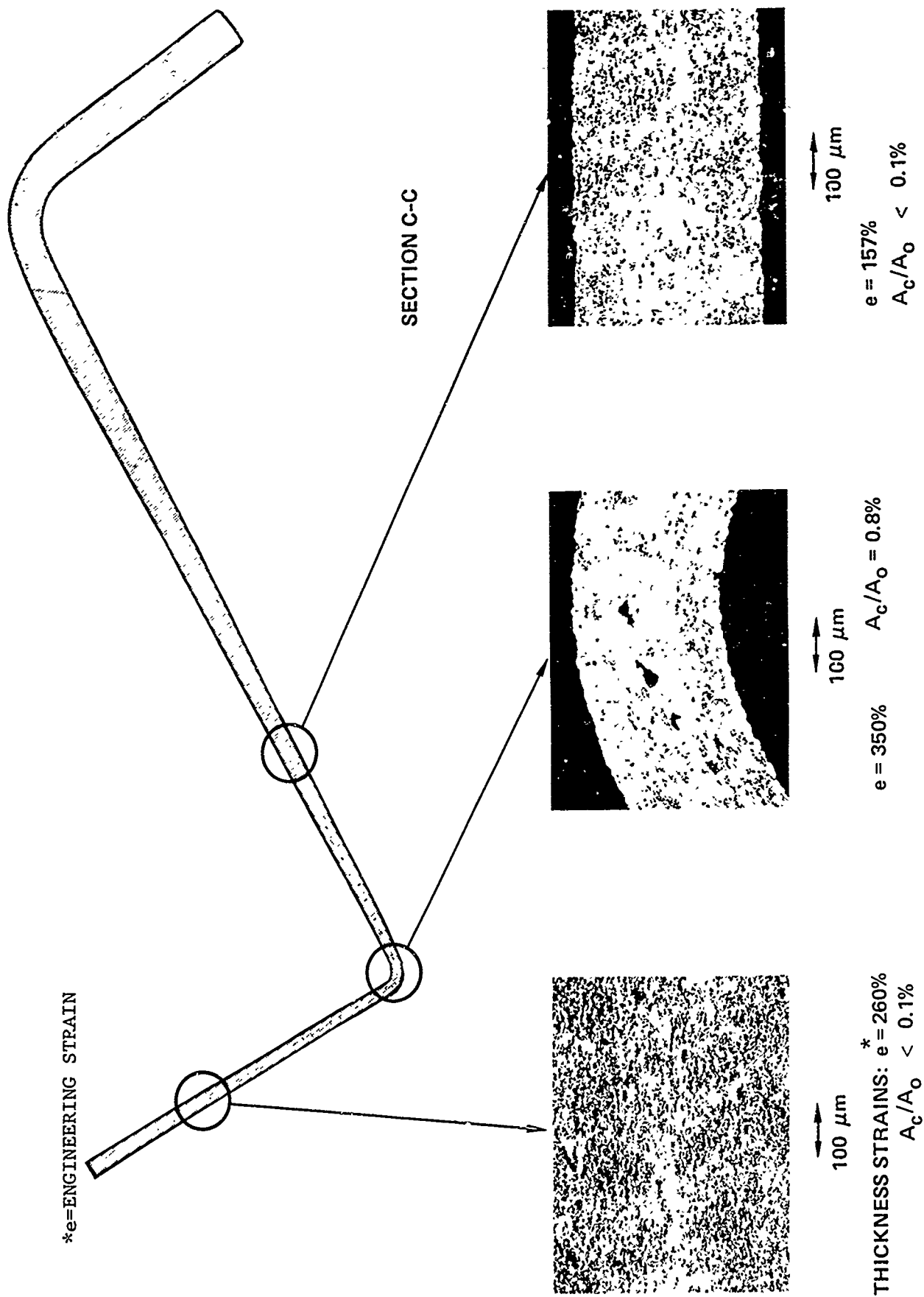


Figure 5-5. Cavitation Measurements for LEX Subcomponent

5.3.1 LEX Subcomponent Redesign

Due to the excessive thinning and cavitation associated with the bottom corner of the original subcomponent, the subcomponent design was modified and a second set of forming was carried out. The corner radius of the acute angle was increased from 1/4 to 3/8 inch to decrease the amount of thinning and cavitation in that area.

A new subcomponent was fabricated with the modified corner radii and the forming was carried out successfully, Figure 5-6. No excessive thinning was noticed with the new radii. This

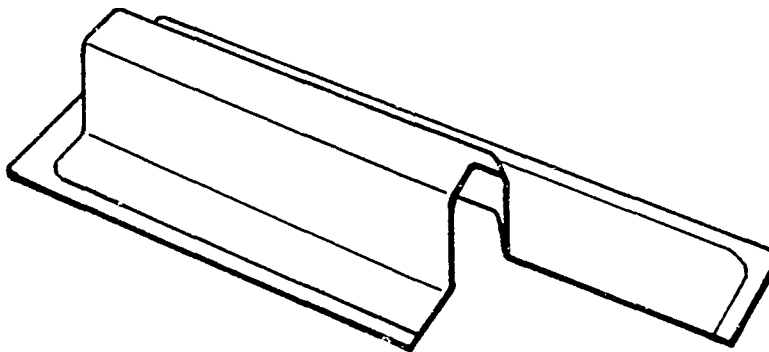
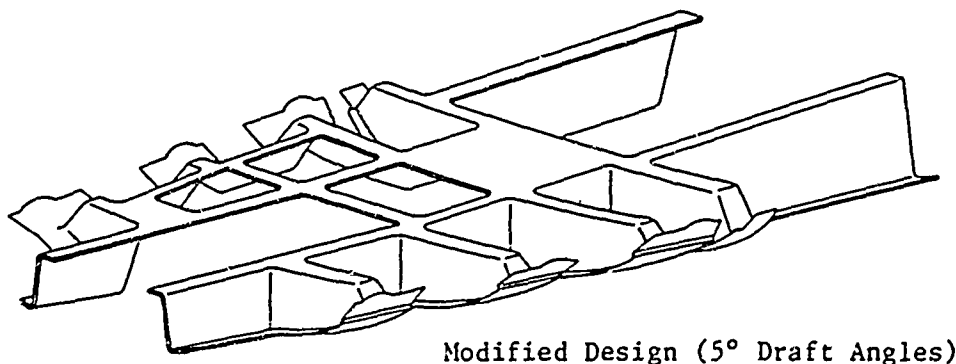


Figure 5-6. Modified LEX Producibility Subcomponent

modified design parameter was also incorporated into the LEX corrugation and tool design.

5.3.2 Avionics Deck Subcomponent Redesign

The unfavorable results of the first subcomponent forming called for a redesign of the subcomponent and the waffle pan. As a result, the pan was redesigned by eliminating the aft center pockets and extending the side pockets to join each other as shown in Figure 5-7. A preliminary analysis of this area showed that the new design was also acceptable from a structural point of view. The wall draft angles were also reduced from 15 degrees to 5 degrees in order to make the thinning more uniform.



Modified Design (5° Draft Angles)

Figure 5-7. Modified Avionics Deck Waffle Pan

The geometry of the subcomponent was scaled by a factor of 0.86 and resulted in a pocket 8 inches long, 3.9 inches wide and 3 inches deep. The bottom moldline was approximated by two straight lines. The part was successfully formed using Reynolds MD254 sheet. The forming was carried out at 970°F, with a back pressure of 400 psi and a strain rate of $3 \times 10^{-4} \text{ sec}^{-1}$. A maximum true thickness strain, ϵ , of 1.9 was measured at the corners. Figure 5-8 shows the machined die insert that was used



Figure 5-8. Modified Avionics Deck Subcomponent Die

to produce the redesigned producibility subcomponent and Figure 5-9 shows the formed subcomponent. The missing portion of the subcomponent was used for metallographic inspection.

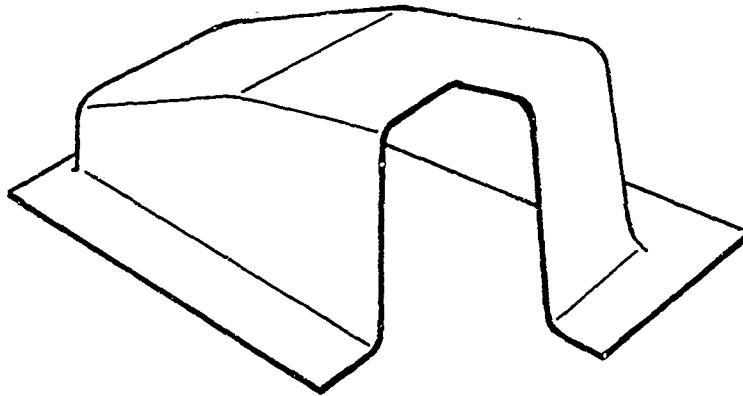


Figure 5-9. Modified Avionics Deck Producibility Subcomponent

The results of this inspection are shown in Figure 5-10. The photographs show the complete section excised from the producibility subcomponent and etched photomicrographs from areas of 64 percent and 260 percent strain. As seen in these photos, there are no signs of significant cavitation. The modified subcomponent basically showed more uniform thinning during the initial portion of forming as well as a better thickness profile. As a consequence, the maximum elongation required to form the part was also reduced.

The modified subcomponent was fully formed using 0.16 inch thick MD254 material. After forming, the part was sectioned for thickness measurements and optical microscopy. An acceptable minimum thickness of 0.024 inch was obtained at the critical corner location. Figure 5-11 shows optical micrographs of the section of the subcomponent. It is evident that cavitation was effectively suppressed with this modified design.

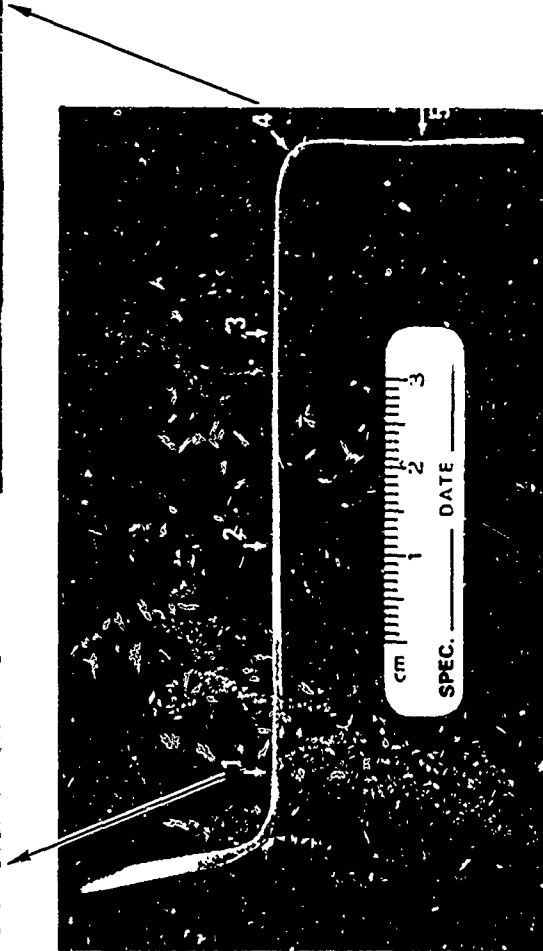
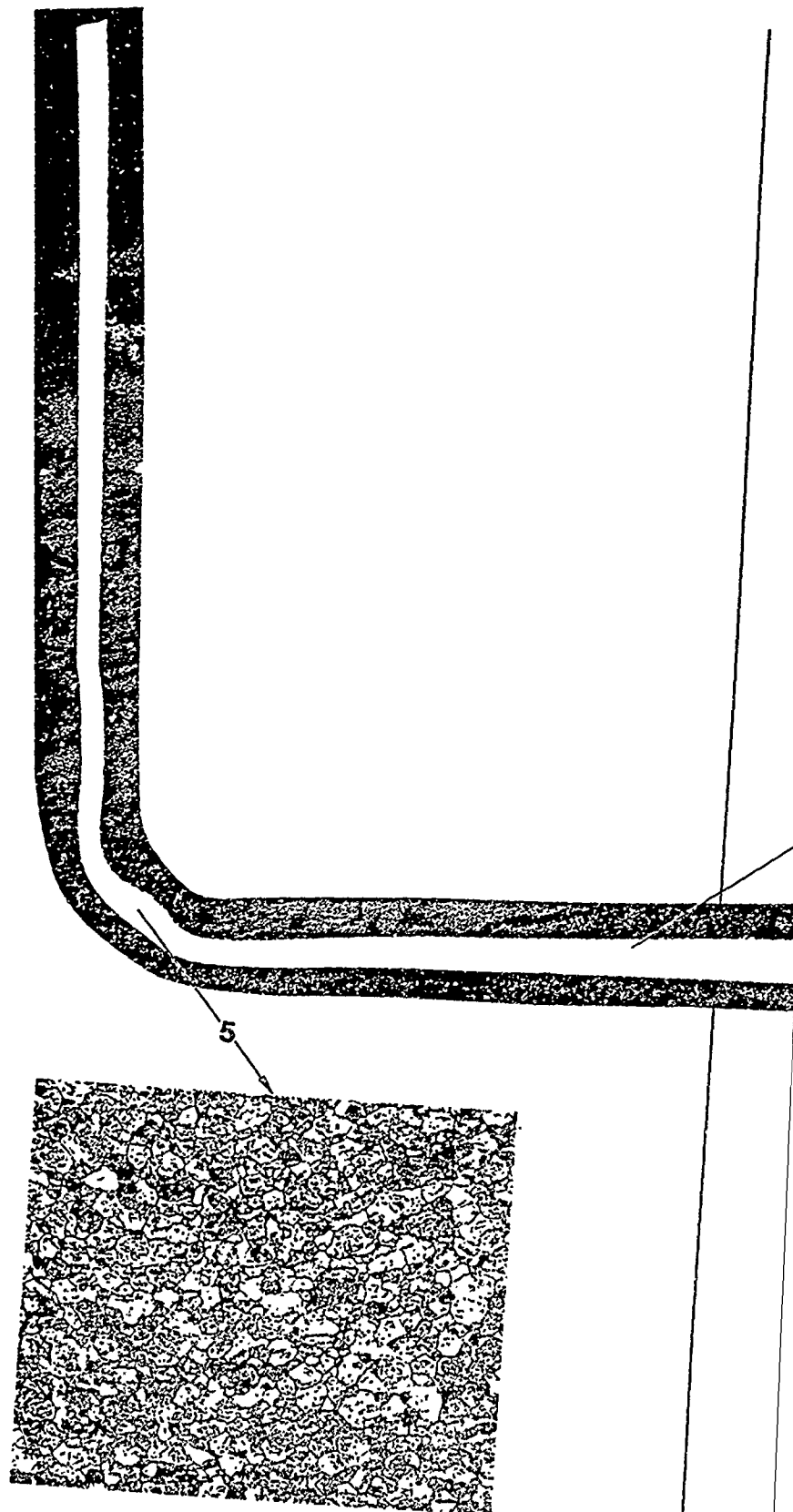


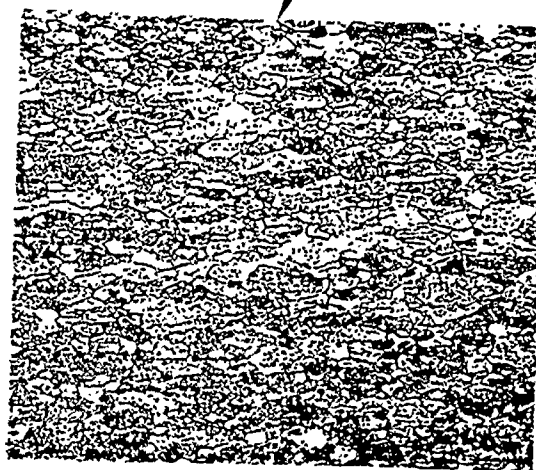
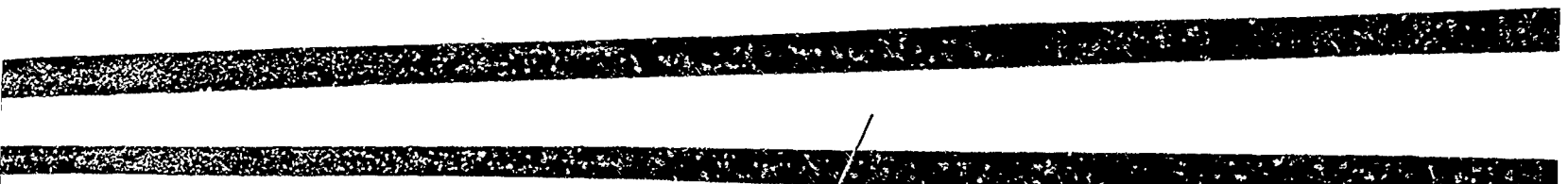
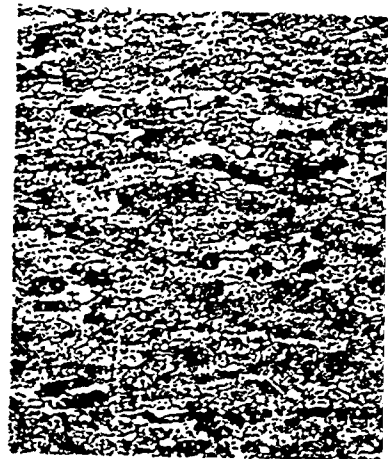
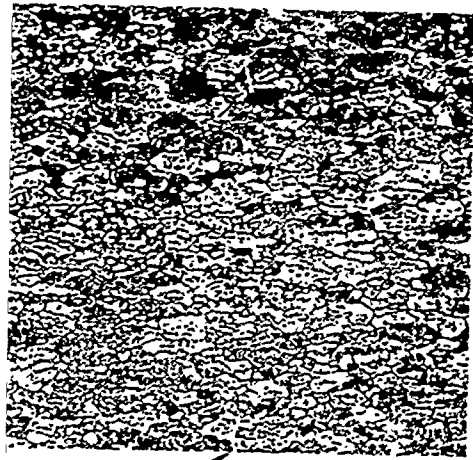
Figure 5-10. Avionics Deck Producibility Subcomponent Microstructure



176

1

AVIONICS DECK - SUBCOMPONENT



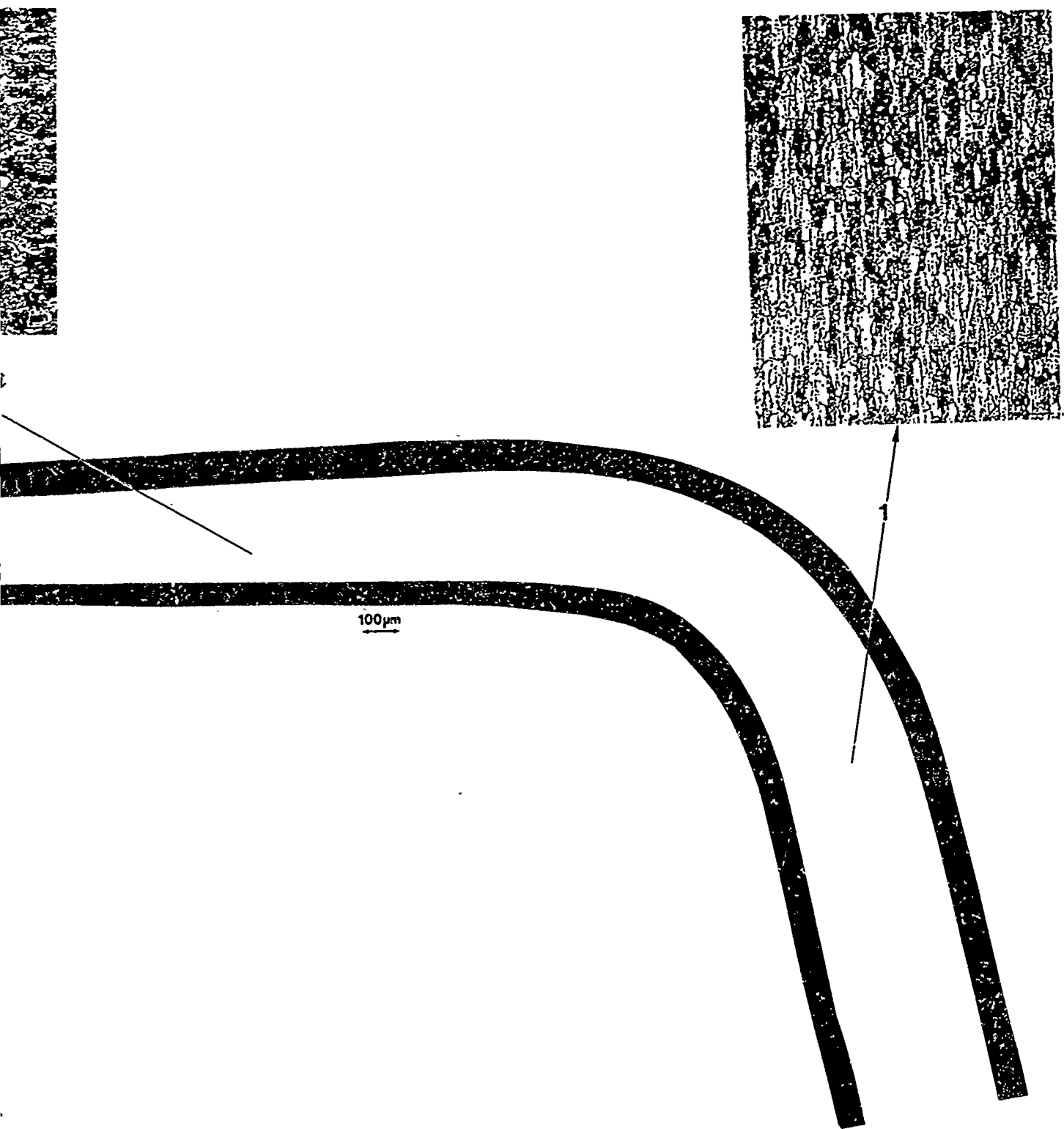


Figure 5-11. Cavitation Measurement for Avionics Deck Subcomponent

3

6. PART AND TOOL FABRICATION

The bulk of the work under Task IV consisted of the fabrication of the SPF dies, the SPF parts and the non-SPF substructural details for the lower avionics deck. This section contains a detailed description of the efforts associated with this phase of Task IV.

6.1 TOOL FABRICATION

The tool fabrication efforts followed the completion of the SPF tool designs. A number of offsite vendors were contacted to support the program schedule. Each vendor was supplied with a set of tool design drawings so they could assess the feasibility of fabricating the dies on schedule.

The conventional profile machining as well as the N/C machining methods were both reviewed for fabrication of the SPF dies. It was decided that the LEX corrugation die would be fabricated using the conventional profile machining and the avionics deck dies would be N/C machined in order to meet the program schedule and to provide better tolerances for the assembly of the final parts.

6.1.1 Conventional Machining of LEX Corrugation Die

The fabrication of the LEX corrugation die proceeded the avionics deck dies since its tool design was the first to be completed. An outside vendor was selected to fabricate the die using the conventional plaster profile machining method. The die material was designated as 4130 steel and the dies outside geometry was machined to fit Northrop's existing production cage. Section cuts for the LEX corrugation were provided by Northrop

using the NCAD/CADAM system so the vendor could utilize them for machining the corrugation die. Layouts of fuselage station cuts and trim line coordinates were also furnished to fabricate the plaster master model. The plaster model was utilized to obtain plaster splashes, blue blocks, die patterns for the skin and was also used to match the inner corrugation moldlines with the outer skins.

The LEX corrugation tool was successfully fabricated and delivered to Northrop. The LEX die was a self-contained tool with seal edge and inlet-outlet gas tubes. Multiport gas inlet-outlet holes were used to prevent gas entrapment and to vent out all of the gas after forming. The LEX die is shown in Figure 6-1.



Figure 6-1. LEX Corrugation Die

6.1.2 Numeric Control Data Generation

The fabrication of the avionics deck dies was done by the N/C machining as opposed to the LEX corrugation die. The N/C method was selected over conventional profile machining due to the complexity of the avionics deck dies, a need to meet the schedule, and to have acceptable tolerances between parts during

the final assembly. The offsite vendor selected for this task had the capability for N/C machining and was selected on that basis.

In order to N/C machine the dies, a N/C tape was to be created and moldline surface data were to be transferred to the vendor through a magnetic tape. The vendor would then use the surface data on their Gerber CAD/CAM system to generate the N/C tapes for the final machining of the dies. Preliminary efforts had indicated that the surface data created on Northrop's 3D NCAD system could be transferred to the vendors Gerber system using the Initial Graphics Exchange Specification (IGES) format. However, subsequent attempts indicated that the NCAD surfaced models and the geometric entities defining them were incompatible with the IGES format.

The IGES system was basically developed for model data transfer between dissimilar CAD/CAM systems. Data would run through a translator and be stored on magnetic tapes or disks prior to up-loading into another system. The Northrop NCAD system defines surface data through a number of parametric equations which are not yet included in the IGES format. As a result, an alternate method of data transfer had to be used through redefining the avionics deck die surfaces.

All three die moldline surfaces were examined for spline/point positioning. Both splines and coordinate points were easily transferrable by IGES and were therefore positioned on all surfaces to create a "wire frame" model of the surface to be transferred. These modified geometric entities were downloaded on a magnetic tape and transferred to the vendors gerber CAD/CAM system. Once in the vendors systems, the "wire frame" models were fully surfaced by the Gerber CAD/CAM system and stored for use in creating numerical control cutter paths for N/C tape generation. The transferred tool designs were also indexed to the part designs so cutter paths could be generated without any tool fixture interference.

6.1.3 Numeric Control Machining

Prior to the N/C machining, all three steel billets were rough cut and profiled to match Northrop's SPF titanium production cage. A plaster of the inside surface of the cage prepared by Northrop's model shop was given to the vendor as a check tool. In addition, the N/C tapes were ran through a tape prove cycle on a block of foam prior to its application on the actual steel billets. The machined foams were then checked and inspected to assure the accuracy of the N/C tapes.

As it turned out, the avionics deck lower and upper skin N/C tapes required minor corrections before they were ready for machining of the final dies. The avionics deck waffle pan N/C tapes however, being the most complex, required several major revisions before they were ready for the final machining. The inspection of the tapes revealed that incorrect surfaces had been created from the data provided by Northrop. The problem was rectified through comparison of the vendor generated data to the one supplied by Northrop. A new cutter path was created and subsequent trial runs were done on foam blocks until the surfaces were within acceptable engineering tolerances.

The cage plaster was used as a master during the profiling of the steel billets. The billets were affixed to a simple mill fixture base by four tooling attach points in an upside down position once they were rough sized. The plaster master and billets were then indexed on the profile mill machine base. After necessary alignments, each billet was profile machined to the geometry of the cage off the plaster master. To further prepare each billet for the final N/C machining, excess stock was removed manually along the surfaces to minimize the N/C machining time. The removal of excess material was done manually and by conventional machining using laycuts of the tool design drawings.

The final N/C machining took place on a vertical N/C mill using the same mill fixture base used in the profiling operation. The lower and upper skin dies were bolted to the mill fixture base and indexed to the machine base for alignment. Each die was machined separately and presented a few problems with the operation of the machine and/or cutter failures. The waffle pan die was mounted to the machine in the same manner as the other two dies. The machining of this die was much slower due to its complexity and excessive failure of cutters during the machining of its deep pockets. The cutters used along the pockets were 0.5-inch diameter, 6.0 inches long round nose and mill cutters made from high speed steel or carbide. Both type of cutters were used over their normal capability. Several trials with different speed and feed rates revealed that the ideal feed rate was 7 inches per minute to preserve a normal cutter life and machining time. As a result of these problems, the waffle pan die took 4 weeks to complete as opposed to the 2 weeks required for each of the skin dies.

Upon the completion of the N/C machining and the subsequent inspections, each die was hand polished to a 64 surface finish and scribe lines were etched on the surface to indicate the rough trim lines for each part. The inspection was done by remounting each die to the mill fixture base and reading the coordinates of pre designated inspection points using the vertical mills digital read out. Figures 6-2 through 6-4 represent the finished dies for the avionics deck. A more detailed description of the inspection is presented in the next paragraph.

6.1.4 Numeric Tool Inspection

All three avionics deck dies were inspected at the completion of the N/C machining. The inspection technique utilized was to use coordinate check points. This method was selected over other methods such as inspection with check fixtures (templates) or maxi check (automated coordinate measurements) as

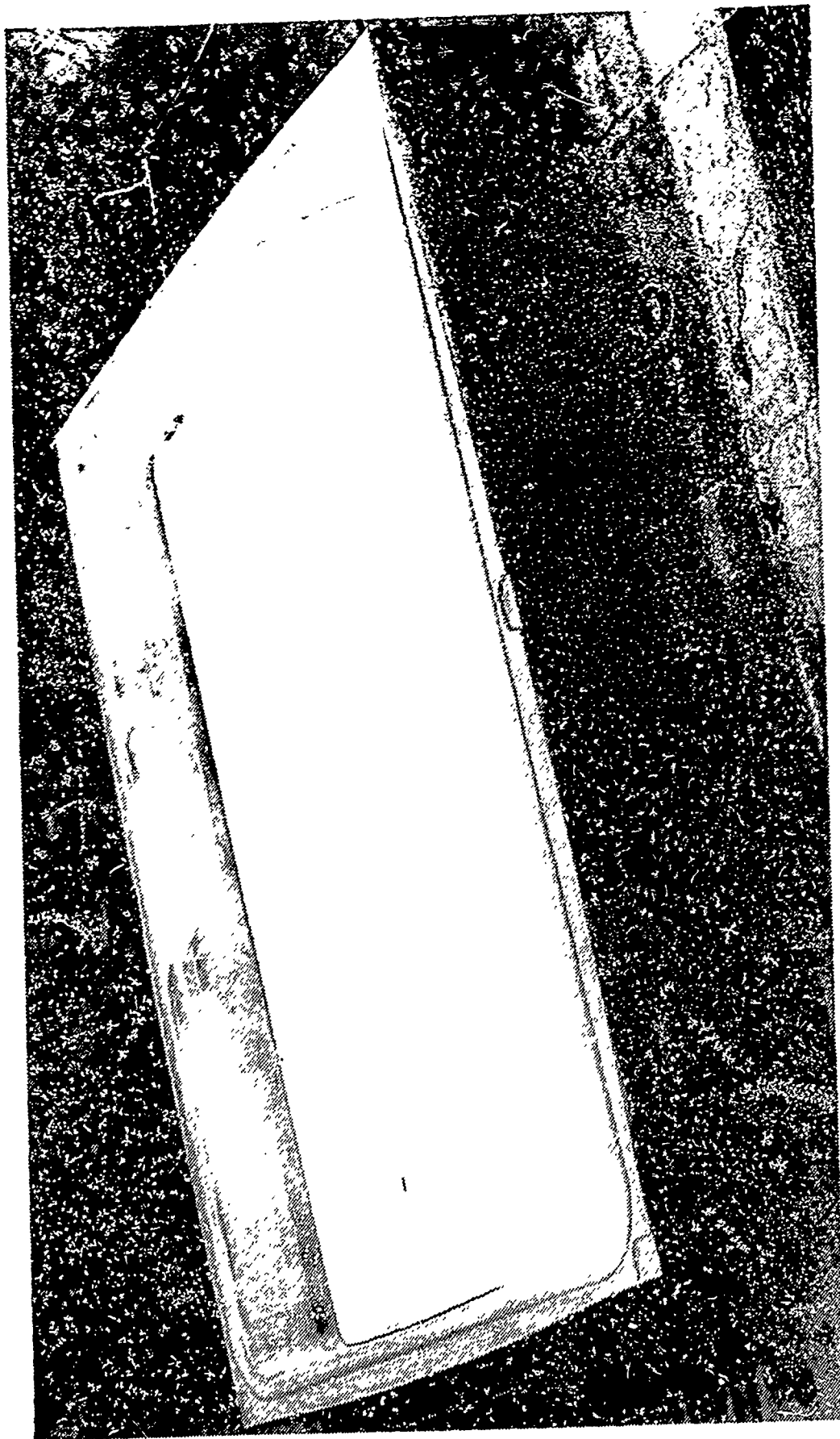


Figure 6-2. Avionics Deck Lower Skin Die



Figure 6-3. Avionics Deck Upper Skin Die

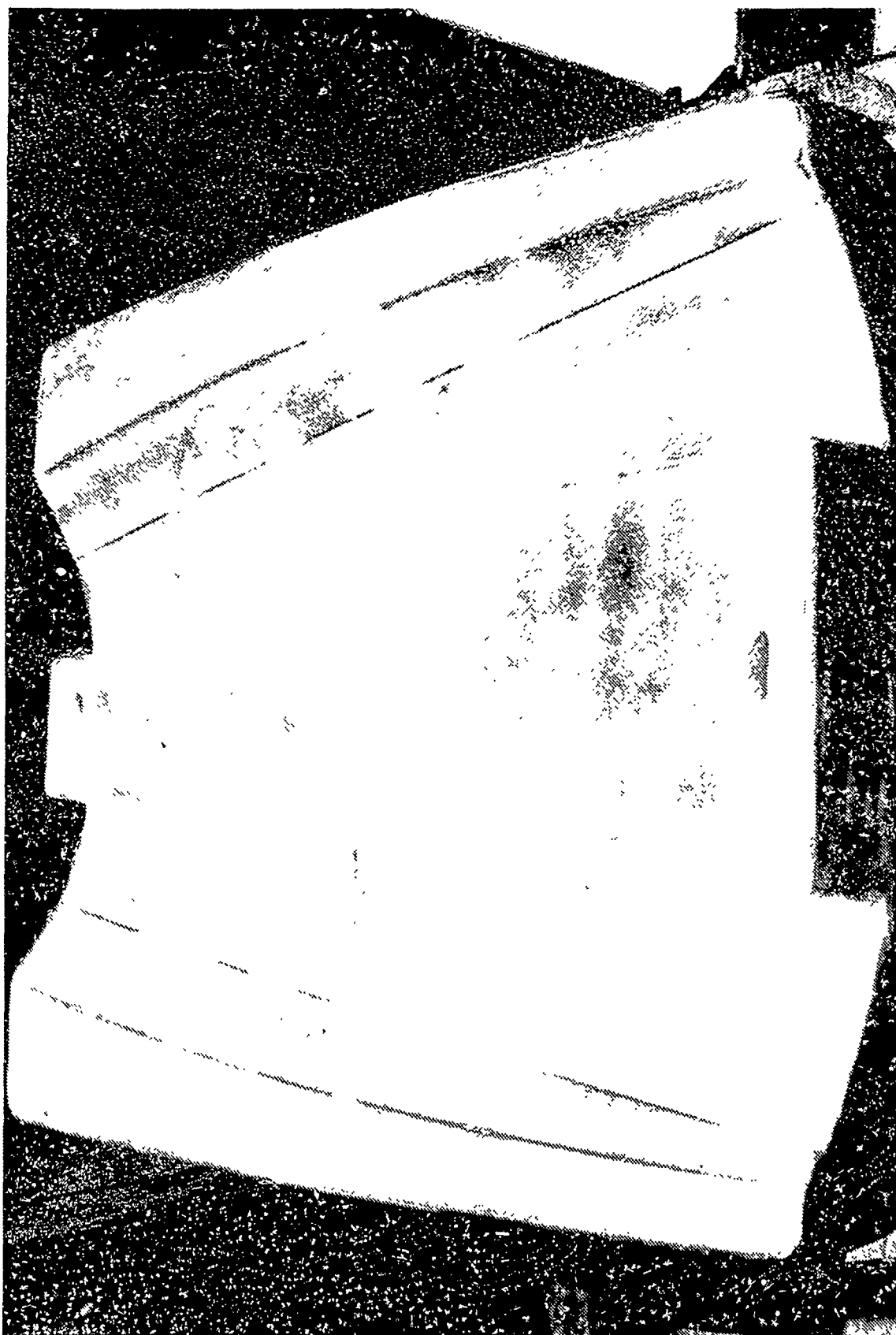


Figure 6-4. Avionics Deck Waffle Pan Die

a time and cost saving measure. Fabricating check templates and/or maxi check would be more costly and would also require transportation of dies from the vendor site to Northrop and back to the vendor. Therefore, it was decided to check the surface of each die through a series of points, coordinates of which had been preidentified by the Northrop NCAD system.

Inspecting the surface of each die through a series of coordinate points was the most efficient method, since all dies were designed in Northrop's NCAD/CADAM system and the identification of point coordinates was an easy task. The inspection points were laid out along the die surface in strategic locations after which their coordinates were analyzed. The coordinate values for each dies' inspection points were recorded by Northrop's Master Dimensions group and verified for accuracy. Once the coordinates of the inspection points were verified, they were used for the final inspection of the die surfaces.

Each die was indexed back on the vertical mill and a "starting" point was located as the origin with coordinates of $x = 0$, $y = 0$, and $z = 0$. The inspection point coordinates along the x,y surface were then manually fed to machines controller. The machine would then automatically locate that point, and a dial indicator would measure the surface height to check the value of the z -coordinate. By using the dial indicator in combination with the mills digital coordinate read out, the height of the die surface was checked as being high or low.

The inspection process consisted of two phases. During the first phase of inspection, the entire die surface was machined to 0.100 inch over the prescribed surface dimensions to avoid any undercutting. An excess material thickness of 0.100 inch would allow a sufficient margin for possible errors during the machining process. Once the first phase of inspection was completed, the areas with excessive material were identified and hand worked until a uniform die surface was created. The second

phase of inspection double checked the accuracy of the hand worked areas.

In case of the upper and lower skin dies, the die surfaces were found to be high in some isolated areas. Those areas were hand worked and polished until an acceptable surface height was obtained. The waffle pan die, however, was found to be high on several different locations. The problem stemmed from two different mill operations and two different setup procedures. The N/C tapes corresponding to those locations had to be reran with the correct setup to correct the areas of problem. Those surfaces were then rechecked and found to be acceptable.

The entire inspection and liason efforts were handled by Northrop personnel at the vendors site. All inspection data was recorded and compared to the point coordinates generated previously. Once the data was found to be acceptable, the dies were approved and delivered to Northrop.

6.2 PART FABRICATION

This task consisted of fabrication of SPF and non SPF parts of the LEX and the lower avionics deck. In case of the LEX, only the SPF corrugation was fabricated to demonstrate its producibility. The avionics deck, however, had three SPF parts (upper skin, lower skin and waffle pan) and seven non SPF details fabricated for the final assembly. The full scale structural parts were superplastically formed using the tooling concepts and fabrication techniques developed in the producibility forming studies (Task III). Reynolds superplastic MD254 aluminum material was utilized for fabrication of alloy SPF parts. The following paragraphs give a detailed description on fabrication of each part.

6.2.1 LEX Corrugation Fabrication

Prior to forming of the LEX corrugation, both the die and aluminum sheets were coated with Boron-Nitride. The forming was carried out at the temperature range of 940 to 980°F. The die was heated up to the forming temperature and the MD254 aluminum sheet was hot loaded. A 0.090-inch thick sheet was used, and the forming was conducted with a back pressure of 400 psi to suppress the cavitation. The theoretical forming strain rate was $2 \times 10^{-4} \text{ sec}^{-1}$, however, the average strain rate measured was slightly lower, $1.4 \times 10^{-4} \text{ sec}^{-1}$. The forming cycle is shown in Figure 6-5. A total of three LEX corrugations were successfully fabricated with no scrap parts.

After forming, the SPF LEX corrugations were heat treated to the T6 temper per Northrop's heat treat specifications (HT-1). The heat treatment was verified through electrical conductivity and hardness measurements. Following the heat treatment, the parts were chemical cleaned, anodized and primed. A SPF LEX corrugation before and after trimming is shown in Figure 6-6.

Figure 6-7 represents a section cut from the deepest channel of the LEX corrugation and optical micrographs from different locations on the section. The micrographs indicated a few areas containing isolated cavities which may be related to the variation in the grain structure. However, the area fraction of cavities in such areas was less than 0.5 percent which was considered acceptable.

6.2.2 Avionics Deck Upper Skin Fabrication

The avionics deck upper skin was superplastically formed utilizing 0.090-inch thick MD254 sheet material. The 0.090 inch sheet thickness was selected since preliminary analysis had indicated that a post-SPF thickness of 0.050 inch would

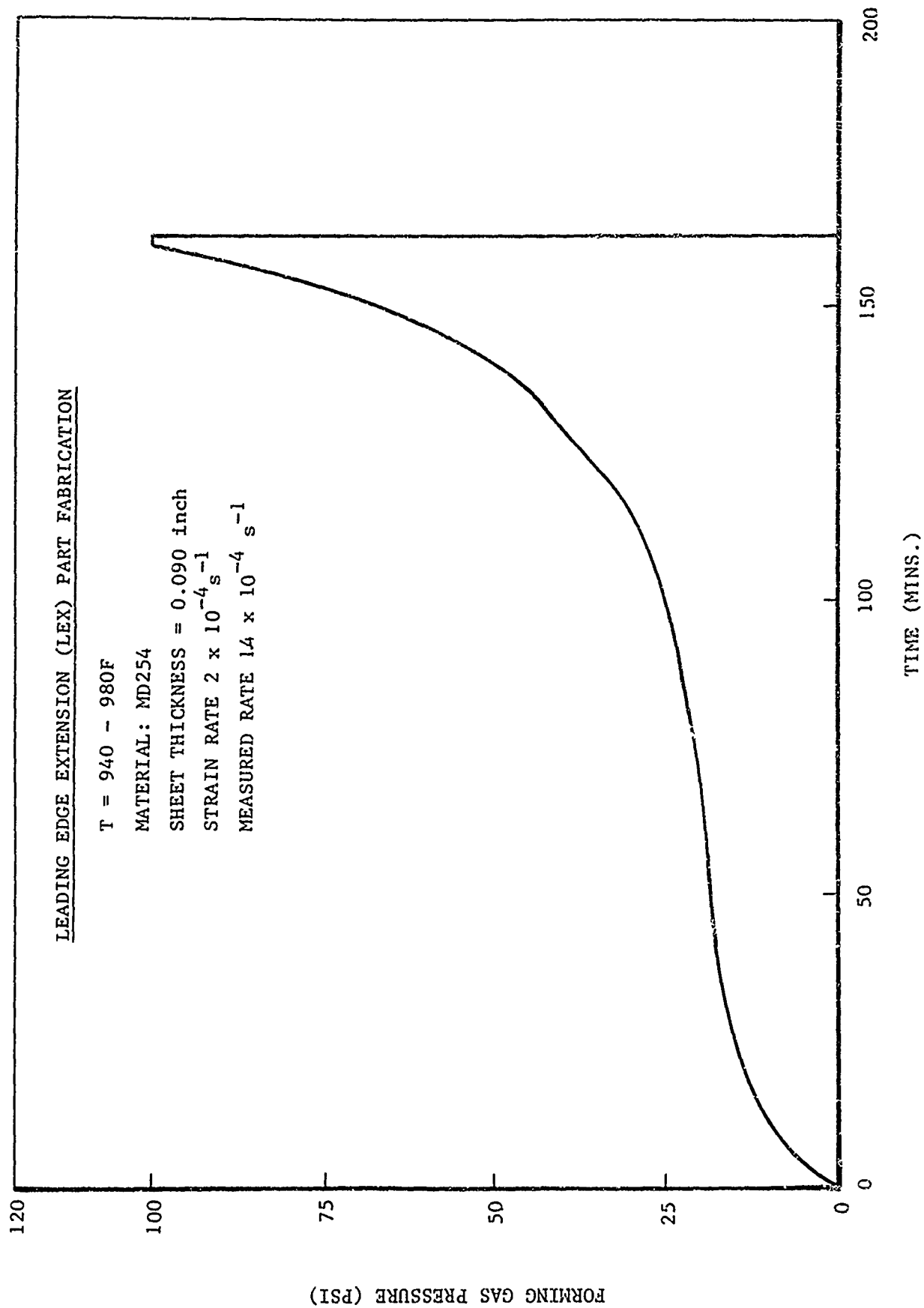
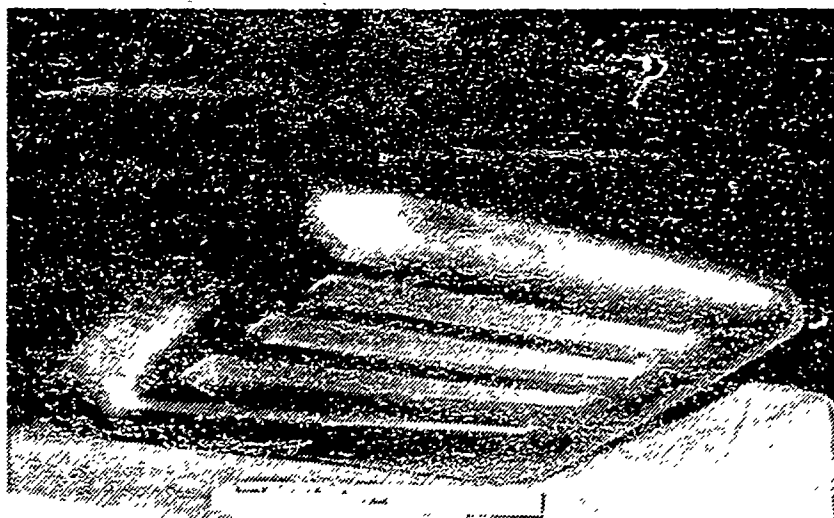
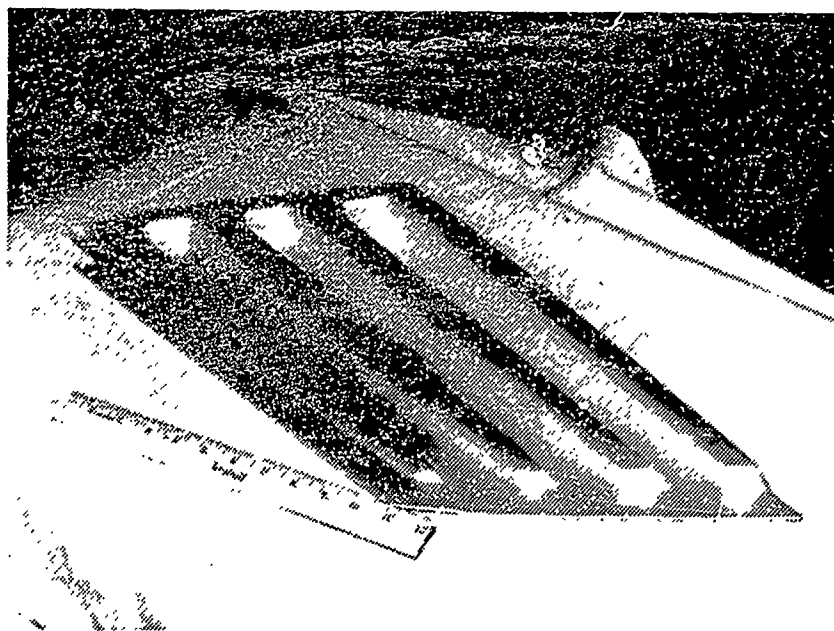


Figure 6-5. Forming Cycle for LEX Corrugation

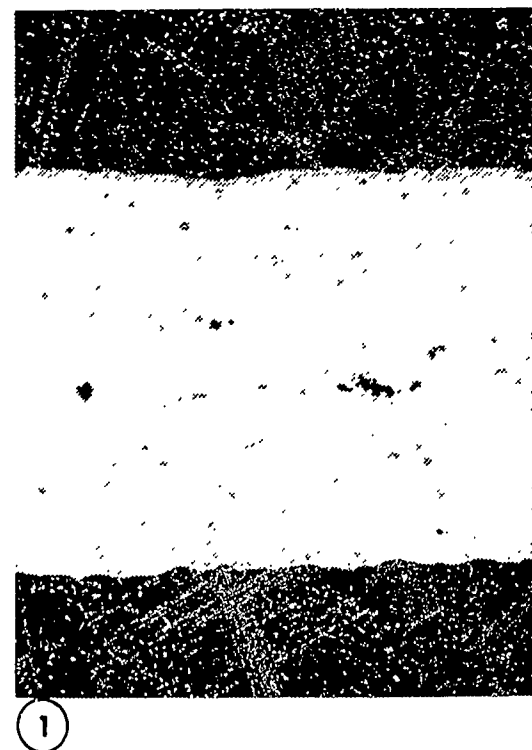
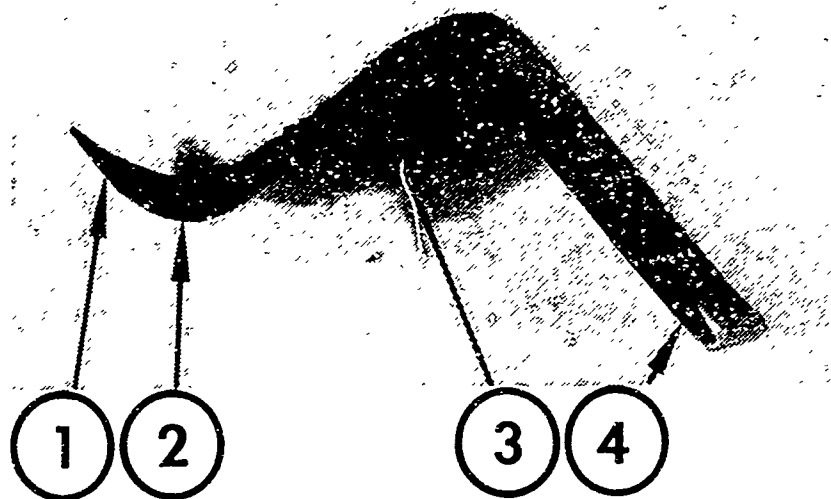


(a) LEX Component Before Trimming



(b) LEX Component After Trimming

Figure 6-6. Superplastically Formed LEX Corrugations



192

1

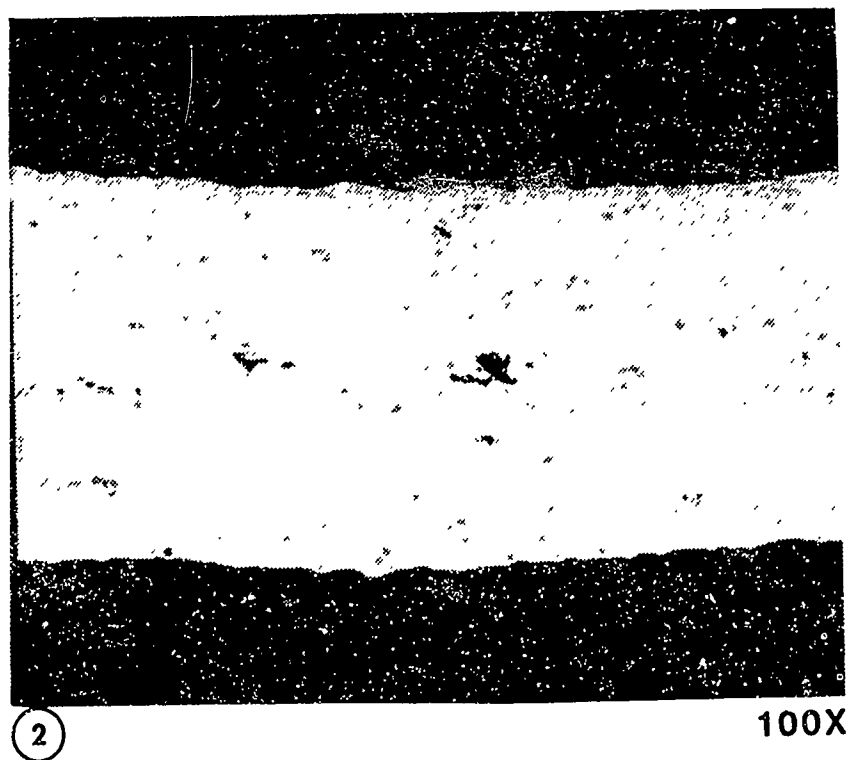
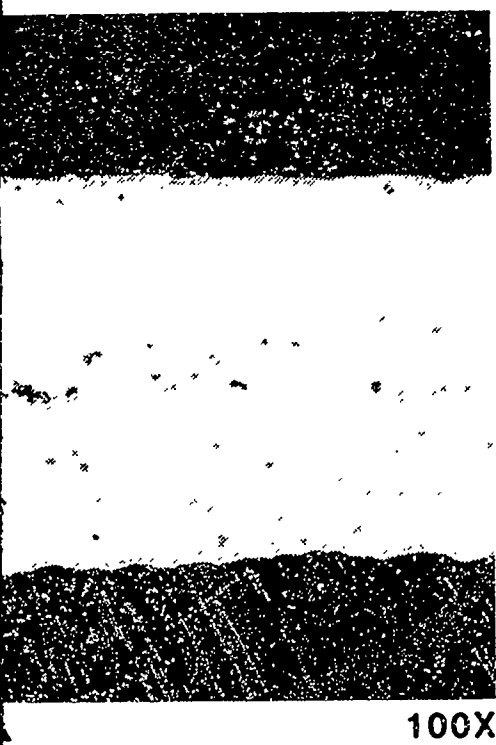
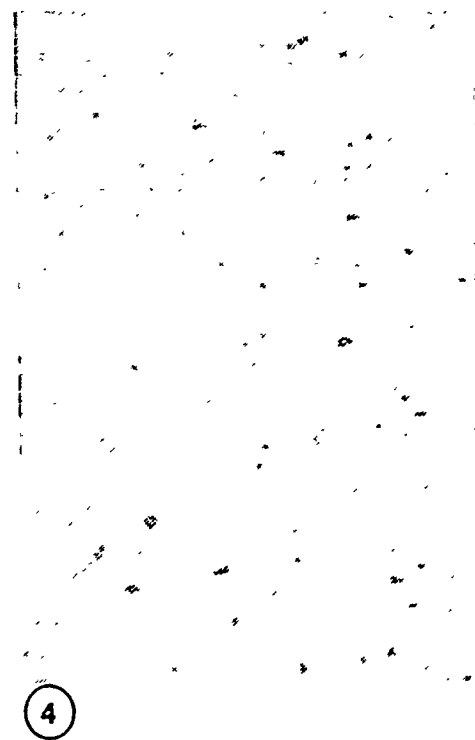
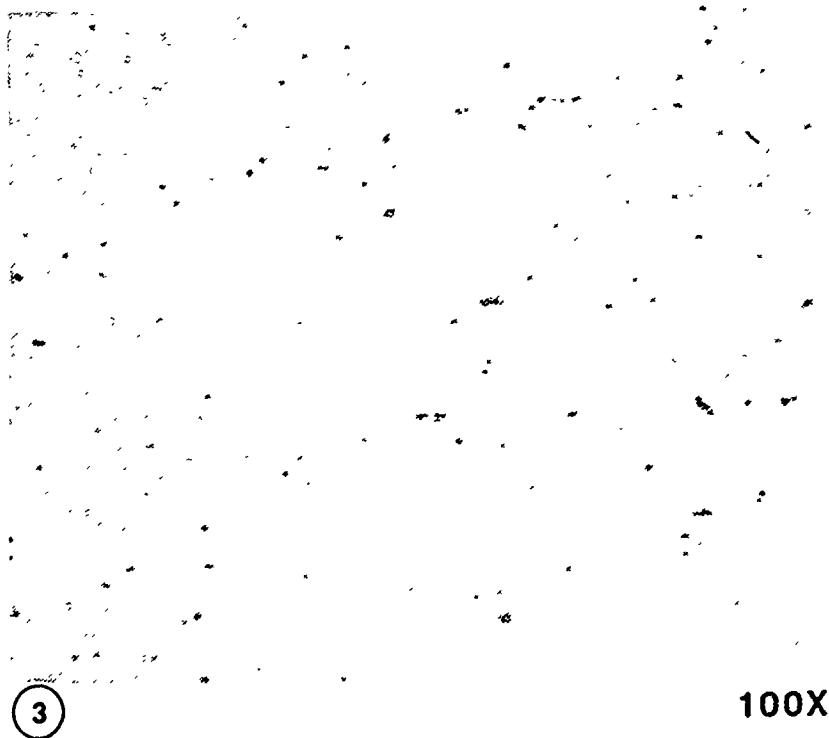


Figure 6-7. SPF L



100X



100X

Figure 6-7. SPF LEX Corrugation Microstructure

be sufficient from a strength point of view. Due to the configuration of the upper skin, it was predicted that there would not be much thinning associated with the forming of the skin. Therefore, a starting gage of 0.090 inch was selected.

The forming cycle for the upper skin is shown in Figure 6-8. Forming was conducted in the temperature range of 940 to 970°F with a back pressure of 400 psi. The strain rate was set at $2 \times 10^{-4} \text{ sec}^{-1}$. Three upper skins were successfully formed with no scrap parts. The SPF upper skins are shown in Figure 6-9. An optical micrograph excised from the upper skin close to its trim line is shown in Figure 6-10, and as noticed, there are no signs of cavitation.



Figure 6-10. SPF Avionics Deck Upper Skin Microstructure

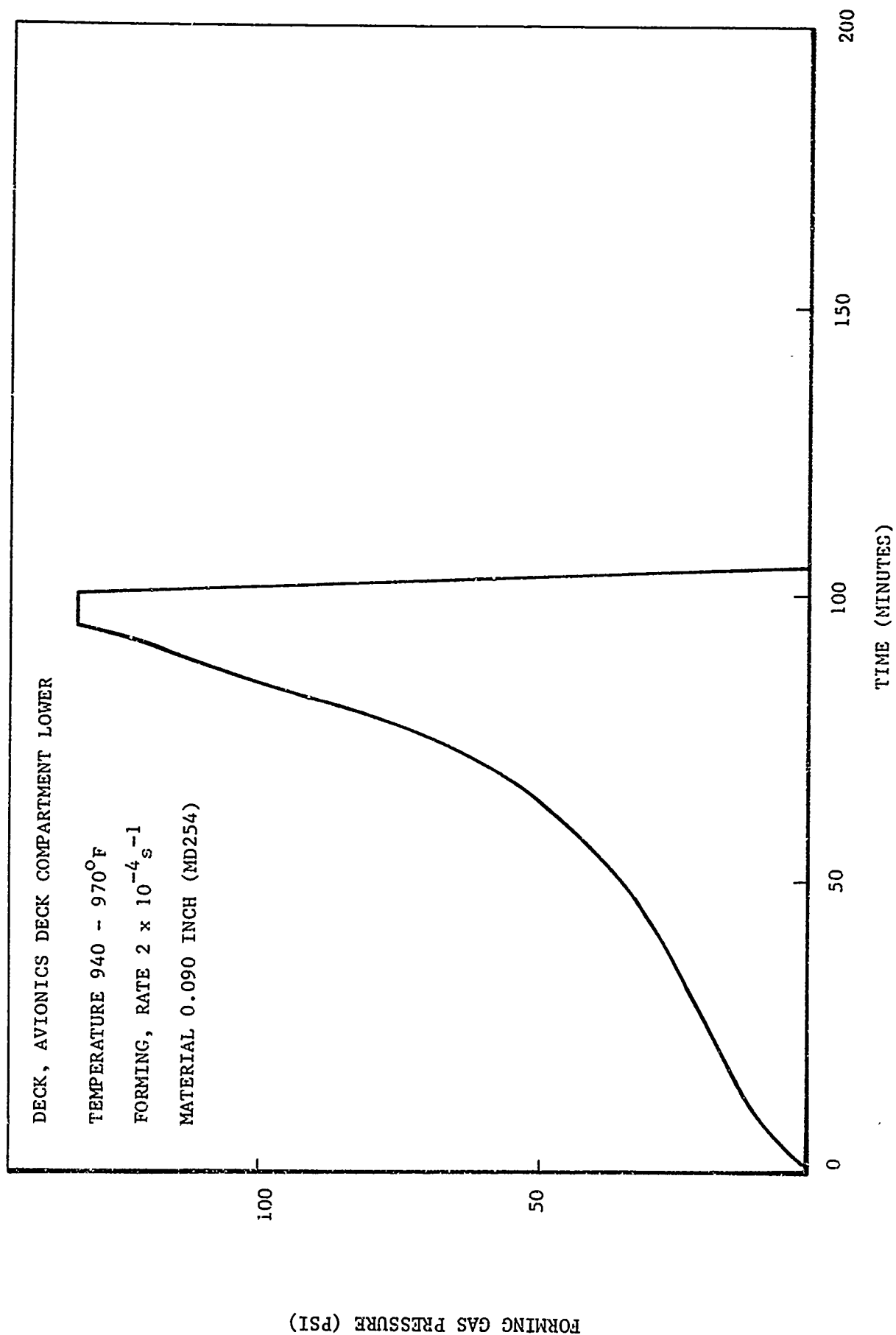


Figure 6-8. Forming Cycle for Superplastic Forming of Avionics Deck Upper Skin

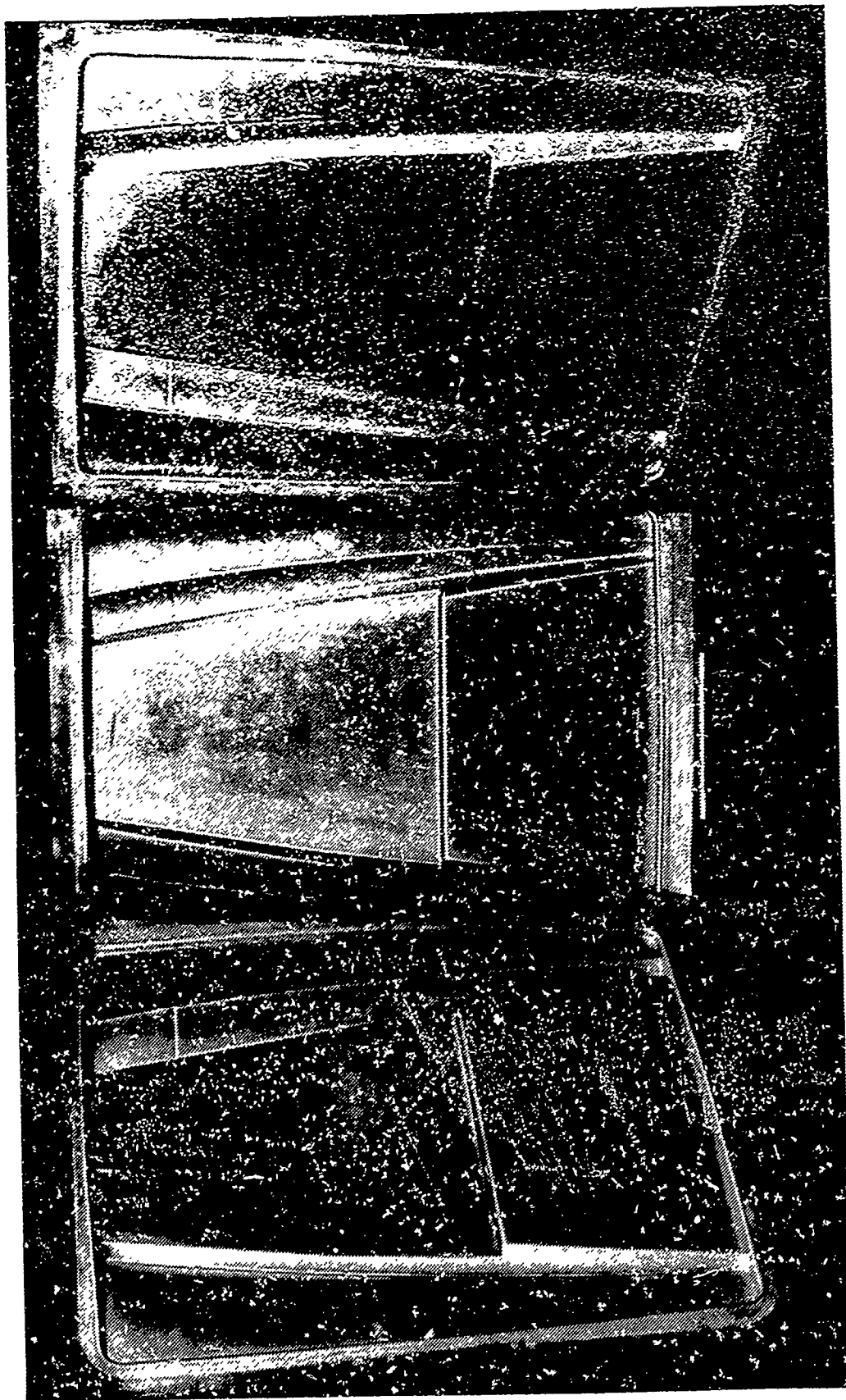


Figure 6-9. Superplastically Formed Upper Skin Parts

5.2.3 Avionics Deck Lower Skin Fabrication

The lower skin was also superplastically formed using 0.090-inch thick MD254 aluminum sheet. Forming was conducted in the temperature range of 943 to 977°F, at a strain rate of $2 \times 10^{-4} \text{ sec}^{-1}$ and a 400 psi back pressure. The forming cycle for the avionics deck lower skin is shown in Figure 6-11. Three skins were formed successfully with no scrap parts and are shown in Figure 6-12. An optical micrograph from the skin ends is shown in Figure 6-13, and as noticed, there are no signs of any cavitation.

6.2.4 Avionics Deck Waffle Pan Fabrication

The forming of the avionics deck waffle pan was more complicated as opposed to the skins. Due to the complex configuration of the pan and the deep pockets associated with its design, there was severe forming involved with this part. As a result, a lower strain rate of $1 \times 10^{-4} \text{ sec}^{-1}$ was used to form the waffle pan. The forming cycle for the avionics deck waffle pan is shown in Figure 6-14. A total of six waffle pans were formed without any rupture. Figure 6-15 represents a typical SPF waffle pan.

Once the forming was completed, thickness measurements were made to check the thickness variation among the different pans. Due to the excessive thinning associated with the pans complex configuration, a 0.160 inch thick MD254 aluminum sheet was used for forming of the pan. Figures 6-16 and 6-17 represent the thicknesses measured on two of the pans before and after trimming.

Due to the excessive material thickness in the flat areas of the waffle pan, Figures 6-16 and 6-17, where thinning was minimal, the pans were chem milled to remove all excessive material. After chem milling and prior to the final assembly,

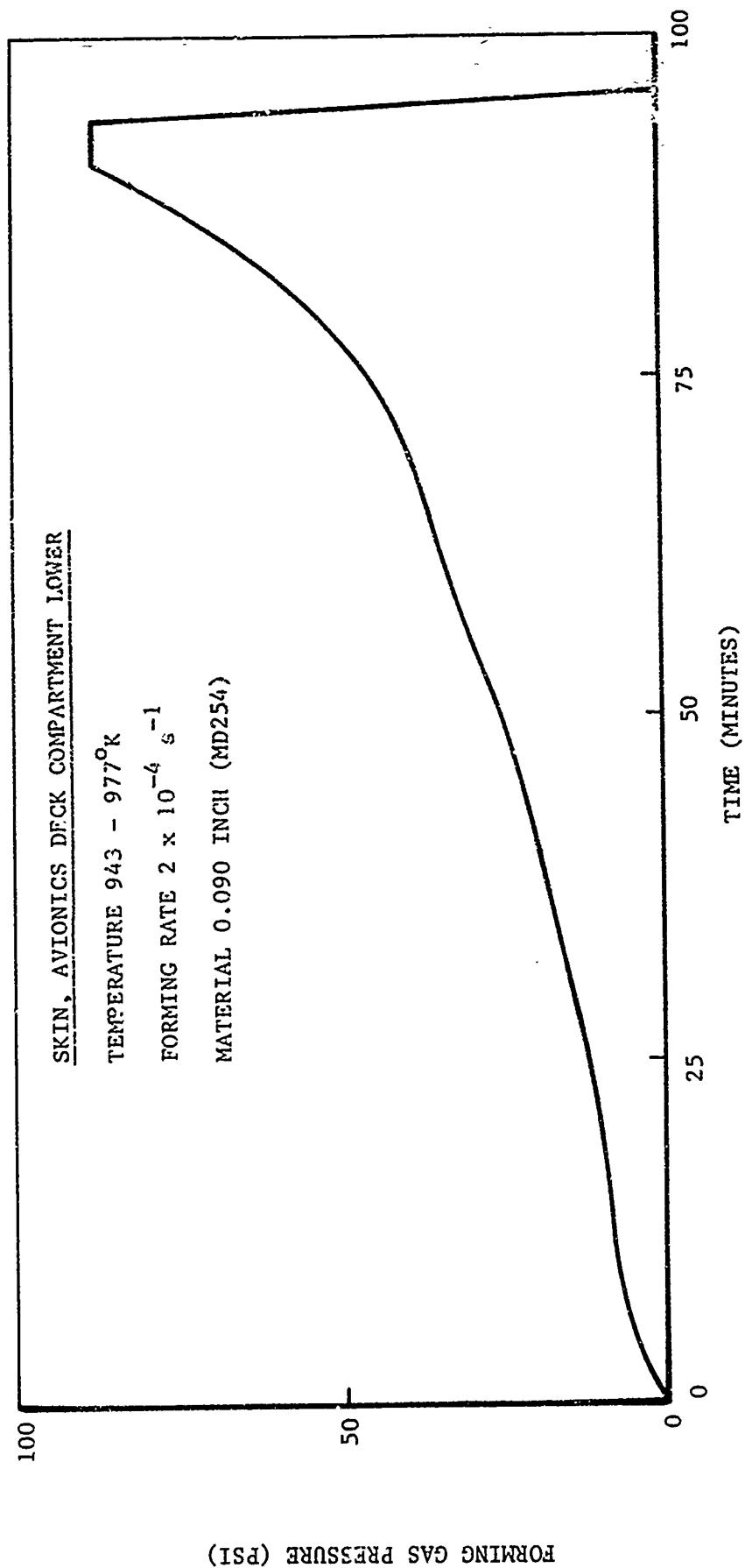


Figure 6-11. Forming Cycle for Superplastic Forming of Avionics Deck Lower Skin

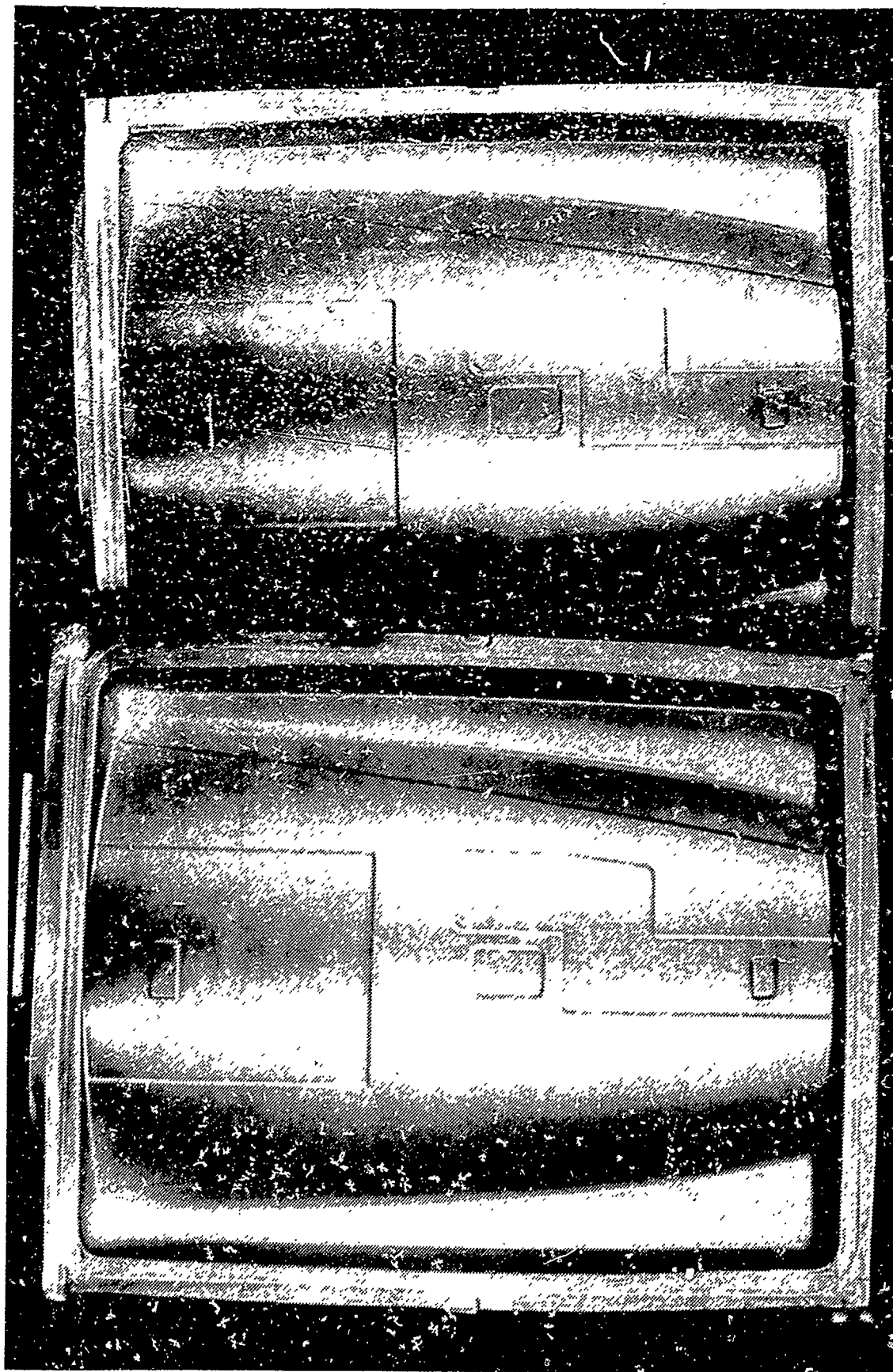


Figure 6-12. Superplastically Formed Lower Skin Parts

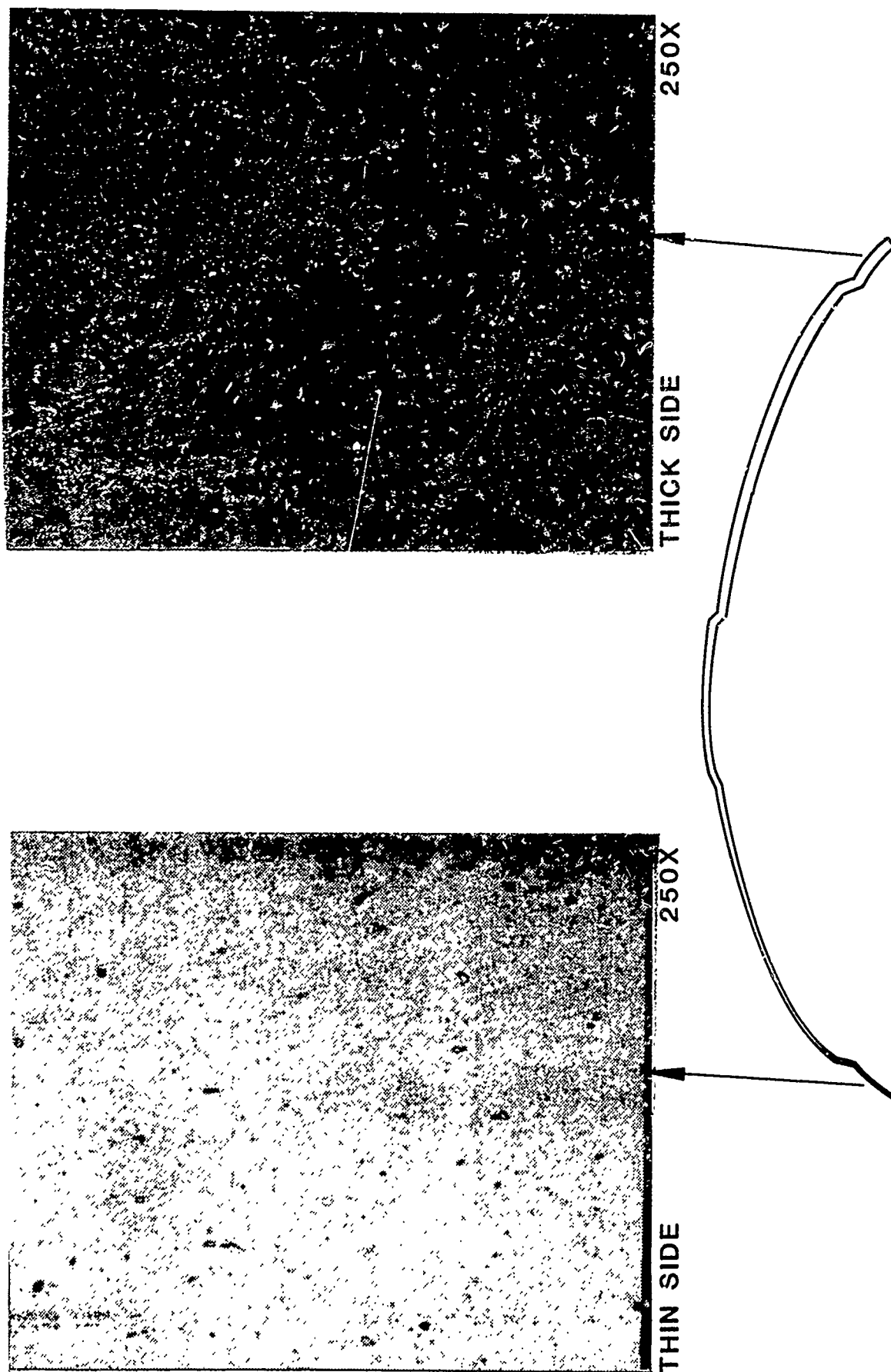


Figure 6-13. Avionics Deck Lower Skin Microstructure

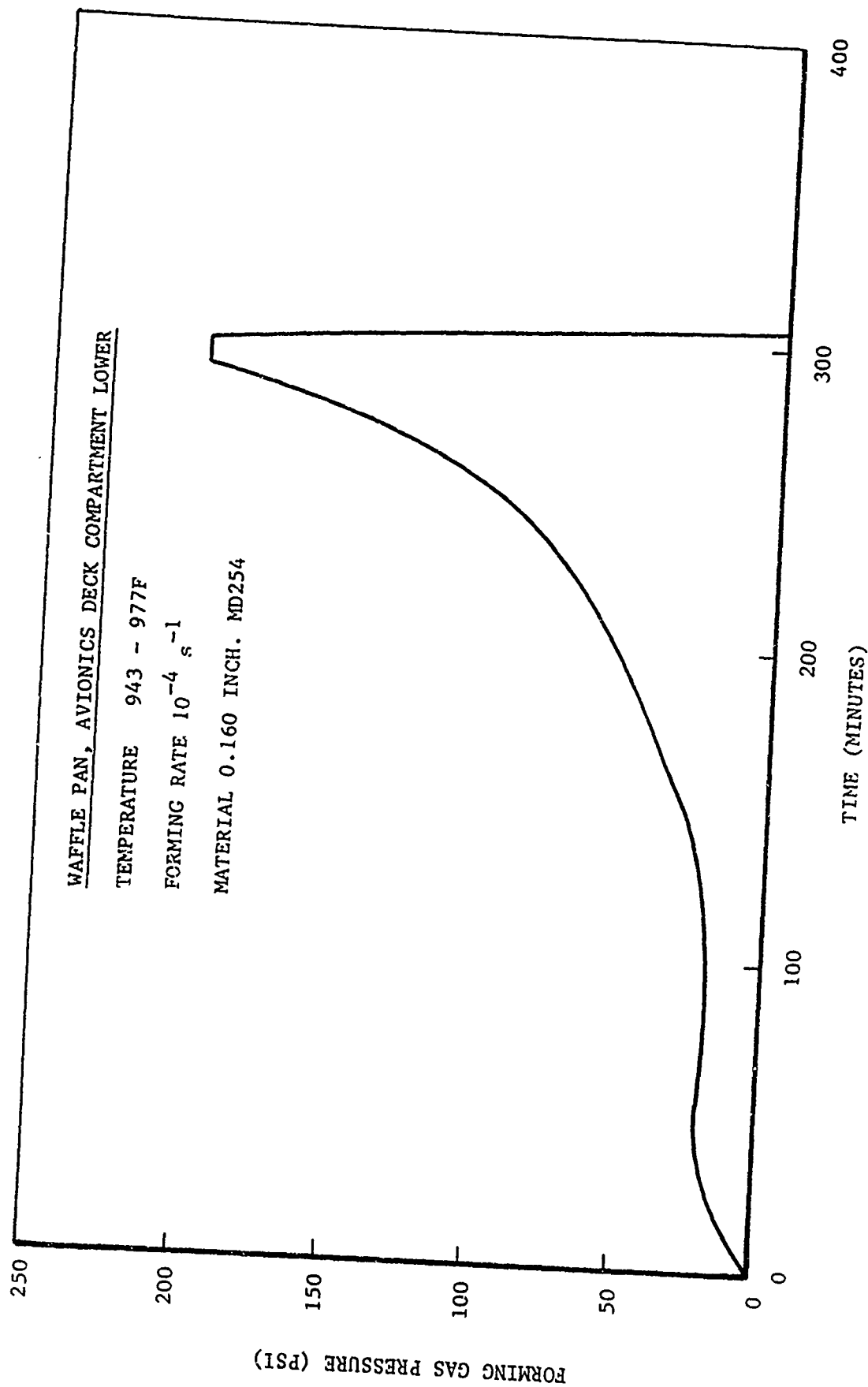


Figure 6-14. Forming Cycle for SPF of Waffle Pan

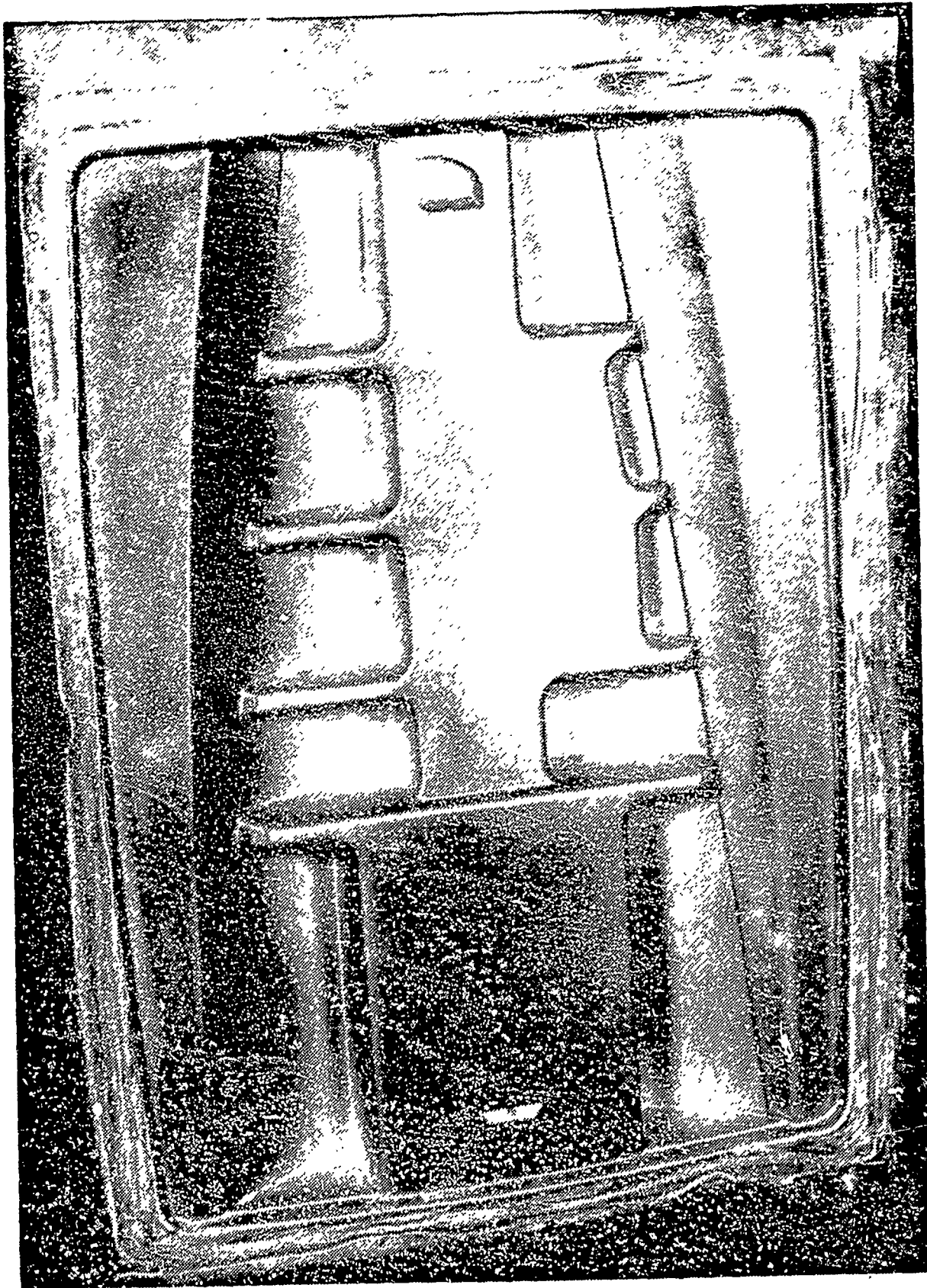


Figure 6-15. Avionics Deck Superplastically Formed Waffle Pan

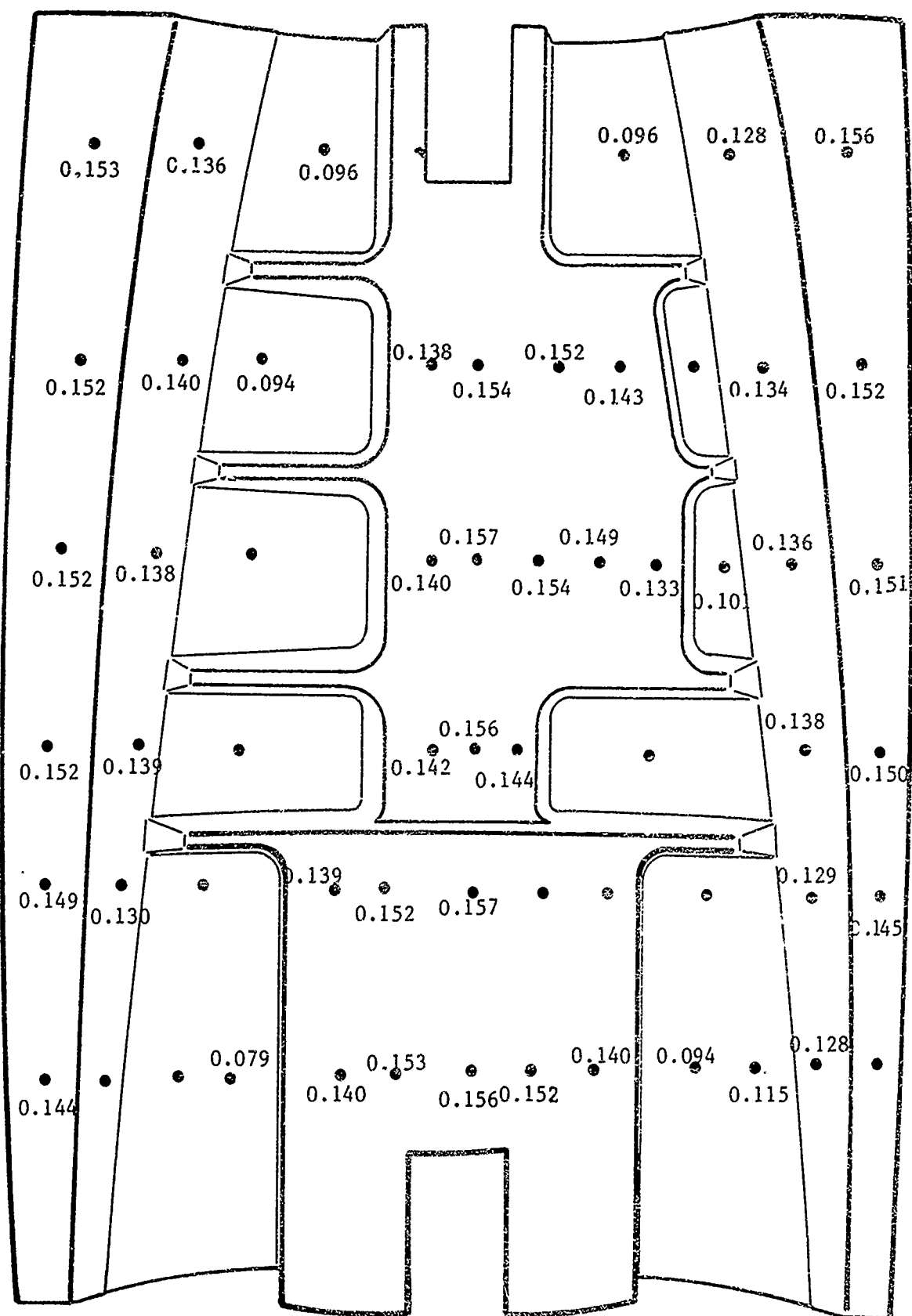


Figure 6-16. Waffle Pan Thicknesses Before Trimming

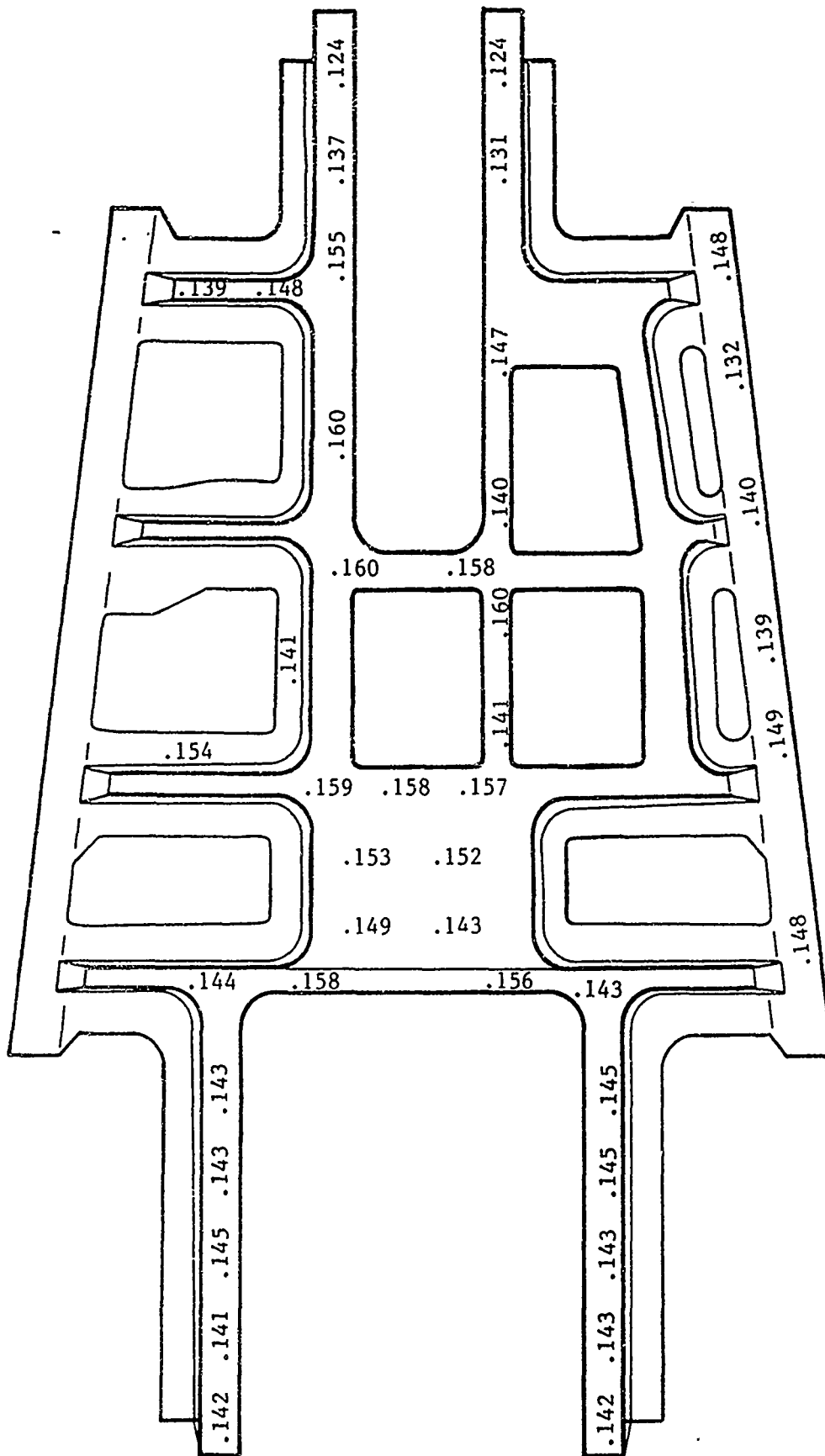


Figure 6-17. Waffle Pan Thicknesses After Trimming

the pan was net trimmed as shown in Figure 6-18. Prior to chem milling, however, the pans were heat treated to T6 temper which was verified through electrical conductivity and hardness measurements. Optical microscopy was performed to determine if there were any cavitation problems. The micrographs were taken from the locations of maximum elongation. Figure 6-19 shows the micrographs, and as seen, there were no signs of any cavitation.

6.3 AVIONICS DECK SUBSTRUCTURE DETAIL FABRICATION

The avionics deck was comprised of seven substructural details which consisted of both sheet metal formed and machined parts. All sheet metal parts were fabricated by hydro-forming using hydro-form blocks. The blocks were profile machined using templates made from flat pattern drawings. The flat patterns were made from the design drawings of each substructural part using the CADAM system. By using templates as profile trace patterns, the shop was able to machine the aluminum formed blocks for use in the fabrication of the intercostals.

The form blocks contained tooling holes for indexing blanked stock prior to forming. The form blocks were inspected to the engineering prints for overall accuracy and to check parameters such as the bevel angels. After the form blocks were completed, 7075 aluminum sheet was cut out to the flat pattern engineering drawings for the fabrication of the details. The material was then drilled for coordination of tooling holes to the form blocks. Prior to the final forming, the material was softened for greater formability through solution heat treat, quenching, and storage in an ice box to prevent natural aging. After forming, the parts were heat treated to a T7 condition and inspected against the engineering prints. Inspections revealed that several parts had not been fully formed. As a result, the form block corner radii were reworked, and a second set of details were formed, which were found to be acceptable.

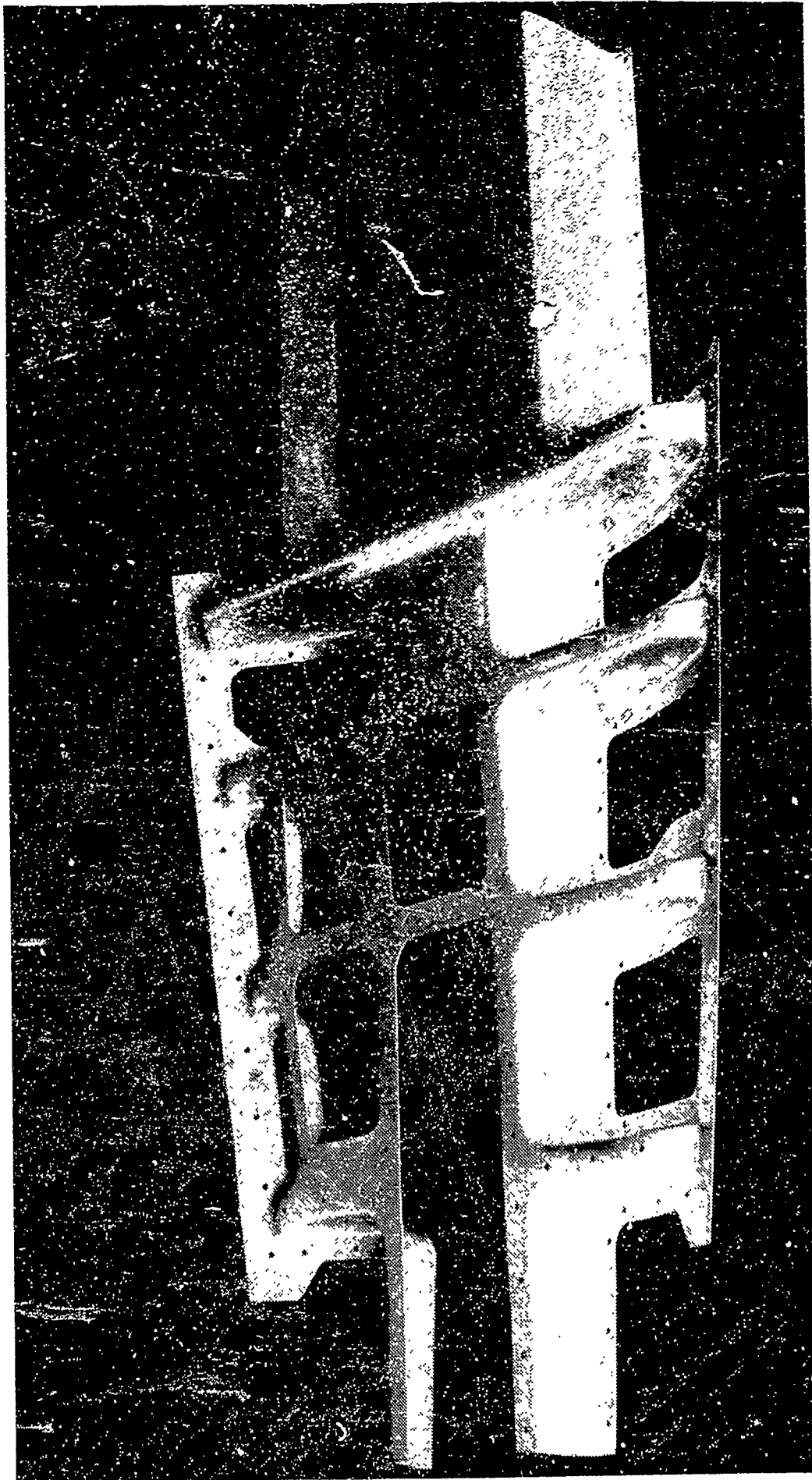
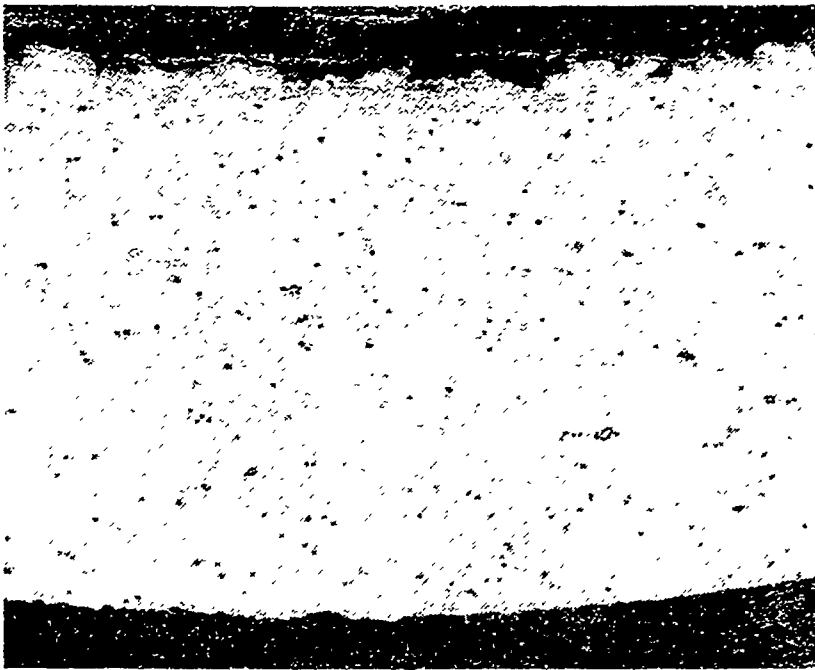
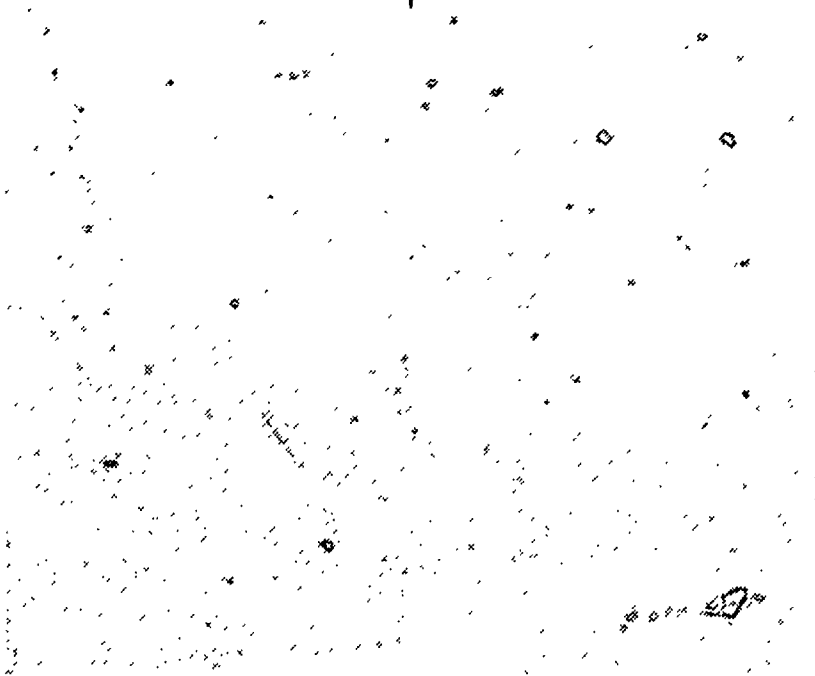


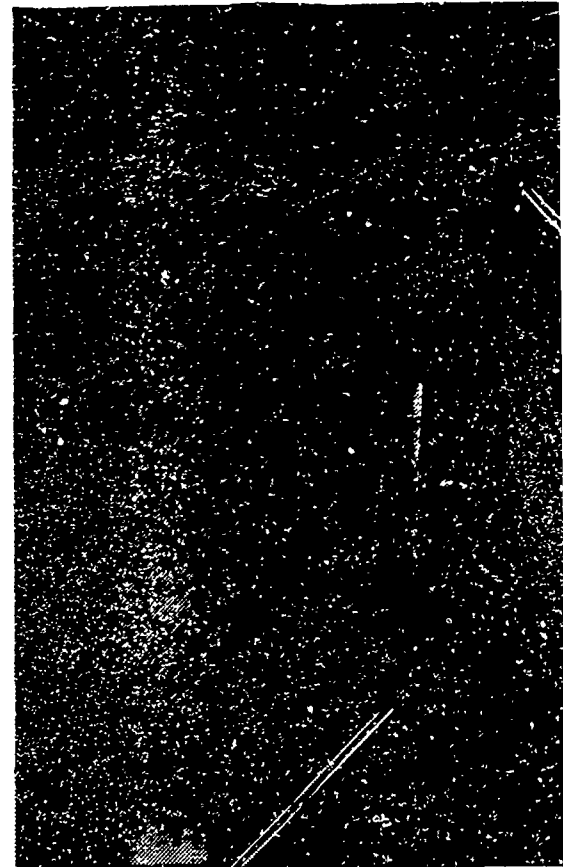
Figure 6-18. Avionics Deck Waffle Pan After Final Trimming



150X



250X



208

1

1

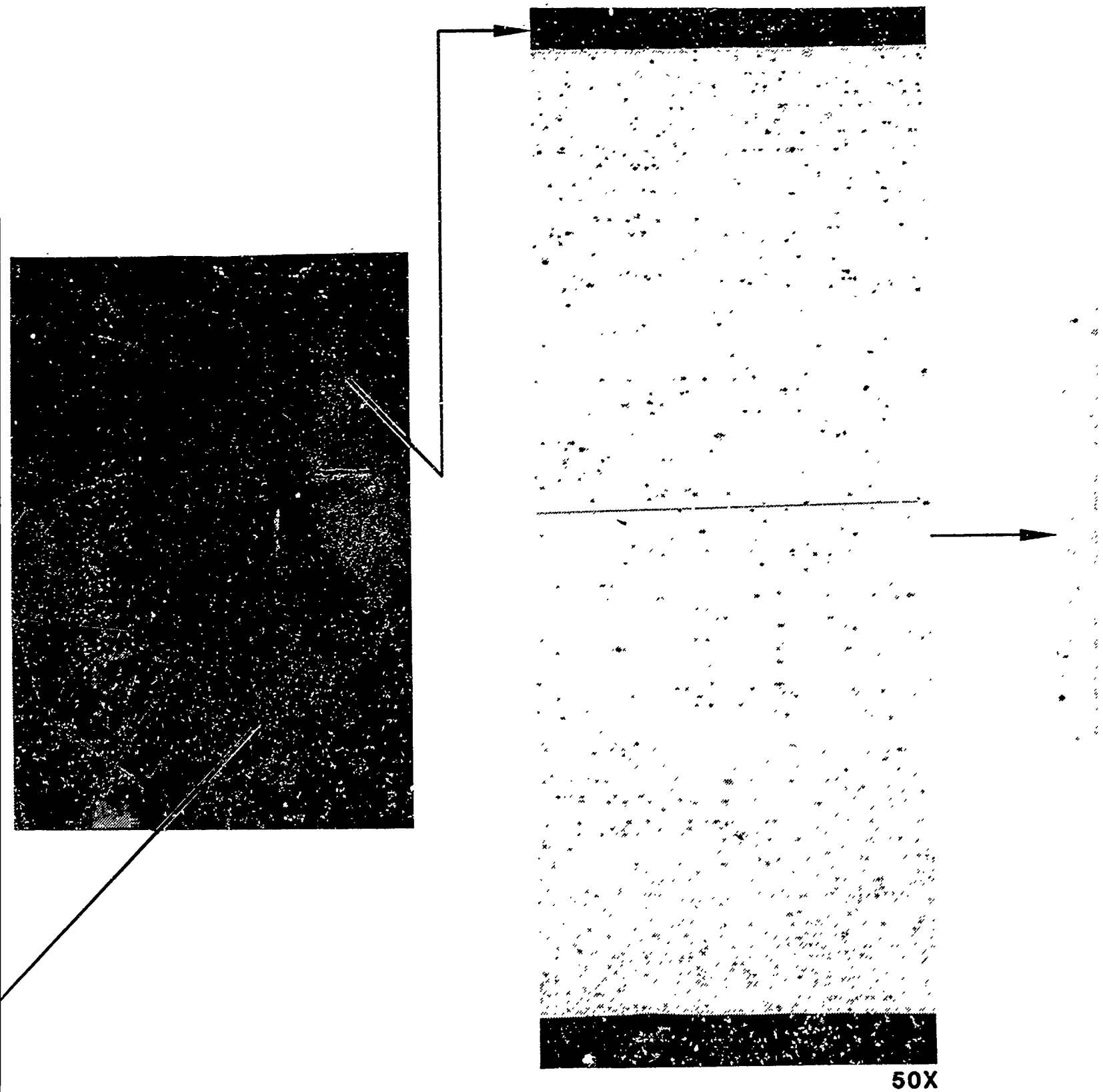
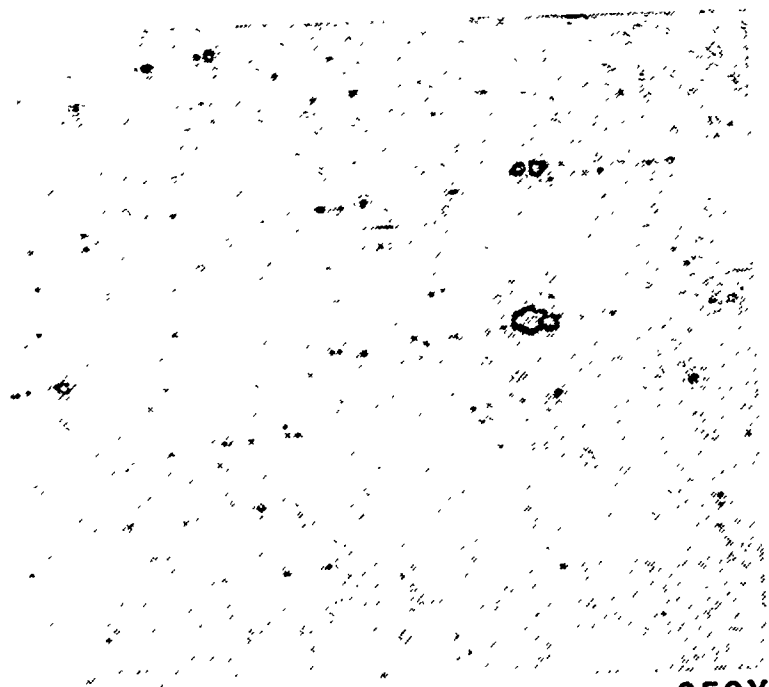


Figure 6-19

2



250X

-19. SPF Avionics Deck Waffle Pan Microstructure

209

3

Other than the hydro-formed parts, there were two machined formers which were machined from 7075-T6 aluminum. These formers were fabricated by trace machining from templates. Templates were made from engineering drawings to serve as a pattern. Templates were made by cutting aluminum sheet to the shape of the details. Actual machining of the part was done manually on a Bridgeport vertical mill. Once the machining was completed, the formers were inspected against full size engineering prints for accuracy of moldlines and dimensions and were found to be acceptable.

210/

7. ASSEMBLY AND TEST

This section contains a detailed description of the assembly of the avionics deck and its static and fatigue testing. The assembly of the deck and its delivery to the Air Force concluded the efforts of Task IV (Part Fabrication), where the testing along the cut-up microstructural evaluations were a part of Task V (Part Evaluation and Structural Verification). The results of the microstructural evaluations were reported earlier in Section 6.2.

7.1 LOWER AVIONICS DECK ASSEMBLY

The original manufacturing plans as described in Section 2.0 called for weldbonding of the waffle pan and substructural details to the lower skin and adhesive bonding of the upper skin to the rest of the structure. However, design modifications on the avionics deck, especially in the flange areas, revealed that weldbonding was not feasible due to access problems associated with the weldbonding machine electric probes. Therefore, with the approval of the Air Force, it was decided to use an alternate technique and assemble the deck through rivet bonding. This procedure was similar to weldbonding except rivets would simulate the bonding pressure instead of spot welds.

7.1.1 Preliminary Assembly

The preliminary assembly process checked the proper mating of all part surfaces. Tolerance checks and adjustments were made to details at this phase to ensure the proper fit up of all parts during the final assembly. Prior to any assembly checks, SPF parts were prepared for secondary processing. Each part was solution heat treated after forming and artificially

aged to T6 condition per Northrop's HT-1 specification. Each part was then rough trimmed per the engineering drawings. Initial trimming was done to 0.5 inch over the actual trim lines to allow for a final trimming after assembly. All three SPF parts; lower skin, waffle pan, and upper skin, were measured for gradient thinning using an ultrasonic digital transducer. Once the thicknesses of different areas on each part were determined, the areas with excessive material thickness were mapped for chem milling. Each part was flow coat dip masked to allow the etching of the exposed areas only. This procedure would also allow a step chem mill procedure where thicker areas were etched first and followed by areas of less thickness. An exception was made on the pocket walls of the waffle pan where step chem milling was extremely difficult due to excessive thinning profiles.

The substructural details, as mentioned earlier, were either conventionally formed or machined and required no chem milling. Each detail was net trimmed according to the developed flat patterns. After trimming and deburring, all details were heat treated to the T6 condition and ice boxed to save them in the as quenched condition. The assembly of the substructural details was assisted by laying them out to the engineering drawings. All details had undersized holes drilled and were held together by C-clamps and/or Clecos (temporary fasteners).

A simple assembly fixture was fabricated to assist the assembly of the avionics deck. A net trimmed lower skin was attached to a series of "female" loft boards rigged on a wooden base to form the fixture. The loft boards were made of loft cuts generated by CADAM. The fixture also had several edge angles to allow clamping when all substructural details were indexed to one another. The rough trimmed lower skin was indexed to the fixture and clamped in position. The substructural detail subassembly was then positioned in place and indexed to the lower skin. The preliminary assembly positioned the waffle pan and upper skin on

top of the substructural details. After the indexing was completed, the tolerances and fit up checks were made between all parts. Modeling clay was applied to contact areas of the lower skin, substructure subassembly, waffle pan, and upper skin to check tolerances. After disassembly, the clay was used to examine bondline thicknesses and was found to be acceptable except for an area between the waffle pan and the upper skin. This area revealed bondline thicknesses in excess of 0.030 inch. Laminated shims were made to fill the gap and the parts were ready for final assembly.

7.1.2 Final Assembly

The final assembly of the avionics rack as mentioned earlier was done using the rivet bonding process. The B.F. Goodrich A-1444B weldbond paste adhesive was used as the primary load carrying element of the joint while rivets simulated the bonding pressure.

Prior to the final assembly, all parts were processed for the bonding procedure. Each detail was vapor degreased and alkaline cleaned by immersing them in a non silicated alkaline solution at 120 to 165°F. The details were then spray rinsed with deionized water and visually inspected for any primer spots. After inspection, the details were deoxidized in an agitated deoxidizer solution at 70 to 80°F and spray rinsed in deionized water. The parts were then immediately immersed in an anodizing solution within the required voltage range, rinsed with deionized water and oven dried. Surfaces of all parts were then primed by spraying a surface treatment primer for the subsequent bonding.

After the processing of all parts and prior to the final assembly, the waffle pan was strain gaged for the structural testing. The final assembly started with indexing the substructural details through the previously drilled pilot holes. The full size holes were drilled for rivet applications and all

details were deburred and prepared for the application of the paste adhesive. The paste adhesive was applied in all contact areas of the substructural details and they were fastened securely with standard aluminum rivets. A decision was made to assemble the remainder of the structure and to cure it in one step.

The lower skin was indexed to the assembly fixture and clamped in place. The substructure subassembly was then located to the underside of the waffle pan. Positioning was done through previously marked index lines. Once the indexing was completed, the assembly was indexed to the upper skin and all full size rivet holes were drilled. All parts were deburred and cleaned prior to the application of the paste adhesive. The adhesive was applied in all contact areas and the rivets were installed. The final phase of the assembly consisted of mating the pan, substructure, and upper skin subassembly to the lower skin. Once the indexing of the subassembly to the lower skin was completed, the adhesive and rivet application concluded the final assembly. Standard aluminum rivets were used in most areas and blind rivets in areas where access was limited.

The complete assembly was now ready for curing. The assembly was immediately transferred to an oven where it was cured at 250°F for one hour. The rivets, as mentioned earlier, provided the pressure during the cure cycle which eliminated the need for an autoclave. The final net trimming followed the curing after which all access doors were installed. The access doors were roll formed in order to match the contoured shape of the avionics deck lower skin. Blind rivets were used to install the doors due to limited access. Flow of the paste adhesive prior and after curing required polishing of certain areas of the deck. However, prior to the delivery of the part to the Air Force, the complete assembly was vapor degreased and sprayed with a primer to cover the polished spots and to prevent corrosion. Figures 7-1 and 7-2 represent two different views of the avionics deck prior to the assembly of the access doors, and Figure 7-3 shows the deck after the installation of the doors.



Figure 7-1. Upper View of Assembled Deck Prior to Door Installation

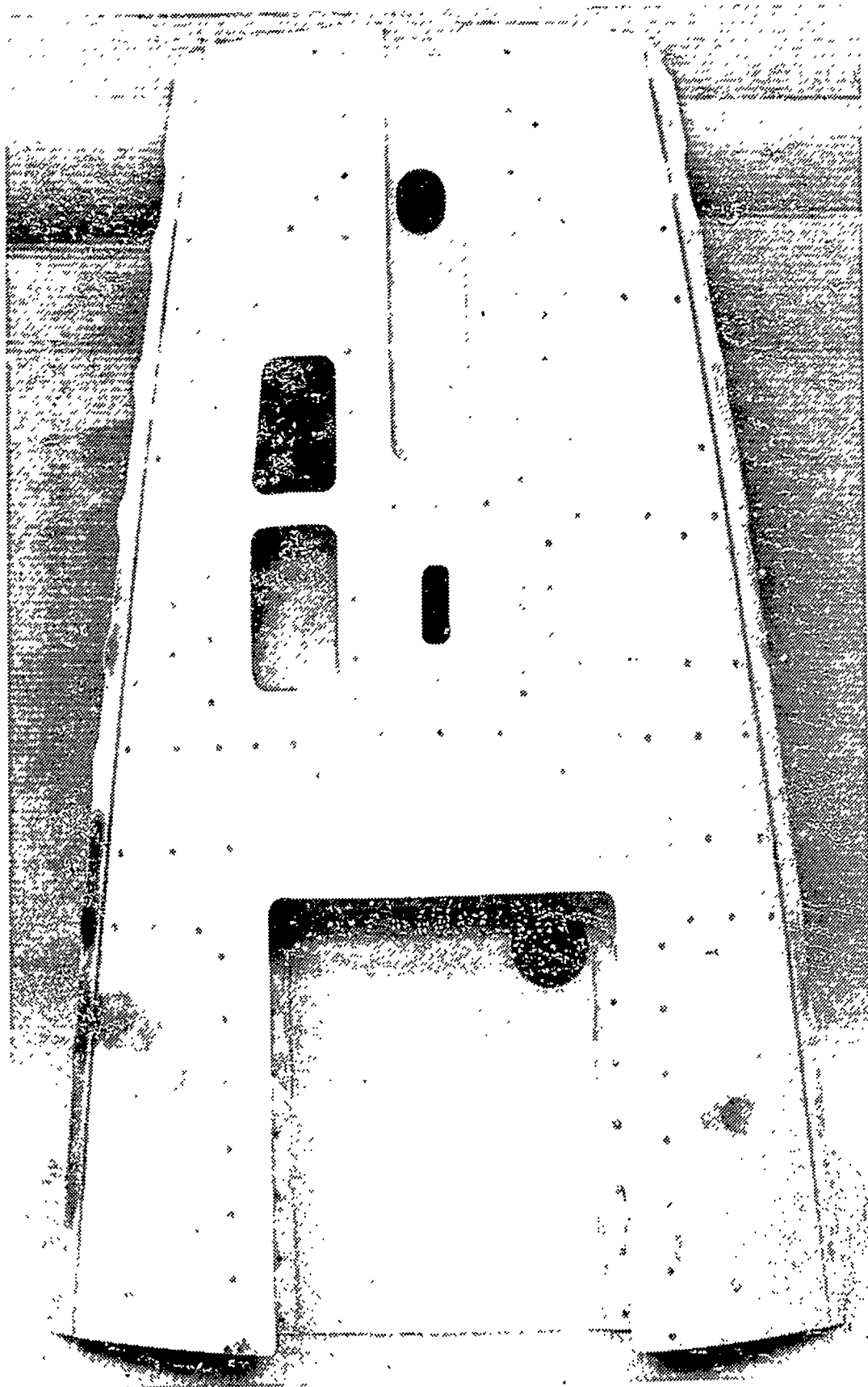


Figure 7-2. Lower View of Assembled Deck Prior to Door Installation

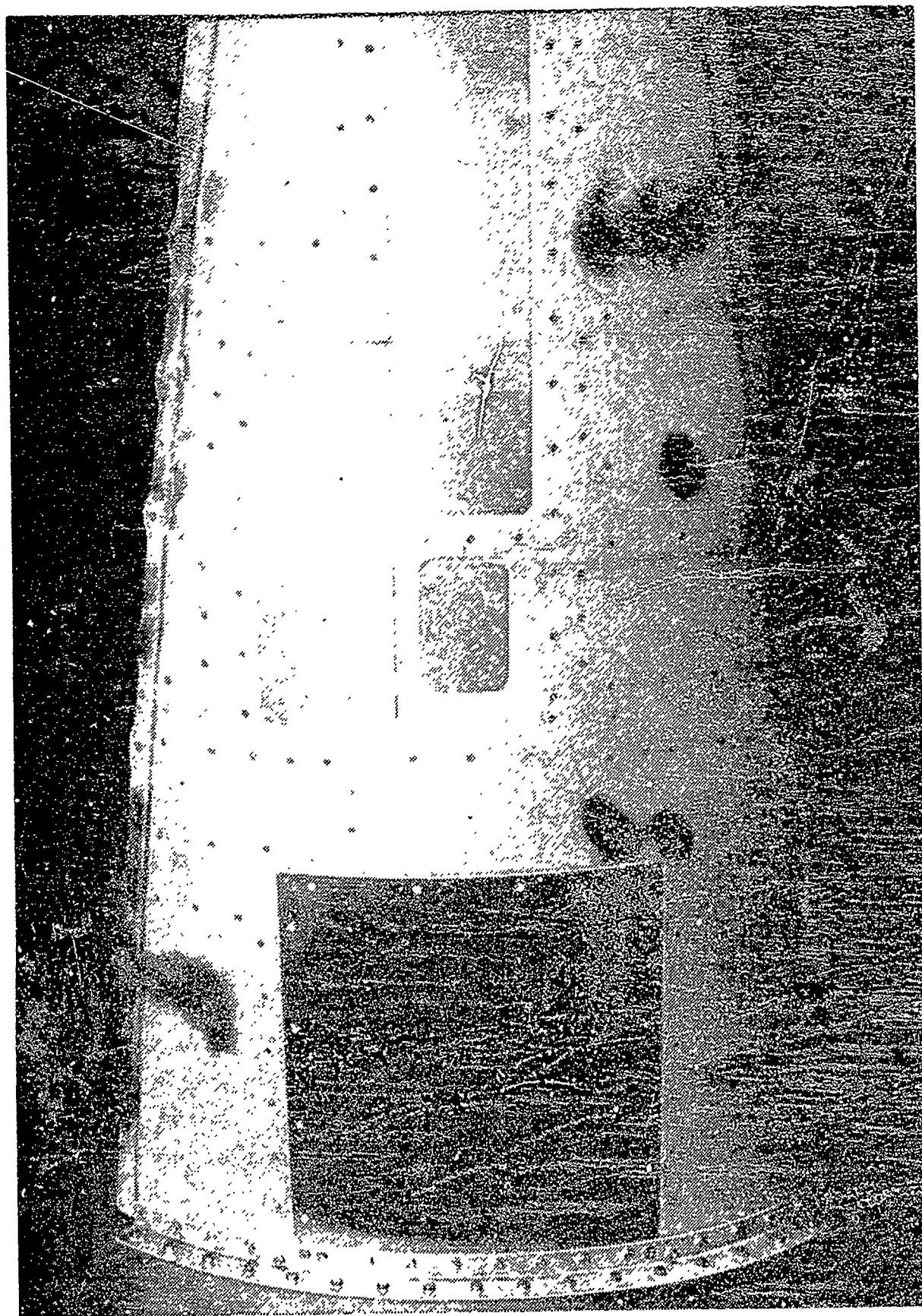


Figure 7-3. Lower View of Assembled Deck After Door Installations

The structural testing of the SPF avionics deck was conducted at the Air Force testing facilities and it marked the completion of the final task of the subject program. A detailed structural test plan was prepared by Northrop and reviewed by Air Force test personnel for their approval. During the preparation of the test plan, a decision was made to test the avionics deck as an individual component instead of an integral part of the forward fuselage. The foregoing decision was made subsequent to a decision to test the avionics deck at the Air Force test facilities. Testing of the avionics deck as an integral part of the forward fuselage was not feasible due to the following reasons:

- (1) A forward fuselage was not available at the time of testing.
- (2) Testing of the entire forward fuselage was not cost effective.
- (3) Transportation of the entire forward fuselage to the Air Force test laboratories and its subsequent testing was not feasible.

As a result, a modified test plan was generated for testing of the avionics deck as an individual component. The fuselage loads were reviewed extensively in order to determine the portion which was reacted by the avionics deck. As a result, a new set of test loads were generated. The test plan was prepared accordingly to introduce the appropriate loads to the avionics deck during testing. With the concurrence of the Air Force, a decision was made to conduct both static and fatigue testing on the avionics deck. The following paragraphs give a more detailed explanation of the test load generation, test plan preparation and the subsequent testing.

7.2.1 Test Load Generation

The forward fuselage structure between F.S. 47.50 and 87.50 is subjected to gun blast pressure due to a gun barrel located on the left-hand side between the upper skin and deck. In addition to gun blast pressure, the substructure between F.S. 47.50 and 87.50 is subjected to internal pressure (cockpit pressure) loading, to external air pressure loads and to the inertia loading of the structure and equipment.

The lower avionics deck box is subjected to the following loading:

- (1) Maximum cockpit bursting pressure of 3.98 psi.
- (2) External air pressure linearly varying from a 1.4 psi collapsing pressure at F.S. 4750 to a 0.8 psi bursting pressure at F.S. 87.50 (bottom centerline pressure for a symmetrical pull up under supersonic mach numbers).
- (3) Inertia loading due to equipment assembled onto the deck.

As a result of preliminary analysis, it was decided that the SAB13010 symmetrical pull up condition will be tested as the most critical condition. SAB13010 as mentioned above is a symmetrical pull up condition with $N_z = 7.33g$ for limit loading.

Table 7-1 represents the bending moment and shear values for the avionics deck compartment under the SAB13010 condition. The bending moment and shear variations across the forward fuselage, F.S. 47.50 to 87.50, are schematically shown in Figures 7-4 and 7-5. Since it was not clear what portion of the loads was carried by the lower deck, certain assumptions were required. As for the shear, since the shear web attaching the

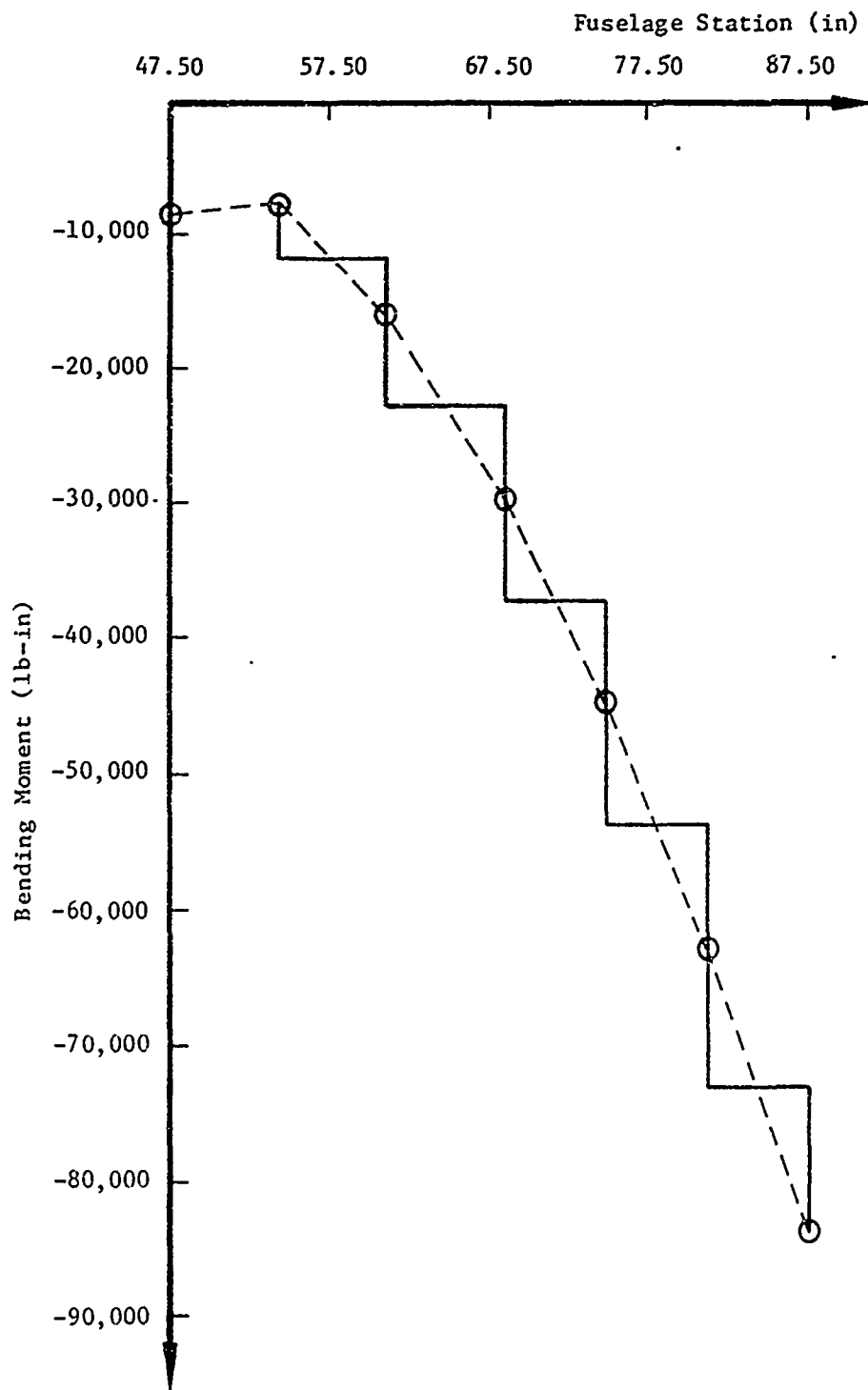


Figure 7-4. F-5F Avionics Compartment Bending Moments (Cond. SAB13010, Symmetrical Pull-Up)

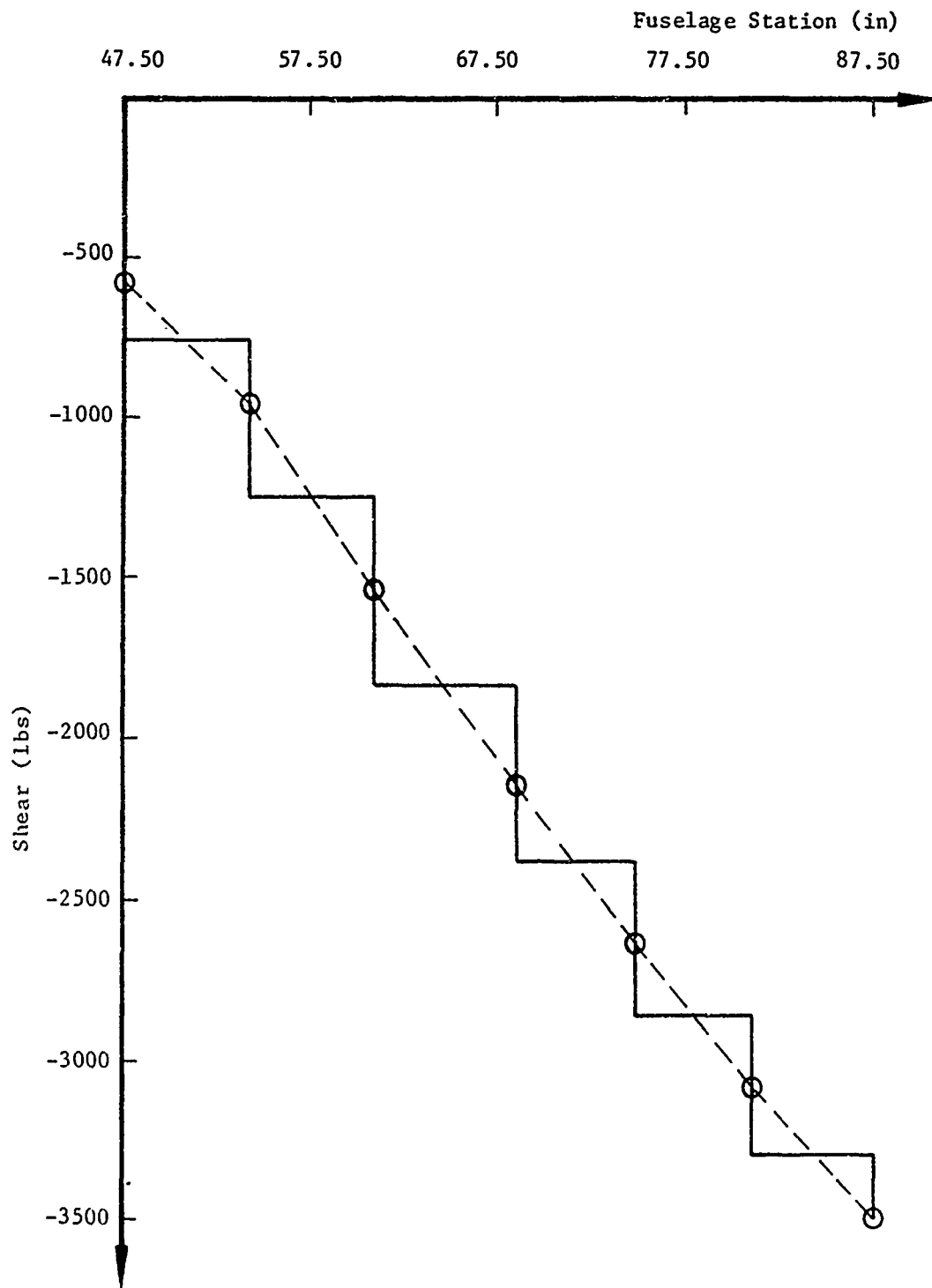


Figure 7-5. F-5F Avionics Compartment Shear Loads (Cond. SAB13010, Symmetrical Pull-Up)

TABLE 7-1. F-5F AVIONICS COMPARTMENT LOADS

FUSELAGE STATION	M _X	V _Z (LBS)	M _Y (LB-IN)	M _Z
47.50	0	- 571.7	- 8382.6	0
54.25	0	- 955.3	- 7562.6	0
61.00	0	-1532.3	-15977.2	0
68.50	0	-2140.0	-29768.2	0
74.80	0	-2626.0	-44792.9	0
81.10	0	-3089.1	-62809.0	0
87.50	0	-3508.0	-83955.4	0

upper and lower boxes extended from F.S. 62.00 to 87.50, it was assumed that the lower deck carried no shear from F.S. 47.50 to 62.00. Instead, all of the lower deck shear loads were to be reacted from F.S. 62.00 to 87.50.

The maximum fuselage shear load as shown in Table 7-1 and Figure 7-5 is -3508 lbs at F.S. 87.50. The following equation was used to calculate the lower avionics deck shear load at F.S. 87.50.

$$V_1 = h/H (V_2)$$

where,

$$V_1 = \text{Avionics deck shear load @ F.S. 87.50}$$

$$h = \text{Depth of avionics deck @ F.S. 87.50 (4.5 inches)}$$

$$H = \text{Depth of fuselage @ F.S. 87.50 (28 inches)}$$

$$V_2 = \text{Fuselage shear @ F.S. 87.50.}$$

Therefore, the lower avionics deck shear load at F.S. 87.50 would be:

$$V_1 = 4.5/28(-3508) = -564 \text{ lbs}$$

Since the shear value of -564 lbs was not severely critical, a constant shear value of -600 lbs was used from F.S. 62.50 to 87.50 in order to simplify the testing.

Simulating the actual bending moments through application of reaction loads was an extremely difficult and complicated task. Therefore, a much simpler approach was undertaken through a review of the avionics deck NASTRAN results. The NASTRAN generated axial loads for the avionics deck upper and lower skins were reviewed and due to the discrepancy between the load values, the lower skin axial load at F.S. 87.50 was used as a baseline. This axial compressive load as determined by NASTRAN was -2117 lbs for F.S. 81.00 to 88.00. This axial load and the depth of the lower avionics deck were used to calculate the avionics deck bending moment as shown below:

$$\begin{aligned} \text{Bending Moment} &= \text{Axial Load} \times \text{Depth} = -2117 \times 4.1 \\ &= -8680 \text{ lb-in} \end{aligned}$$

(4.1 inch was used as depth of the avionics deck)

Comparing this value to the actual fuselage bending moments shown in Table 7-1 indicated that the moment carried by the avionics deck was an average 12 percent of the total fuselage bending moment. Therefore, a similar ratio was used to calculate the avionics deck moments at other stations, as shown in Table 7-2.

TABLE 7-2. AVIONICS DECK BENDING AND AXIAL LOADS
(CONDITION SAB13010)

FUSELAGE STATION	BENDING MOMENT (IN-LBS)	LOWER SKIN AXIAL LOAD (LBS)	UPPER SKIN AXIAL LOAD (LBS)
47.5 - 54.0	- 943	- 368	- 262
54.0 - 61.0	-1392	- 480	- 341
61.0 - 68.5	-2706	- 820	- 583
68.5 - 75.0	-4410	-1098	- 780
75.0 - 81.1	-6365	-1623	-1154
81.1 - 87.5	-8680	-2117	-1505

Also shown in Table 7-2 are the upper skin and lower skin axial loads. The bending moment values were used to determine the lower skin axial loads. The upper skin axial loads were determined by using the lower skin loads and adjusting the distance to the neutral axis of the fuselage. The equation used for calculation of the upper skin axial loads is shown below:

$$P_1 = [(H/2 - h)/(H/2)](P_2)$$

where,

P_1 = Upper skin axial load

H = Depth of fuselage (assume fuselage \bar{c} is @ neutral axis)

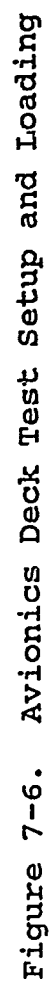
h = Depth of avionics deck

P_2 = Lower skin axial load.

The avionics deck test loads were selected to satisfy the generated deck loads shown in Table 7-2. As shown in Figure 7-6, there were basically four reaction loads P_1 , P_2 , P_3 and P_4 required for the test. All loads were selected to satisfy the shear and axial skin loads of the deck. The function of each load is described below:

P_1 : To satisfy the upper and lower skin axial loads between F.S. 47.50 and 62.50. This load as shown in Figure 7-6, is applied slightly above the centerline of the deck in order to distribute the upper and lower skin axial loads in an appropriate manner.

P_2 : This load basically offsets the moment induced tension loads of the upper skin. In addition,



since this load is being applied above the center-line of the deck, it also contributes to generation of the deck bending moments.

P₃: This load has basically the same function as P₂ except it is applied at a different location. The location of this reaction (F.S. 75.00) was also selected to satisfy the deck loading.

P₄: This load basically introduces the avionics deck shear load and has a great contribution towards the deck bending moments.

It is important to realize that the lower avionics deck is positioned below the neutral axis of the aircraft fuselage. As a result, both upper and lower skins are subjected to compressive loads under the symmetrical pull up condition SAB13010. When testing the deck by itself, application of bending moment would induce compressive axial loads on the lower skin and tensile loads on the upper skin. Therefore, in order to offset the tensile axial loads of the upper skin, the compressive reactions P₂ and P₃ were added to the avionics deck test loads.

The values of these loads were selected to satisfy the deck shear, moment, and skin axial loads discussed before. The ultimate reaction loads were as follows:

$$P_1 = 1500 \text{ lbs}$$

$$P_2 = P_3 = 1000 \text{ lbs}$$

$$P_4 = 600 \text{ lbs}$$

(All values are ultimate)

7.2.2 Test Setup

Since testing of the avionics deck as an integral part of the F-5F forward fuselage structure was not feasible, certain modifications were required in order to test the deck as an individual component. The lower avionics deck was set up in such a way that it simulated the actual loading of the lower deck box. To simulate the actual boundary conditions of the deck, since the bending moments at the forward end, F.S. 47.50, were minimal and much higher at the aft end, F.S. 87.50, it was decided to brick wall the deck at the aft end and leave the forward end free as shown in Figure 7-6. Application of an off center axial load at the forward end would induce its required bending moment.

In addition, a plate simulating the web was attached to the upper skin of the deck to linearly distribute the off setting compressive reactions applied to the upper skin. The actual test setup shown in Figure 7-7 was designed by Northrop and assembled by Air Force test personnel. Northrop delivered the deck to AFWAL with the end plate attached at F.S. 87.50, and the installation of the web plate and the remaining test fixturing was done by the Air Force test personnel.

The scope of the testing was to determine the room temperature loads versus strain response to limit load (2/3 of ultimate load) for two conditions, Condition I (Loading Check Out) and Condition II (Critical Load Condition, SAB13010). The second phase of testing established the room temperature fatigue followed by a static residual strength test. The details of the static and fatigue testing are discussed in the following paragraphs.

7.2.3 Instrumentation

The instrumentation of the avionics deck for detecting strains was limited to strain gaging. A number of axial and



Figure 7-7. Avionics Deck Actual Test Setup

rossette gages were applied on the critical locations of the waffle pan, upper skin, and lower skin. The internal strain gages consisted of six rossette gages as shown in Figure 7-8. These gages were applied by Northrop prior to the assembly and delivery of the avionics deck to AFWAL. Figure 7-9 represents the external gages which consisted of both axial and rossette gages. The locations of these gages were determined by Northrop and the gages were applied by the Air Force test personnel.

7.2.4 Preliminary Static Testing

The preliminary static test, as discussed earlier in Section 7.2.2, consisted of room temperature loading of the deck to limit load for two conditions. The purpose of this initial loading was to assess the validity of the strain gage data and to assess the structural integrity of the part up to limit load prior to initiation of the fatigue testing.

The avionics deck successfully carried the limit load without any signs of failure. The strain data from both internal and external gages were recorded and reviewed by Air Force and Northrop personnel for any anomalies.

Prior to the initial strain survey, a non destructive inspection (NDI) of the deck was conducted by Air Force personnel to assure that there were no severe adhesive disbond and/or rivet failures prior to the testing. After NDI, the strain survey was resumed. The actual reaction loads applied were:

$$P_1 = 938 \text{ lbs (Ultimate load} = 1500 \text{ lbs)}$$

$$P_2 = P_3 = 633 \text{ lbs (Ultimate load} = 1000 \text{ lbs)}$$

$$P_4 = 402 \text{ lbs (Ultimate load} = 600 \text{ lbs)}$$

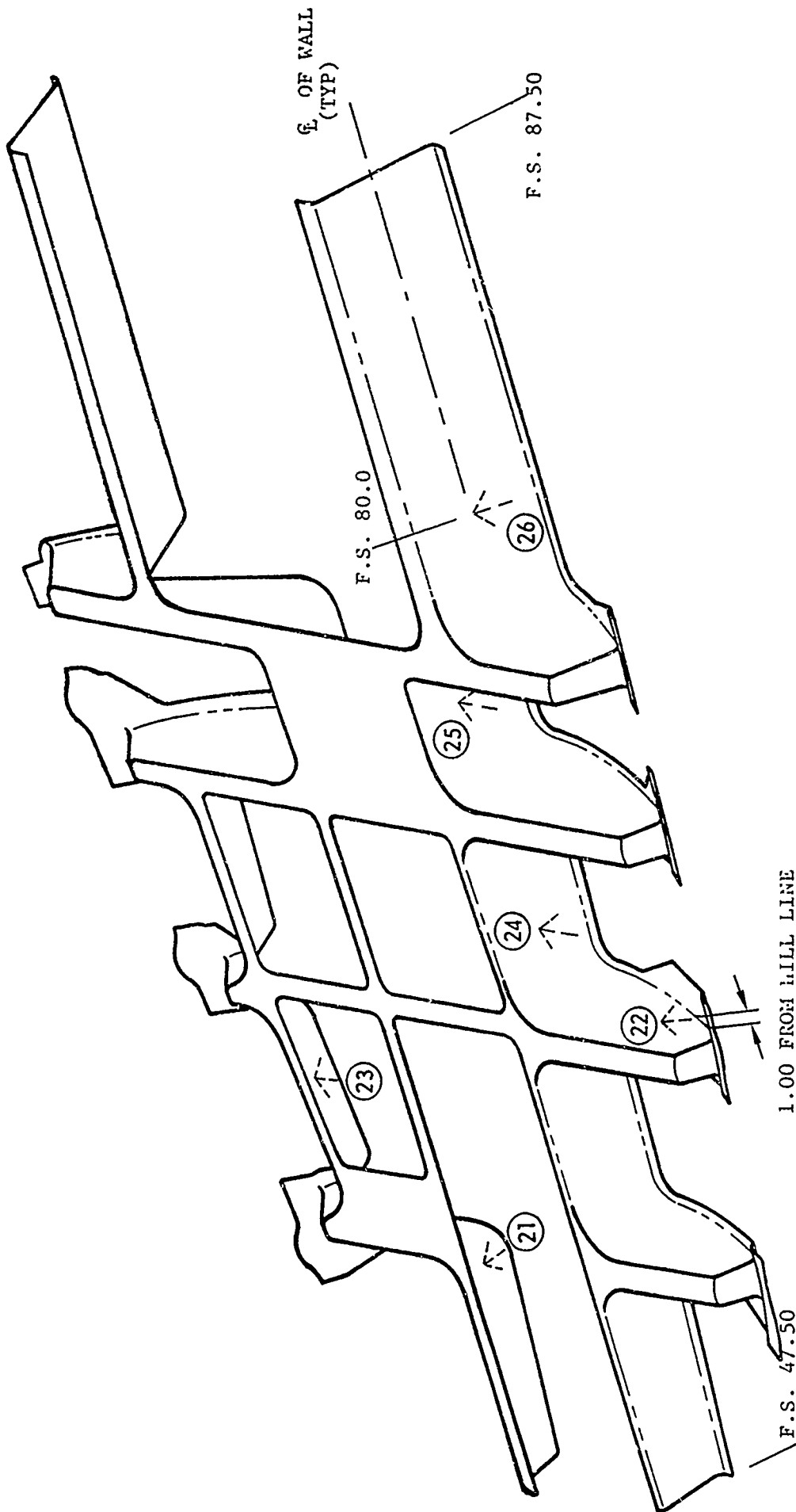


Figure 7-8. Location of Avionics Deck Internal Strain Gages

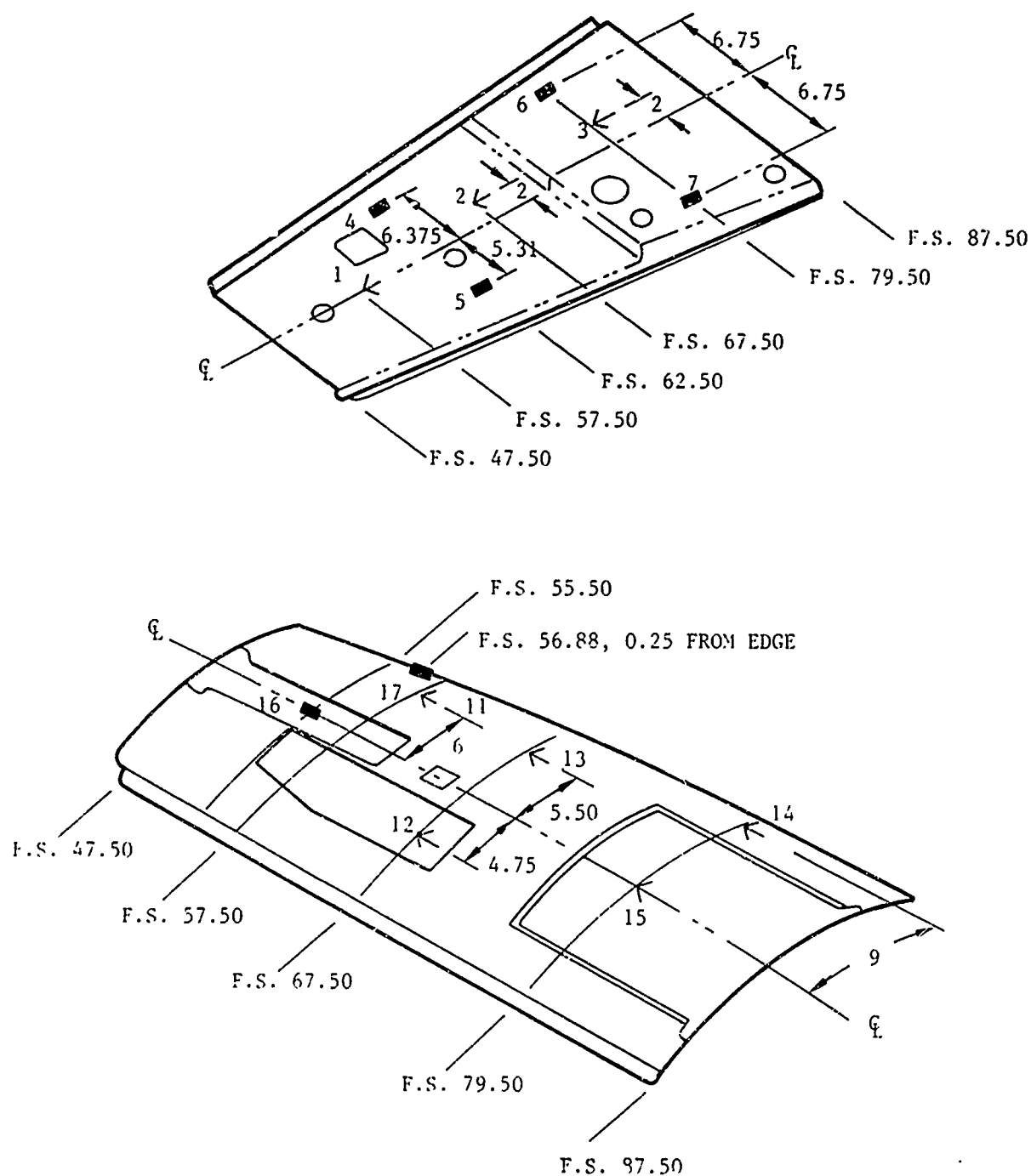


Figure 7-9. Locations of Avionics Deck External Strain Gages

The values of P_1 , P_2 and P_3 reactions were slightly lower than the actual limit load values due to the limitations on loading at the time of test. However, the differences were small enough to be neglected. Figure 7-10 gives a schematic representation of the strain survey loading. The maximum and minimum strain values for each strain gage is shown in Table 7-3.

In addition to the strain values, maximum and minimum principal stresses and maximum shear stresses were calculated and recorded for the rosette gages. The axial gage stresses were calculated and recorded. Table 7-4 represents the maximum and minimum principal stresses associated with the rosette gages. As shown, the highest stress value detected was -2124 psi for strain gage no. 14. A hand analysis was conducted to verify the accuracy of the strain gage strain data. The recorded strain data correlated well with the results of the hand analysis.

TABLE 7-4. STRAIN SURVEY TESTING, MAXIMUM AND MINIMUM PRINCIPAL STRESSES

STRAIN GAGE NO.	MAXIMUM PRINCIPAL STRESS (PSI)	MINIMUM PRINCIPAL STRESS (PSI)
1A *	92.2	- 361.9
2A	730.2	- 655.4
3A	447.1	- 994.5
11A	220.7	- 344.6
12A	196.0	- 347.9
13A	518.4	- 210.7
14A	487.7	- 2123.8
15A	598.2	- 168.3
21A	278.4	- 142.4
22A	298.5	- 83.7
23A	177.6	- 418.4
24A	306.0	- 266.0
25A	302.3	- 439.6
26A	487.7	- 658.7

* Letter 'A' indicates the A leg of the rosette gage.

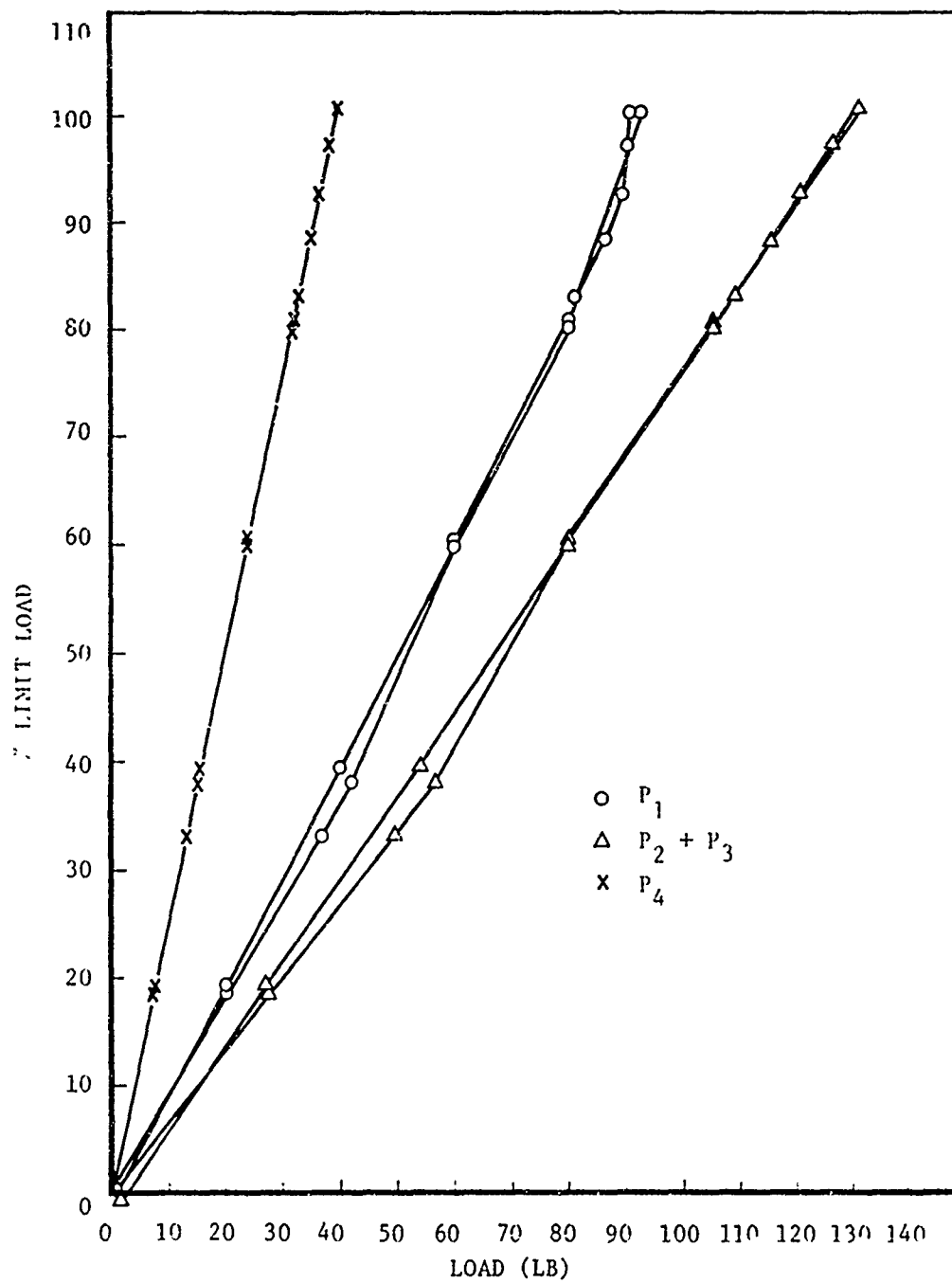


Figure 7-10. Avionics Deck Strain Survey Loading

TABLE 7-3. STRAIN SURVEY TESTING, MAXIMUM AND MINIMUM STRAIN VALUES

STRAIN GAGE NO.	MAXIMUM STRAIN (μ IN/IN)	MINIMUM STRAIN (μ IN/IN)	STRAIN GAGE NO.	MAXIMUM STRAIN (μ IN/IN)	MINIMUM STRAIN (μ IN/IN)
1A	2.3	- 21.0	14A	3.5	-107.6
1B	3.5	- 35.5	14B	2.3	-205.2
1C	2.4	- 19.8	14C	14.0	- 32.0
2A	84.9	- 4.7	15A	19.7	- 3.6
2B	31.0	- 3.5	15C	31.5	- 12.9
2C	4.7	- 80.3	16	11.9	-274.7
3A	64.0	- 10.5	17	83.7	-478.1
3B	19.8	- 15.0	21A	24.7	- 3.5
3C	3.5	-100.0	21B	24.4	- 9.3
4	131.8	-119.8	21C	9.4	- 9.4
5	60.3	-180.8	22A	18.8	8.2
6	478.2	-107.6	22B	8.1	- 12.8
7	214.6	- 71.5	22C	17.7	- 2.4
11A	22.5	- 1.1	23A	5.9	- 20.0
11B	4.6	- 29.9	23B	27.9	2.3
11C	7.0	- 32.9	23C	10.6	- 12.9
12A	14.2	- 10.6	24A	25.9	0
12B	6.9	- 31.0	24B	9.3	- 9.3
12C	5.9	- 28.1	24C	7.0	- 28.2
13A	18.7	- 8.2	25A	38.9	- 8.2
13B	3.5	- 31.2	25B	3.5	- 19.7
13C	22.2	- 10.5	25C	9.4	- 47.1
26A	50.7	0	26C	7.0	- 53.0
26B	44.3	- 3.5			

7.2.5 Fatigue Testing

In order to fully verify the structural integrity of the deck and SPF aluminum, Northrop proposed fatigue testing of the SPF avionics deck. Since the avionics deck was located at the F-5F forward fuselage, which was a non-critical fatigue area, a substitute fatigue spectrum was proposed. The proposed fatigue spectrum was the F-5F dorsal longeron which is a moderately severe tension dominated spectrum. Since this was not representative of a realistic spectrum and due to the difficulties associated with spectrum fatigue testing at the Air Force test facilities, it was decided to conduct a constant amplitude fatigue test.

As a result, a constant amplitude test was designed which was representative of the dorsal longeron spectrum loading. The fatigue testing consisted of four phases. The first and second phase loading applied Blocks I through IV, while the third and fourth phase loading consisted of 20 repetitions of Block IV. Description of each block is given below:

Block I - 6000 cycles at 65 percent of limit load

Block II - 120 cycles at 90 percent of limit load

Block III - 20 cycles at 110 percent of limit load

Block IV - 1 cycle at 125 percent of limit load.

Table 7-5 represents the four phases of fatigue testing conducted on the avionics deck.

The subject fatigue schedule was designed by assuming that each life time consisted of 4000 flight hours. A block equivalent to 200 flight hours was designed to consist of 300 cycles at 65 percent of design limit load (DLL), 6 cycles at 90

TABLE 7-5. AVIONICS DECK FATIGUE LOADING SCHEDULE

PHASE NO.	TYPE OF BLOCK LOADING
1	BLOCKS I, II, III AND IV
2	BLOCKS I, II, III AND IV
3	20 REPETITIONS OF BLOCK IV
4	20 REPETITIONS OF BLOCK IV

percent of DLL, one cycle at 100 percent, and one cycle at 125 percent of DLL as shown in Figure 7-11. A life time consisting of 20 blocks was proposed by Northrop which initiated the Air Force to arrive at the fatigue schedule shown in Table 7-5. It should be noted that the four phases shown in Table 7-5 are actually equivalent to two real life times of fatigue. However, since minor adhesive disbands were detected on the edge of deck prior to testing, it was decided to separate the 20 cycles at 125 percent of DLL from the first and second phases of fatigue loading for conducting NDI inspections before and after loading. Such an investigation would isolate the possible effects of each phase on the adhesive disbands.

In order to monitor the fatigue testing and the possible residual effects due to fatigue loading, it was decided to record strain data for 3 cycles after every 1500 cycles of Block I and for at least 3 cycles of each other block. The cycles for which strain data was recorded are as follows:

(1) Lifetime No. 1

BLOCK I: - Cycles 1499-1501, Cycles 2999-3001,
Cycles 4499-4501, Cycles 5998-6000.

BLOCK II: - Cycles 71-73, Cycles 118-120.

BLOCK III: - Cycles 18-20.

BLOCK IV: - Cycle I.

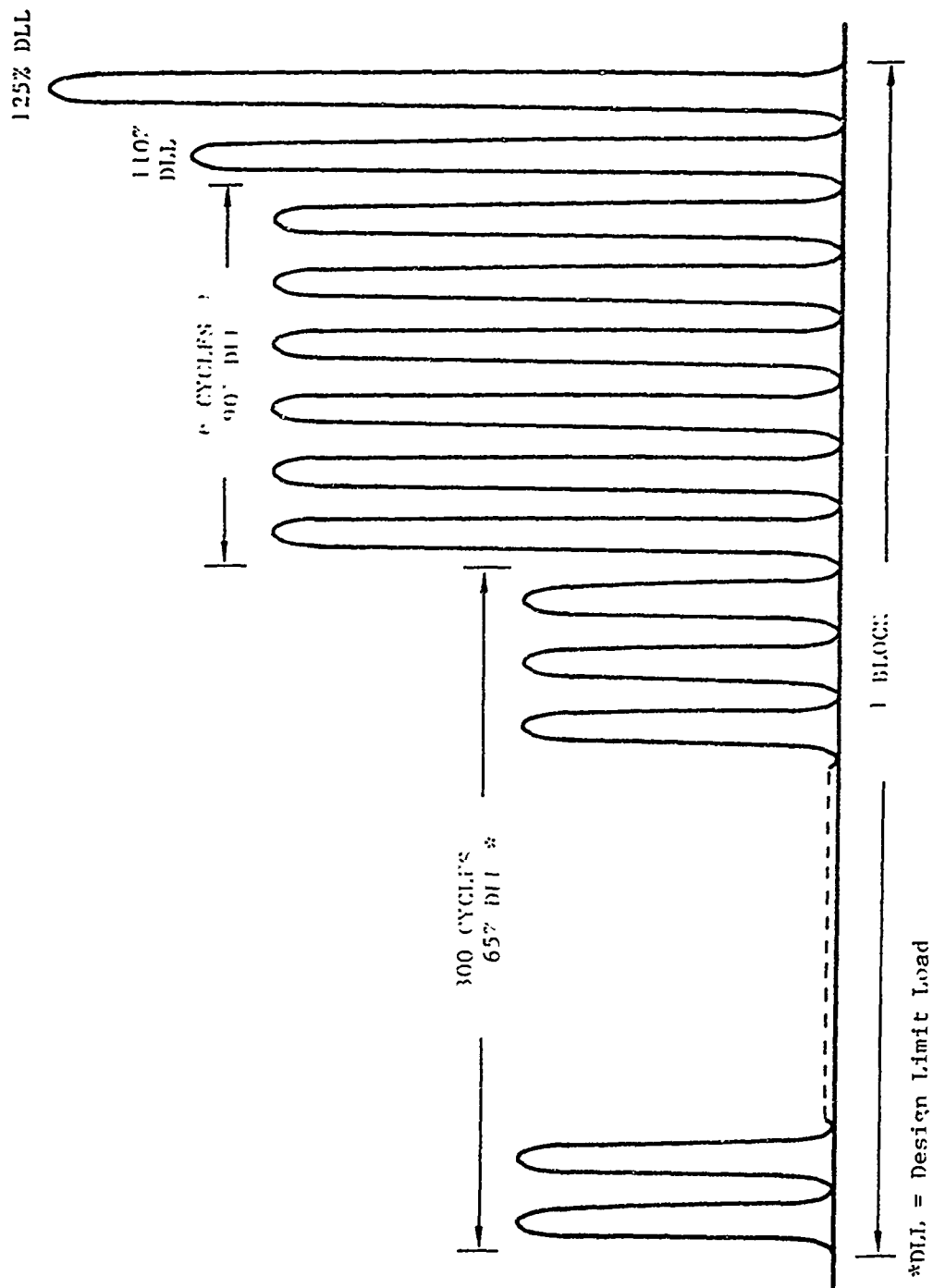


Figure 7-11. Typical Block Designed for Constant Amplitude Fatigue Loading

(2) Lifetime No. 2

BLOCK I: - (Same as Lifetime No. 1)

BLOCK II: - Cycles 59-61, Cycles 118-120.

BLOCK III: - Cycles 18-20.

BLOCK IV: - Cycle I.

(3) Lifetime Nos. 3 and 4

BLOCK IV: - Cycles 18-20.

Figure 7-12 represents an example of the time during which the strain data for 3 cycles of loading was recorded. A sinewave cyclic loading was selected for applying the fatigue loading cycles. Prior to conducting the static residual strength test, the fatigue test recorded strain data were delivered to Northrop for review. The fatigue strain data were thoroughly reviewed to assess any significant change in the strain data due to fatigue loading. Similar to the initial static loading, strains as well as maximum principal stresses, minimum principal stresses and maximum shear stresses were recorded for the rosette gages and strains and axial stresses were recorded for the axial gages.

To assess the effects of fatigue more clearly, the most critical strain gage data was investigated. The most highly loaded gages for the upper skin, lower skin and waffle pan were selected and their initial static loading and post fatigue strain response were compared. Figures 7-13 through 7-15 represent comparison of strain data before and after fatigue. Strain gage No's 15, 3A and 26A were selected from the lower skin, upper skin and waffle pan, respectively. These gages were selected since they were located in the aft area of the deck and were representative of the highest stress levels.

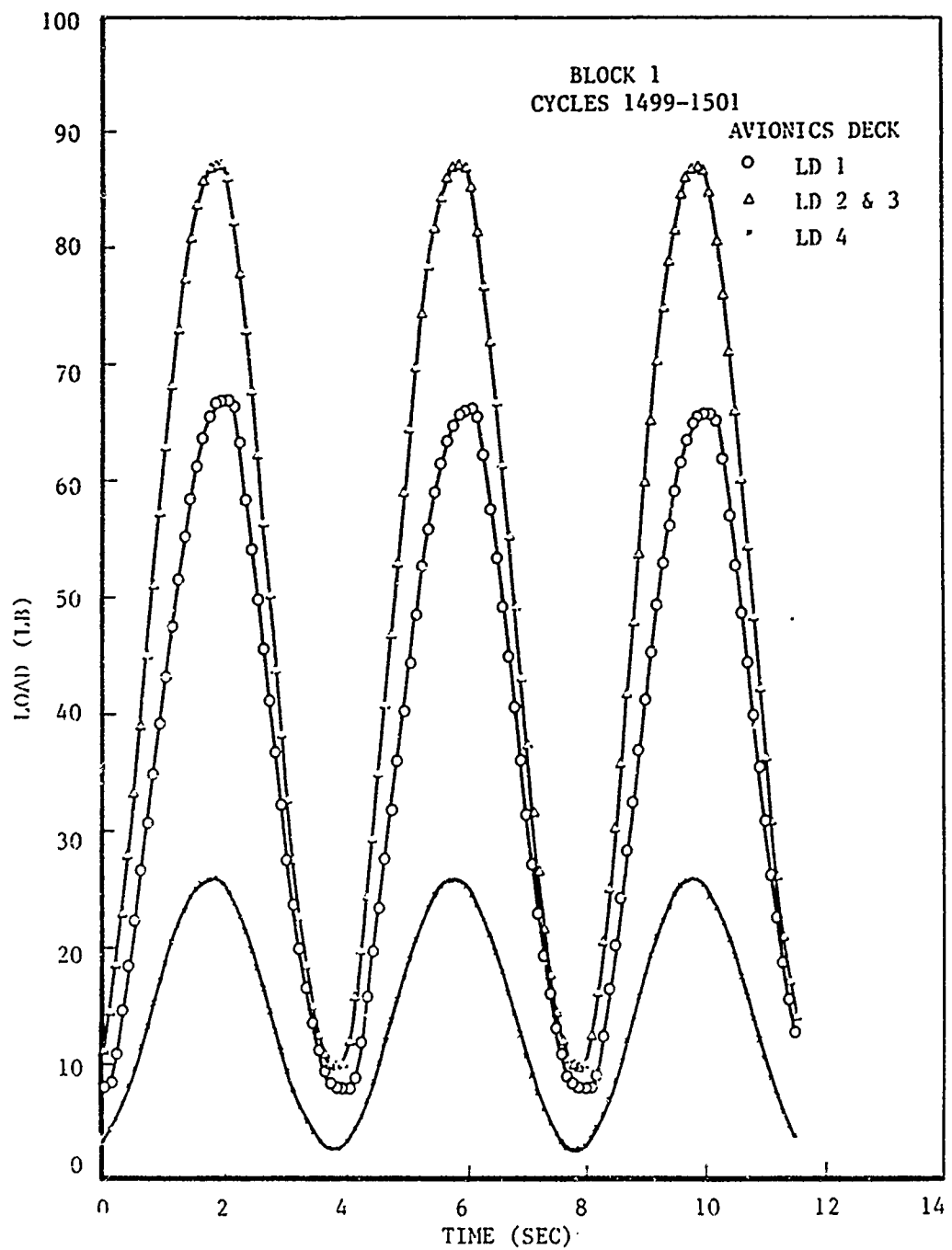


Figure 7-12. Typical Fatigue Cycle Loading Versus Time

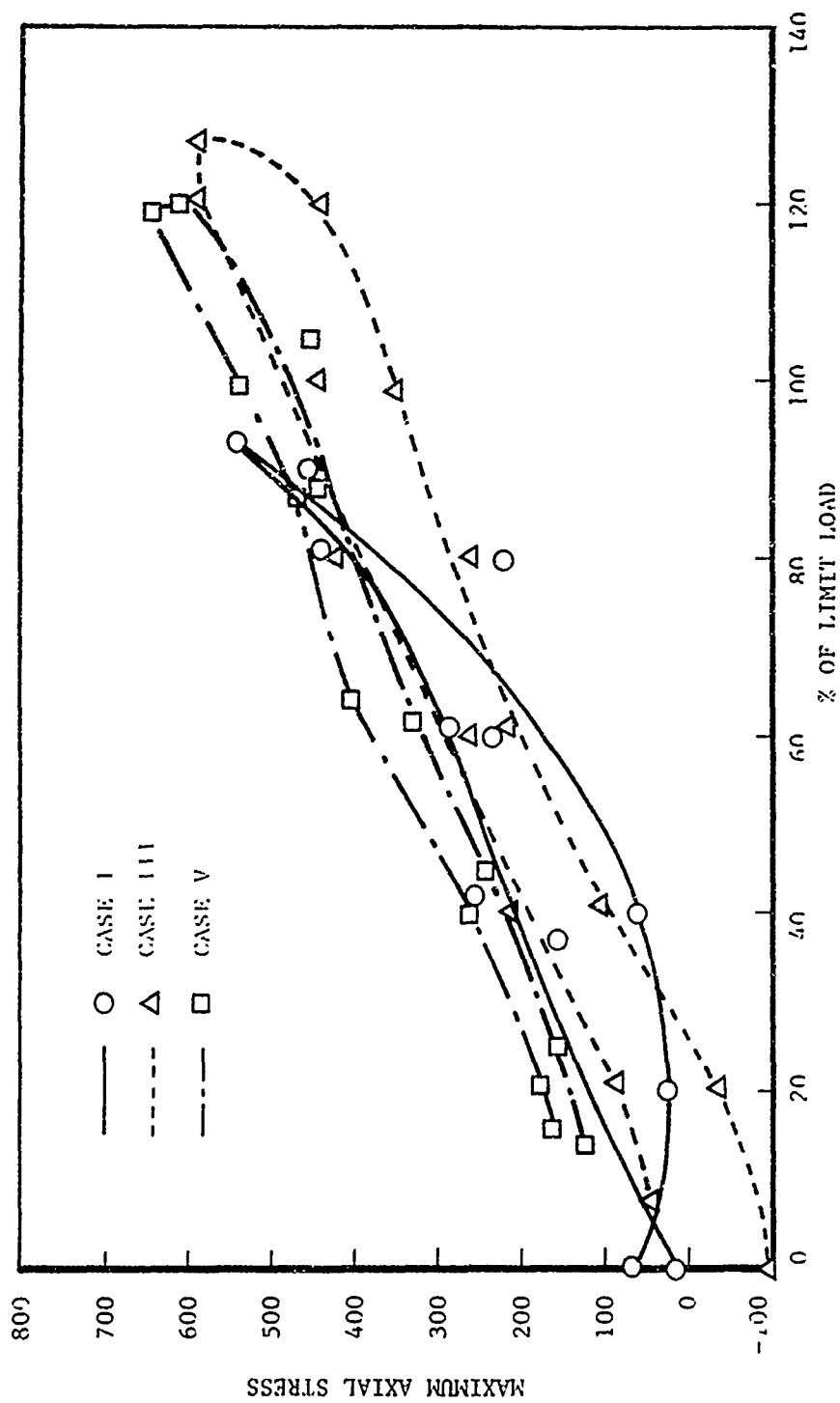


Figure 7-13. Initial Static Loading Versus Fatigue Loading Strain Response (Strain Gage No. 15, Lower Skin)

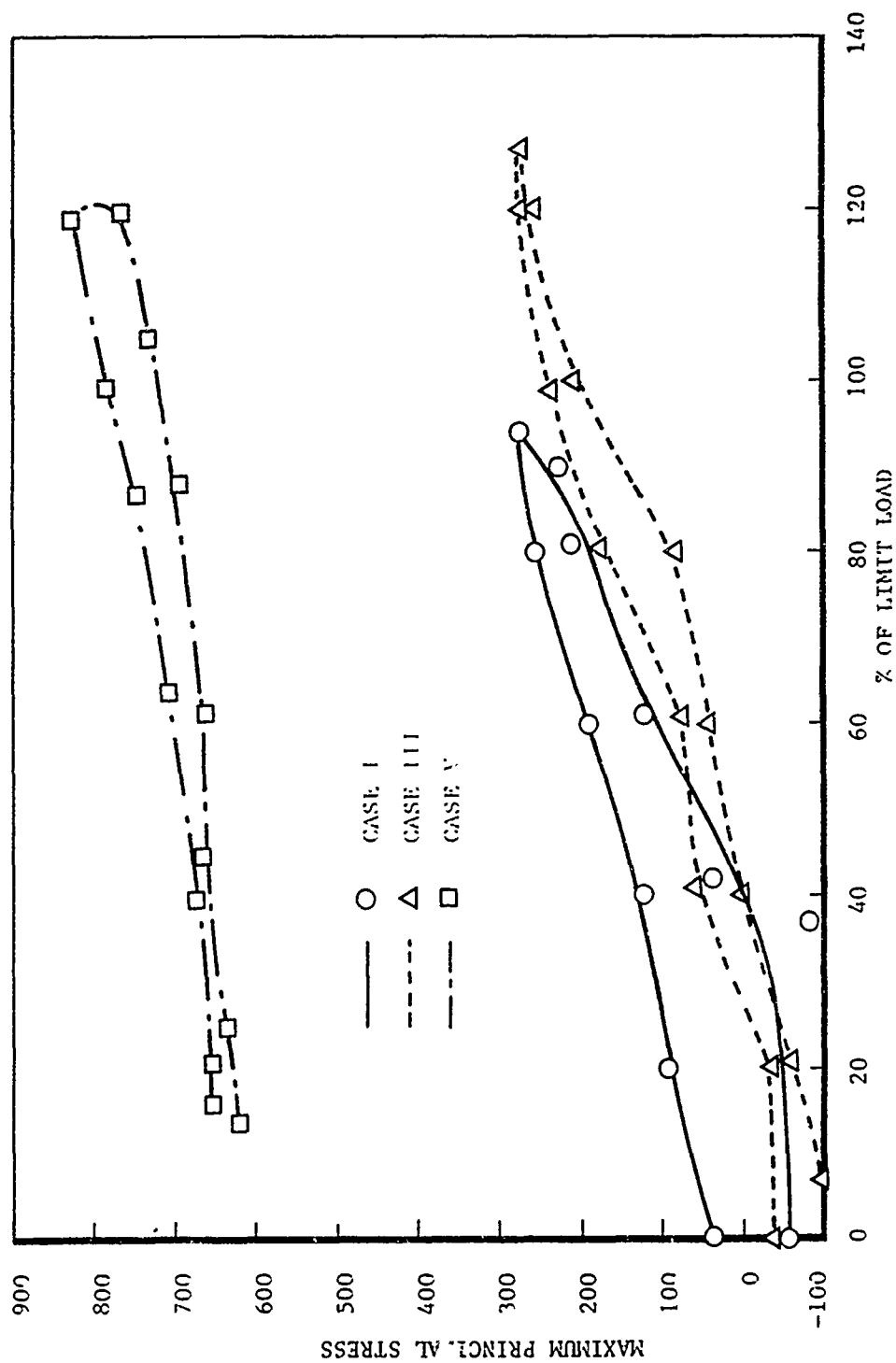


Figure 7-14. Initial Static Loading Versus Fatigue Loading Strain Response (Strain Gage No. 3A, Upper Skin)

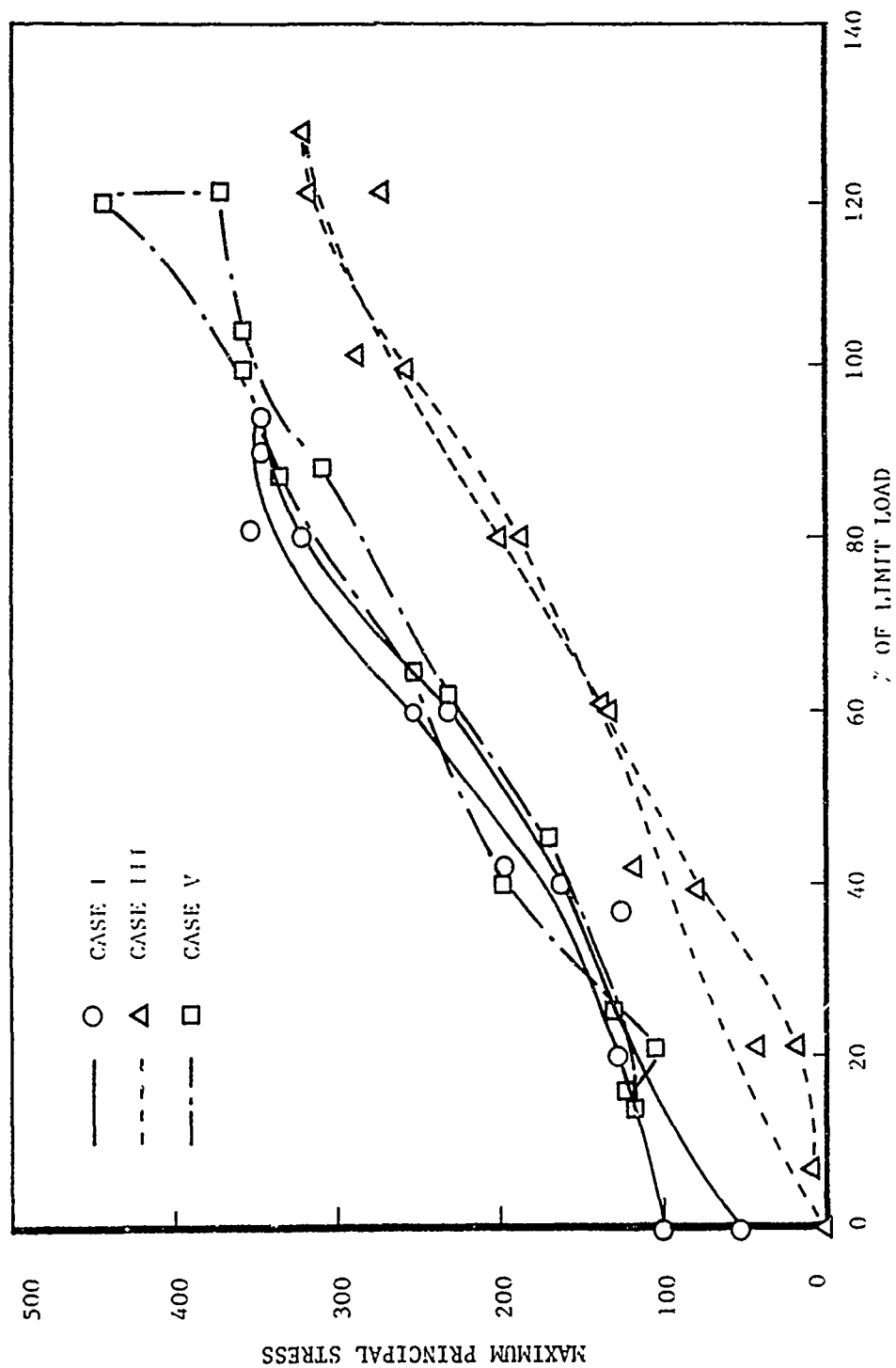


Figure 7-15. Initial Static Loading Versus Fatigue Loading Strain Response (Strain Gage No. 26A, Waffle Pan)

In Figures 7-13 through 7-15, the stress versus percent of limit load was plotted for the initial static loading at the end of the second and fourth phase of fatigue loading. The first and third phase fatigue data were not shown for clarity. As noticed there was no significant effect in the stress values due to fatigue loading. However, we should notice that due to the low levels of stress monitored during testing, the error factor is fairly high due to noise levels and other side effects. Therefore, minor scatter in stress data are not necessarily due to fatigue and due to the errors associated with the test equipment. After concluding that there were no effects due to fatigue loading, it was decided to statically test the deck to failure.

7.2.6 Residual Strength Testing

Upon the completion of the fatigue loading, the avionics deck was statically loaded to assess its residual strength. However, due to limitations with the test equipment, the part could not be loaded higher than 200 percent of ultimate load. This limitation on loading had been set in advance and after coordinating with Air Force test personnel, we decided that testing of the deck to 200 percent of its ultimate load would be adequate. Therefore, the static test was conducted and as expected, the deck successfully carried the load without any signs of failure.

Figure 7-16 represents a plot of the left- and right-hand deflections of the deck during testing. The deflection pattern was symmetrical, and there was a 0.16-inch deflection after unloading which is an indication of some permanent set. The maximum and minimum strains and principal stresses are shown in Tables 7-6 and 7-7, respectively. The successful completion of the static residual strength testing marked an end to the successful completion of the program. The success of both fatigue and static testing of the avionics deck is an indication of

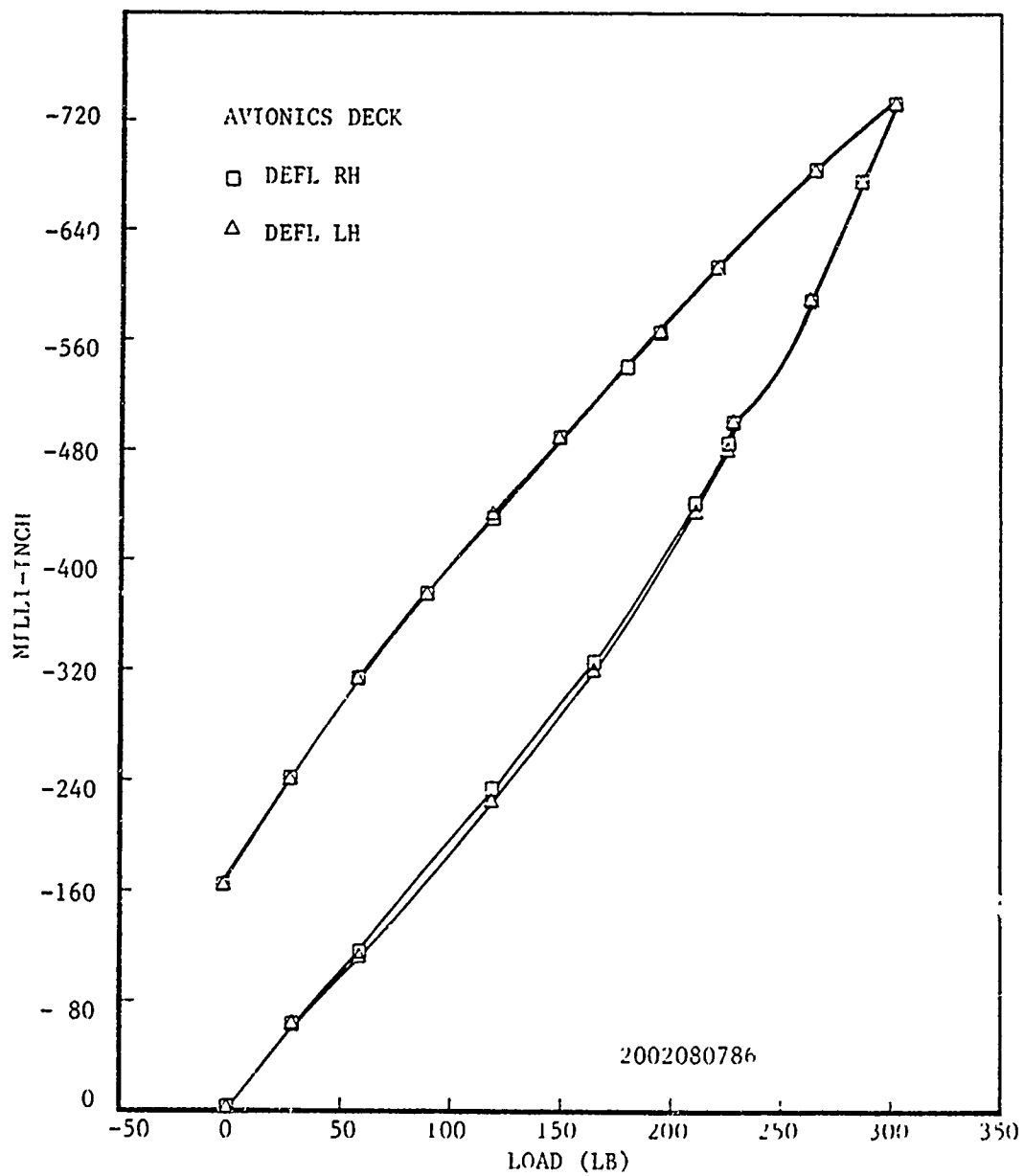


Figure 7-16. Avionics Deck Left Hand and Right Hand Deflections for Residual Strength Testing

TABLE 7-6. RESIDUAL STRENGTH TESTING, MAXIMUM AND MINIMUM PRINCIPAL STRESSES

STRAIN GAGE NO.	MAXIMUM STRAIN (μ IN/IN)	MINIMUM STRAIN (μ IN/IN)	STRAIN GAGE NO.	MAXIMUM STRAIN (μ IN/IN)	MINIMUM STRAIN (μ IN/IN)
1A	1.5	- 26.8	14C	-53.4	-104.8
1B	- 39.0	- 75.8	15A	42.0	10.0
1C	- 21.0	- 43.4	15B	- 3.9	- 29.5
2A	282.3	190.2	15C	56.3	-984.5
2B	112.8	71.3	16	-507.7	-894.4
2C	-138.9	-231.1	17	-480.3	-984.5
3A	189.7	107.0	21A	53.1	28.3
3B	-----	-----	21B	50.1	18.6
3C	-195.4	-290.8	21C	7.0	- 17.8
4	-119.4	-406.0	22A	18.8	1.1
5	- 72.3	-229.0	22B	9.2	- 1.2
6	1510.8	851.3	22C	21.3	4.7
7	1098.4	608.8	23A	10.6	- 7.0
11A	36.8	16.8	23B	68.9	28.0
11B	- 22.9	- 64.4	23C	3.5	- 16.5
11C	- 45.0	- 71.0	24A	43.7	18.9
12A	9.8	- 6.8	24B	- 9.3	- 31.3
12B	- 25.3	- 78.2	24C	-31.8	- 63.6
12C	- 16.4	- 51.7	25A	94.5	48.5
13A	44.6	10.5	25B	-20.9	- 41.8
13B	- 61.5	-102.0	25C	-71.9	-141.3
13C	15.0	- 2.6	26A	104.2	61.6
14A	-175.8	-291.8	26B	108.2	75.6
14B	-422.8	-644.4	26C	0	-176.9

TABLE 7-7. RESIDUAL STRENGTH TESTING, MAXIMUM AND MINIMUM PRINCIPAL STRESSES

STRAIN GAGE NO.	MAXIMUM PRINCIPAL STRESS (PSI)	MINIMUM PRINCIPAL STRESS (PSI)
1A *	122.1	- 787.2
2A	2565.6	- 1744.2
3A	---	---
11A	28.1	- 814.0
12A	209.3	- 834.9
13A	1409.4	- 652.0
14A	890.9	- 6596.9
15A	1125.6	31.1
21A	641.3	- 108.5
22A	395.0	66.1
23A	541.1	- 598.4
24A	325.6	- 607.3
25A	635.6	- 1311.2
26A	1039.7	- 2144.8

* Letter 'A' indicates the A leg of the rosette gage.

the structural integrity of a full scale SPF component against fatigue and static loading.

8. SUMMARY AND CONCLUSIONS

8.1 SUMMARY

A five-task program was carried out to exploit the applications of SPF aluminum and to develop and demonstrate the SPF process as a viable means of fabricating full scale structural parts which are more efficient and cost effective than their conventionally produced counterparts.

The major emphasis was on reduction of piece count and assembly costs. A number of airframe structural components were identified where application of the SPF process would provide potential cost and weight savings. These components were ranked and the two components promising the most benefits were selected for fabrication. The two components were the F-5F LEX and the lower avionics deck.

Several aluminum alloys were evaluated for their SPF potential, post-SPF properties and availability. Reynold's MD254 aluminum alloy was found to have the highest SPF potential and post-SPF properties. The post-SPF static and fatigue properties of this material were found to be comparable to those of the conventional 7075-T6 aluminum alloy.

Producibility forming tests were conducted to assess the forming feasibility of the components based on the preliminary design and forming parameters. Based on the outcome of these tests, the preliminary component designs were modified and parameters such as draft angles, and corner and edge radii, were modified to eliminate problems, such as cavitation and non uniform thinning.

After the completion of the producibility forming studies and the subsequent design modifications, the LEX corrugation and three avionics deck parts; lower skin, upper skin, and waffle pan, were superplastically formed using the MD254 aluminum alloy. Three of each part was successfully formed without any scrap parts. Subsequent to forming, the SPF parts were heat treated, trimmed, cleaned, and prepared for the component assembly. The avionics deck was assembled using the rivet bonding concept, the application of rivets simulated bonding pressure so the component could be cured in an oven as opposed to an autoclave. In production, weldbonding would have been used.

The assembled deck was delivered to the Air Force for the final static and fatigue testing. The deck was tested under static loading, to design limit load and constant amplitude fatigue loading. Four phases of fatigue loading were conducted which were equivalent to two lifetimes, typical of the F-5F aircraft. Upon the completion of the fatigue testing, the deck successfully carried twice the design ultimate load without failure.

8.2 CONCLUSIONS

The following conclusions can be derived from the studies conducted under this program:

- (1) Fabrication of airframe structural parts utilizing SPF technology can result in significant cost and weight savings.
- (2) Careful selection of potential SPF components can provide the maximum cost and weight savings. During the selection process, emphasis should be on reduction of piece count and assembly costs.

- (3) Superplastic forming of complex components should be accompanied by forming feasibility studies. Subcomponents representing the most critical forming areas of the component should be formed to verify the preliminary design parameters.
- (4) Based on the results of the forming feasibility studies, slight design modifications may be necessary to avoid possible cavitation and non uniform thinning problems.
- (5) 7475 aluminum (specifically MD254) is the best of aluminum alloys for superplastic forming, and its post-SPF properties are comparable to the conventional 7075-T6 alloy.

Prior to the delivery of the avionics deck to the Air Force, the component was weighed. Data indicated that the SPF avionics deck provided a 28.2 percent weight saving against its baseline design. The SPF avionics deck weighed 19.0 lbs, as opposed to the 26.47 lbs for its baseline design. Most of this weight saving was accomplished by reduction of the piece count from 63 (Baseline deck) down to 10 (SPF design). This reduction in piece count also eliminated a large number of fasteners and substantially reduced the machining and assembly costs.

In fact, cost studies conducted subsequent to forming of the deck indicated that the SPF avionics deck would also provide an average of 32 percent cost saving over its baseline design. Another factor that needs to be considered is that the substantial reduction of piece count associated with the SPF process also reduces the number of production engineering drawings associated with the component. As a result, a substantial saving in engineering design cost could also be achieved with application of this process. Table 8-1 represents a summary of the SPF avionics deck design benefits.

TABLE 8-1. SPF AVIONICS DECK DESIGN BENEFITS

DESIGN BENEFITS	BASELINE	SPF DESIGN	SAVINGS
PIECE COUNT	63	10	53
FASTENER COUNT	1,009	276	733
NONRECURRING COSTS (Tooling, Planning,	\$423,860	\$280,408	\$143,452 (33.8%)
RECURRING COSTS			
T1	\$ 7,946	\$ 5,440	\$2,506 (31.5%)
T500	5,551	3,782	1,769 (31.9%)
T1000	5,888	4,042	1,846 (31.3%)
STRUCTURAL WEIGHT	26.36 lb	18.98 lb	7.38 lb (28.0%)

REFERENCES

1. Ghosh, A.K., U.S. Patent No. 4,352,280, 5 October 1982.
2. Hamilton, C.H., U.S. Patent No. 4,354,369, 19 October 1982.
3. Agrawal, S.P., U.S. Patent No. 4,516,419, 14 May 1985.
4. Ghosh, A.K., and Hamilton, C.H., Met. Trans A, 1980, Vol. 11A, pp. 1915-1918.
5. Mackay, T.L., Sastry, S.M.L., and Yolton, C.F., "Metal-lurgical Characterization of Superplastic Forming," Technical Report AFWAL-TR-80-4038. Wright-Patterson AFB, Ohio, September 1980.
6. Woodford, D.A., Trans. Quart. ASM, 1969, Vol. 62, p. 291.
7. Hosford, W.F. and Caddell, R.M., "Metal Forming: Mechanics and Metallurgy," Prentice-Hall, Inc., pp. 80-102, 1983.
8. Gosh, A.K. and Hamilton, C.H., "Mechanical Behavior and Hardening Characteristics of a Superplastic Ti-6Al-4V Alloy," Metallurgical Transactions, v. 10A, p. 699, June 1979.
9. Agrawal, S.P. and Weisert, E.D., "Grain Size Effects and the Practice of Superplastic Forming/Diffusion Bonding of Titanium Alloys," Seventh North American Metalworking Research Conference Proceedings, p. 197, SME (1979).

10. Gosh, A.K., "Dynamics of Microstructural Changes in a Superplastic Aluminum Alloy," Proceedings of the 2nd Riso International Symposium on Metallurgy and Materials Science, Riso National Laboratory, Denmark (1981).
11. Agrawal, S.P., Bernhardt, L. and Vastava, R., "Near-Net-Structural Airframe Parts by Superplastic Forming of Aluminum," paper presented at the 113th Annual AIME Meeting, Los Angeles, CA, February 29, 1984.
12. Agrawal, S. P. and Tuss, J. M., "Superplastic Forming and Post-SPF Behavior of an Aluminum Alloy for Airframe Applications," Superplasticity in Aerospace-Aluminum, Proceedings of an International Conference held at Cranfield, England, UK, 12-15 July 1985, R. Pearce, L. Kelly, editors, Ashford Press, UK, pp. 296-325.
13. Mahoney, M. W. and Hamilton, C. H., "Superplastic Aluminum Evaluation," Technical Report, AFWAL-TR-81-3051, Wright-Patterson AFB, Ohio, June 1981.
14. Cervay, R. R., "Engineering Design Data for Aluminum Alloy 7475 in the T761 and T61 Condition," Technical Report, AFML-TR-72-173, Wright-Patterson AFB, Ohio, September 1972.
15. Mehr, P.L., Alcoa 7475 Sheet and Plate, Alcoa Green Letter, Third Revised Edition, Alcoa Technical Center, Pennsylvania, February 1978.
16. Bohlen, J.W. and Ping, S.W., "Development of High Strength, Fatigue Crack Growth Resistant Aluminum Alloys by Rapid Solidification Technology," Final Report on Contract N60921-82-C-0043, Naval Surface Weapons Center, Silver Spring, Maryland, December 1983.